CONTROLLED SUBSTRUCTURE IDENTIFICATION FOR SHEAR STRUCTURES

by

Dongyu Zhang

A Dissertation Presented to the
FACULTY OF THE USC GRADUATE SCHOOL
UNIVERSITY OF SOUTHERN CALIFORNIA
In Partial Fulfillment of the
Requirements for the Degree
DOCTOR OF PHILOSOPHY
(CIVIL ENGINEERING)

December 2010

Dedication

To my parents, father (Yulong Zhang) and mother (Qingwen Feng), for giving and guiding my life.

To my wife (Li), daughter (Angela) and son (Gary) for encouraging me to pursue my academic dream.

Acknowledgements

First, I would like to express the deepest thank to my advisor, Professor Erik A. Johnson, for his friendship, encouragement and support. Without his guidance and persistent help this dissertation would not have been possible.

I would also like to gratefully thank for other committee members, Prof. Sam F. Masri, Prof. Roger Ghanem, Prof. Vincent W. Lee, Prof. Robert L. Nigbor, for their invaluable suggestions and advices on this research.

I would like to thank many people who gave me so many help during my study at USC: Tat Fu to provide excellent suggestions for the research, Charles DeVore to help me on the experiment tests, Mahmoud Kamalzare, Elham Hemmat Abiri, Yuanhai Ryan Zheng, Wael Elhaddad,…

The author gratefully acknowledges the partial financial support of this research work by National Science Foundation (NSF) through the following grants: CMS 00-94030, ANI 03-25875, CMMI 08-26634; by the University of Southern California through Teaching Assistantship.

Table of Contents

List of Tables

List of Figures

Abstract

Shear structure models are widely used to model the dynamics of building structures; therefore, developing the techniques that can accurately identify the parameters of a shear structure plays a vital role in establishing efficient and reliable structural health monitoring systems for building structures.

In this dissertation, applying the "divide and conquer" strategy of substructure identification (SI), a series of innovative SI methods for shear structure are developed. A shear structure is divided into many two-story standard substructures. A novel inductive identification procedure is applied to identify the parameters of the whole structure from top to bottom. Numerical simulations verify that these substructure identification methods provide accurate identification results.

One of the most important features of these SI methods is that an approximate analytical expression for the identification error is obtained, which demonstrates that the identification accuracy is simply controlled by the frequency responses of the substructure near the substructure natural frequency. This important discovery provides the ability to easily improve the identification accuracy by appropriately changing the substructure responses via specially designed structural control systems. Several controlled substructure identification methods are proposed, using different structural control systems to improve the accuracy of the SI method. Furthermore, since the accuracy of the proposed controlled SI methods directly depends on the close-loop controlled structural responses rather than on the control systems themselves, these controlled SI methods are proven to be quite robust to possible control system errors.

To expand the applicability of the SI methods, a loop substructure identification method is proposed which makes use of the dynamic equilibrium of only one standard substructure to formulate a loop identification sequence and identify all parameters of that substructure once. Compared with the previous SI methods, the loop SI method is able to perform the structural identification of any part of a shear structure with only three floor acceleration responses; also importantly, the loop substructure identification can be carried out without knowing structural mass information.

Several shake table experiments are conducted on a two-story bench-scale test structure; the results show that the proposed SI methods can accurately identify the structural parameters and that, by using appropriately designed passive control system, the identification accuracy can be further improved.

Finally, a new approach is proposed to extend the SI methods originally developed for shear structures to more realistic frame structures. The study shows that the proposed approach is able to accurately structural damage of columns in a frame structure.

In summary, the SI methods developed in this dissertation are able to accurately identify the structural parameters of a shear structure, forming a solid foundation to design efficient SHM systems for building structures. Furthermore, combined with structural control systems, the proposed controlled SI methods not only further improve the accuracy of damage detection but also have a potential to enhance the performance of control systems to reduce the structural vibration by providing more accurate structural model for control algorithms design, both of which greatly enhance the safety and reliability of the structures.

Chapter 1

Introduction

Civil structures, such as high-rise buildings, bridges, dams, etc., begin to deteriorate once they are built and used. They may also be damaged in severe events like strong earthquakes. Due to the essential roles of civil structures in our modern society, it is vital to frequently check the health status of structures and detect damage, if any has occurred, at the earliest possible stage so that timely repair work can be made to ensure the safe and reliable operation of the structures. According to a recent report from Federal Highway Administration (FHWA, 2008), 15% percent of the nearly 600,000 highway bridges in the United States are rated as “structural deficient”, requiring signification maintenance and repair to remain in service. Clearly, there is urgent need to develop efficient techniques that can accurately detect damage in aging civil structures nationwide. Recent catastrophes such as the collapse of the I-35W Bridge in Minneapolis are another reminder that frequent and rapid assessment of structural health is a vital need.

<http://www.america2050.org/2007/08/minnesota-bridge-collapse-unde-2.html>

Figure 1.1 The collapse of the I-35W Bridge in Minneapolis (August 1, 2007)

Visual inspection, which is labor-intensive and expensive, is still the most widely used method to date to check structural safety. However, it is a very *subjective* process as the accuracy of the damage detection depends highly on the expertise of the inspection staff. Moreover, many instances of structural damage, like the corrosion of steel bars in reinforce concrete structure, are hidden inside the structure and cannot be observed from the outside; under such circumstances, visual inspection cannot accomplish its mission.

Hence, in research communities there is intensive interest in developing efficient structural health monitoring (SHM) techniques, which provide an *objective* way to assess the structural health condition and detect the existence of the damage. Generally, SHM techniques are classified into two large categories. The first kind of techniques is also known as nondestructive evaluation (NDE), including acoustic emission monitoring, ultrasonic wave, radiography imagining, eddy current detection, and many other methods (Chang *et al.*, 2003). These techniques need to carry out some experiment tests in the immediate vicinity of the damage locations to detect the damage. In order to perform NDE testing, the locations of the damage must be known *a priori* and be accessible for testing, making these methods unsuitable to detect structural damage in the entirety of a complex structure. The second kind of techniques, also known as vibration-based structural health monitoring methods, makes use of structural vibration responses to detect and locate structural damage on a global structure basis. The basic premise of these SHM methods is that structural damage will alter the structural stiffness, mass and/or energy dissipation, which in turn change the dynamic behaviors of structures (Farrar *et al*., 2001). Thus, by tracking these changes SHM systems can theoretically detect the occurrence of structural damage, and even locate and quantify them. Relative to NDE tools, vibration-based SHM methods have the advantages of discovering and locating multiple structural damage locations across the entire structure. In order to make the notation simpler, hereafter SHM methods will exclusively refer to the vibration-based SHM methods unless otherwise stated.

1.1 The State-of-art of Vibration Based SHM

Many SHM techniques utilize structural modal features, such as natural frequencies, mode shapes and modal flexibility, to detect damage in the structure. These techniques are usually realized via system and/or parameter identification techniques. A structural model, often a finite element model, is selected to represent the behavior of the real structure; the parameters of the structural model, such as structural mass, stiffness and damping, are estimated by minimizing the difference between the modal features of the structural model and that of real structure derived from the measured structural responses. By comparing the values of these identified parameters before and after the damage, the structural damage can be detected, located and quantified.

Unfortunately, current global vibration-based SHM techniques cannot yet be considered sufficiently accurate, efficient and robust for real applications. Many factors contribute to the failure, including:

1. Structural modal properties such as natural frequency and mode shape are generally not sensitive to structural damage, which makes the inverse problems associated with SHM methods ill-conditioned, resulting in inaccurate identified structural parameters and, thus, inaccurate damage detection results.

2. In order to represent the behavior of a large structure, usually a complex model with tens or even hundreds of parameters is needed. Solving the inverse identification problem for damage detection with this kind of model is very challenging. Ill-condition and non-global identifiability features for this kind of identification problem pose huge challenges to correctly identifying the structural damage. Thus, the complexity of a real structure becomes one of the most difficult challenges for SHM methods.

3. The structure model is only an approximation of a real structure; it may not exactly describe the full behavior of the real structure. Efficient SHM methods must be able to accommodate the modeling errors caused by the imperfect match between the structural model and the real structure.

4. Other factors like the periodic variation of environmental effects (*e.g.*, temperature) also induce changes in the structure modal properties, masking the effect of real damage.

5. Since controlled excitation experiments are quite expensive for the long-term structural health monitoring of civil structures, ambient excitation tests usually have to be adopted to identify the structural modal properties. However, it is much more challenging to perform SHM identification using ambient excitation than using controlled force excitation. First, ambient excitation cannot be directly measured in most cases, which requires that the SHM methods be performed without the information of the excitation. Several methods have been proposed to carry out structural identification without excitation information,

such as the natural excitation technique (James *et al.*, 1993; Caicedo *et al.*, 2004), random decrement (Yang *et al.*, 1976, Huang *et al.*, 1999). Second, ambient excitation is generally very small, resulting in small structural responses; thus, usually the measured structural responses will be significantly corrupted by measurement noise, resulting in large identification errors for SHM.

To the best of the author's knowledge, there is not an all-in-one solution to all challenges previously mentioned. Many researchers have proposed some new techniques, trying to solve one or several above problems and increase the accuracy for damage detection. Two of these techniques, substructure identification methods and controlled identification methods, are discussed herein.

1.1.1 Substructure Identification

Substructure identification methods provide an effective means for SHM systems to tackle the difficulty of identifying complex real structures. A substructure identification method, applying a "divide and conquer" strategy (Koh, 1991), divides a large complex structure into many simple substructures and carries out system identification and damage detection for each substructure as an independent structure. Since the identification problem of each substructure is much simpler than that of the whole structure, the convergence and ill-conditioning problems frequently encountered in global SHM methods are alleviated; more accurate damage detection and localization can be achieved. In additional to the improvement of identification accuracy, substructure identification methods have many other promising features.

1. The identification of one substructure generally does not require measuring the excitation forces applied outside this substructure; thus, substructure identification methods partially solve the common difficulty facing many SHM methods – how to perform the identification without excitation information.
2. Each identification step in a substructure identification method only utilizes the structural responses related to one substructure and can be carried out almost independently. Consequently, substructure identification methods do not need to simultaneously measure all structural responses of a large structure, which may greatly reduce the cost of SHM systems especially when power-limited wireless sensors are used to collect and transmit the measured data.
3. Since structural damage inside one substructure usually only affects the identified parameters of that substructure, substructure identification methods make it easy to detect structural damage at the substructure level.

1.1.2 Controlled Identification

Another promising technique is to use structural control (SC) systems to improve the accuracy of SHM. These techniques try to change the structural responses by some specially designed structural control strategies, so that either SHM methods are more sensitive to the damage or multiple information sets of structural features are available to improve the identification accuracy.

Traditionally, structural control systems are designed and installed to reduce the excessive structural vibration due to strong earthquakes or high-speed winds. However, compared with the whole service life of structures, such large natural hazards occur rarely and only last for very short durations; the remainder of the time, the expensive structural control system remains unused in an idle state. When no external hazard is present, the capacity of the control system to measure and control structural responses may be re-tasked to monitor the structural health and detect potential structural damage. Incorporating SHM functionality into current structural control systems not only adds useful functions to current control systems at a very small cost, making control systems more cost-efficient, but also has potential to enhance the performance of control systems to reduce structural vibration by providing a more accurate structural model for the control algorithm. As shown in Figure 1.2, the synergy of structural control (SC) systems and structural health monitoring (SHM) systems leads to more reliable and safe structures.

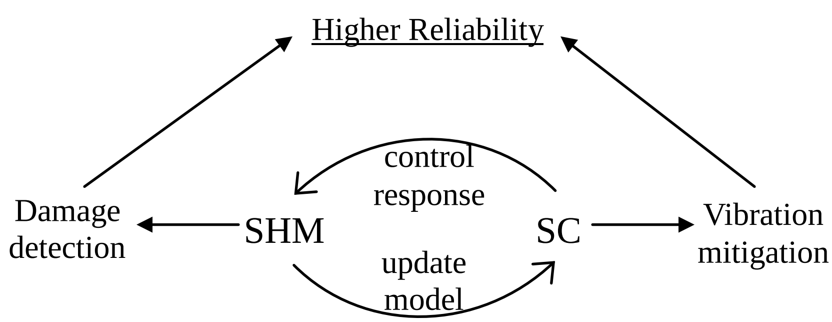

Figure 1.2 Mutual benefit of combining structural control and structural health monitoring systems

1.2 Overview of This Dissertation Work

A shear structure, shown in Figure 1.3, is widely used to model the dynamic behaviors of building structures. Therefore, developing efficient identification methods, which can accurately identify the parameters of a shear model, plays a vital role in establishing efficient and accurate SHM systems for building structures.

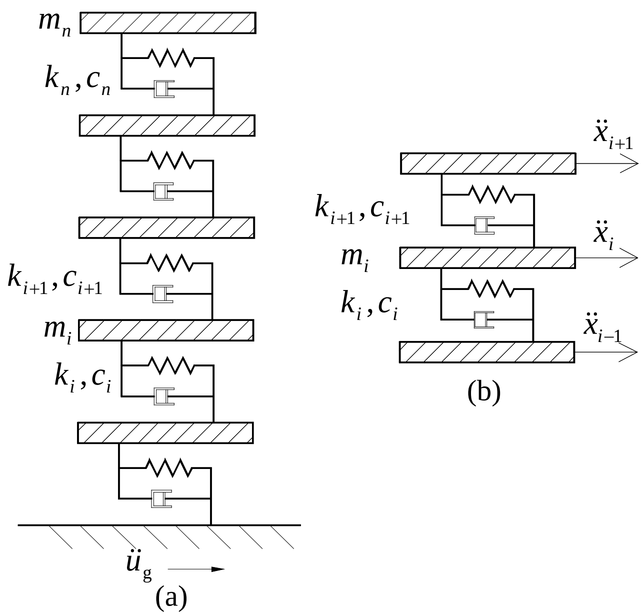

Figure 1.3 (a) An *n*-story shear structure (b) the two-story standard substructure

1.2.1 Substructure Identification for Shear Structures

Following the "divide and conquer" strategy, a substructure identification method for shear structures is developed in this study. A standard two-story substructure, shown in Figure 1.4, is used to divide a large shear structure into many small substructures. An inductive identification method is formulated in which the parameters of the whole structure are identified from top to bottom iteratively. In each step of the substructure identification, only two or three floors' acceleration responses are needed for the identification procedure, making this method easy to be implemented.

When long stationary structural responses are available and there is only one excitation source in the structure, a more accurate transfer-function based substructure identification method (FT_SUBID), formulated by using the transfer functions among different substructure responses, can be adopted to improve the identification accuracy.

Moreover, a cross power spectrum based substructure identification (CSD_SUBID) method is developed from the differential equation governing random structural responses to stochastic excitation; not only does this approach overcome the limitation of only one excitation source required for the FT_SUBID approach, it also further improves the identification accuracy. This substructure identification method possesses some superb properties compared with its two predecessors. 1) It is an asymptotically unbiased and consistent estimator for structural parameters, being able to provide arbitrarily accurate identification results given that sufficiently long stationary structural response measurements are available. 2) The explicit formulae to calculate the approximate variance of identification errors are developed, which provide the confidence level along with the estimated parameters, crucial information for damage detection tasks. 3) Although this new SI method is first developed assuming that the structural responses are wide sense stationary (WSS), it is proved theoretically as well as through simulation that this method, with little modification, can be directly extended to perform the identification tasks with non-stationary structural responses and still provide very accurate identification results.

Numerical simulations demonstrate that all proposed substructure identification methods offer good estimation results as expected.

1.2.2 Controlled Substructure Identification for Shear Structures

In contrast with previous work on substructure identification, which have mainly focused on reducing the size of the identification problem to increase the accuracy and efficiency of the system identification, this study also makes some important attempts to discuss how the uncertain factors in the identification process, such as measurement noise, will influence the accuracy of the identification result. To accomplish this goal, an approximate identification error analysis for a least-square-error (LSE) identification problem is proposed and applied to the proposed substructure methods. A simple analytical result of the identification error is obtained, which demonstrates that the identification accuracy is simply controlled by two substructure responses within a very narrow frequency band centered at the substructure natural frequency. This important discovery provides the ability to easily improve the identification accuracy by appropriately changing the substructure responses via specially designed structural control systems.

Several controlled substructure identification methods are proposed herein, using different structural control systems to improve the accuracy of the substructure identification methods. Furthermore, since the accuracy of the proposed controlled substructure identification methods directly depend on the close-loop controlled structural responses rather than on the control systems themselves, these controlled substructure identification methods are proven to be quite robust to possible control system errors, making them excellent candidates to provide accurate and reliable identification results with imperfect structural control systems.

Combined with the controlled substructure identification methods, a fast substructure identification method is also developed, which only makes use of the responses of one standard two-story standard substructure to formulate a loop-identification sequence and identify all four parameters of that substructure once together even without knowing structural mass. This new method can directly, quickly and accurately identify any structural parameters in a large shear structure with as few as one set of substructure response data and no information about the structural mass, making it a very promising technique for real-world applications, like immediate post-earthquake damage evaluation for buildings.

1.2.3 Damage Detection in Frame Structures via Substructure Identification

The proposed substructure identification methods and their identification error analyses are all based on a fundamental assumption that the identified structure is a shear model structure. Although the shear model is widely used to model the dynamic behavior of frame structures, it is only a simplification of a complex real building structure. Furthermore, finding the damage in complex real building structures, like the frame structure in Figure 1.5, is of much more practical interest than just identifying the parameter values in a shear model structure (Yan *et al.*, 2006). However, directly performing identification in a complex structure model to find damage is often in vain due to the greater complexity of the search space in the identification problems.

Using the methodology of substructuring, a substructure identification method for frame structures is successfully developed. The dynamic equilibrium of one floor substructure is used to formulate the identification problem, in which the equivalent story stiffness parameters are identified. In addition to the horizontal floor responses, the rotational responses at beam-column joints are needed in the new formulation. Surprisingly, the new substructure identification method for frame structures has a similar format as the substructure identification methods for shear structures. As a consequence, the results of the identification error analysis can also be applied to the new substructure identification methods with some modifications. This new method can identify the structural damage occurring in the columns of the structure.

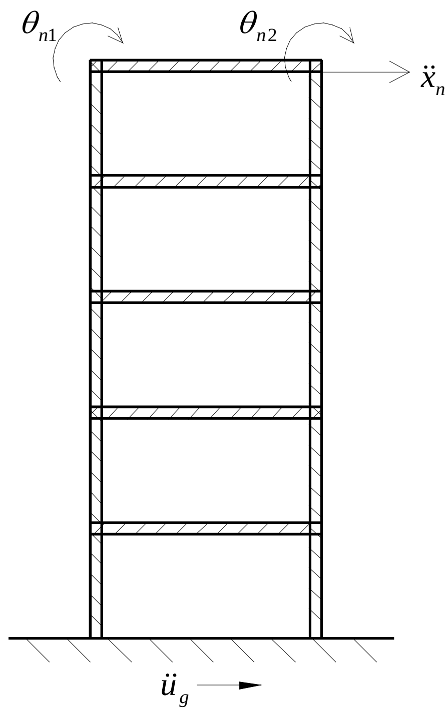

Figure 1.4 A simple one-bay frame structure

In summary, the substructure identification methods developed in this work are able to accurately identify the structural parameters of a shear structure, forming a solid foundation to design efficient SHM systems for building structures. Furthermore, combined with structural control systems, the proposed controlled SI methods not only further improve the accuracy of damage detection but also have the potential to enhance the performance of control systems to reduce the structural vibration by providing more accurate structural models for control algorithm design, both of which greatly raise the safety and reliability of the structures.

Chapter 2
Background and Literature Review

Aging of civil structures gradually deteriorates the load-resistant capacity of structures. The need for assessing the health status of structures and detecting structural damage, if present, at the earliest possible stage has urged development of research in structural health monitoring.

Generally, structural health monitoring methods fall roughly into two categories: one is localized experimental methods, also known as nondestructive evaluation (NDE) techniques, including acoustic emission monitoring, ultrasonic wave, radiography imagining, eddy current detection, and many other methods (Chang *et al.*, 2003); the other is global vibration-based methods which make use of the change of structural vibration features (frequency, mode shape, etc.) to identify the onset, location and severity of the damage.

NDE methods typically require carrying out some experiment near the damage location to test the physical properties of the structural materials and detect the onset and severity of the damage inside the structure. For example, ultrasonic methods will generate incident ultrasonic sound waves on the surface of a structural component and measure the reflective waves from the structure. If there are cracks inside the structure, some additional reflective waves will be produced by these cracks and captured by sensors. Therefore, by analyzing the reflective waves, the hidden structural damage will be detected. Usually, such a method will provide accurate information about the structural damage. However, because NDE methods require *a priori* knowledge of likely damage locations and also need to carry out experiments near every possible damage location, they are, by themselves, impractical for detecting structural damage in the entirety of a complex structure. A good review of local SHM methods is given by Rens *et al.* (1997). This chapter will only focus on global vibration-based SHM methods.

In this chapter, first a brief review of the major vibration-based global structural health monitoring methods is given. Then the common deficiencies of these methods are summarized. Last, some recently developed methods are introduced that intend to overcome some of the deficiencies and improve the accuracy of damage detection.

2.1 Major Structural Health Monitoring Methods

Structural health monitoring and damage detection have been hot research topics for several decades; hundreds of approaches have been proposed using various hardware and algorithms. This chapter will only refer to a few representative approaches; extensive reviews could be found in Doebling *et al.* (1996) and Sohn *et al.* (2003).

Rytter (1993) proposed to classify the damage identification methods into four levels:

- Level 1: Determination if damage is present in the structure
- Level 2: Determination of the geometric location of the damage
- Level 3: Quantification of the severity of the damage
- Level 4: Prediction of the remaining service life of the structure

The vibration-based SHM methods generally fall into Level 1, Level 2, or Level 3 methods because they are directly associated with structural dynamics testing, modeling and structure identification. While Level 4 methods, predicting the effect of structural damage on the structural loading-resistant capacity given that structural damage have been identified, are related to the fields of fracture mechanics, fatigue life analysis, or structural design assessment.

In general, damage can be defined as changes within a structural system which adversely affect its current and future performance (Farrar *et al*., 2000). Accordingly, structural damage is usually associated with changes to geometric and material properties of the structure, such as the occurrence of cracks in structural components, gradual deterioration of Young's module of the structural materials and the yielding of some structural components. Some structural damage is caused by unexpected excessive loadings such as strong earthquakes and blast loading; others are the result of accumulated corrosion caused by environment factors such as humidity. However, structural damage is difficult to directly measure and quantify; therefore, most researchers tend to use the change in the mechanical properties of the structure, which could be directly measured or indirectly estimated from structural responses, to represent the existence of structural damage. The general mechanical properties used for damage detection can be classified in two categories: structural modal parameters (*e.g.,* natural frequency, damping ratio and mode shape) and structural model parameters like the stiffness of structural components. Structural damage is detected and evaluated by monitoring the changes of these parameters before and after damage. Hence, identifying these features or parameters becomes an essential step for SHM.

Usually a mathematical or computational prediction model that replicates the behavior or features of the structure system is needed first; then, by applying system identification techniques that fit the model to experimental data, the optimal model parameters can be estimated. Different types of structural models are most amenable to different system identification techniques, which can be roughly divided into the methods based on structural modal properties, frequency domain, time domain, and ERA and other subspace identification.

2.1.1 Structural Modal Property Based Methods

Structural modal methods are probably the most abundant of SHM methods. They typically use structural modal parameters, such as natural frequency and mode shape, to detect the damage in the structure. These methods can be further classified, by how the modal characteristics are used, as forward methods and inverse methods. For the forward methods, some damage indices are calculated from structural modal parameters. Large changes in these indices are used to indicate the occurrence of damage. Usually this kind of method can only suggest whether or not there is some damage, and cannot provide information such as the location and severity of the damage. Inverse methods typically use the structural modal parameters as the prediction model; by solving some inverse problem, the parameters of the physical structural model (like stiffness) are estimated. Hence, inverse methods can offer information about the location and severity of the damage.

a) Natural Frequency Based Methods

The tangible relation between the changes of structural stiffness and the changes of structural natural frequency makes it a natural choice to use the estimated structural frequencies to identify damage. Another reason that the structural frequency based identification methods prevail is the ease of identifying the natural frequencies (in many cases only a single sensor is required). Salawu (1997) reviewed 65 publications dealing with the detection of structural damage through frequency changes.

Most of the early work was based on very simple structures and structural elements. Adams *et al*. (1978) and Cawley *et al*. (1979) demonstrated that the ratio of the frequency changes in two modes is only a function of damage location. A collection of possible damage points was considered, and an error term was constructed that relates the measured frequency shifts to those predicted local stiffness reduction. A number of mode pairs were considered for each potential damage location, and the pair that give the lowest error indicated the location of the damage.

Stubbs *et al*. (1990a,b) discussed a method for damage identification which relates changes in the structural frequencies to changes in the stiffness of structural members by using a sensitivity relation. The sensitivity matrix of structural frequency with respect to both structural stiffness and mass was constructed and used to calculate the changes of structural stiffness and mass.

Brincker *et al*. (1995) applied a statistical analysis method to detect damage in two concrete beams using changes in the measured vibration frequencies. The authors introduced a significance indicator for the i^{th} modal frequency, defined by scaling the observed change in modal frequency by the estimated standard deviation of the frequencies. A similar significance indicator was defined for the measured modal damping ratio. By summing the frequency and damping significance indicators over several measured modes, a unified significance indicator was defined and used to detect damage. This significance indicator was a sensitive indicator of structural damage, but it was not able to provide an estimate of damage location.

It is worth pointing out that structural frequency shifts have some significant limitations for detecting the structural damage in real complex structures. The low sensitivity of frequency shifts to damage requires either very precise measurements or large levels of damage, in order to accurately detect the occurrence of structural damage. For example, in offshore platforms, frequency shifts resulting from mass changes due to marine growth are much larger than damage-induced frequency shifts (Whittome e*t al.*, 1983). Tests conducted on the I-40 Bridge (Farrar *et al.*, 1994) also demonstrated this point. When the cross-sectional stiffness at the centre of a main plate girder had been reduced by 96%, reducing the bending stiffness of the overall bridge cross section by 21%, no significant reductions in the modal frequencies were observed.

b) Mode Shape Based Methods

Since the structural natural frequency is insensitive to structural damage, researchers turned to more damage-sensitive modal properties (*i.e.*, mode shape) for help. The Modal Assurance Criterion (MAC) (Allemeng *et al.*, 1982) and Coordinate Modal Assurance Criterion (COMAC) (Lieven *et al.*, 1988) are two commonly used methods to compare two sets of mode shapes. The MAC value is a measure of the similarity of two mode shape vectors. A MAC value of 1 means a perfect match (exactly parallel vectors) and a value of 0 means they are completely dissimilar (orthogonal). Thus, the reduction of a MAC value may be considered as an indication of damage. The COMAC is a pointwise measure of the difference between two sets of mode shapes and takes a value between 1 and 0. A low COMAC value would indicate discordance at a point and, thus, is also a possible damage location indicator.

West (1984) demonstrated the possibility of using mode shape information for locating structural damage. The modal assurance criterion (MAC) was used to determine the correlation of the modes before and after damage. The mode shape was partitioned using various schemes and the change in the MAC across the different partitioning techniques was used to localize the structural damage.

Salawu *et al.* (1995) tested a reinforced concrete bridge before and after repair. Although the natural frequency shift, due to structural damage, was less than 3% for each of the first seven modes, the MAC values show substantial change, which indicated that comparison of mode shapes is a more sensitive and robust technique for damage detection than shifts in natural frequencies.

Frỳba *et al.* (2001) used the COMAC method for checking the quality of the repair of a pre-stressed concrete bridge segment after part of the superstructure had spontaneously slid off its bearings. The COMAC analysis was used to confirm that the repaired segment responses were consistent with the undamaged segment.

Williams *et al.* (1999) formulated a frequency Multiple Damage Location Assurance Criterion (MDLAC) method. In this method, a correlation coefficient MDLAC was calculated, which compared changes in a structure's resonant frequencies with predictions based on a frequency-sensitivity model derived from a finite element model. When the MDLAC approaches 1, it implies that the frequencies calculated from the damage scenario of the finite element model match very well with the structural frequencies estimated from measured quantities.

In addition to these methods, several other assurance criteria have also been proposed to assess the consistence of modal shapes and other structural dynamic properties like frequency response function as well. These techniques include the frequency response assurance criterion (Heylen *et al.*, 1996), coordinate orthogonality check (Avitabile *et al.*, 1994), frequency scaled modal assurance criterion (Fotsch *et al.*, 2001), partial modal assurance criterion (Heylen, 1990), scaled modal assurance criterion (Brechlin *et al.*, 1998), and modal assurance criterion using reciprocal modal vectors (Wei *et al.*, 1990).

c) Mode Shape Curvature Based Methods

Since structural damage in simple structures, like a beam, causes larger local changes of the mode shape curvatures than that of mode shapes, many researchers propose to use mode shape curvatures, instead of mode shapes, to detect structural damage. The curvature is often calculated from the measured displacement mode shapes using a central difference approximation,

$$\phi''_{ji} = \frac{\phi_{(j+1)i} - 2\phi_{ji} + \phi_{(j-1)i}}{L^2} \tag{2.1}$$

where i = mode shape number; j = node number; L is the distance between the nodes (assuming equidistant).

Pandey *et al.* (1991) presented a method to detect damage in a beam structure by using absolute changes in mode shape curvatures. The curvature values were computed from the displacement mode shape using a central difference approximation. Chance *et al.* (1994) found that curvature calculated numerically from mode shapes resulted in unacceptable errors. They proposed using measured strains instead to infer curvature, which dramatically improved results.

Wahab *et al.* (1999) successfully applied a curvature based method to the Z24 Bridge in Switzerland. They introduced a damage indicator which is determined by the difference in curvature before and after damage averaged over a number of modes. They concluded that the use of modal curvature to locate damage in civil engineering structures seems promising.

d) Modal Strain Energy Based Methods

When a particular vibration mode stores a large amount of strain energy in some structural members, the frequency and shape of that mode are highly sensitive to the changes in those structural members. Thus, changes in modal strain energy might be considered as logical choice of the indicator of damage location.

Kim *et al.* (1995) applied a damage identification algorithm to locate and quantify a single crack in an experimental plate girder. Cubic spline functions were used to interpolate the incomplete mode shapes and produce a curvature function to calculate the modal strain energy. A damage indicator was proposed based on the ratio of modal strain energy of elements before and after the damage. A statistical hypothesis technique was applied to classify the significance of the value of the damage indicator. The method was also demonstrated to locate up to two damage sites in a simulated plate girder.

Law *et al.* (1998) proposed to use the elemental energy quotient (EEQ), defined as the ratio of the modal strain energy of an element to its kinetic energy, to detect the damage in structural members. The difference in the EEQ before and after damage was normalized and averaged over several modes and used as a damage location indicator. This method was demonstrated on a simulated space frame. The method was also successfully applied to an experimental two-story plane frame with up to two joints loosened to simulate damage.

e) Dynamically Measured Flexibility Matrix Based Methods

Another class of damage identification methods uses the dynamically measured flexibility matrix to estimate changes in the static behavior of the structure. The measured flexibility matrix is estimated from the mass-normalized measured mode shapes and frequencies as

$$\mathbf{G} = \sum_i \frac{1}{\omega_i^2} \boldsymbol{\varphi}_i \boldsymbol{\varphi}_i^{\mathrm{T}} \tag{2.2}$$

where $\mathbf{G}$ is the flexibility matrix of the structure; ω_i is the natural frequency of the i^{th} mode; and $\boldsymbol{\varphi}_i$ is the i^{th} mass normalized mode shape. This formulation indicates that only the first few modes of the structure (typically the lowest-frequency modes) are needed to construct the flexibility matrix.

Li *et al.* (1999) proposed an approach for damage identification by utilizing the flexibility matrix in slender structures, such as tall buildings and chimneys. The method assumed that damage in each story of a building could be represented by just two variables and, thus, only a minimal number of modes were needed for successful identification. However, the authors did not tackle any issues of sparse measurements or compare cantilever models to more complex models.

Bernal (2000, 2006, 2010) pointed out that changes in the dynamic flexibility matrix are sometimes more desirable to monitor than changes in the stiffness matrix. Since the dynamic flexibility matrix is dominated by the lower modes, and good approximations can be obtained even when only a few lower modes are measured. Bernal outlines a state-space realization procedure to identify the modes at sensor locations and presents closed form solutions for computing mass normalized mode shapes when classical damping is assumed.

2.1.2 Frequency Domain Techniques

Frequency domain identification techniques refer to the methods that employ a transfer function (TF) or frequency response function (FRF) to identify the damage in a structure. Because the TF or FRF cannot be measured directly, many methods (*e.g.*, empirical transfer function estimate (ETFE), correlation method, etc.), which calculate the FRF from measured structural time history responses, have been proposed. Detailed information about these methods is found in Ljung (1999).

As Lee and Shin (2002) pointed out, there are two main advantages of using the FRF data. Firstly, modal data can be contaminated by modal extraction errors in addition to measurement errors, because they are derived data sets. Secondly, a complete set of modal data cannot be measured in all but the simplest structures. FRF data can provide much more information on damage in a desired frequency range compared to modal data that is extracted from a very limited range around resonances.

Crohas *et al.* (1982) described a “vibro-detection device” that was attached to structural members of an offshore oil platform. The device was able to apply an excitation to the structure and simultaneously measure its response. Frequency response functions were then determined for the measured the acceleration response that results from the excitation.

Park *et al.* (1999) observed that the changing environmental and operational conditions will alter the structure's vibration signals, which often lead to false assessments of structural damage for conventional modal-based SHM. They used a piezoelectric transducer (PZT) bonded to the structure as an actuator and sensor simultaneously, and carry out damage detection via the transfer function obtained from PZT. Many related studies are reported in the literature.

Fanning *et al.* (2003) proposed a damage detection method based on a single-input single-output (SISO) measurement. A numerically efficient method was proposed to calculate a single FRF from the SISO measurements. The method requires a correlated numerical model of the structure in its initial state and a single measured FRF of the damaged system sampled at several frequencies to detect structural changes. The method successfully detected stiffness changes in a numerically simulated 2-D frame structure (Fanning *et al.*, 2004).

2.1.3 Time Domain Techniques

Time domain identification techniques here refer to the methods that directly make use of the structural time history response to detect structural damage. These methods typically first select a mathematical model to represent the structure; then, the parameters of the model are identified by minimizing the difference between the measured structural responses and that predicted by the model.

Auto regressive (AR) and auto regressive moving average (ARMA) are probably two of the most adopted models for time domain methods. By minimizing the error between the measured and computed structural time history responses, the parameters of these models are estimated. Structural damage is detected by relating the identified parameters to the structural model parameters, such as stiffness of structural members. However, for a complex structure, the relation between the parameters of an ARX or ARMA model and that of structural model becomes so complicated that detecting the damage becomes a non-trivial task.

Shinozuka *et al.* (1982) demonstrated a method of parameter estimation for linear multi-degree-of-freedom structural dynamical systems based on observed records of the external forces and the structural responses. The ARMA model was used for simulating the dynamic response of the structure. The parameter values of the ARMA model were estimated using least-square-error criterion. To check the estimation accuracy, analytical simulation studies were performed on the basis of simulated data dealing with the aerodynamic coefficient matrices that appear in the equations of motion of a two-dimensional model of a suspension bridge. Then, these methods were applied to the same equations to identify the coefficient matrices using the field measurement data, yielding good estimates of the system parameters even under large output noise conditions.

Beck (1978) proposed a method applying a minimum output error approach to identify the modal parameters of the structure from earthquake records. Beck (1998) also extended his method with a Bayesian probability framework, which treats the identified parameter as random variables rather than fixed value parameters. By applying Bayesian updating techniques, the probability density function (PDF) of the identified parameters was calculated. This method gave not only the optimal values of the identified parameters, but also quantified uncertainty in the identified parameters, which is of great importance for evaluating the credibility of the identification results.

Zheng *et al.* (2008) introduced a new damage indicator, denoted by the distance between ARMA models, to identify structural damage including its location and severity. They pointed out that two commonly used distances, the cepstral metric and subspace angles, of ARMA models have limitation in accurately predicting the damage when there are multiple inputs with strong correlations. To overcome this difficulty, a pre-whitening filter was applied. Therefore, the proposed damage indicator was applicable for varieties of excitation types in civil engineering, such as wind, traffic loading and earthquake excitations. A five-story building model was used for performance verification when subjected to different excitations.

The state-space model is another commonly used model especially for multivariable input/output systems to model the dynamics behaviors of structures. A variety of methods, such as extended Kalman filter, unscented Kalman filter, ensemble Kalman filter etc., have been proposed to estimate the state space response of the model as well as the parameters of the model.

Hoshiya *et al.* (1984) utilized extended Kalman filter (EKF) to perform system identification of seismic structural systems. To obtain the stable and convergent solutions, a weighted global iteration procedure with an objective function was incorporated into the extended Kalman filter algorithm for stable estimation. The effectiveness of this present method was verified on multiple degree-of-freedom linear systems, bilinear hysteretic systems, and equivalent linearization of bilinear hysteretic systems.

Yang *et al.* (2007) proposed an EKF approach with unknown inputs (EKF-UI) to identify the structural parameters, such as the stiffness, damping and other nonlinear parameters, as well as the unmeasured excitations. An analytical solution for the proposed

EKF-UI approach was derived and presented. An adaptive tracking technique was also implemented in the proposed EKF-UI approach to track the variations of structural parameters due to damages. Simulation results for linear and nonlinear structures demonstrated that the proposed approach was capable of identifying the structural parameters and their variations due to damage and unknown excitations.

Ghanem *et al.* (2006) pointed out that the accuracy of EKF relies on the simple structure of linear dynamical systems excited by Gaussian noise. In situations where either the noise is significantly non-Gaussian or the dynamics is highly non-linear, the accuracy associated with filtering the linearized system may not be acceptable. To tackle the above challenges, they presented a combination of the ensemble Kalman filter (EnKF) and non-parametric modelling techniques. EnKF relies on the traditional corrector equation of the standard Kalman filter, except that the gain is calculated from the error covariance provided by the ensemble of model states. Both location and time of occurrence of damage were accurately detected in spite of measurement and modeling noise. A comparison between ensemble and extended Kalman filters was also presented, highlighting the benefits of the approach.

Another technique to handle the difficulty of EKF in dealing with strong nonlinear system is the unscented Kalman filter (UKF). The UKF uses a deterministic sampling technique known as the unscented transform to pick a minimal set of sample points (called sigma points) around the mean. These sigma points are then propagated through the non-linear functions, from which the mean and covariance of the estimate are then recovered. Compared with EKF, UKF more accurately captures the true mean and covariance of the estimation. In addition, UKF removes the requirement to explicitly calculate Jacobian, which for complex functions can be a difficult task in itself. Wu *et al.* (2007) compared EKF and UKF in estimating the dynamic responses of nonlinear structures, whose results show that the UKF produces better state estimation and parameter identification than the EKF and is also more robust to measurement noise levels.

2.1.4 ERA and Subspace Identification Methods

The Eigensystem Realization Algorithm (ERA), one of most commonly used subspace identification methods, was proposed by Juang and Pappa (1985). ERA uses a singular-value decomposition to derive a minimum-order state-space representation of a linear time-invariant system. First, a Hankel matrix is assembled by arranging the structure's impulse responses into the blocks of the Hankel matrix. The order of the structural system is determined by examining the magnitude of the singular values of the Hankel matrix. A state-space realization is constructed by using the shift block Hankel matrix. After obtaining the state-space representation, all modal parameters can be easily calculated.

Later Juang *et al*. (1988) also introduced a modification to the ERA algorithm, called the ERA data correlation algorithm (ERA/DC). ERA/DC uses correlation data of structure responses rather than the impulse response to formulate the Hankel matrix. It was found that ERA/DC can reduce the effects of measurement noises without over-specification.

Caicedo *et al*. (2004) combined the Natural Excitation Technique (NExT) (James *et al*., 1993) and the ERA to study the phase I IASC-ASCE benchmark structure. The benchmark structure is a 2×2 bays 4-story braced frame structure. The damage is simulated by removing some story braces. The NExT technique was first used to obtain the cross-correlation function from ambient vibration, which in turn served as input to ERA. After natural frequency and mode shape data of the structure were calculated from ERA, the least-square criterion was then applied to identify the structure stiffness. The simulation results showed that the NExT and ERA are successful in identifying the structural damage.

De Callafon *et al*. (2008) developed a generalized realization algorithm (GRA) to identify the modal parameters of linear multiple-degrees-of-freedom dynamic systems subject to measured arbitrary input from known initial condition. The GRA extends the eigensystem realization algorithm by allowing an arbitrary input signal in the realization algorithm. This generalization was obtained by performing a weighted Hankel matrix decomposition, where the weighting was determined by the loading. The state-space matrices were identified in a two-step procedure that includes a state reconstruction followed by a least-squares optimization to get the minimum prediction error for the response. The statistical properties of the modal parameter estimators provided by the GRA were investigated through numerical simulation based on a benchmark problem.

2.2 Challenges for SHM

Although many vibration-based SHM methods have been developed so far, no method could be regarded sufficiently accurate, efficient and robust to widely apply to real applications. The reasons are discussed in the following subsections.

2.2.1 Modeling for SHM

Picking the right model is crucial in SHM. The model is used to mimic the responses or behaviors of the structure; thus, the model should closely replicate the behaviors of the real structure. However, due to simplifications in the modeling process and the inherent structural uncertainties like material property variation, the model cannot be expected to perfectly predict the full behavior of the structure. Moreover, a model which can predict the structural behavior very well may be so complicated that it will generate very large errors in a subsequent identification procedure (discussed further in the next subsection). A trade-off between the accuracy in predicting the structural behavior and the simplicity of the model must be made to select an appropriate model for SHM.

2.2.2 Identifiability and Ill-Conditioning in Identification Optimization

Usually a large complex structure requires a complicated model with many unknown parameters to simulate its full behavior. Solving an identification optimization problem with a large number of unknown parameters poses significant challenges. First, the optimization problem may possess many local minima/maxima, causing the result of gradient-based optimization algorithms to be largely dependent on the (guessed) initial searching point. Improper selection of the initial point will result in completely wrong identified structural parameters and, thus, incorrect conclusions for the damage detection. With an increase in the numbers of unknown parameters, this problem becomes more significant. Second, when the number of unknown parameters becomes large, the identification problem is prone to be ill-conditioned, meaning that small noise in the measured responses will generate very large identification errors in the identified parameters, which of course is a disaster for any structural health monitoring and damage detection method.

2.2.3 Insensitivity to Structural Damage

Commonly used methods for damage detection, such as structural natural frequency, mode shape and so forth, are not very sensitive to local structural damage. As a result, small or moderate structural damage are very difficult, if at all possible, to detected. In addition, other factors (like environmental temperature) may often lead to larger changes in the structural frequency and mode shape than those caused by the damage, making the damage detection even more difficult.

2.3 Methods to Improve the Accuracy of SHM

In order to improve the accuracy of the damage detection for SHM, some new methods have been proposed recently.

2.3.1 Substructure Identification

Substructure identification methods, which apply a 'divide and conquer' strategy, provide a feasible solution to identify a large complex structure. Basically, the substructure identification method divides a large structure into many manageable smaller substructures, each of which has far fewer DOFs and unknown parameters, and carries out system identification for each substructure independently. Frequently, the response of the interface DOFs between adjacent substructures are needed to account for the interaction force at the interface. Since substructure identification methods greatly reduce the number of unknown parameters for the optimization, the aforementioned problems of identifiability and ill-condition are alleviated.

Koh *et al.* (1991) first proposed a substructure system identification method in the time domain. A large structure is divided into many smaller substructures and an extended Kalman filter (EKF) is used to identify the unknown structural parameters of each substructure separately.

Yun *et al.* (1997) applied a discrete auto-regressive and moving average (ARMAX) model to simulate the structural time history responses. The sequential prediction error method is used for the estimation of unknown parameters of each substructure with noisy measurements. Example analyses are given for idealized structural models of a multistory building and a truss bridge. The results indicate that the method is effective for local damage estimation of complex structures.

Tee *et al.* (2005) presented both first and second-order models for substructure identification. The eigensystem realization algorithm (ERA) and the observer/Kalman filter identification are used for the first order model, and a least-square method for structural time history responses is used for second order model. Numerical examples of a 12-DOF system and a larger structural system with 50 DOFs are conducted with the effects of noisy responses. Laboratory experiments involving an eight-story frame model are performed to illustrate the performance of the proposed method. The identification results show that the proposed methodology is able to locate and quantify damage fairly accurately.

Hou *et al.* proposed to isolate the concerned substructures from the global structure via adding virtual forces on the boundary of the substructure. The values of the virtual forces are calculated from the measured substructure response in a way that the substructure responses on the boundary are zero. The original substructure is converted into an equivalent substructure with the fixed boundary. Then Eigensystem Realization Algorithms is applied to identify the model parameters of the fixed boundary substructure, which in turn is used to detect the damage in the substructure.

In order to overcome the difficulties of substructure identification that the responses of some boundary DOFs (like rotation) of the substructures cannot be measured and thus the interaction forces between adjacent substructures cannot be calculated, Koh *et al.* (2003) proposed a frequency-domain approach for substructure identification without the need for measuring of the interface responses. This method uses the product of measured substructure responses and the transfer function from boundary interaction force to these responses to replace the interaction forces calculated by substructure boundary responses. Several numerical examples are given, demonstrating that this method works well when the structure is simple and input/output measurement noises are too large. Yuen *et al.* (2006) further combined this method with a Bayesian identification framework to provide a probability measure of the identification accuracy.

2.3.2 Controlled Identification Methods

To increase the accuracy of damage detection, some researchers have turned to structural control techniques for help. The basic idea underlying these methods is that, since a structure control system can change the behavior of the structure, by carefully choosing the configuration of the control system either more information about the structure could be obtained or the sensitivity of the model to the structural damage can be improved.

Lew *et al.* (2002) presented an approach to structural damage detection using virtual passive controllers attached to a structure. The authors formulate an inverse problem that uses n measured frequencies to identify the stiffness of r elements. When $n<r$, this inverse problem becomes intractable. To solve this rank deficiency problem, m virtual passive controllers are introduced into structure. A direct output feedback algorithm is used to drive the virtual passive controllers. The frequencies of both open-loop and close-loop systems are measured. Therefore, the total number of the original system's frequencies and the feedback loop frequencies becomes $n(m+1)$, which is greater than r. Then, the frequency changes are approximated as linear functions of the element stiffness using a truncated Taylor expansion, and this inverse problem is solved by a least squares projection.

Elmasry and Johnson (2002) and Elmasry (2005) utilized variable stiffness and damping devices (VSSD) to greatly increase the stiffness and damping of certain parts of a structure, and use the frequency response function (FRF) to identify the structural parameters. Both numerical and experiment results show that this technique can increase the accuracy of the identification. However, while that research has established that there are controllable passive strategies that can improve structural parameter identification, means of determining where or how much change in VSDD parameters has not yet been developed.

Koh and Ray (2004) proposed using state-feedback control to shift lower structural frequencies downward so that the sensitivity of the frequency to the structural damage is increased and the damage can be more accurately detected. However, decreases in natural frequencies are likely not welcomed by owners of civil structures and could not be easily achieved with controllable passive (semiactive) devices; further, it is well established that natural frequencies are less sensitive to damage than other measured or computed quantities.

Jiang *et al.* (2007) showed that the sensitivity of the natural frequency shift to the damage in a multi-degree-of-freedom structure can be significantly influenced by the placement of both the eigenvalues and the eigenvectors. And a method is proposed to find the optimal assignment of both the closed-loop eigenvalues and eigenvectors and achieve the desired closed-loop eigenstructure.

However, none of these controlled identification studies addresses the question of how an imperfect control system will affect the identification results. In reality, there always exists some kind of error in the control system, such as time delay for computation, measurement noise in the feedback, etc. Since the structural control system is involved in the system identification procedure for the aforementioned methods, it is inevitable that these errors will affect the final estimates. Indeed, small error in the control system may completely offset all of the benefit obtained from the close-loop control system identification.

2.4 Parameter Identification of Shear Structures

A shear structure, as shown in Figure 2.1, is widely used to model the dynamic behavior of building structures. Thus, accurately identifying the parameters of shear structures plays a vital role in evaluating the building’s health status and discovering the potential damage in the structure.

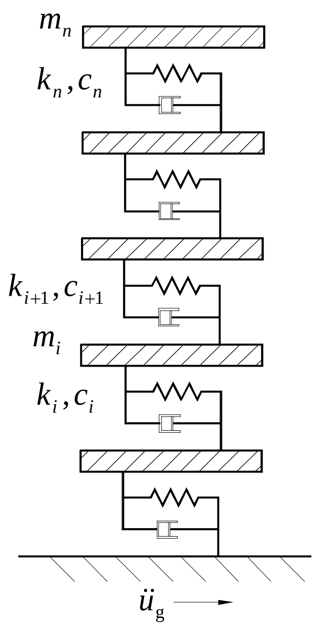

Figure 2.1 A shear structure

Udwadia *et al.* (1987) studied the uniqueness of the identification of stiffness and damping distribution of a shear structure. An induction procedure was developed to estimate structural stiffness and damping from the measured excitation and structural responses. Although the authors discussed the uniqueness of the identified parameters for the proposed method, they did not investigate the effect of measurement noise on the accuracy of identified parameters.

Masri *et al.* (1982) proposed a non-parametric identification method for chain-like structures (*e.g.*, shear structure). The internal forces between any two adjacent floors were represented as nonlinear functions of the interstory displacement and velocity responses. These internal forces were expanded in terms of two-dimensional orthogonal polynomials. The parameters of the expansion were estimated via a recursive procedure. The technique was applied to a model of a steel frame to demonstrate its effectiveness. Hernandez-Garcia *et al.* (2010) applied this method to a three-story test structure; both simulation and experimental results showed that the approach was able to detect the presence of structural changes, accurately locate the structural section where the change occurred, and provide an accurate estimate of the actual level of change. Nayeri *et al.* (2008) also applied this method to estimate the structural modal properties of a full-scale 17-story building based on ambient vibration measurements; the estimated structural natural frequencies and mode shapes were consistent with the modal parameters estimated using the NExT/ERA method.

In this dissertation, the author will present new identification methods for shear structures, developed based on the substructuring methodology. The analyses and simulations in this study will show that this method, and some variants of this method, can provide very accurate estimation for the parameters of a shear structure. Moreover, the accuracy of this method can be further improved by changing the structural responses via some specifically designed structural control systems.

Chapter 3

Fourier Transform Based Substructure Identification Method

By applying "divide and conquer" strategy of substructure identification, an innovative substructure identification method, named FFT_SUBID, is proposed in this chapter to identify the parameters of a shear structure as shown in Figure 3.1a.

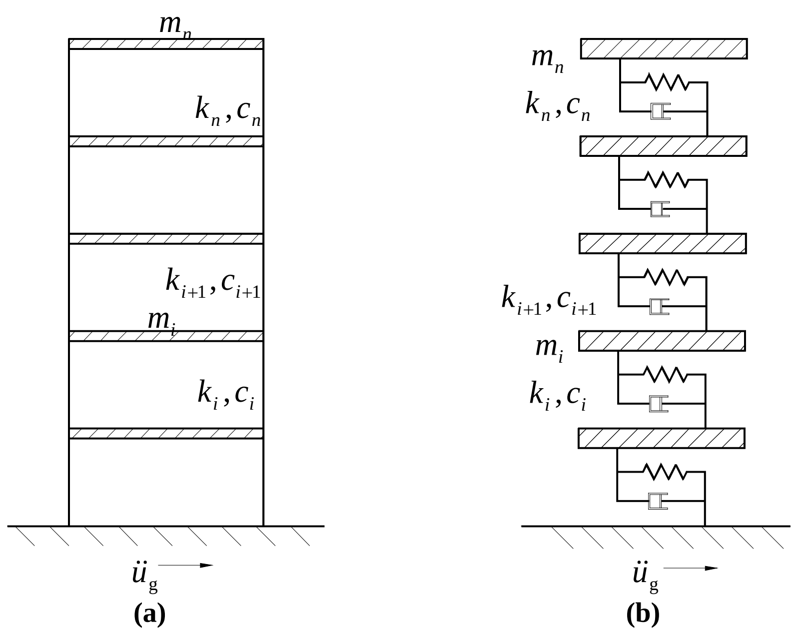

Figure 3.1 (a) An *n*-story shear structure (b) the equivalent mechanics model of the shear structure

This chapter is organized as follows. First, the FFT_SUBID identification method is formulated, using the Fourier transform of structure floor acceleration responses, to identify the parameters of a shear structure (*e.g.*, the story stiffness and damping). Second, an approximate method to analyze the identification error of least-square-error identification problem is developed and applied to the proposed FFT_SUBID method. The results reveal the most important factors determining the identification accuracy for the proposed substructure method. Next, by using the results of the identification error analysis, the statistical moments of the identification error are analyzed. A damage detection strategy is proposed based on the identified structural parameters. Finally, a numerical example of a 5-story building is used to illustrate the efficacy of the proposed substructure identification method and the damage detection strategy.

3.1 Method formulation

Figure 3.1a shows an *n*-story shear structure and Figure 3.1b shows the equivalent mechanics model of this shear structure. When the inertial coordinate is used to quantify the motion of the structure, the dynamic equation of the structure subject to ground motion u_g can be written in separate equation forms as follows:

Top floor (i=n):

$$m_n \ddot{x}_n + c_n(\dot{x}_n - \dot{x}_{n-1}) + k_n(x_n - x_{n-1}) = 0 \tag{3.1}$$

Middle floor (2≤i≤n-1):

$$m_i \ddot{x}_i + c_i(\dot{x}_i - \dot{x}_{i-1}) + k_i(x_i - x_{i-1}) + c_{i+1}(\dot{x}_i - \dot{x}_{i+1}) + k_{i+1}(x_i - x_{i+1}) = 0 \tag{3.2}$$

Bottom floor (i=1):

$$m_1 \ddot{x}_1 + c_1(\dot{x}_1 - \dot{u}_g) + k_1(x_1 - u_g) + c_2(\dot{x}_1 - \dot{x}_2) + k_2(x_1 - x_2) = 0 \tag{3.3}$$

where m_i is the mass of the i^{th} floor; c_i and k_i are the damping coefficient and stiffness of the i^{th} story; x_i is the displacement of the i^{th} floor relative to an inertial reference frame; u_g is the displacement of the ground; overdots represent derivative with respect to time; and n is the number of floors in the structure. It is assumed herein that the mass of the structure is known, though a similar analysis with unknown mass is possible.

The motion of the top floor is affected only by the top story structural parameters as well as by the motion of the top two floors. The proposed substructure identification method begins with the top story. Adding $-m_n\ddot{x}_{n-1}$ to both sides of Equation (3.1) gives

$$m_n(\ddot{x}_n - \ddot{x}_{n-1}) + c_n(\dot{x}_n - \dot{x}_{n-1}) + k_n(x_n - x_{n-1}) = -m_n\ddot{x}_{n-1} \tag{3.4}$$

Taking Fourier transform of Equation (3.4)

$$m_n(\ddot{X}_n - \ddot{X}_{n-1}) + c_n(\dot{X}_n - \dot{X}_{n-1}) + k_n(X_n - X_{n-1}) = -m_n\ddot{X}_{n-1} \tag{3.5}$$

where $X_i, \dot{X}_i, \ddot{X}_i$ are the Fourier transforms (or the frequency responses) of the i^{th} floor displacement, velocity and acceleration responses $x_i, \dot{x}_i, \ddot{x}_i$, respectively. ($X_i, \dot{X}_i, \ddot{X}_i$ are functions of frequency $j\omega$ which is omitted for notational simplicity.) Assuming that the structure is stationary at the beginning and the ending time when the structural responses are recorded, we can obtain the following two relations that $X_i = \ddot{X}_i \big/ (j\omega)^2$ and $\dot{X}_i = \ddot{X}_i \big/ j\omega$, where j^2=–1. Substituting these two relations back into Equation (3.5) gives

$$(\ddot{X}_n - \ddot{X}_{n-1})\left(m_n + \frac{c_n}{j\omega} + \frac{k_n}{(j\omega)^2}\right) = -m_n\ddot{X}_{n-1} \tag{3.6}$$

Rearranging Equation (3.5), it can be obtained that

$$\frac{1}{1 - jc_n\big/(m_n\omega) - k_n\big/(m_n\omega^2)} = \frac{\ddot{X}_{n-1} - \ddot{X}_n}{\ddot{X}_{n-1}} \tag{3.7}$$

The right side of Equation (3.7) only involves the frequency responses (Fourier transforms) of the structural acceleration responses, which can be calculated from the measured acceleration responses. Then, the structural parameters of the top story $[k_n\ c_n]^{\mathrm{T}}$ can be identified by solving the following optimization problem, which minimizes the second norm of the difference between the two sides of Equation (3.7) over all possible frequencies.

$$\underset{k_n, c_n}{\arg\min} \quad J(k_n, c_n) = \sum_{l=1}^{N} \left| f_l(k_n, c_n) - \hat{f}_l\left(\hat{\ddot{X}}_{n-1}, \hat{\ddot{X}}_n \right) \right|^2 \tag{3.8}$$

where $f_l(k_n, c_n) = \dfrac{1}{1 - j\, c_n / (m_n \omega_l) - k_n / (m_n \omega_l^2)}$, $\hat{f}_l\left(\hat{\ddot{X}}_{n-1}, \hat{\ddot{X}}_n \right) = \dfrac{\hat{\ddot{X}}_{n-1,l} - \hat{\ddot{X}}_{n,l}}{\hat{\ddot{X}}_{n-1,l}}$.

$\hat{\ddot{X}}_{i,l}$ stands for the frequency response of the i^{th} measured floor acceleration at frequency ω_l; $\omega_l = l \cdot \Delta\omega \quad (l = 1, 2, \cdots, N)$ are the discrete frequencies at which the discrete Fourier transform of the structural responses are calculated; and $\Delta\omega$ is the frequency interval.

After the top story parameters $[k_n \; c_n]^T$ are identified, the following induction method can be applied to identify the structural parameters of other stories iteratively. Adding the term $-m_i \ddot{x}_{i-1}$ to both sides of Equation (3.2) and following a procedure similar to that for Equation (3.7) will give:

$$\frac{1}{1 - j\, c_i / (m_i \omega) - k_i / (m_i \omega^2)} = \frac{\ddot{X}_{i-1} - \ddot{X}_i}{\ddot{X}_{i-1} + (\ddot{X}_{i+1} - \ddot{X}_i)\left[j c_{i+1} / (m_i \omega) + k_{i+1} / (m_i \omega^2) \right]} \tag{3.9}$$

Assuming that structural parameters $[k_{i+1} \; c_{i+1}]^T$ in the equation are known, the right side of the equation can be directly calculated from the measured acceleration responses. Then, a similar optimization problem, shown in Equation (3.10), is formulated to identify structural parameters $[k_i \; c_i]^T$ on the left side of the equation.

$$\underset{k_i, c_i}{\arg\min} \quad J(k_i, c_i) = \sum_{l=1}^{N} |\varepsilon_l|^2 = \sum_{l=1}^{N} \left| g_l(k_i, c_i) - \hat{g}_l\left(\hat{\ddot{X}}_{i-1}, \hat{\ddot{X}}_i, \hat{\ddot{X}}_{i+1} \right) \right|^2 \tag{3.10}$$

where $g_l(k_i, c_i) = \dfrac{1}{1 - j\, c_i / (m_i \omega_l) - k_i / (m_i \omega_l^2)}$;

$$\hat{g}_l\left(\hat{\ddot{X}}_{i-1},\hat{\ddot{X}}_i,\hat{\ddot{X}}_{i+1}\right)=\frac{\hat{\ddot{X}}_{i-1,l}-\hat{\ddot{X}}_{i,l}}{\hat{\ddot{X}}_{i-1,l}+\left(\hat{\ddot{X}}_{i+1,l}-\hat{\ddot{X}}_{i,l}\right)\left[jc_{i+1}/(m_i\omega_l)+k_{i+1}/(m_i\omega_l^2)\right]}$$

Since identification problem (3.10) is applicable to the parameter identification of every story in the structure except for the top (n^{th}) story, an induction identification step is essentially established by Equation (3.10) in which the parameters of any i^{th} story $[k_i\ \ c_i]^{\text{T}}$ can be identified if the parameters of the story above (the $(i+1)^{\text{th}}$ story) $[k_{i+1}\ c_{i+1}]^{\text{T}}$ are known. The top story structural parameters $[k_n\ c_n]^{\text{T}}$ identified from the optimization problem (3.8) are already available to initiate the above induction identification process. Thus, all structural parameters $[k_i\ \ c_i]^{\text{T}}$ $(i=1,\ldots,n)$ can be identified iteratively by following the identification procedure in Equation (3.10). It is noted that when the parameters of the first floor are to be identified, a simple replacement of $\hat{\ddot{X}}_{i-1}$ by $\hat{\ddot{U}}_{\text{g}}$ in the optimization problem (3.10) is needed.

The proposed substructure identification method has several advantages.

1) It is not required in the method formulation that the substructure identification for every floor be performed at the same time; thus, there is no need to simultaneously measure the acceleration of all floors. For each step of the substructure identification, only the acceleration responses of two or three floors are needed. This potentially reduces the cost of SHM systems, particularly in the case of wireless sensor networks when the number of sensors may be limited but moving sensors is relatively easy.
2) In each step of the optimization procedure, there are only two optimization variables, making the optimization procedure much easier to execute and much

more likely to converge. Moreover, the formulation of each substructure identification step is simple and similar (except for the top story substructure identification), making it very convenient to analyze which are the most important factors that control the accuracy in the identification process (discussed in more detail in a subsequent section).

3) Since each substructure identification step only makes use of the dynamic equilibrium of a certain floor substructure in formulating the identification problem, the excitation forces, not directly applied on this floor, do not need to be measured and will not affect the accuracy of this step identification. This property provides two additional attractive features for the proposed method. First, the excitation force generated by normal use of the building (such as the movement of people in buildings) is usually very difficult to measure. But the unknowns of these forces will not affect identification accuracy of the substructure method unless they directly apply on the floor where the substructure identification is being performed. Therefore, if properly scheduled, the proposed substructure method can be implemented with a little interference of the normal use of the building: when the substructure identification is performed on a certain floor, only this floor will be restricted for the use while other floors can still be accessed as normal. Second, as discussed in the chapter 6, the proposed substructure identification method is combined with structural control techniques to further improve the accuracy. When the control forces are not directly applied on the floor where the substructure identification is carried out, the measurement errors in the control forces will not directly affect the accuracy of the identification.

Thus, the proposed controlled substructure identification is robust to the side effects of control system errors.

However, there is an obvious drawback for this method: since, for each identification step (except for the top story), the previous identification results are used as known parameters, the uncertainty in the previous identification step(s) will be accumulated for later identification, which may result in large identification error in the lower floors. This possible error accumulation problem is discussed in more detail in the following identification error analysis section; however, first the methodology for approximating the error for a general Least-square-error identification is proposed in the following section, which will be applied later to derive the identification error for the proposed substructure method.

3.2 Approximate Error Analysis for Least-square-error Identification

Least-square-error (LSE) identification is one of the most widely used identification methods. Through minimizing the second norm of the difference between the prediction of a representative model and the measurement of a real system, the system parameters are estimated. A LSE identification problem usually has the following form:

$$\arg\min_{\boldsymbol{\theta}} \quad \sum_{l=1}^{N} \left\| \varepsilon_l(\boldsymbol{\theta}) \right\|_2^2 = \sum_{l=1}^{N} \left\| M_l(\boldsymbol{\theta}) - \hat{M}_l(\hat{\mathbf{x}}) \right\|_2^2 \tag{3.11}$$

where $M_l(\boldsymbol{\theta})$ is the l^{th} output of the model used to predict the behaviors of the real system and is a function of parameter vector $\boldsymbol{\theta} = [\theta_1 \cdots \theta_M]^{\mathrm{T}}$ to be identified, assumed to be real (non-complex); $\hat{M}_l(\hat{\mathbf{x}})$ is the l^{th} measurement of the system which is a function of the direct measurement of the structural responses $\hat{\mathbf{x}} = [\hat{X}_1 \cdots \hat{X}_p]^{\mathrm{T}}$, assumed to be equal to true responses $\mathbf{x} = [X_1 \cdots X_p]^{\mathrm{T}}$ plus some random measurement noises $\hat{\mathbf{N}} = [\hat{N}_1 \cdots \hat{N}_p]^{\mathrm{T}}$ (*i.e.*, $\hat{\mathbf{X}} = \mathbf{X} + \hat{\mathbf{N}}$).

Assume that the true values of the system parameters are $\boldsymbol{\theta}_0$ and there is no modeling error for the system; thus,

$$M_l(\boldsymbol{\theta}_0) = \hat{M}_l(\mathbf{x}) \tag{3.12}$$

Using a Taylor series to expand $M_l(\boldsymbol{\theta})$ about point $\boldsymbol{\theta}_0$ and $\hat{M}_l(\hat{\mathbf{x}})$ about point $\mathbf{x}$, respectively, and neglecting the second and higher order terms gives:

$$M_l(\boldsymbol{\theta}) \approx M_l(\boldsymbol{\theta}_0) + \left.\frac{\partial M_l}{\partial \boldsymbol{\theta}}\right|_{\boldsymbol{\theta}=\boldsymbol{\theta}_0} (\boldsymbol{\theta} - \boldsymbol{\theta}_0) = M_l(\boldsymbol{\theta}_0) + \mathbf{h}_l \Delta\boldsymbol{\theta} \tag{3.13}$$

$$\hat{M}_l(\hat{\mathbf{x}}) \approx \hat{M}_l(\mathbf{x}) + \left.\frac{\partial \hat{M}_l}{\partial \hat{\mathbf{X}}}\right|_{\hat{\mathbf{x}}=\mathbf{x}} (\hat{\mathbf{x}} - \mathbf{x}) = \hat{M}_l(\mathbf{x}) + \hat{\mathbf{h}}_l \hat{\mathbf{N}} \tag{3.14}$$

where $\Delta\boldsymbol{\theta} = \boldsymbol{\theta} - \boldsymbol{\theta}_0$ is defined as the parameter identification error, and

$$[\mathbf{h}_l]_{1\times M} = \left.\frac{\partial M_l}{\partial \boldsymbol{\theta}}\right|_{\boldsymbol{\theta}=\boldsymbol{\theta}_0} ; [\hat{\mathbf{h}}_l]_{1\times P} = \left.\frac{\partial \hat{M}_l}{\partial \hat{\mathbf{x}}}\right|_{\hat{\mathbf{x}}=\mathbf{x}}$$

Substituting Equation (3.12) ~ (3.14) back into Equation (3.11), the original optimization problem can be approximated by

$$\underset{\Delta\boldsymbol{\theta}}{\arg\min} \quad \sum_{l=1}^{N} \left\| \varepsilon_l(\Delta\boldsymbol{\theta}) \right\|_2^2 \approx \sum_{i=1}^{N} \left\| \mathbf{h}_l \cdot \Delta\boldsymbol{\theta} - \hat{\mathbf{h}}_l \cdot \hat{\mathbf{N}} \right\|_2^2 \tag{3.15}$$

To solve the optimization problem (3.15), take the derivative of (3.15) with respect to $\Delta\boldsymbol{\theta}$ and set those equations to zero

$$\frac{\partial}{\partial \Delta\boldsymbol{\theta}}\sum_{l=1}^{N}\left\|\varepsilon_l\left(\Delta\boldsymbol{\theta}\right)\right\|_2^2 = \frac{\partial}{\partial \Delta\boldsymbol{\theta}}\sum_{l=1}^{N}(\mathbf{h}_l\Delta\boldsymbol{\theta}-\hat{\mathbf{h}}_l\hat{\mathbf{N}})\cdot(\mathbf{h}_l\Delta\boldsymbol{\theta}-\hat{\mathbf{h}}_l\hat{\mathbf{N}})^*$$
$$= \sum_{l=1}^{N}\mathbf{h}_l(\mathbf{h}_l\Delta\boldsymbol{\theta}-\hat{\mathbf{h}}_l\hat{\mathbf{N}})^* + \mathbf{h}_l^*(\mathbf{h}_l\Delta\boldsymbol{\theta}-\hat{\mathbf{h}}_l\hat{\mathbf{N}}) = \mathbf{0}_{1\times M} \tag{3.16}$$

Noting that the terms in parentheses are scalars, transposing and rearranging gives

$$\sum_{l=1}^{N}(\mathbf{h}_l^{\mathrm{T}}\mathbf{h}_l^* + \mathbf{h}_l^{\mathrm{H}}\mathbf{h}_l)\Delta\boldsymbol{\theta} - (\mathbf{h}_l^{\mathrm{T}}\hat{\mathbf{h}}_l^*\hat{\mathbf{N}}^* + \mathbf{h}_l^{\mathrm{H}}\hat{\mathbf{h}}_l\hat{\mathbf{N}}) = \mathbf{0}_{M\times 1} \tag{3.17}$$

where superscript “*” stands for complex conjugate, superscript “T” stands for transpose and superscript “H” stands for complex conjugate transpose. Noting that $\mathbf{h}_l^{\mathrm{T}}\mathbf{h}_l^* = (\mathbf{h}_l^{\mathrm{H}}\mathbf{h}_l)^*$ and $\mathbf{h}_l^{\mathrm{T}}\hat{\mathbf{h}}_l^*\hat{\mathbf{N}}^* = (\mathbf{h}_l^{\mathrm{H}}\hat{\mathbf{h}}_l\hat{\mathbf{N}})^*$, the imaginary parts of the terms in parentheses cancel and (3.17) simplifies to

$$\sum_{l=1}^{N}\mathrm{Re}(\mathbf{h}_l^{\mathrm{T}}\mathbf{h}_l^*)\Delta\boldsymbol{\theta} = \sum_{l=1}^{N}\mathrm{Re}(\mathbf{h}_l^{\mathrm{H}}\hat{\mathbf{h}}_l\hat{\mathbf{N}}) \tag{3.18}$$

where $\mathrm{Re}(\cdot)$ stands for the real part of a complex number. Then the identification error $\Delta\boldsymbol{\theta}$ could be obtained

$$\Delta\boldsymbol{\theta} = \left[\sum_{l=1}^{N}\mathrm{Re}(\mathbf{h}_l^{\mathrm{T}}\mathbf{h}_l^*)\right]^{-1}\sum_{l=1}^{N}\mathrm{Re}(\mathbf{h}_l^{\mathrm{H}}\hat{\mathbf{h}}_l\hat{\mathbf{N}}) \tag{3.19}$$

Although the identification error (3.19) is an approximation, valid only under the condition that the measurement noise of the structural response $\hat{\mathbf{N}}$ is not too large and the solution $\boldsymbol{\theta}$ of optimization problem (3.8) is near the true value $\boldsymbol{\theta}_0$, it does provide a way to estimate the accuracy of the identification method without resorting to time-consuming numerical simulations.

3.3 Identification Error Analysis for FFT_SUBID Method

The parameters to be identified in the substructure identification method belong to different categories with different units and vastly different magnitudes (*e.g.*, stiffness and damping coefficient). To fairly evaluate the efficiency of the identification method for every parameter, it is better to compare the identification error on a relative basis. Define the integrity index as

$$\beta_{ik} = \hat{k}_i \big/ k_i \quad \text{and} \quad \beta_{ic} = \hat{c}_i / c_i \,, \quad \left(i = 1, \cdots, n\right) \tag{3.20}$$

where k_i and c_i are the true (unknown) values of the stiffness and damping coefficients of the i^{th} story; $\hat{k}_i$ and $\hat{c}_i$ are the corresponding estimated parameter values. Instead of using absolute error value $(\hat{k}_i - k_i)$ and $(\hat{c}_i - c_i)$ in analyzing the identification error, relative error $(\beta_{ik} - 1)$ and $(\beta_{ic} - 1)$ will be used herein.

3.3.1 Top Story Identification Error

Using the relative parameter values, the identification problem (3.8) is rewritten as

$$\underset{\beta_{nk},\beta_{nc}}{\arg\min} \quad J\left(\beta_{nk}, \beta_{nc}\right) = \sum_{l=1}^{N} \left|\varepsilon_l\right|^2 = \sum_{l=1}^{N} \left| f_l\left(\beta_{nk}, \beta_{nc}\right) - \hat{f}_l\left(\hat{\ddot{X}}_{n-1}, \hat{\ddot{X}}_n\right)\right|^2 \tag{3.21}$$

where $f_l\left(\beta_{nk}, \beta_{nc}\right) = \dfrac{1}{1 - j\beta_{nc}\, c_n \big/ (m_n\omega_l) - \beta_{nk}\, k_n \big/ (m_n\omega_l^2)}$; $\hat{f}_l\left(\hat{\ddot{X}}_{n-1}, \hat{\ddot{X}}_n\right) = \dfrac{\hat{\ddot{X}}_{n-1,l} - \hat{\ddot{X}}_{n,l}}{\hat{\ddot{X}}_{n-1,l}}$.

Following the procedure proposed in section 3.2,

$$\mathbf{h}_l = \left[\frac{\partial f_l}{\partial \beta_{nk}} \quad \frac{\partial f_l}{\partial \beta_{nc}} \right]_{\beta_\bullet = 1}$$

$$= \left[\frac{k_n / (m_n \omega_l^2)}{\left[1 - j c_n / (m_n \omega_l) - k_n / (m_n \omega_l^2)\right]^2} \quad \frac{j c_n / (m_n \omega_l)}{\left[1 - j c_n / (m_n \omega_l) - k_n / (m_n \omega_l^2)\right]^2} \right] \tag{3.22}$$

$$\hat{\mathbf{h}}_l = \left[\frac{\partial \hat{f}_l}{\partial \hat{\ddot{X}}_{n-1}} \quad \frac{\partial \hat{f}_l}{\partial \hat{\ddot{X}}_n} \right]_{\hat{\ddot{X}}_\bullet = \ddot{X}_\bullet} = \left[\frac{\ddot{X}_{n,l}}{\ddot{X}_{n-1,l}^{\ 2}} \quad \frac{-1}{\ddot{X}_{n-1,l}} \right] \tag{3.23}$$

where $\beta_\bullet = 1$ is the abbreviation for $\beta_{kn} = 1$ and $\beta_{cn} = 1$; $\hat{\ddot{X}}_\bullet = \ddot{X}_\bullet$ is the abbreviation of $\hat{\ddot{X}}_{n-1,l} = \ddot{X}_{n-1,l}$ and $\hat{\ddot{X}}_{n,l} = \ddot{X}_{n,l}$ for the sake of notational simplicity. Rearranging Equation (3.7) gives

$$\ddot{X}_{n-1,l} = [1 - j c_n / (m_n \omega_l) - k_n / (m_n \omega_l^2)](\ddot{X}_{n-1,l} - \ddot{X}_{n,l}) \tag{3.24}$$

Using the right side of Equation (3.24) to replace the terms in Equation (3.23) that equal the left side of Equation (3.23), Equation (3.23) is simplified as

$$\hat{\mathbf{h}}_l = \frac{1}{(\ddot{X}_{n,l} - \ddot{X}_{n-1,l})} \begin{bmatrix} \dfrac{j c_n / (m_n \omega_l) + k_n / (m_n \omega_l^2)}{\left[1 - j c_n / (m_n \omega_l) - k_n / (m_n \omega_l^2)\right]^2} \\ \dfrac{1}{\left[1 - j c_n / (m_n \omega_l) - k_n / (m_n \omega_l^2)\right]} \end{bmatrix}^{\mathrm{T}} \tag{3.25}$$

Using the result of Equation (3.19), the approximate relative identification error of the top story parameters $[k_n \ \ c_n]^{\mathrm{T}}$ becomes

$$\begin{bmatrix} \theta_{kn} \\ \theta_{cn} \end{bmatrix} \approx \sum_{l=1}^{N} \mathrm{Re} \left\{ \begin{bmatrix} W_{11,l} & W_{12,l} \\ W_{21,l} & W_{22,l} \end{bmatrix} \cdot \begin{bmatrix} N_{n-1,l} / (\ddot{X}_{n,l} - \ddot{X}_{n-1,l}) \\ N_{n,l} / (\ddot{X}_{n,l} - \ddot{X}_{n-1,l}) \end{bmatrix} \right\} \tag{3.26}$$

where $\theta_{kn}=\beta_{kn}-1$ and $\theta_{cn}=\beta_{cn}-1$ are the relative identification error of the n^{th} story parameters k_n and c_n respectively; $N_{i,l} = \hat{\ddot{X}}_{i,l} - \ddot{X}_{i,l}$ (i=1,…,n) are the Fourier transform of the measurement noise of the i^{th} floor acceleration at frequency ω_l; $W_{ij,l}$ are some deterministic factors which are the functions of the substructure parameters m_n, c_n and k_n as well as frequency ω_l. The expression of $W_{ij,l}$ are listed as follows,

$$W_{11,l} = \frac{1}{A_1} \cdot \frac{k_n/(m_n\omega_l^2) \cdot \left[j\,c_n/(m_n\omega_l) + k_n/(m_n\omega_l^2) \right]}{\left| 1 - j\,c_n/(m_n\omega_l) - k_n/(m_n\omega_l^2) \right|^4}$$

$$W_{21,l} = \frac{1}{A_2} \cdot \frac{-jc_n/(m_n\omega_l) \cdot \left[j\,c_n/(m_n\omega_l) + k_n/(m_n\omega_l^2) \right]}{\left| 1 - j\,c_n/(m_n\omega_l) - k_n/(m_n\omega_l^2) \right|^4}$$

$$W_{12,l} = \frac{1}{A_1} \cdot \frac{k_n/(m_n\omega_l^2)}{\left| 1 - j\,c_n/(m_n\omega_l) - k_n/(m_n\omega_l^2) \right|^2 \left[1 + j\,c_n/(m_n\omega_l) - k_n/(m_n\omega_l^2) \right]}$$

$$W_{22,l} = \frac{1}{A_2} \cdot \frac{-jc_n/(m_n\omega_l)}{\left| 1 - j\,c_n/(m_n\omega_l) - k_n/(m_n\omega_l^2) \right|^2 \left[1 + j\,c_n/(m_n\omega_l) - k_n/(m_n\omega_l^2) \right]}$$

where $|\cdot|$ stands for the magnitude of a complex number and

$$A_1 = \sum_{l=1}^{N} \frac{k_n^2/(m_n^2\omega_l^4)}{\left| 1 - j\,c_n/(m_n\omega_l) - k_n/(m_n\omega_l^2) \right|^4},\; A_2 = \sum_{l=1}^{N} \frac{c_n^2/(m_n^2\omega_l^2)}{\left| 1 - j\,c_n/(m_n\omega_l) - k_n/(m_n\omega_l^2) \right|^4}$$

Note that the off-diagonal terms of $h_l^{\mathrm{T}} h_l^*$ are purely imaginary and the diagonal terms are purely real. Thus, the inverse in Equation (3.19) is straightforward with the diagonal terms of $1/A_1$ and $1/A_2$ and zero off-diagonal terms.

Figure 3.2 shows how the magnitude of four factors $W_{ij,l}$ changes with different frequency ω_l. In the figure, instead of plotting the magnitude of the factors with respect to the absolute frequency ω_l, the normalized frequency ω_l/ω_{n0} is used, where ω_{n0} is the natural frequency of the n^{th} story substructure ω_{n0}, defined as $\omega_{n0} = \sqrt{k_n/m_n}$. Figure 3.2 shows an interesting phenomenon that all four weighting factors are significantly large near frequency ω_{n0} and diminish quickly moving away from ω_{n0}. For this example, the structural parameters of the top story substructure are chosen here: $c_n / m_n = 2\xi_n \omega_{n0}$ and $\xi_n = 0.1$. Changing the values of the damping coefficient c_n or damping ratio ξ_n only affects the sharpness of the peak near the frequency ω_{n0}, but does not invalidate the location of the peak (unless the damping is significantly large, which seldom occurs for civil structures).

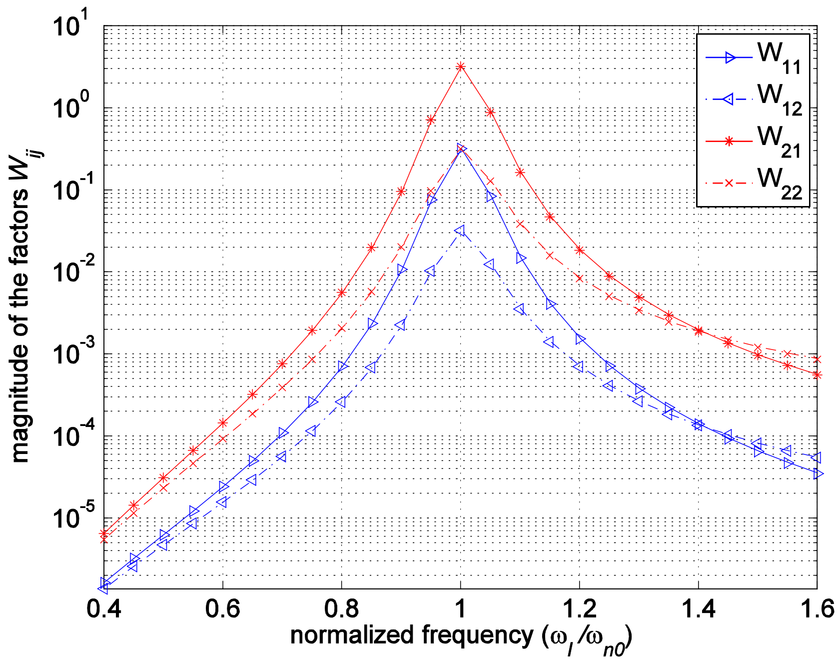

Figure 3.2 Magnitude of factors W_{ij}

Equation (3.26) suggests several insightful points regarding the relationship between measurement noise and identification error. First, the terms $N_{n-1,l} / (\ddot{X}_{n,l} - \ddot{X}_{n-1,l})$ and $N_{n,l} / (\ddot{X}_{n,l} - \ddot{X}_{n-1,l})$ can be considered as the measurement uncertainty of the structural responses, which lead to the identification errors. Since the true structural response of the n^{th} interstory acceleration $(\ddot{X}_{n,l} - \ddot{X}_{n-1,l})$ is in the denominator of all uncertainty terms, larger n^{th} interstory acceleration response gives smaller measurement uncertainty and, thus, more accurate identification. Second, $W_{ij,l}$ can be treated as weighing factors that represent the relative importance of the measurement uncertainty in determining final parameter identification errors; the uncertainty terms with larger weighting factor contribute more to the identification error than those with smaller weighting factor. Since all four weighting factors, as shown in Figure 3.2, are significantly large near the substructure natural frequency of the top story, ω_{n0}, and diminish quickly when moving away from ω_{n0}, the identification errors are mainly determined by the measurement uncertainty near the frequency ω_{n0}. Furthermore, if compared with the factors $W_{1j,l}$ and $W_{2j,l}$, which represent the contributions to the identification error of stiffness and damping parameters respectively from the same measurement uncertainty term, the magnitude of $W_{1j,l}$ is much smaller than that of $W_{2j,l}$, indicating that the damping estimate of the top story will be less accurate than the stiffness estimate of the same floor. Third, while the measurement noises $N_{n-1,l}$ and $N_{n,l}$ can be reduced by using more expensive sensor, cable and data acquisition systems, they cannot be eliminated and the cost to reduce them significantly may be prohibitive. However, the structural responses could be controlled or adjusted by some structural control techniques less expensively, if such a structural control system has been installed in the structure to mitigate structural responses due to earthquake or high wind. Equation (3.26) suggests that if the structural response is controlled such that $(\ddot{X}_{n,l} - \ddot{X}_{n-1,l})$ is large within some frequency range around ω_{n0}, an equivalent or even better reduction of measurement uncertainty can be achieved relative to an expensive measuring system and, thus, more accurate identification results can be obtained.

3.3.2 Non-top Story Identification Error

In the parameter identification of the i^{th} story ($i < n$), the identified parameters of the $(i+1)^{\text{th}}$ story are used as known input; thus, the identification error of these parameters from the previous step will inevitably affect the accuracy of the current identification step. Therefore, besides the structural response noises, the uncertainties of identification results from previous identification steps must be considered. Using the relative parameters β_{ki} and β_{ci}, the identification problem in (3.10) could be rewritten as

$$\underset{\beta_{ki},\beta_{ci}}{\arg\min} \quad J(\beta_{ki},\beta_{ci}) = \sum_{l=1}^{N} \left| g_l(\beta_{ki},\beta_{ci}) - \hat{g}_l\left(\hat{\ddot{X}}_{i-1}, \hat{\ddot{X}}_{i}, \hat{\ddot{X}}_{i+1}, \beta_{k(i+1)}, \beta_{c(i+1)}\right) \right|^2 \qquad (3.27)$$

where $g_l(\beta_{ki},\beta_{ci}) = \dfrac{1}{1 - j\beta_{ci}\, c_i/(m_i\omega_l) - \beta_{ki}\, k_i/(m_i\omega_l^2)}$

$$\hat{g}_l\left(\hat{\ddot{X}}_{i-1}, \hat{\ddot{X}}_{i}, \hat{\ddot{X}}_{i+1}, \beta_{k(i+1)}, \beta_{c(i+1)}\right) = \frac{\hat{\ddot{X}}_{i-1,l} - \hat{\ddot{X}}_{i,l}}{\hat{\ddot{X}}_{i-1,l} + (\hat{\ddot{X}}_{i+1,l} - \hat{\ddot{X}}_{i,l})\left[j\beta_{k(i+1)}c_{i+1}/(m_i\omega_l) + \beta_{c(i+1)}k_{i+1}/(m_i\omega_l^2)\right]}$$

Following a procedure similar to the top story gives

$$\mathbf{h}_l = \begin{bmatrix} \dfrac{\partial g_l}{\partial \beta_{ki}} & \dfrac{\partial g_l}{\partial \beta_{ci}} \end{bmatrix}_{\beta_\bullet = 1} = \begin{bmatrix} \dfrac{k_i/(m_i\omega_l^2)}{\left[1 - j\,c_i/(m_i\omega_l) - k_i/(m_i\omega_l^2)\right]^2} \\ \dfrac{jc_i/(m_i\omega_l)}{\left[1 - j\,c_i/(m_i\omega_l) - k_i/(m_i\omega_l^2)\right]^2} \end{bmatrix}^{\mathrm{T}} \qquad (3.28)$$

$$\hat{\mathbf{h}}_l = \left[\frac{\partial \hat{g}_l}{\partial \hat{\ddot{X}}_{i-1}} \quad \frac{\partial \hat{g}_l}{\partial \hat{\ddot{X}}_{i}} \quad \frac{\partial \hat{g}_l}{\partial \hat{\ddot{X}}_{i+1}} \quad \frac{\partial \hat{g}_l}{\partial \beta_{k(i+1)}} \quad \frac{\partial \hat{g}_l}{\partial \beta_{c(i+1)}} \right]_{\substack{\hat{\ddot{X}}_\bullet = \ddot{X}_\bullet \\ \beta_\bullet = 1}}$$

$$= \begin{bmatrix} \dfrac{\left\{\ddot{X}_{i-1,l} + (\ddot{X}_{i+1,l} - \ddot{X}_{i,l})\left[jc_{i+1}/(m_i\omega_l) + k_{i+1}/(m_i\omega_l^2)\right]\right\} - (\ddot{X}_{i-1,l} - \ddot{X}_{i,l})}{\left\{\ddot{X}_{i-1,l} + (\ddot{X}_{i+1,l} - \ddot{X}_{i,l})\left[jc_{i+1}/(m_i\omega_l) + k_{i+1}/(m_i\omega_l^2)\right]\right\}^2} \\ \dfrac{-1 + \dfrac{\left[jc_{i+1}/(m_i\omega_l) + k_{i+1}/(m_i\omega_l^2)\right]}{\left[1 - j\,c_i/(m_i\omega_l) - k_i/(m_i\omega_l^2)\right]}}{\left\{\ddot{X}_{i-1,l} + (\ddot{X}_{i+1,l} - \ddot{X}_{i,l})\left[jc_{i+1}/(m_i\omega_l) + k_{i+1}/(m_i\omega_l^2)\right]\right\}} \\ \dfrac{(\ddot{X}_{i,l} - \ddot{X}_{i-1,l})\left[jc_{i+1}/(m_i\omega_l) + k_{i+1}/(m_i\omega_l^2)\right]}{\left\{\ddot{X}_{i-1,l} + (\ddot{X}_{i+1,l} - \ddot{X}_{i,l})\left[jc_{i+1}/(m_i\omega_l) + k_{i+1}/(m_i\omega_l^2)\right]\right\}^2} \\ \dfrac{(\ddot{X}_{i,l} - \ddot{X}_{i-1,l})(\ddot{X}_{i+1,l} - \ddot{X}_{i,l})\,k_{i+1}/(m_i\omega_l^2)}{\left\{\ddot{X}_{i-1,l} + (\ddot{X}_{i+1,l} - \ddot{X}_{i,l})\left[jc_{i+1}/(m_i\omega_l) + k_{i+1}/(m_i\omega_l^2)\right]\right\}^2} \\ \dfrac{(\ddot{X}_{i,l} - \ddot{X}_{i-1,l})(\ddot{X}_{i+1,l} - \ddot{X}_{i,l})\; jc_{i+1}/(m_i\omega_l)}{\left\{\ddot{X}_{i-1,l} + (\ddot{X}_{i+1,l} - \ddot{X}_{i,l})\left[jc_{i+1}/(m_i\omega_l) + k_{i+1}/(m_i\omega_l^2)\right]\right\}^2} \end{bmatrix}^{\mathrm{T}} \tag{3.29}$$

Rearranging Equation (3.9) gives

$$\begin{aligned} &\ddot{X}_{i-1,l} + (\ddot{X}_{i+1,l} - \ddot{X}_{i,l})\left[jc_{i+1}/(m_i\omega_l) + k_{i+1}/(m_i\omega_l^2)\right] = \\ &(\ddot{X}_{i-1,l} - \ddot{X}_{i,l})\left[1 - j\,c_i/(m_i\omega_l) - k_i/(m_i\omega_l^2)\right] \end{aligned} \tag{3.30}$$

Using the right side of (3.30) to replace the terms in (3.29) that equal the left side of (3.30) and simplifying will give

$$\hat{\mathbf{h}}_l = \begin{bmatrix} \dfrac{1}{(\ddot{X}_{i,l} - \ddot{X}_{i-1,l})} \dfrac{j\,c_i/(m_i\omega_l) + k_i/(m_i\omega_l^2)}{\left[1 - j\,c_i/(m_i\omega_l) - k_i/(m_i\omega_l^2)\right]^2} \\ \dfrac{1}{(\ddot{X}_{i,l} - \ddot{X}_{i-1,l})} \dfrac{1 - j\left(c_{i+1} + c_i\right)/(m_i\omega_l) - \left(k_{i+1} + k_i\right)/(m_i\omega_l^2)}{\left[1 - j\,c_i/(m_i\omega_l) - k_i/(m_i\omega_l^2)\right]^2} \\ \dfrac{1}{(\ddot{X}_{i,l} - \ddot{X}_{i-1,l})} \dfrac{j\,c_{i+1}/(m_i\omega_l) + k_{i+1}/(m_i\omega_l^2)}{\left[1 - j\,c_i/(m_i\omega_l) - k_i/(m_i\omega_l^2)\right]^2} \\ \dfrac{(\ddot{X}_{i+1,l} - \ddot{X}_{i,l})}{(\ddot{X}_{i,l} - \ddot{X}_{i-1,l})} \dfrac{k_{i+1}/(m_i\omega_l^2)}{\left[1 - j\,c_i/(m_i\omega_l) - k_i/(m_i\omega_l^2)\right]^2} \\ \dfrac{(\ddot{X}_{i+1,l} - \ddot{X}_{i,l})}{(\ddot{X}_{i,l} - \ddot{X}_{i-1,l})} \dfrac{j\,c_{i+1}/(m_i\omega_l)}{\left[1 - j\,c_i/(m_i\omega_l) - k_i/(m_i\omega_l^2)\right]^2} \end{bmatrix}^{\mathrm{T}} \tag{3.31}$$

Then the relative identification error of the optimization problem (3.10) can be obtained as

$$
\begin{aligned}
\begin{bmatrix}\theta_{ki}\\ \theta_{ci}\end{bmatrix} \approx \sum_{l=1}^{N}\mathrm{Re}\left\{\begin{bmatrix}U_{11,l} & U_{12,l} & U_{13,l}\\ U_{21,l} & U_{22,l} & U_{23,l}\end{bmatrix}\cdot\begin{bmatrix}N_{i-1,l}\big/(\ddot{X}_{i,l}-\ddot{X}_{i-1,l})\\ N_{i,l}\big/(\ddot{X}_{i,l}-\ddot{X}_{i-1,l})\\ N_{i+1,l}\big/(\ddot{X}_{i,l}-\ddot{X}_{i-1,l})\end{bmatrix}\right\}\\
+\sum_{l=1}^{N}\mathrm{Re}\left\{\begin{bmatrix}U_{14,l} & U_{15,l}\\ U_{24,l} & U_{25,l}\end{bmatrix}\cdot\begin{bmatrix}\dfrac{(\ddot{X}_{i+1,l}-\ddot{X}_{i,l})}{(\ddot{X}_{i,l}-\ddot{X}_{i-1,l})}\theta_{k(i+1)}\\ \dfrac{(\ddot{X}_{i+1,l}-\ddot{X}_{i,l})}{(\ddot{X}_{i,l}-\ddot{X}_{i-1,l})}\theta_{c(i+1)}\end{bmatrix}\right\}
\end{aligned}
\tag{3.32}
$$

where $\theta_{k(i+1)}=\beta_{k(i+1)}$-1 and $\theta_{k(i+1)}=\beta_{c(i+1)}$-1 are the relative identification error of the $(i+1)^{\text{th}}$ story parameters k_{i+1} and c_{i+1}, respectively. $U_{ij,l}$ are deterministic factors as follows,

$$U_{11,l} = \frac{1}{B_1}\cdot\frac{k_i\big/(m_i\omega_l^2)\cdot\left[jc_i\big/(m_i\omega_l)+k_i\big/(m_i\omega_l^2)\right]}{\left|1-j\,c_i\big/(m_i\omega_l)-k_i\big/(m_i\omega_l^2)\right|^4}$$

$$U_{21,l} = \frac{1}{B_2}\cdot\frac{-jc_i\big/(m_i\omega_l)\cdot\left[jc_i\big/(m_i\omega_l)+k_i\big/(m_i\omega_l^2)\right]}{\left|1-j\,c_i\big/(m_i\omega_l)-k_i\big/(m_i\omega_l^2)\right|^4}$$

$$U_{12,l} = \frac{1}{B_1}\cdot\frac{k_i\big/(m_i\omega_l^2)\cdot\left[1-j(c_{i+1}+c_i)\big/(m_i\omega_l)-(k_{i+1}+k_i)\big/(m_i\omega_l^2)\right]}{\left|1-j\,c_i\big/(m_i\omega_l)-k_i\big/(m_i\omega_l^2)\right|^4}$$

$$U_{22,l} = \frac{1}{B_2}\cdot\frac{-jc_i\big/(m_i\omega_l)\cdot\left[1-j(c_{i+1}+c_i)\big/(m_i\omega_l)-(k_{i+1}+k_i)\big/(m_i\omega_l^2)\right]}{\left|1-j\,c_i\big/(m_i\omega_l)-k_i\big/(m_i\omega_l^2)\right|^4}$$

$$U_{13,l} = \frac{1}{B_1}\cdot\frac{k_i\big/(m_i\omega_l^2)\cdot\left[jc_{i+1}\big/(m_i\omega_l)+k_{i+1}\big/(m_i\omega_l^2)\right]}{\left|1-j\,c_i\big/(m_i\omega_l)-k_i\big/(m_i\omega_l^2)\right|^4}$$

$$U_{23,l} = \frac{1}{B_2}\cdot\frac{-jc_i\big/(m_i\omega_l)\cdot\left[jc_{i+1}\big/(m_i\omega_l)+k_{i+1}\big/(m_i\omega_l^2)\right]}{\left|1-j\,c_i\big/(m_i\omega_l)-k_i\big/(m_i\omega_l^2)\right|^4}$$

$$U_{14,l} = \frac{1}{B_1} \cdot \frac{k_i k_{i+1} \big/ (m_i^2 \omega_l^4)}{\left|1 - j\,c_i \big/ (m_i \omega_l) - k_i \big/ (m_i \omega_l^2)\right|^4}\,,\; U_{24,l} = \frac{1}{B_2} \cdot \frac{-\,jk_{i+1} c_i \big/ (m_i^2 \omega_l^3)}{\left|1 - j\,c_i \big/ (m_i \omega_l) - k_i \big/ (m_i \omega_l^2)\right|^4}$$

$$U_{15,l} = \frac{1}{B_1} \cdot \frac{jk_i c_{i+1} \big/ (m_i^2 \omega_l^3)}{\left|1 - j\,c_i \big/ (m_i \omega_l) - k_i \big/ (m_i \omega_l^2)\right|^4}\,,\; U_{25,l} = \frac{1}{B_2} \cdot \frac{c_i c_{i+1} \big/ (m_i^2 \omega_l^2)}{\left|1 - j\,c_i \big/ (m_i \omega_l) - k_i \big/ (m_i \omega_l^2)^4\right|}$$

where $B_1 = \sum_{l=1}^{N} \frac{k_i^2 \big/ \left(m_i^2 \omega_l^4\right)}{\left|1 - j\,c_i \big/ (m_i \omega_l) - k_i \big/ (m_i \omega_l^2)\right|^4}$, $B_2 = \sum_{l=1}^{N} \frac{c_i^2 \big/ \left(m_i^2 \omega_l^2\right)}{\left|1 - j\,c_i \big/ (m_i \omega_l) - k_i \big/ (m_i \omega_l^2)\right|^4}$.

The identification error in Equation (3.32), indeed, does come from two kinds of uncertainty sources: The first part of the right side of the equation is directly related to measurement noise and the second is due to the uncertainty from parameter estimates of the story above. As shown in Figure 3.3, all factors $U_{ij,l}$ possess characteristics similar to factors $W_{ij,l}$: the magnitudes of the factors have peaks near the natural frequency of the i^{th} story substructure ω_{i0}, defined by $\omega_{i0} = \sqrt{k_i / m_i}$, and decay very fast when moving to lower and higher frequency. (It is assumed in Figure 3.3 that $k_i = k_{i+1}$, $c_i = c_{i+1}$ and $c_i / m_i = 2\xi_i \omega_{i0}$ where $\xi_i = 0.1$.) As in the top story identification, the weighting factor $U_{1j,l}$ has a much smaller magnitude than that of $U_{2j,l}$, which indicates a similar conclusion that the damping estimates are less accurate than the stiffness estimates.

Following an analysis methodology similar to that used in the top story case, it can be easily concluded that the identification error of the i^{th} story parameters can be reduced by (a) maximizing the frequency response of the i^{th} interstory acceleration $(\ddot{X}_{i,l} - \ddot{X}_{i-1,l})$ in a frequency range around the i^{th} story substructure natural frequency ω_{i0}, which reduces the errors due to the measurement uncertainty; (b) minimizing the frequency response ratio between the $(i+1)^{th}$ interstory acceleration and the i^{th} interstory acceleration, $(\ddot{X}_{i+1,l} - \ddot{X}_{i,l})/(\ddot{X}_{i,l} - \ddot{X}_{i-1,l})$, in the same frequency range, which reduces the propagation errors caused by the parameter estimate errors of the $(i + 1)^{th}$ story.

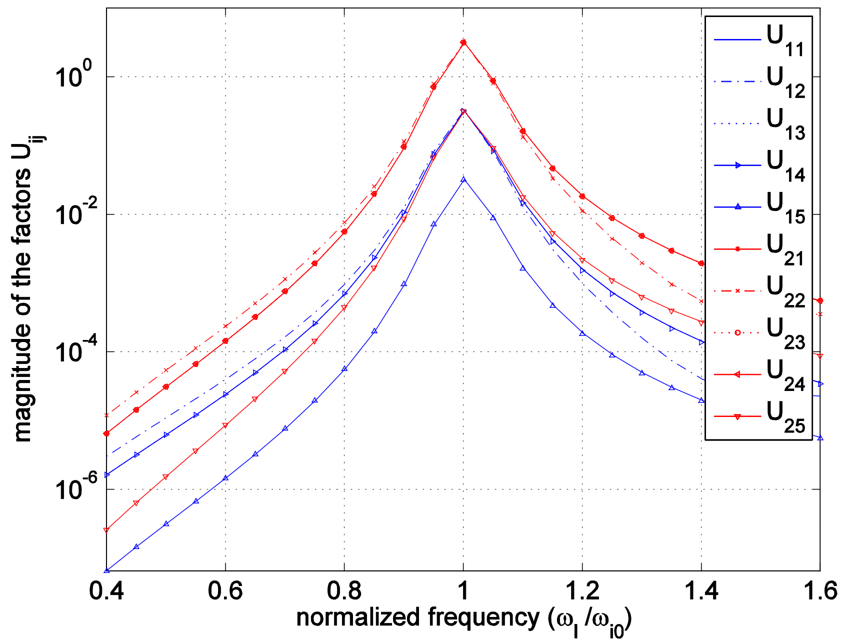

Figure 3.3 Magnitude of factors U_{ij}

3.4 Statistical Moments for Identification Error

Since the proposed substructure identification method uses LSE identification to estimate structural parameters, it only offers the optimal estimate of these parameters, but does not provide much information as to how accurate their estimates will be, which is of importance for giving users confidence in the identification results. Based on the previous result of the approximate identification error analysis, a method to estimate the first two statistical moments (mean and variance) of the identification error is studied in this section. The result not only helps to better comprehend the performance of the proposed substructure method in real uncertain circumstances, but also provides some important suggestions to further improve its accuracy.

3.4.1 Top Story Identification Case

From the result of Equation (3.25), identification errors of top story parameters are associated with three kinds of terms: Fourier transforms of noise $N_{j,l}$, Fourier transforms of the n^{th} true (noiseless) interstory acceleration $(\ddot{X}_{n,l} - \ddot{X}_{n-1,l})$, and the weighting factors $W_{ij,l}$. Factors $W_{ij,l}$ are only related to the structural parameters of the top story and, thereby, are deterministic values; in contrast, the measurement noise terms and the structural response terms change for every identification and are considered to be random in nature. For the sake of notational simplicity, define complex noise vector $\overline{\mathbf{N}}_n = \begin{bmatrix} N_{n-1,1} & N_{n,1} & \cdots & N_{n-1,N} & N_{n,N} \end{bmatrix} \in \mathbf{C}^{2N}$ and structural response vector $\overline{\mathbf{X}}_n = \begin{bmatrix} \Delta_{n,1} & \cdots & \Delta_{n,N} \end{bmatrix} \in \mathbf{C}^{N}$ where $\Delta_{n,l} = \ddot{X}_{n,l} - \ddot{X}_{n-1,l}$. Since the true structural responses $\Delta_{n,l}$ appear in the dominator of the uncertainty terms in Equation (3.25), if the magnitude of any of them is zero the identification error given in Equation 3.25 will tend to infinity. In order to prevent the occurrence of such a situation, an event **A**, which occurs when the magnitude of all structural responses $\left|\Delta_{n,l}\right| \quad (l = 1 \cdots N)$ are no less than a very small positive value $\varepsilon_{n,l}\ (l = 1 \cdots N)$, is defined. Instead of directly calculating the statistic moments of the identification error θ (for notational simply, generic symbol θ is introduced here to represent the identification errors of stiffness θ_{kn} and damping θ_{cn})

with respect to all possible realization of random variables $\overline{\mathbf{N}}_n$ and $\overline{\mathbf{X}}_n$, the statistical moments conditional on event **A** is computed as follows,

$$\begin{aligned}
\mathrm{E}\left[g(\theta)\,|\,\mathbf{A}\right] &= \iint g(\theta)\cdot p_{\overline{\mathbf{N}}_n,\overline{\mathbf{X}}_n|\mathrm{A}}\left(\overline{\mathbf{N}}_n,\overline{\mathbf{X}}_n\,|\,\mathbf{A}\right)d\overline{\mathbf{N}}_n d\overline{\mathbf{X}}_n \\
&= \int\left\{\int g(\theta)\cdot p_{\overline{\mathbf{N}}_n|\overline{\mathbf{X}}_n,\mathrm{A}}\left(\overline{\mathbf{N}}_n\,|\,\overline{\mathbf{X}}_n,\mathbf{A}\right)d\overline{\mathbf{N}}_n\right\}p_{\overline{\mathbf{X}}_n|\mathrm{A}}\left(\overline{\mathbf{X}}_n\,|\,\mathbf{A}\right)d\overline{\mathbf{X}}_n \\
&= \int\left\{\int g(\theta)\cdot p_{\overline{\mathbf{N}}_n}\left(\overline{\mathbf{N}}_n\right)d\overline{\mathbf{N}}_n\right\}p_{\overline{\mathbf{X}}_n|\mathrm{A}}\left(\overline{\mathbf{X}}_n\,|\,\mathbf{A}\right)d\overline{\mathbf{X}}_n \\
&= \int\left\{\mathrm{E}\left[g(\theta)\,|\,\overline{\mathbf{X}}_n,\mathbf{A}\right]\right\}p_{\overline{\mathbf{X}}_n|\mathrm{A}}\left(\overline{\mathbf{X}}_n\,|\,\mathbf{A}\right)d\overline{\mathbf{X}}_n
\end{aligned} \tag{3.33}$$

where $g(\theta)$ equals θ when calculating the mean and equals $(\theta\text{-E}[\theta|\mathbf{A}])^2$ when computing the variance; $p_{\overline{\mathbf{N}}_n,\overline{\mathbf{X}}_n|\mathrm{A}}\left(\overline{\mathbf{N}}_n,\overline{\mathbf{X}}_n\,|\,\mathbf{A}\right)$ is the joint probability distribution function of noises $\overline{\mathbf{N}}_n$ and structural responses $\overline{\mathbf{X}}_n$ conditional on the event **A**; $p_{\overline{\mathbf{N}}_n|\overline{\mathbf{X}}_n,\mathrm{A}}\left(\overline{\mathbf{N}}_n\,|\,\overline{\mathbf{X}}_n,\mathbf{A}\right)$ is the conditional probability of noise $\overline{\mathbf{N}}_n$ on given structural response $\overline{\mathbf{X}}_n$ in the event **A**, which equals $p_{\overline{\mathbf{N}}_n}\left(\overline{\mathbf{N}}_n\right)$ due to the assumption that the measurement noise and structural responses are independent; $p_{\overline{\mathbf{X}}_n|\mathrm{A}}\left(\overline{\mathbf{X}}_n\,|\,\mathbf{A}\right)$ is the conditional probability distribution function of structural responses $\overline{\mathbf{X}}_n$ in event **A**; $\mathrm{E}\left[g(\theta)\,|\,\overline{\mathbf{X}}_n,\mathbf{A}\right]$ is the conditional statistic moment of identification error θ on given structural response $\overline{\mathbf{X}}_n$ in the event **A**.

In order to simplify the analysis, three assumptions are made hereafter:

1. The measurement noise and the true structural response are statistically independent.
2. The measurement noise is a zero-mean white Gaussian vector process and the measurement noises of different structural responses are statistically independent.

3. The true structural responses can be modeled as one or several independent zero-mean white Gaussian processes passing through a linear time invariant (LTI) system.

Based on the above three assumptions, it is shown in the Appendix A that (a) any element in the random vector $\overline{\mathbf{X}}_n$ (and $\overline{\mathbf{N}}_n$) is a zero-mean circular complex Gaussian random variable, which implies that the real and imaginary part of a complex random variable are independent zero-mean Gaussian variables with the same variance, equal to one half of the variance of the magnitude of the complex variable; and (b) any two elements in the vector $\overline{\mathbf{X}}_n$ (and $\overline{\mathbf{N}}_n$) are independent of each other.

Define two new complex random variables,

$$\begin{bmatrix} \Theta_{nk} \\ \Theta_{nc} \end{bmatrix} = \sum_{l=1}^{N} \left\{ \begin{bmatrix} W_{11,l} & W_{12,l} \\ W_{21,l} & W_{22,l} \end{bmatrix} \cdot \begin{bmatrix} N_{n-1,l} \big/ (\ddot{X}_{n,l} - \ddot{X}_{n-1,l}) \\ N_{n,l} \big/ (\ddot{X}_{n,l} - \ddot{X}_{n-1,l}) \end{bmatrix} \right\} \tag{3.34}$$

Obviously, the identification errors of top story parameter θ_{nc} and θ_{nc} just become the real part of the newly defined complex variable Θ_{nk} and Θ_{nc}, respectively. Applying the result of Lemma 1 in Appendix A, it can be easily shown that, for a given deterministic realization of structural response $\overline{\mathbf{X}}_n$ in the event **A**, the conditional random variables "$\Theta_{nk} \mid \overline{\mathbf{X}}_n, \mathsf{A}$" and "$\Theta_{nc} \mid \overline{\mathbf{X}}_n, \mathsf{A}$" become zero-mean complex circular Gaussian random variables. Therefore, the conditional mean and variance of the identification error on given structural responses $\overline{\mathbf{X}}_n$ in the event **A** can be calculated as

$$\mathrm{E}\left[\theta_{nk} \mid \overline{\mathbf{X}}_n, \mathrm{A}\right] = \mathrm{Re}\left\{\mathrm{E}\left[\Theta_{nk} \mid \overline{\mathbf{X}}_n, \mathrm{A}\right]\right\} = \mathrm{Re}\left\{\sum_{l=1}^{N} W_{11,l} \frac{\mathrm{E}\left[N_{n-1,l}\right]}{\Delta_{n,l}} + W_{12,l} \frac{\mathrm{E}\left[N_{n,l}\right]}{\Delta_{n,l}}\right\} = 0 \tag{3.35}$$

$$\mathrm{E}\left[\theta_{nc} \mid \overline{\mathbf{X}}_n, \mathrm{A}\right] = \mathrm{Re}\left\{\mathrm{E}\left[\Theta_{nc} \mid \overline{\mathbf{X}}_n, \mathrm{A}\right]\right\} = \mathrm{Re}\left\{\sum_{l=1}^{N} W_{21,l} \frac{\mathrm{E}\left[N_{n-1,l}\right]}{\Delta_{n,l}} + W_{22,l} \frac{\mathrm{E}\left[N_{n,l}\right]}{\Delta_{n,l}}\right\} = 0 \tag{3.36}$$

$$\mathrm{VAR}\left[\theta_{nk} \mid \overline{\mathbf{X}}_n, \mathrm{A}\right] = \frac{1}{2}\mathrm{E}\left[\left|\Theta_{nk}\right|^2 \mid \overline{\mathbf{X}}_n, \mathrm{A}\right] = \frac{1}{2}\sum_{l=1}^{N}\left|W_{11,l}\right|^2 \frac{\sigma_{n-1,l}^2}{\left|\Delta_{n,l}\right|^2} + \left|W_{12,l}\right|^2 \frac{\sigma_{n,l}^2}{\left|\Delta_{n,l}\right|^2} \tag{3.37}$$

$$\mathrm{VAR}\left[\theta_{nc} \mid \overline{\mathbf{X}}_n, \mathrm{A}\right] = \frac{1}{2}\mathrm{E}\left[\left|\Theta_{nc}\right|^2 \mid \overline{\mathbf{X}}_n, \mathrm{A}\right] = \frac{1}{2}\sum_{l=1}^{N}\left|W_{21,l}\right|^2 \frac{\sigma_{n-1,l}^2}{\left|\Delta_{n,l}\right|^2} + \left|W_{22,l}\right|^2 \frac{\sigma_{n,l}^2}{\left|\Delta_{n,l}\right|^2} \tag{3.38}$$

where $\sigma_{n-1,l}^2 = \mathrm{E}\left[\left|N_{n-1,l}\right|^2\right]$ and $\sigma_{n,l}^2 = \mathrm{E}\left[\left|N_{n,l}\right|^2\right]$.

Furthermore, integrating Equation (3.35)~(3.38) with respect to all structural responses $\overline{\mathbf{X}}$ in event **A** gives

$$\mathrm{E}\left[\theta_{kn} \mid \mathrm{A}\right] = 0,\ \mathrm{E}\left[\theta_{cn} \mid \mathrm{A}\right] = 0 \tag{3.39}$$

$$\mathrm{VAR}\left[\theta_{kn} \mid \mathrm{A}\right] = \frac{1}{2}\sum_{l=1}^{N}\left[\left|W_{11,l}\right|^2 \sigma_{n-1,l}^2 + \left|W_{12,l}\right|^2 \sigma_{n,l}^2\right] \cdot \mathrm{E}\left[1 \big/ \left|\Delta_{n,l}\right|^2 \Big| \left|\Delta_{n,l}\right| \geq \varepsilon_{n,l}\right] \tag{3.40}$$

$$\mathrm{VAR}\left[\theta_{cn} \mid \mathrm{A}\right] = \frac{1}{2}\sum_{l=1}^{N}\left[\left|W_{12,l}\right|^2 \sigma_{n-1,l}^2 + \left|W_{22,l}\right|^2 \sigma_{n,l}^2\right] \cdot \mathrm{E}\left[1 \big/ \left|\Delta_{n,l}\right|^2 \Big| \left|\Delta_{n,l}\right| \geq \varepsilon_{n,l}\right] \tag{3.41}$$

Since the structural responses $\Delta_{n,l}$ $(l = 1 \cdots N)$ are mutually independent zero-mean circular complex Gaussian variables, the probability density function (PDF) of the random variable $\left|\Delta_{n,l}\right|$ follows Rayleigh distribution

$$f_{\left|\Delta_{n,l}\right|}(x) = \frac{x}{\sigma_{\Delta n,l}^2}\exp\left(\frac{-x^2}{2\sigma_{\Delta n,l}^2}\right) \tag{3.42}$$

where $\sigma_{\Delta n,l}^2 = \mathrm{E}\left[\left|\Delta_{n,l}\right|^2\right]$; then, the conditional PDF of $\left|\Delta_{n,l}\right|$ given that $\left|\Delta_{n,l}\right| \geq \varepsilon$ becomes

$$f_{|\Delta_{n,l}|}\left(x \middle\| \Delta_{n,l}\right| \geq \varepsilon_{n,l}\Big) = \begin{cases} 0 & \text{if } x < \varepsilon_{n,l} \\ \dfrac{1}{C_n}\dfrac{x}{\sigma_{\Delta n,l}^2}\exp\left(\dfrac{-x^2}{2\sigma_{\Delta n,l}^2}\right) & \text{if } x \geq \varepsilon_{n,l} \end{cases} \tag{3.43}$$

where $C_n = \mathrm{P}(x \geq \varepsilon_{n,l}) = \exp\left(-\varepsilon_{n,l}^2 \big/ 2\sigma_{\Delta n,l}^2\right)$. Therefore, the expectation value in the right side of Equation (3.40) and (3.41) can be computed as

$$\mathrm{E}\left[1\Big/\left|\Delta_{n,l}\right|^2 \middle\| \Delta_{n,l}\right| \geq \varepsilon_{n,l}\Big] = \int_{\varepsilon_{n,l}}^{\infty} \frac{1}{x^2}\frac{1}{C_n}\frac{x}{\sigma_{\Delta n,l}^2}\exp\left(\frac{-x^2}{2\sigma_{\Delta n,l}^2}\right)dx \tag{3.44}$$

Changing the integration variable, define $z = x\big/\sigma_{\Delta n,l}$. Then,

$$\mathrm{E}\left[1\Big/\left|\Delta_{n,l}\right|^2 \middle\| \Delta_{n,l}\right| \geq \varepsilon_{n,l}\Big] = \frac{1}{\sigma_{\Delta n,l}^2} \cdot \int_{\varepsilon_{n,l}/\sigma_{\Delta n,l}}^{\infty} \frac{1}{C_n z}\exp\left(-\frac{z^2}{2}\right)dz \tag{3.45}$$

Putting the result of Equation (3.45) back into Equation (3.40) and (3.41), the conditional variance of the identification errors, $\mathrm{VAR}[\theta_{kn} \mid \mathrm{A}]$ and $\mathrm{VAR}[\theta_{cn} \mid \mathrm{A}]$, will be

$$\mathrm{VAR}[\theta_{kn} \mid \mathrm{A}] = \frac{1}{2}\sum_{l=1}^{N}\left[\left|W_{11,l}\right|^2 \frac{\sigma_{n-1,l}^2}{\sigma_{\Delta n,l}^2} + \left|W_{12,l}\right|^2 \frac{\sigma_{n,l}^2}{\sigma_{\Delta n,l}^2}\right] \cdot Q_l \tag{3.46}$$

$$\mathrm{VAR}[\theta_{cn} \mid \mathrm{A}] = \frac{1}{2}\sum_{l=1}^{N}\left[\left|W_{12,l}\right|^2 \frac{\sigma_{n-1,l}^2}{\sigma_{\Delta n,l}^2} + \left|W_{22,l}\right|^2 \frac{\sigma_{n,l}^2}{\sigma_{\Delta n,l}^2}\right] \cdot Q_l \tag{3.47}$$

where $Q_l = \dfrac{1}{C_n}\displaystyle\int_{\varepsilon_{n,l}/\sigma_{\Delta n,l}}^{\infty} \frac{1}{z}\exp\left(-\frac{z^2}{2}\right)dz$.

The conditional variance in Equation (3.46) & (3.47) for the top story substructure depict the scatter of the identification error given that the event **A** occurs. Clearly, we need to pick the values for $\varepsilon_{n,l} \quad (l = 1, \ldots, N)$ such that event A is *very likely* to occur; thus, the conditional variances in Equation (3.46) and (3.47) approximately reflect the real situation of the scatter of the identification error. One of simplest ways to select $\varepsilon_{n,l}$ values is that let $\varepsilon_{n,l} = \alpha\sigma_{\Delta n,l} \;\forall l$, where α is a very small positive scalar value that reflects the user-chosen possibility of the occurrence of event **A**. Then, the probability of event **A** can simply be calculated as

$$P(\mathrm{A}) = \prod_{l=1}^{N} \mathrm{P}\left(\left|\Delta_{n,l}\right| \geq \varepsilon_{n,l}\right) = \prod_{l=1}^{N} \exp\left(-\varepsilon_{n,l}^{2} \big/ 2\sigma_{\Delta n,l}^{2}\right) = \left[\exp\left(-\alpha^{2}/2\right)\right]^{N} \tag{3.48}$$

and Q_l in Equation (3.44) and (3.45) are also simplified as

$$Q_l = Q(\alpha) = \exp\left(\frac{\alpha^2}{2}\right)\int_{\alpha}^{\infty}\frac{1}{z}\exp\left(-\frac{z^2}{2}\right)dz \tag{3.49}$$

3.4.2 Non-top Story Identification Case

Similar to the top story analysis case, two new complex random variables are defined for the non-top story identification as

$$\begin{aligned}\begin{bmatrix}\Theta_{ki}\\ \Theta_{ci}\end{bmatrix} &= \sum_{l=1}^{N}\begin{bmatrix}U_{11,l} & U_{12,l} & U_{13,l}\\ U_{21,l} & U_{22,l} & U_{23,l}\end{bmatrix}\cdot\begin{bmatrix}N_{i-1,l}\big/(\ddot{X}_{i,l}-\ddot{X}_{i-1,l})\\ N_{i,l}\big/(\ddot{X}_{i,l}-\ddot{X}_{i-1,l})\\ N_{i+1,l}\big/(\ddot{X}_{i,l}-\ddot{X}_{i-1,l})\end{bmatrix}\\ &\quad+\sum_{l=1}^{N}\begin{bmatrix}U_{14,l} & U_{15,l}\\ U_{24,l} & U_{25,l}\end{bmatrix}\cdot\begin{bmatrix}\dfrac{(\ddot{X}_{i+1,l}-\ddot{X}_{i,l})}{(\ddot{X}_{i,l}-\ddot{X}_{i-1,l})}\theta_{k(i+1)}\\ \dfrac{(\ddot{X}_{i+1,l}-\ddot{X}_{i,l})}{(\ddot{X}_{i,l}-\ddot{X}_{i-1,l})}\theta_{c(i+1)}\end{bmatrix}\end{aligned} \tag{3.50}$$

Then, the identification errors, θ_{ki} and θ_{ci}, become the real parts of these newly defined complex variables. For the sake of notational simplicity, define complex noise vector $\overline{\mathbf{N}}_i = \begin{bmatrix}N_{i-1,1} & N_{i,1} & N_{i-1,1} & \cdots & N_{i-1,N} & N_{i-1,N} & N_{i-1,N}\end{bmatrix} \in \mathbf{C}^{3N}$ and structural response vector $\overline{\mathbf{X}}_i = \begin{bmatrix}\Delta_{i,1} & \cdots & \Delta_{i,N}\end{bmatrix} \in \mathbf{C}^{N}$ where $\Delta_{i,l} = \ddot{X}_{i,l} - \ddot{X}_{i-1,l}$. Similar as in the analysis of the top story, an event B, which occurs when the magnitude of any structural responses $\left|\Delta_{i,l}\right|$ is no less than a very small positive value $\varepsilon_{i,l}$, is introduced. $\varepsilon_{i,l}$ is equal to the standard deviation of the structural response $\sigma_{\Delta i,l}$ multiplied by a positive number α. The mean and variance of identification error conditional on the event B are calculated.

As seen from Equation (3.50), the identification errors of the i^{th} story parameters, θ_{ki} and θ_{ci}, are related to the measurement uncertainty as well as the identification errors from the $(i+1)^{\text{th}}$ story. In order to reduce the problem difficulty to a manageable level, besides the three assumptions previously made in the top story identification analysis, two additional more restrictive assumptions are made here.

4. The identification error of the $(i+1)^{\text{th}}$ story parameters, $\theta_{k(i+1)}$ and $\theta_{c(i+1)}$, are considered to be deterministic values when calculating the statistical moments of the identification errors of the i^{th} story parameters.
5. There is only one independent excitation in the structure, other excitations (*e.g.*, control forces from structural control systems in the subsequent chapter of controlled substructure identification), if existed, can be determined by this independent excitation.

Since the PDF of the identification errors of the $(i+1)^{\text{th}}$ story parameters are unknown and difficult to obtain, the first assumption provides a solution to overcome such a difficulty. As for the second assumption, it is shown that, based on this assumption, the ratio between the $(i+1)^{\text{th}}$ and i^{th} interstory acceleration responses, $(\ddot{X}_{i+1,l} - \ddot{X}_{i,l})/(\ddot{X}_{i,l} - \ddot{X}_{i-1,l})$, become a function of the structural parameters only that will not change under different random excitations (assuming infinitely long records to determine the Fourier transforms). Therefore, the second part of Equation (3.50), related to the (i+1)th story parameter errors, becomes a deterministic value during different identifications.

The estimate error (3.50) has two parts: the first part, related to the errors from the measurement uncertainty, is a random term with characteristics similar to those on the right side of Equation (3.34); the second part turns out to be some deterministic values in this analysis because of assumption 4 and 5. Applying a technique similar to that for the top story, the conditional mean and variance of the identification errors can be computed as

$$\mathrm{E}\left[\theta_{ki} \mid \mathrm{B}\right] = \mathrm{Re}\left\{\sum_{l=1}^{N} H_l \left[U_{14,l}\theta_{k(i+1)} + U_{15,l}\theta_{c(i+1)}\right]\right\} \tag{3.51}$$

$$\mathrm{E}\left[\theta_{ci} \mid \mathrm{B}\right] = \mathrm{Re}\left\{\sum_{l=1}^{N} H_l \left[U_{24,l}\theta_{k(i+1)} + U_{25,l}\theta_{c(i+1)}\right]\right\} \tag{3.52}$$

$$\mathrm{VAR}\left[\theta_{ki} \mid \mathrm{B}\right] = \frac{1}{2}\sum_{l=1}^{N}\left[\left|U_{11,l}\right|^2 \frac{\sigma_{i-1,l}^2}{\sigma_{\Delta i,l}^2} + \left|U_{12,l}\right|^2 \frac{\sigma_{i,l}^2}{\sigma_{\Delta i,l}^2} + \left|U_{13,l}\right|^2 \frac{\sigma_{i+1,l}^2}{\sigma_{\Delta i,l}^2}\right]\cdot Q(\alpha) \tag{3.53}$$

$$\mathrm{VAR}\left[\theta_{ci} \mid \mathrm{B}\right] = \frac{1}{2}\sum_{l=1}^{N}\left[\left|U_{21,l}\right|^2 \frac{\sigma_{i-1,l}^2}{\sigma_{\Delta i,l}^2} + \left|U_{22,l}\right|^2 \frac{\sigma_{i,l}^2}{\sigma_{\Delta i,l}^2} + \left|U_{23,l}\right|^2 \frac{\sigma_{i+1,l}^2}{\sigma_{\Delta i,l}^2}\right]\cdot Q(\alpha) \tag{3.54}$$

where $H_l = (\ddot{X}_{i+1,l} - \ddot{X}_{i,l}) \big/ (\ddot{X}_{i,l} - \ddot{X}_{i-1,l})$ is the transfer function from the ith interstory acceleration response $\left(\ddot{x}_i - \ddot{x}_{i-1}\right)$ to the (i+1)th interstory acceleration response $\left(\ddot{x}_{i+1} - \ddot{x}_i\right)$; $\sigma_{j,l}^2 = \mathrm{E}\left[\left|N_{j,l}\right|^2\right]$ $\left(j = i-1, i, i+1\right)$ is the variance of measurement noise; $\sigma_{\Delta i,l}^2 = \mathrm{E}\left[\left|\Delta_{i,l}\right|^2\right]$ is the variance of the ith interstory acceleration response; $Q(\alpha)$ is given in Equation (3.49).

Different from the result of the top story case, the conditional means for the non-top story estimate errors are not zeros, so there exists a bias in the estimates of non-top story parameters, which are related to the parameter estimate errors of the story above as well as the frequency response ratio between two adjacent interstory accelerations $(\ddot{X}_{i+1,l} - \ddot{X}_{i,l}) / (\ddot{X}_{i,l} - \ddot{X}_{i-1,l})$. The smaller this response ratio, the smaller the bias will be. The conditional variances possess similar features as that of top story estimate; the variance of interstory acceleration responses near this story substructure natural frequency ω_{i0} plays a critical role in determine the variance of identification errors, with larger response variance leading to smaller variance of identification errors.

3.4.3 Comments on Statistical Moments of Identification Error

The conditional variances in Equations (3.46) & (3.47) for the top story substructure and Equations (3.53) & (3.54) for the non-top story substructure depend on the value of α. As α goes to zero the probabilities of the events **A** and **B,** P(**A**) and P(**B**), approaches to unity and the conditional variances in Equations (3.46) & (3.47) and Equations (3.53) & (3.54) will converge to the (unconditional) variances of the identification error. However, as shown in Figure 3.4, the integral value $Q_n(\alpha)$ increases with the decrease of α value. Moreover, it can also be shown that as α goes to zero, the value $Q_n(\alpha)$ tends to infinity. Does this result really imply that the variance of the identification errors for the identification problems (3.8) & (3.10) is infinity? (This is a horrible conclusion if it were true.) In author's opinion, the answer should be negative. Because the conditional variance in Equations (3.46) & (3.47) and Equations (3.53) & (3.54) are derived on the basis of the result of the identification error analysis shown in Equations (3.26) and (3.32) which are obtained based on the assumption that the identification error is not too large. Recall that these estimates of the relative identification errors are approximate due to the first-order truncation of the Taylor series expansion in Equations (3.13) and (3.14). Thus, if the identification error is too large, Equations (3.26) and (3.32) are not appropriate to exactly calculate the distribution of the identification errors. Therefore, the conditional variance in Equations (3.46) & (3.47) and Equations (3.53) & (3.54) can only offer good approximation of the error variance when the identification errors are not too large. If Equations (3.46) & (3.47) and Equations (3.53) & (3.54) provide very large variance estimation, that results may not be reliable.

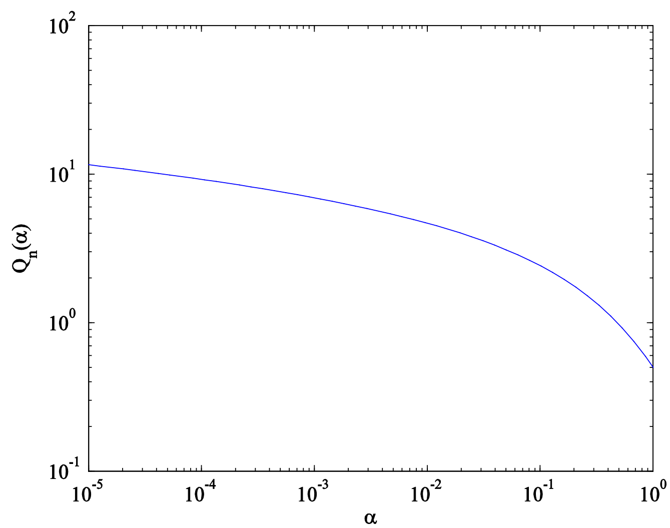

Figure 3.4 The value of function $Q(\alpha)$

However, the analysis of the identification error variances does point out an important fact that the proposed substructure identification method in (3.8) and (3.10) may give estimation results with very large errors, when some of the interstory acceleration responses $\Delta_{i,l}\ (i=1,...,n)$ are very small. If many substructure identification tests have been carried out, it is very likely that some tests provide *outlier* results that are far away from the true values of the structural parameters.

Furthermore, since all weighting factors $W_{ij,l}$ and $U_{ij,l}$ are *significantly large* near the substructure natural frequency and diminish very fast when moving away from that frequency, the variances of the identification errors are mainly determined by the variances of the magnitude of the interstory acceleration responses near the key substructure natural frequency. The larger structural responses, the smaller identification error variances are. This result complies well with the identification error analysis (3.26) in the previous section, except that the previous result depicts the identification error in one identification experiment while this result offers the statistics of many random experiments. Moreover, this result also implies that magnifying the variance of the magnitude of the n^{th} interstory acceleration responses near the key frequency ω_{n0} (*e.g.*, by some structural control technique) can significantly reduce the variance of identification error and, thus, improve identification accuracy.

3.5 Damage Detection Strategy

Structural damage is often associated with the reduction of the stiffness of structural members and the increase of structural damping. Thus, continuously monitoring the change of the structural stiffness and damping parameters, identified by the proposed substructure identification method, provides a way to detect the onset and location of structural damage. However, due to the existence of inevitable uncertain factors, like measurement noise, in the identification process, there are always some variations in the identification results among different tests even for the same structure. In order to discriminate whether the change of the identified parameters results from the normal variation of the identification results or is caused by the onset of structural damage, a statistical hypothesis test is performed. It is assumed herein that before conducting any damage detection, many substructure identification tests have been carried out for the healthy (undamaged) structure, providing data of "normal" scatter of parameter estimates, particularly the mean and the standard deviation of the identified structural parameters from the undamaged structure.

A hypothesis, H_0, is established which states that the structure being tested is undamaged or, equivalently, the structural stiffness and damping parameters are not changed compared with that of the undamaged structure. To verify the correctness of this hypothesis, the structural parameters are estimated via the substructure identification method for the structure of unknown condition (damaged or undamaged). If one observes a significant decrease in the estimated structural stiffness parameters and/or a considerable increase of the estimated structural damping parameters, compared with the normal distribution of parameters form the undamaged structure, then the hypothesis will be rejected, indicating that damage has occurred in the structure; otherwise the hypothesis will be accepted, implying that the structure is undamaged.

Let $\hat{\boldsymbol{\theta}}$ denote the estimated values of the structural parameter vector $\boldsymbol{\theta}$ used to detect structural damage; let $\mathbf{m}_{\boldsymbol{\theta}}$ be the mean vector, and $\mathbf{S}_{\boldsymbol{\theta}}$ be the variance matrix of the parameter vector $\boldsymbol{\theta}$ for the undamaged structure. The conclusion about the hypothesis test is made as follows: if the Mahalanobis distance (Mahalanobis, 1936) between the estimated parameters $\hat{\boldsymbol{\theta}}$ and the mean value of the parameters $\mathbf{m}_{\boldsymbol{\theta}}$ are large, *i.e.*,

$\sqrt{(\hat{\boldsymbol{\theta}}-\mathbf{m}_{\boldsymbol{\theta}})^{\mathrm{T}}\mathbf{S}_{\boldsymbol{\theta}}^{-1}(\hat{\boldsymbol{\theta}}-\mathbf{m}_{\boldsymbol{\theta}})} > \beta$, then the hypothesis is rejected, indicating the occurrence of the structural damage; otherwise the hypothesis is accepted, implying that the structure is intact. β is a positive scalar parameter, which is adjustable to reflect the user's preferences in the damage detection process.

There are two kinds of errors associated with this hypothesis test. The first error is miss detection, that is, when the structure is damaged but the hypothesis is accepted, indicating that the structure is undamaged. The failure to detect the existent damage may pose a great threat to the structural safety and lead to catastrophic results, which should definitely be avoided. The second error is faulty detection, that is, when the structure is undamaged but the hypothesis is rejected, implying the occurrence of the damage in the structure. Although the consequence of the faulty detection is not as severe as the miss reporting, this error should also be avoided as much as possible. Too many false alarms about the structural damage will quickly make the damage detection system lose the trust of the public, leading to the system being abandoned. Changing the β value mentioned in the last paragraph can adjust the probability of these two errors. However, no matter how one changes the parameter β, when the probability of one error decreases, the probability of the other increases.

In order to improve the accuracy of damage detection and reducing both kinds of possible errors in the process, a new hypothesis test procedure, the majority vote of *n* tests, is proposed herein. In the new procedure, *n* (*n* is an odd number) substructure identification tests are carried out and a hypothesis test with the same β is performed for each identification results independently. Then, the final decision of the hypothesis for the damage detection is determined by the majority results of all individual hypothesis testing. For example, if three individual hypothesis tests are carried out and the two of them suggest rejecting the hypothesis (indicating the structure is damaged), then final decision is to reject the hypothesis.

The performance of newly proposed hypothesis testing method is analyzed as follows. Let p be the probability that one individual hypothesis test will make the wrong decision and P_n be the probability that the majority of n hypothesis tests will make the wrong decision. Since all n tests are independent each other, the probability P_n follows a binomial distribution. Thus, one can easily calculate the probability P_n with n=1,3,5 as

$$P_1(p) = p \tag{3.55}$$

$$P_3(p) = \binom{3}{2} p^2 (1-p) + p^3 \tag{3.56}$$

$$P_5(p) = \binom{5}{3} p^3 (1-p)^2 + \binom{5}{4} p^4 (1-p) + p^5 \tag{3.57}$$

It is worth pointing out that P_n is a function of the error probability p and P_1 corresponds to the error probability of the original hypothesis test when only one test is performed. Figure 3.5 shows the value P_n/P_1 (n=3,5) changes with different p value, which demonstrates that if p is less than 0.5, the value P_n/P_1 are always less than unity, indicating the improvement of the detection accuracy. Moreover, when the p value is close to zero, P_n/P_1 are very small, which suggests the great reduction in the probability that the majority of n test will make the wrong decision. For example, if p=0.1, P_3/P_1=28% and P_5/P_1=9%, implying the 72% and 91% reduction in the error probability, respectively, if 3 or 5 tests are performed together to make the decision about the structural damage instead of only one test being performed.

Since p can be the error probability for either the first or the second kind of error of the hypothesis testing, the newly proposed the hypothesis testing method, majority vote of n tests, can simultaneously reduce both kind of errors in the hypothesis testing if p is less than 0.5.

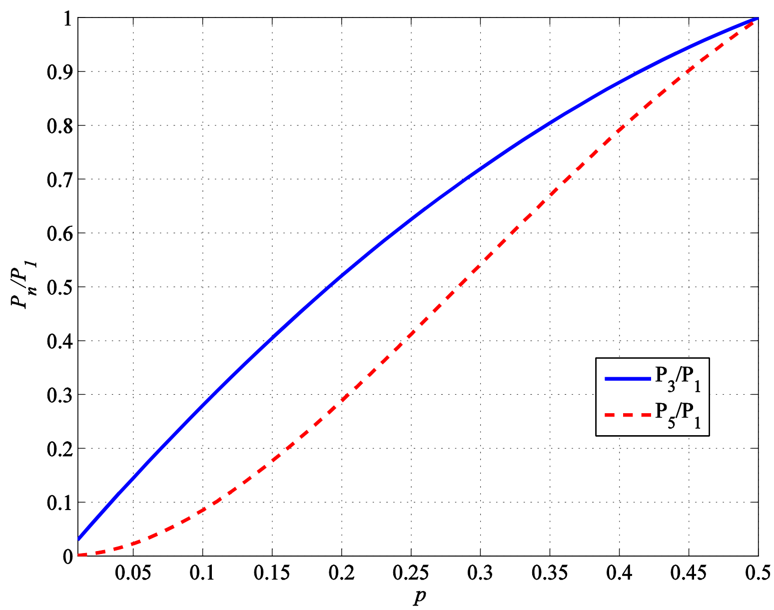

Figure 3.5 How P_n/P_1 changes with different p values

3.6 Illustrative Examples

A 5-story uniform shear structure excited by ground acceleration is used to illustrate the effectiveness of the proposed substructure identification method. The parameters of the structure are chosen to be m_i=1×10^5 kg, c_i=8×10^5 N·sec/m, and k_i=16×10^7 N/m (i=1…5). The natural frequencies and damping ratios of the structure are listed in Table 3.1.

The ground excitation $\ddot{u}_g$ is generated by a Gaussian random pulse process passing through a 4-th order band pass Butterworth filter with the low cut-off frequency at 1Hz and the high cut-off frequency at 12Hz.

Table 3.1 Modal properties of the 5-story structure

Mode Number	1	2	3	4	5
Frequency (radian/second)	11.3	33.2	52.4	67.3	76.8
Damping Ratio (%)	2.85	8.31	13.1	16.8	19.2

3.6.1 Substructure Identification with Undamaged Structure

To check if the proposed identification method works consistently well, 100 identification tests are performed. In each test, 120 second ground and floor acceleration responses, with a sampling rate of 200Hz, are generated and used to carry out substructure identification. Substructure identification is carried out using the Fourier transform of the noisy floor accelerations up to 12Hz.

Two levels of noise, 5% and 20%, are added to the simulated structural responses to mimic the effect of the measurement noise. 5% (or 20%) noise means that the root-mean-square (RMS) value of the measurement noise is equal to 5% (or 20%) of the RMS of the ground excitation. It is also assumed herein that magnitude of the measurement noise of all acceleration responses is the same. The measurement noise is modeled by a band-limited Gaussian white noise with the cut-off frequency at 100Hz. Figure 3.6 shows an example of first two seconds of the 5th story acceleration response, which demonstrates how much the structural response is distorted by the measurement noise. From the figure, it can be seen that 5% noise represents a relatively small level of the disturbance, which is almost unnoticeable without zooming in; 20% noise represents a medium level of disturbance which does not greatly change the structural responses but can be easily observed.

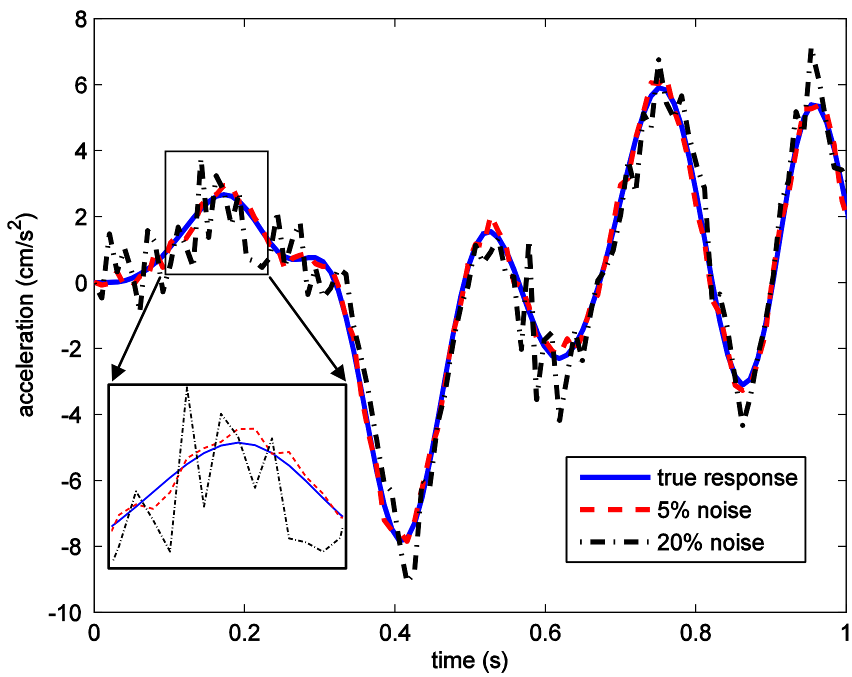

Figure 3.6 The 5th floor noisy acceleration response with and without measurement noise

When identifying the i^{th} story parameters $[k_i \;\; c_i]^T$ ($i \neq n$, thus not the top story), the parameters of the $(i+1)^{th}$ story $[k_{i+1} \; c_{i+1}]^T$ are needed. Hence, two identification scenarios are considered here: 1) 100 tests are carried out independently, that is, the j^{th} identification test result (j=1,…,100) for the $(i+1)^{th}$ story parameters are used to perform the j^{th} identification test for the i^{th} story parameters; 2) To reduce the identification errors in the i^{th} story parameters caused by the identification of the $(i+1)^{th}$ story parameters, in the second scenario, the mean values of 100 substructure identification results for the

$(i+1)^{th}$ story parameters are used to perform all 100 substructure identification tests for the i^{th} story parameters.

a) Identification Results with 5% Noise

The statistics of the identification results of the 100 tests with 5% noise disturbance are listed in Tables 3.2 and 3.3 for the above two scenarios respectively. From the identification results of both scenarios, it can be seen that with 5% measurement noise the proposed substructure identification provides quite accurate estimates for the stiffness parameters. For example, the largest relative root-mean-square-error (RMSE) of the story stiffness estimate (RMSE value divided by the true parameter value) is only about 3.8%. However, the accuracy of the identified damping parameter is just mediocre, which attests numerically to the error analysis result that the damping estimates are less accurate than stiffness estimates. For the results of the second identification scenario, since instead of all 100 estimates of the $(i+1)^{th}$ story parameters, the more accurate mean values of these estimates are used to perform substructure identification for the i^{th} story parameters, which actually reduces the identification error in the i^{th} story parameters caused by the errors in the $(i+1)^{th}$ story estimated parameters. Therefore, almost all identified parameters become more accurate in the second scenario compared with those in the first scenario except for the top story parameters.

Table 3.2 The statistics of the identification results with 5% noise (scenario 1: all substructure identification are carried out independently)

Story number	Story stiffness $\hat{k}_i$ ($\times 10^5$N/m)			Story damping $\hat{c}_i$ ($\times 10^5$N·sec/m)		
	mean	relative RMSE	relative STD	mean	relative RMSE	relative STD
1	1626 (1.6%)*	2.5%	1.9%	7.84 (-2.0%)*	7.5%	7.3%
2	1633 (2.0%)	2.7%	1.8%	8.11 (1.3%)	7.1%	7.0%
3	1633 (2.1%)	3.8%	3.2%	9.64 (20.1%)	25.7%	16.0%
4	1604 (0.2%)	1.1%	1.0%	8.62 (7.9%)	10.9%	7.6%
5	1602 (0.2%)	0.8%	0.8%	8.33 (4.1%)	6.8%	5.5%

*: relative error for mean estimate

Table 3.3 The statistics of the identification results with 5% noise (scenario 2: the parameters of the (i+1)th story are taken as the average of all previous identification results)

Story number	Story stiffness $\hat{k}_i$ ($\times 10^5$N/m)			Story damping $\hat{c}_i$ ($\times 10^5$N·sec/m)		
	mean	relative RMSE	relative STD	mean	relative RMSE	relative STD
1	1626 (1.7%)	1.8%	0.6%	7.84 (-2.0%)	3.3%	2.7%
2	1635 (2.2%)	2.3%	0.5%	8.12 (1.5%)	3.5%	3.2%
3	1635 (2.2%)	2.8%	1.8%	9.61 (20.0%)	24.3%	13.7%
4	1601 (0.1%)	0.6%	0.6%	8.60 (7.6%)	8.5%	3.8%
5	1601 (0.1%)	0.8%	0.8%	8.34 (4.2%)	8.0%	6.8%

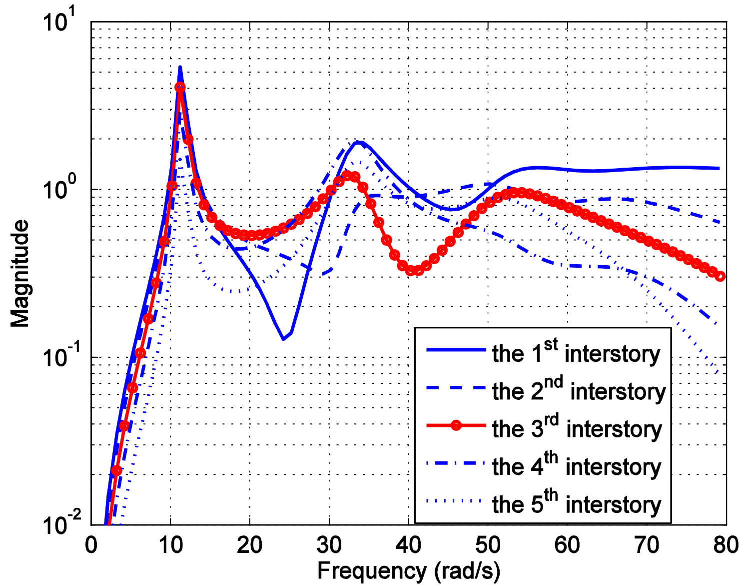

Figure 3.7 Magnitude of the transfer functions from ground excitation to interstory acceleration

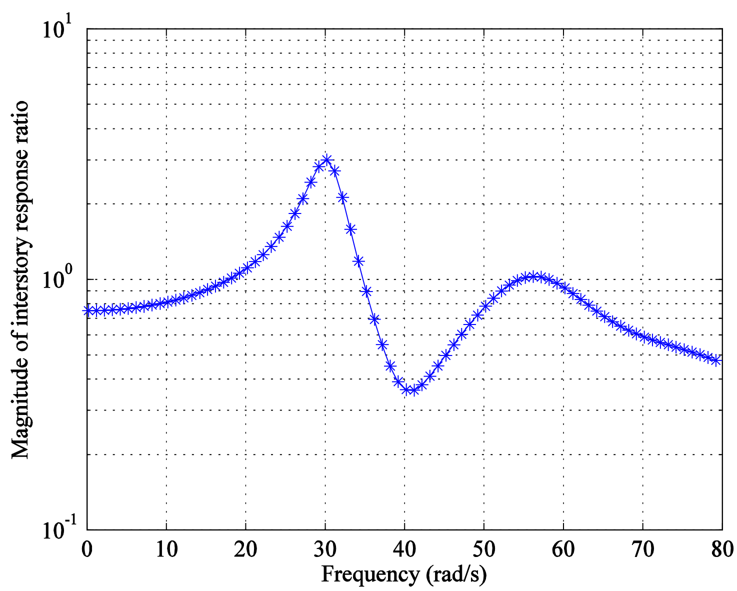

Figure 3.8 Magnitude of the frequency response ratio between the third and second interstory acceleration

Comparing the accuracy of the parameter estimates in different stories in both scenarios shows an interesting phenomenon. Although the proposed substructure method has a drawback of identification error accumulation from the top story to the bottom as previously mentioned in the identification error analysis section, in the simulation the largest parameter identification error in terms of relative RMSE value does not occur in the first story but in the third story.

To explain this phenomenon, first recall the results of the previous identification error analysis, which states that the identification accuracy of the i^{th} story ($i \neq n$) parameters are significantly influenced by two structural responses: 1) the frequency response of i^{th} interstory acceleration $(\ddot{X}_i - \ddot{X}_{i-1})$ near the substructure natural frequency, which affects the identification error due to the measurement uncertainty; 2) the frequency response ratio between two adjacent interstory acceleration $(\ddot{X}_{i+1} - \ddot{X}_i)/(\ddot{X}_i - \ddot{X}_{i-1})$ near the same substructure natural frequency, which affects the identification error caused by the error accumulation from the estimates of the story above. As shown in Figure 3.7, the transfer function from ground excitation to the third interstory acceleration has a relatively small magnitude near the story substructure natural frequency 40 radian/sec, which indicates that the third interstory acceleration response is small near the story substructure natural frequency. Therefore, it is expected that the third story estimates should contain much larger error. Moreover, Figure 3.8 shows the magnitude of the frequency response ratio between the third and second interstory acceleration, which is very small magnitude near the substructure natural frequency 40 radian/sec. This observation in Figure 3.8 explains the fact that although the estimated third story parameters contain large errors, their error accumulation to the second story parameter estimation will still be quite small due to the small frequency response ratio

$(\ddot{X}_3 - \ddot{X}_2)/(\ddot{X}_2 - \ddot{X}_1)$ near the substructure natural frequency and, thus, the largest identification error occurs in the third but not in the second or first story.

Table 3.4The statistics of the identification results with 20% noise (scenario 1: all substructure identifications are carried out independently)

Story number	Story stiffness $\hat{k}_i$ (×10^5N/m)			Story damping $\hat{c}_i$ (×10^5N·sec/m)		
	mean	relative RMSE	relative STD	mean	relative RMSE	relative STD
1	1785 (11.6%)	12.5%	5.0%	10.9 (36.6%)	42.7%	22.2%
2	1754 (9.6%)	10.2%	3.3%	11.9 (48.5%)	51.5%	17.2%
3	1601 (0.1%)	12.6%	12.6%	15.9 (99.4%)	99.4%	3.7%
4	1570 (-1.9%)	4.1%	3.7%	11.4 (43.3%)	47.2%	18.8%
5	1589 (-0.7%)	1.8%	1.6%	9.1 (13%)	16.4%	9.6%

Table 3.5 The statistics of the identification results with 20% noise (scenario 2: the parameters of the (i+1)th story are taken as the average of all previous identification results)

Story number	Story stiffness $\hat{k}_i$ (×10^5N/m)			Story damping $\hat{c}_i$ (×10^5N·sec/m)		
	mean	relative RMSE	relative STD	mean	relative RMSE	relative STD
1	1769 (10.6%)	11.0%	3.0%	10.61 (32.6%)	35.0%	12.7%
2	1750 (9.4%)	9.7%	2.5%	11.64 (45.5%)	47.0%	11.9%
3	1601 (0.1%)	5.4%	5.4%	15.71 (96.4%)	96.9%	10.0%
4	1560 (-2.4%)	3.2%	2.0%	11.29 (41.1%)	42.5%	10.8%
5	1587 (-0.8%)	1.6%	1.4%	9.06 (13.3%)	14.7%	6.2%

b) Identification Results with 20% Noise

The statistics of the identification results of the tests with 20% noise disturbance are listed in Tables 3.4 and 3.5 for the both identification scenarios respectively. As the noise level increases 4 times from 5% to 20%, the RMSE of the identified parameters are also drastically increased, indicating very large errors in the identified parameters. Hence, under the medium level (20%) of noise disturbance, the proposed substructure identification method cannot provide any accurate results for the parameter identification.

3.6.2 Damage Detection via Substructure Identification

In this section, the damage detection strategy proposed in the section 3.5 is applied to perform the damage detect for the structure. It is assumed that the structural damage occurs at the first, third and fifth stories, which results in the reduction of the story stiffness by 5% and the increase of the story damping by 20%.

The results of the substructure identification of the undamaged structure show that with 5% noise the substructure identification method provides relatively good estimation results, while with the noise increasing to 20% the identification results become very noisy. Therefore, the damage detection tests are only performed at the 5% noise level, which means that the noise level in the substructure identification tests are all 5% for both undamaged and damaged structure.

To establish the "normal" distribution of the identified parameters for the undamaged structure, 100 substructure identifications are performed on the undamaged structure under the same level of noise disturbance. The identification results of these tests are used to calculate the mean and covariance of the identified structural parameters, which, in turn, are used to carry out the hypothesis tests. In order to test the performance of the proposed damage detection strategy to correctly identify the health status of the structure, 1500 independent substructure identifications are carried out on the damaged structure and used in the hypothesis test to determine whether or not the structure is damaged. To see the effect of the number of identifications used for each hypothesis test, these 1500 identifications are grouped as 1500 sets of one identification each (n=1), 500 sets of three identifications each (n=3), and 300 sets of five identification each (n=5). A hypothesis test is performed for each group using the method proposed in section 3.5. The percentages of the hypothesis tests that give the correct health status of the structure are shown in Table 3.6. The β value is selected as 3 in the hypothesis tests (i.e., "damage" is assumed if the parameter vector has changed by more than three standard deviations from the healthy state).

The results in Table 3.6 shows that when only one identification is used in the hypothesis testing, the damage in each of the first and the fifth stories is almost 100% percent correctly identified; however, there is about a 15% chance that the undamaged second and fourth story are mistakenly reported as the damaged, and 20% chance that the damage at the third story are not detected. As the number of the identifications used in each hypothesis test increases, the chances that hypothesis tests make the corrected decision also increase, verifying that the proposed hypothesis test method, using n identifications together to make the decision, is effective in improving the probability to make the right decision about the health status of the structure.

Table 3.6 The percentage of the hypothesis tests which give the corrected conclusion about the structural health status

Floor Number	*n*		
	1	3	5
1	99%	100%	100%
2	84%	94%	96%
3	80%	90%	94%
4	85%	94%	98%
5	100%	100%	100%

Although using more identification results to perform the hypothesis test improves the accuracy of the damage detection, it does requires more substructure identifications be carried out, increasing the costs of running the SHM system. Moreover, as shown in Figure 3.5, if the error probability p is close to 0.5, the improvement of the accuracy of the hypothesis test by using more identification results is very limited.

Thus, the key to increasing the accuracy of damage detection lies in improving the accuracy of parameter identification in substructure identification method.

Chapter 4

Transfer Function Based Substructure Identification Method

It is well known that structural acceleration measurements are generally very noisy, which will have a large effect on identification accuracy, especially when the frequency response of the interstory acceleration of the story being identified is very small near its substructure natural frequency. To reduce the effect of the noise and improve the identification accuracy, an improved transfer function based substructure identification method, TF_SUBID, is proposed in this chapter. Instead of directly using the Fourier transform of noisy acceleration response, this method utilizes transfer functions of structural response at different times, averaged together in the frequency domain, to formulate the identification problem. Although the TF_SUBID method can only be applied if certain constraints are satisfied (discussed later), it is shown herein that the improved method does greatly reduce the identification error caused by measurement noise.

4.1 Using Transfer Functions to Formulate Substructure Identification

Equation 4.1 shows the key identification equation for the top story substructure identification in the Fourier transform based method in Chapter 3.

$$\frac{1}{1 - j\,c_n/(m_n\omega) - k_n/(m_n\omega^2)} = \frac{\ddot{X}_{n-1} - \ddot{X}_n}{\ddot{X}_{n-1}} \tag{4.1}$$

Dividing both numerator and denominator of the right side of Equation (4.1) by $\ddot{X}_{n-1}$ gives

$$\frac{1}{1 - jc_n/(m_n\omega) - k_n/(m_n\omega^2)} = 1 - H_{\ddot{x}_n\ddot{x}_{n-1}} \tag{4.2}$$

where $H_{\ddot{x}_n\ddot{x}_{n-1}} = \ddot{X}_n / \ddot{X}_{n-1}$.

$H_{\ddot{x}_n\ddot{x}_{n-1}} = \ddot{X}_n / \ddot{X}_{n-1}$ can be interpreted as the transfer function from the (n-1)th floor acceleration response $\ddot{x}_{n-1}$ to the n^{th} floor acceleration response $\ddot{x}_n$, if such a transfer function exists. This observation inspires the author to think of using the transfer function(s) between structural acceleration responses rather than the Fourier transform of the acceleration responses to formulate the identification problem. There is an averaging technique which can provide more accurate estimation of the transfer function, compared with the above method of calculating the transfer function by directly taking the frequency response ratio between input and output of the system. More accurate estimation of the transfer function will, in turn, lead to more accurate estimation of the structural parameters in the substructure identification. However, to apply this averaging technique requires that 1) the estimated transfer function should not change with different inputs and 2) long stationary input and output responses are available. In order to satisfy these requirements, the following three assumptions are made in this study.

1. There is only one excitation source in the structure. As a consequence, the frequency response ratios between any two noise-free structural responses become a deterministic transfer function, which is a function of the structural parameters only and is independent of the excitation.
2. The noise measurements of different sensors are wide sense stationary (WSS) (*i.e.*, the first and second moments of the noise do not vary with respect to time), zero-

mean, independent of one another and also independent of the true structural responses.

3. All structural responses involved in each substructure identification step are required to be jointly wide sense stationary, which ensures that the power spectrum and cross power spectrum of structural responses do not change with time. Therefore, by averaging the structural response at various times, the effects of measurement noise can be reduced and, thus, more accurate transfer functions can be obtained.

4.2 Transfer Function Estimation via Averaging Method

A review of the method for estimating the transfer function of a single-input-single-output (SISO) system using long stationary noisy measurements is given in this section.

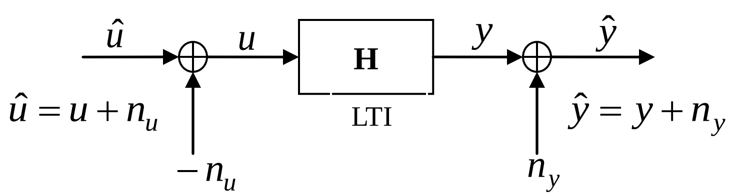

Figure 4.1 The flowchart of a linear SISO system H

Figure 4.1 shows a linear SISO time-invariant system (LTI) **H.** u and y here are the true (noiseless) input and output of the system respective. Let $H(j\omega)$ denote the transfer function (or frequency response function) of the system **H** that satisfies the equation: $Y = H(j\omega)U$, where U and Y are the Fourier transforms of the input u and output y, respectively. The measurements of the input and output signals are corrupted by additive white noise, such that $\hat{U} = U + N_u$ and $\hat{Y} = Y + N_y$, where N_u and N_y are the Fourier transforms of the measurement noises. It is assumed here that measurement noises are white noises that are statistically independent of the true structural responses and mutually statistically independent of each other; *i.e.*,

$$\mathrm{E}\left[UN_u{}^*\right] = \mathrm{E}\left[UN_y{}^*\right] = \mathrm{E}\left[YN_u{}^*\right] = \mathrm{E}\left[YN_y{}^*\right] = \mathrm{E}\left[N_u N_y{}^*\right] = 0 \tag{4.3}$$

Then, the transfer function $H(j\omega)$ can be estimated by the following method (Pintelon *et al.*, 2001)

$$\begin{aligned}
\hat{H}(j\omega) &= \frac{\mathrm{E}\left[\hat{Y}\hat{U}^*\right]}{\mathrm{E}\left[\hat{U}\hat{U}^*\right]} = \frac{\mathrm{E}\left[(Y+N_y)(U+N_u)^*\right]}{\mathrm{E}\left[(U+N_u)(U+N_u)^*\right]} \\
&= \frac{\mathrm{E}\left[YU^* + YN_u^* + N_y U^* + N_y N_u^*\right]}{\mathrm{E}\left[UU^* + UN_u^* + N_u U^* + N_u N_u^*\right]} = \frac{\mathrm{E}\left[UY^*\right]}{\mathrm{E}\left[UU^*\right] + \mathrm{E}\left[N_u N_u^*\right]} \\
&= \frac{\mathrm{E}\left[UY^*\right]}{\mathrm{E}\left[UU^*\right]} \cdot \frac{1}{1 + \mathrm{E}\left[N_u N_u^*\right] / \mathrm{E}\left[UU^*\right]} = H(j\omega)\frac{1}{1+\alpha_u(j\omega)}
\end{aligned} \tag{4.4}$$

where $\hat{H}(j\omega)$ denotes the estimated transfer function from the noisy measurements, $\mathrm{E}[\cdot]$ is the expectation operator, and $\alpha_u(j\omega) = \mathrm{E}[N_u N_u^*] / \mathrm{E}[UU^*]$ is the noise-to-signal-ratio (NSR) of the input u at the frequency ω. The derivation of Equation (4.4) uses the conclusions from Equation (4.3), which states that by averaging long stationary structural responses some noise effects are eliminated.

It is worth pointing out that the error of the estimated transfer function from (4.4) is only related to the input noise N_u and has nothing with the output noise N_y. Reducing the NSR of the input u can improve the accuracy of the estimated transfer function.

4.3 Transfer Function Based Substructure Identification (TF_SUBID)

Using the result from section 4.2, the transfer functions among different responses are estimated and used to formulate the identification problems in the new transfer function based substructure identification method.

4.3.1 Top Story Identification

Equation (4.1), the key identification equation for the top story substructure, is related to two structural responses, $\ddot{x}_{n-1}$ and $\ddot{x}_n$, on its right side. Treating either of these two responses as the input and the other as the output when calculating the transfer functions used in the substructure identification problem, the key identification equation can be rewritten as either of the following two equations

$$\frac{1}{1-j\,c_n/(m_n\omega)-k_n/(m_n\omega^2)}=\frac{\ddot{X}_{n-1}-\ddot{X}_n}{\ddot{X}_{n-1}}=1-H_{\ddot{x}_n\ddot{x}_{n-1}} \tag{4.5}$$

$$\frac{1}{1-j\,c_n/(m_n\omega)-k_n/(m_n\omega^2)}=\frac{\ddot{X}_{n-1}-\ddot{X}_n}{\ddot{X}_{n-1}}=1-\frac{1}{H_{\ddot{x}_{n-1}\ddot{x}_n}} \tag{4.6}$$

where $H_{\ddot{x}_n\ddot{x}_{n-1}}$ and $H_{\ddot{x}_{n-1}\ddot{x}_n}$ stand for the transfer function from $\ddot{x}_{n-1}$ to $\ddot{x}_n$ and the transfer function from $\ddot{x}_n$ to $\ddot{x}_{n-1}$, respectively.

When there is no measurement noise, both transfer functions $H_{\ddot{x}_n\ddot{x}_{n-1}}$ and $H_{\ddot{x}_{n-1}\ddot{x}_n}$ are equal to their true value, so using either Equation (4.5) or (4.6) to formulate the identification problem will give the same and exact results of the structural parameters. However, if the noisy structural responses are used to estimate these transfer functions, the accuracy of the two transfer functions will be different. According to the results from the last section that the accuracy of the estimated transfer function is determined by the

NSR of the input $\alpha_u(j\omega)$ (with a smaller value of $\alpha_u(j\omega)$ leading to a more accurately estimated transfer function), it would be wise to select the transfer function that is more accurate than the other (or, in another words, which has smaller input NSR), to formulate the substructure identification problem to improve the accuracy of the parameter identification. Furthermore, since the NSR $\alpha_u(j\omega)$ is a function of the frequency ω, the above selection procedure can be carried out at each frequency individually. Therefore, the new substructure identification problem for the top story substructure is formulated via the transfer functions between the structural responses,

$$\underset{k_n, c_n}{\arg\min} \quad J(k_n, c_n) = \sum_{l=1}^{N} \left\{ \left| f_l(k_n, c_n) - \hat{f}_l^{\,1}\left(\hat{H}_{\ddot{x}_n \ddot{x}_{n-1}, l}\right) \right|^2 \text{ or } \left| f_l(k_n, c_n) - \hat{f}_l^{\,2}\left(\hat{H}_{\ddot{x}_{n-1} \ddot{x}_n, l}\right) \right|^2 \right\} \qquad (4.7)$$

where $f_l(k_n, c_n) = \dfrac{1}{1 - j\,c_n / (m_n \omega_l) - k_n / (m_n \omega_l^2)}$; $\hat{f}_l^{\,1}\left(\hat{H}_{\ddot{x}_n \ddot{x}_{n-1}, l}\right) = 1 - \hat{H}_{\ddot{x}_n \ddot{x}_{n-1}, l}$;

$$\hat{f}_l^{\,2}\left(\hat{H}_{\ddot{x}_{n-1} \ddot{x}_n, l}\right) = 1 - 1 \big/ \hat{H}_{\ddot{x}_{n-1} \ddot{x}_n, l} \, .$$

where $\hat{H}_{\ddot{x}_n \ddot{x}_{n-1}, l}$ and $\hat{H}_{\ddot{x}_{n-1} \ddot{x}_n, l}$ stand for the estimated transfer functions from the noisy measurements $\hat{\ddot{x}}_{n-1}$ and $\hat{\ddot{x}}_n$ using the method given in Equation (4.4) at frequency ω_l. At the frequency ω_l, which measurement, $\hat{f}_l^{\,1}(\hat{H}_{\ddot{x}_n \ddot{x}_{n-1}, l})$ or $\hat{f}_l^{\,2}(\hat{H}_{\ddot{x}_{n-1} \ddot{x}_n, l})$, will be used in the identification problem (4.7) depends on which structural response, $\ddot{x}_n$ or $\ddot{x}_{n-1}$, has smaller NSR at that frequency. If it is assumed that the noise level for every measured structural responses are same (the term in the numerator of NSR), then the above criterion can be simplified to chose the structural response which has larger power spectrum (the term in the denominator of NSR) at the frequency ω_l in formulating the identification problem (4.7).

4.3.2 Non-top Story Identification

Following a similar procedure, the key identification equation for the i^{th} non-top story substructure (Equation 3.9) can be rewritten into the following three equations by using different structural responses as the system input.

$$\frac{1}{1-jc_i/(m_i\omega)-k_i/(m_i\omega^2)}=\frac{1-H_{\ddot{x}_i\ddot{x}_{i-1}}}{1+\left(H_{\ddot{x}_{i+1}\ddot{x}_{i-1}}-H_{\ddot{x}_i\ddot{x}_{i-1}}\right)\left[jc_{i+1}/(m_i\omega)+k_{i+1}/(m_i\omega^2)\right]} \tag{4.8}$$

$$\frac{1}{1-jc_i/(m_i\omega)-k_i/(m_i\omega^2)}=\frac{H_{\ddot{x}_{i-1}\ddot{x}_i}-1}{H_{\ddot{x}_{i-1}\ddot{x}_i}+\left(H_{\ddot{x}_{i+1}\ddot{x}_i}-1\right)\left[jc_{i+1}/(m_i\omega)+k_{i+1}/(m_i\omega^2)\right]} \tag{4.9}$$

$$\frac{1}{1-jc_i/(m_i\omega)-k_i/(m_i\omega^2)}=\frac{H_{\ddot{x}_{i-1}\ddot{x}_{i+1}}-H_{\ddot{x}_i\ddot{x}_{i+1}}}{H_{\ddot{x}_{i-1}\ddot{x}_{i+1}}+\left(1-H_{\ddot{x}_i\ddot{x}_{i+1}}\right)\left[jc_{i+1}/(m_i\omega)+k_{i+1}/(m_i\omega^2)\right]} \tag{4.10}$$

where $H_{\ddot{x}_k\ddot{x}_j}$ denotes the transfer function from the response $\ddot{x}_j$ to the response $\ddot{x}_k$. Based on these three equations, the new substructure identification problem for the i^{th} non-top story substructure can be formulated as.

$$\underset{k_i,c_i}{\arg\min}\quad J(k_i,c_i)=\sum_{l=1}^{N}\left\{\begin{array}{l}\left|g_l(k_i,c_i)-\hat{g}_l^{\,1}(\hat{H}_{\ddot{x}_i\ddot{x}_{i-1},l},\hat{H}_{\ddot{x}_{i+1}\ddot{x}_{i-1},l})\right|^2 \text{ or}\\ \left|g_l(k_i,c_i)-\hat{g}_l^{\,2}(\hat{H}_{\ddot{x}_{i-1}\ddot{x}_i,l},\hat{H}_{\ddot{x}_{i+1}\ddot{x}_i,l})\right|^2 \text{ or}\\ \left|g_l(k_i,c_i)-\hat{g}_l^{\,3}(\hat{H}_{\ddot{x}_{i-1}\ddot{x}_{i+1},l},\hat{H}_{\ddot{x}_i\ddot{x}_{i+1},l})\right|^2\end{array}\right\} \tag{4.11}$$

where $g_l(k_i,c_i)=\dfrac{1}{1-jc_i/(m_i\omega_l)-k_i/(m_i\omega_l^2)}$

$$\hat{g}_l^{\,1}\left(\hat{H}_{\ddot{x}_i\ddot{x}_{i-1},l},\hat{H}_{\ddot{x}_{i+1}\ddot{x}_{i-1},l}\right)=\frac{1-\hat{H}_{\ddot{x}_i\ddot{x}_{i-1},l}}{1+(\hat{H}_{\ddot{x}_{i+1}\ddot{x}_{i-1},l}-\hat{H}_{\ddot{x}_i\ddot{x}_{i-1},l})\left[jc_{i+1}/(m_i\omega_l)+k_{i+1}/(m_i\omega_l^2)\right]}$$

$$\hat{g}_l^{\,2}\left(\hat{H}_{\ddot{x}_{i-1}\ddot{x}_i,l},\hat{H}_{\ddot{x}_{i+1}\ddot{x}_i,l}\right)=\frac{\hat{H}_{\ddot{x}_{i-1}\ddot{x}_i,l}-1}{\hat{H}_{\ddot{x}_{i-1}\ddot{x}_i,l}+(\hat{H}_{\ddot{x}_{i+1}\ddot{x}_i,l}-1)\left[jc_{i+1}/(m_i\omega_l)+k_{i+1}/(m_i\omega_l^2)\right]}$$

$$\hat{g}_l^{\,3}\left(\hat{H}_{\ddot{x}_{i-1}\ddot{x}_{i+1},l},\hat{H}_{\ddot{x}_i\ddot{x}_{i+1},l}\right)=\frac{\hat{H}_{\ddot{x}_{i-1}\ddot{x}_{i+1},l}-\hat{H}_{\ddot{x}_i\ddot{x}_{i+1},l}}{\hat{H}_{\ddot{x}_{i-1}\ddot{x}_{i+1},l}+(1-\hat{H}_{\ddot{x}_i\ddot{x}_{i+1},l})\left[jc_{i+1}/(m_i\omega_l)+k_{i+1}/(m_i\omega_l^2)\right]}$$

where $\hat{H}_{\ddot{x}_k\ddot{x}_j,l}$ denotes the estimated transfer function from the measured response $\hat{\ddot{x}}_j$ to the measured response $\hat{\ddot{x}}_k$ at frequency ω_l by using the averaging method in Equation (4.4). Which measurement ($\hat{g}_l^{\,1}(\hat{H}_{\ddot{x}_i\ddot{x}_{i-1},l},\hat{H}_{\ddot{x}_{i+1}\ddot{x}_{i-1},l})$, $\hat{g}_l^{\,2}(\hat{H}_{\ddot{x}_{i-1}\ddot{x}_i,l},\hat{H}_{\ddot{x}_{i+1}\ddot{x}_i,l})$ or $\hat{g}_l^{\,3}(\hat{H}_{\ddot{x}_{i-1}\ddot{x}_{i+1},l},\hat{H}_{\ddot{x}_i\ddot{x}_{i+1},l})$) will be used in the identification problem (4.11) at the frequency ω_l depends on which structural response ($\ddot{x}_{i-1}$, $\ddot{x}_i$ or $\ddot{x}_{i+1}$) has the largest power spectrum at that frequency.

4.4 Identification Error Analysis

In this section, the identification error analysis method proposed in section 3.2 is used to analyze the identification error of the newly proposed TF_SUBID method.

4.4.1 Top Story Identification Error

Since the optimization problem (4.7) has two possible measurements, $\hat{f}_l^{\,1}(\hat{H}_{\ddot{x}_n\ddot{x}_{n-1},l})$ and $\hat{f}_l^{\,2}(\hat{H}_{\ddot{x}_{n-1}\ddot{x}_n,l})$, that can be used in the identification at each frequency, and since a different choice may be used in the identification at different frequencies, the identification error analysis method proposed in the section 3.2 cannot be directly applied here. However, the proposed selection algorithm, choosing which transfer function is used in the identification at each frequency, is designed to make the identification results more accurate. Therefore, the identification errors for identification problem (4.7) should be less than the errors if either of the two transfer functions ($\hat{f}_l^{\,1}(\hat{H}_{\ddot{x}_n\ddot{x}_{n-1},l})$ and $\hat{f}_l^{\,2}(\hat{H}_{\ddot{x}_{n-1}\ddot{x}_n,l})$) were used exclusively. Using the error analysis method proposed in the section 3.2, the identification errors using either of the two measurement exclusively in the identification could be calculated, which will serve as some upper bound of the identification error for identification problem (4.7).

Similar to the identification error analysis for the Fourier transform based method in Chapter 3, the error analysis for the new method is also carried out for the relative identification errors of the structural parameters. Using the relative parameter values, identification problem (4.7) is rewritten into two separate identification problems (4.12 and 4.13), in each of which one of the two transfer functions is exclusively used.

$$\underset{\beta_{kn},\beta_{cn}}{\arg\min} \quad J(\beta_{kn},\beta_{cn}) = \sum_{l=1}^{s} \left| f_l(\beta_{kn},\beta_{cn}) - \hat{f}_l^{\,1}(\hat{H}_{\ddot{x}_n\ddot{x}_{n-1},l}) \right|^2 \tag{4.12}$$

where $f_l(\beta_{kn},\beta_{cn}) = \dfrac{1}{1-\beta_{cn}\, j\, c_n/(m_n\omega_l) - \beta_{kn}\, k_n/(m_n\omega_l^2)}$,

$\hat{f}_l^{\,1}\left(\hat{H}_{\ddot{x}_n\ddot{x}_{n-1},l}\right) = 1-\hat{H}_{\ddot{x}_n\ddot{x}_{n-1},l} = 1-\gamma_{n-1,l}H_{\ddot{x}_n\ddot{x}_{n-1},l}$, where $\gamma_{n-1,l} = \hat{H}_{\ddot{x}_n\ddot{x}_{n-1},l} \big/ H_{\ddot{x}_n\ddot{x}_{n-1},l}$

$$\underset{\beta_{kn},\beta_{cn}}{\arg\min} \quad J(\beta_{kn},\beta_{cn}) = \sum_{l=1}^{s} \left| f_l(\beta_{kn},\beta_{cn}) - \hat{f}_l^{\,2}(\hat{H}_{\ddot{x}_{n-1}\ddot{x}_n,l}) \right|^2 \tag{4.13}$$

where $f_l(\beta_{kn},\beta_{cn}) = \dfrac{1}{1-\beta_{cn}\, j\, c_n/(m_n\omega_l) - \beta_{kn}\, k_n/(m_n\omega_l^2)}$,

$\hat{f}_l^{\,2}\left(\hat{H}_{\ddot{x}_n\ddot{x}_{n-1},l}\right) = 1-1\big/\hat{H}_{\ddot{x}_{n-1}\ddot{x}_n,l} = 1-1\big/(\gamma_{n,l}H_{\ddot{x}_{n-1}\ddot{x}_n,l})$, where $\gamma_{n,l} = \hat{H}_{\ddot{x}_{n-1}\ddot{x}_n,l} \big/ H_{\ddot{x}_{n-1}\ddot{x}_n,l}$.

a) *The identification errors for identification problem 4.12*

Following the error analysis procedure proposed in section 3.2,

$$\mathbf{h}_l = \left[\frac{\partial f_l}{\partial \beta_{kn}} \quad \frac{\partial f_l}{\partial \beta_{cn}} \right]_{\beta_\bullet = 1} \\ = \left[\frac{k_n / (m_n \omega_l^2)}{\left[1 - j c_n / (m_n \omega_l) - k_n / (m_n \omega_l^2)\right]^2} \quad \frac{j c_n / (m_n \omega_l)}{\left[1 - j c_n / (m_n \omega_l) - k_n / (m_n \omega_l^2)\right]^2} \right] \tag{4.14}$$

$$\hat{\mathbf{h}}_l = \left[\frac{\partial \hat{f}_l^1}{\partial \gamma_{n-1,l}} \right]_{\gamma_{n-1,l} = 1} = \left[-H_{\ddot{x}_n \ddot{x}_{n-1},l} \right] \tag{4.15}$$

Rearranging Equation (4.5) gives both to the following

$$H_{\ddot{x}_n \ddot{x}_{n-1},l} = \frac{- j c_n / (m_n \omega_l) - k_n / (m_n \omega_l^2)}{1 - j c_n / (m_n \omega_l) - k_n / (m_n \omega_l^2)} \tag{4.16}$$

$$\frac{1}{(1 - H_{\ddot{x}_n \ddot{x}_{n-1},l}) \left[1 - j c_n / (m_n \omega_l) - k_n / (m_n \omega_l^2)\right]} = 1 \tag{4.17}$$

Put the result of Equations (4.16) and (4.17) back into Equation (4.15) to get

$$\hat{\mathbf{h}}_l = \frac{1}{(1 - H_{\ddot{x}_n \ddot{x}_{n-1},l})} \frac{j c_n / (m_n \omega_l) + k_n / (m_n \omega_l^2)}{\left[1 - j c_n / (m_n \omega_l) - k_n / (m_n \omega_l^2)\right]^2} \tag{4.18}$$

Using the results of the identification error analysis in Equation (3.19) as well as the relation that the true transfer function equals the ratio between the Fourier transform of the noiseless input and output signals, the approximate relative identification errors of identification problem (4.12) becomes

$$\begin{bmatrix} \theta_{kn}^{(1)} \\ \theta_{cn}^{(1)} \end{bmatrix} \approx \sum_{l=1}^{N} \mathrm{Re} \left\{ \begin{bmatrix} W_{11,l} \\ W_{21,l} \end{bmatrix} \cdot \frac{\ddot{X}_{n-1,l} \left[\gamma_{n-1,l} - 1\right]}{(\ddot{X}_{n,l} - \ddot{X}_{n-1,l})} \right\} \tag{4.19}$$

where the superscript (1) on the left side of the above equation is used to denote that this identification error is calculated by exclusively using the transfer function $\hat{f}_l^{\,1}(\hat{H}_{\ddot{x}_n\ddot{x}_{n-1},l})$. The expressions of the deterministic factors $W_{11,l}$ and $W_{21,l}$ are give in Equation (3.26).

From the results of the transfer function estimation in the section 4.2, it can be obtained that $\gamma_{n-1,l} = 1/(1+\alpha_{n-1,l})$, where $\alpha_{n-1,l} = \mathrm{E}\left[|\, N_{n-1,l}\,|^2\right] / \mathrm{E}\left[|\, \ddot{X}_{n-1,l}\,|^2\right]$ is the NSR of the structural response $\ddot{x}_{n-1}$ at the frequency ω_l. Using the approximation that $1/(1+\alpha_{n-1,l}) \approx 1-\alpha_{n-1,l}$ if $\alpha_{n-1,l} << 1$, the identification errors in Equation (4.19) are simplified as

$$\begin{bmatrix} \theta_{kn}^{(1)} \\ \theta_{cn}^{(1)} \end{bmatrix} \approx \sum_{l=1}^{N} \mathrm{Re}\left\{ \begin{bmatrix} W_{11,l} \\ W_{21,l} \end{bmatrix} \cdot \frac{\ddot{X}_{n-1,l}\left[-\alpha_{n-1,l}\right]}{(\ddot{X}_{n,l} - \ddot{X}_{n-1,l})} \right\} \tag{4.20}$$

b) The identification errors for problem 4.13

Following a similar procedure, the identification error for problem (4.13) can be derived as follows.

$$\begin{aligned} \mathbf{h}_l &= \left[\frac{\partial f_l}{\partial \beta_{kn}} \quad \frac{\partial f_l}{\partial \beta_{cn}} \right]_{\beta_\bullet = 1} \\ &= \left[\frac{k_n/(m_n\omega_l^2)}{\left[1 - j\,c_n/(m_n\omega_l) - k_n/(m_n\omega_l^2)\right]^2} \quad \frac{jc_n/(m_n\omega_l)}{\left[1 - j\,c_n/(m_n\omega_l) - k_n/(m_n\omega_l^2)\right]^2} \right] \end{aligned} \tag{4.21}$$

$$\hat{\mathbf{h}}_l = \left[\frac{\partial \hat{f}_l^{\,2}}{\partial \gamma_{n,l}} \right]_{\gamma_{n,l}=1} = \left[1 / H_{\ddot{x}_{n-1}\ddot{x}_n,l} \right] \tag{4.22}$$

Rearranging Equation (4.6) gives both of the following

$$\frac{1}{H_{\ddot{x}_{n-1}\ddot{x}_n,l}} = \frac{-\,j\,c_n/(m_n\omega_l) - k_n/(m_n\omega_l^2)}{1 - j\,c_n/(m_n\omega_l) - k_n/(m_n\omega_l^2)} \tag{4.23}$$

$$\frac{1}{(1-1/H_{\ddot{x}_n\ddot{x}_{n-1},l})\left[1-jc_n/(m_n\omega_l)-k_n/(m_n\omega_l^2)\right]}=1 \tag{4.24}$$

Put the result of Equations (4.22) and (4.24) back into (4.22)

$$\hat{\mathbf{h}}_l=\frac{1}{(1-1/H_{\ddot{x}_n\ddot{x}_{n-1},l})}\frac{-jc_n/(m_n\omega_l)-k_n/(m_n\omega_l^2)}{\left[1-jc_n/(m_n\omega_l)-k_n/(m_n\omega_l^2)\right]^2} \tag{4.25}$$

Using the result of (3.19), the approximate relative identification error of the identification problem (4.13) becomes

$$\begin{bmatrix}\theta_{kn}^{(2)}\\ \theta_{cn}^{(2)}\end{bmatrix}\approx\sum_{l=1}^{N}\mathrm{Re}\left\{\begin{bmatrix}W_{11,l}\\ W_{21,l}\end{bmatrix}\cdot\frac{\ddot{X}_{n-1,l}\left[\alpha_{n,l}\right]}{(\ddot{X}_{n,l}-\ddot{X}_{n-1,l})}\right\} \tag{4.26}$$

where the superscript (2) on the left side of Equation (4.26) is used to denote that this identification error is calculated by only using the second transfer function $\hat{f}_l^{\,2}\left(\hat{H}_{\ddot{x}_{n-1}\ddot{x}_n,l}\right)$; $\alpha_{n,l}=\mathrm{E}\left[\| N_{n,l}|^2\right]/\mathrm{E}\left[\|\ddot{X}_{n,l}|^2\right]$ is the NSR of the structural response $\ddot{x}_n$ at the frequency ω_l; the expressions of the deterministic factors $W_{11,l}$ and $W_{21,l}$ are given in Equation (3.26).

c) Comments on the results of the identification error analysis

As noted in Chapter 3, factors $W_{11,l}$ and $W_{21,l}$ in Equation (4.20) and (4.26) are significantly large only near the n^{th} story substructure natural frequency $\omega_{n0}=\sqrt{k_n/m_i}$; thus, the identification errors are mainly determined by the measurement uncertainties near frequency ω_{n0}. To reduce the identification error, the uncertainty terms, $\alpha_{n-1,l}$ and $\alpha_{n,l}$, should be as small as possible in that frequency range; alternately, the corresponding structural responses $\mathrm{E}\left[\|\ddot{X}_{n-1,l}|^2\right]$ and $\mathrm{E}\left[\|\ddot{X}_{n,l}|^2\right]$ (the denominator of the uncertainty terms) should be as large as possible in the same frequency range.

Moreover, Equations (4.20) and (4.26) contain some of the same terms such as deterministic factors $W_{11,l}$ and $W_{21,l}$ as well as the frequency response ratio $\ddot{X}_{n-1,l} \big/ (\ddot{X}_{n,l} - \ddot{X}_{n-1,l})$; hence, comparing the magnitude of the identification errors calculated by these two equations simplifies to comparing the magnitudes of the uncertainty terms ($\alpha_{n-1,l}$ and $\alpha_{n,l}$) in these equations. Assuming that the power spectra of measurement noise at different locations are same (the numerator of the uncertainty terms $\alpha_{n-1,l}$ and $\alpha_{n,l}$, $\mathrm{E}\big[| N_{n-1,l} |^2\big] = \mathrm{E}\big[| N_{n,l} |^2\big]$, are same), the identification errors in the two equation are determined by the magnitudes of power spectra $\mathrm{E}\big[| \ddot{X}_{n-1,l} |^2\big]$ and $\mathrm{E}\big[| \ddot{X}_{n,l} |^2\big]$ (the denominators of $\alpha_{n-1,l}$ and $\alpha_{n,l}$).

From Equation (3.7), it can be easily derived that

$$\ddot{X}_{n,l} = \frac{j c_n \big/ (m_n \omega_l) + k_n \big/ (m_n \omega_l^2)}{1 - j c_n \big/ (m_n \omega_l) - k_n \big/ (m_n \omega_l^2)} \ddot{X}_{n-1,l} \tag{4.27}$$

Then, the power spectra $\mathrm{E}\big[| \ddot{X}_{n-1,l} |^2\big]$ and $\mathrm{E}\big[| \ddot{X}_{n,l} |^2\big]$ have the following relation

$$\mathrm{E}\big[| \ddot{X}_{n,l} |^2\big] = \left| \frac{j c_n \big/ (m_n \omega_l) + k_n \big/ (m_n \omega_l^2)}{1 - j c_n \big/ (m_n \omega_l) - k_n \big/ (m_n \omega_l^2)} \right|^2 \mathrm{E}\big[| \ddot{X}_{n-1,l} |^2\big] \tag{4.28}$$

Since the deterministic transfer function on the right side of Equation (4.28) (the part in front of $\mathrm{E}\big[| \ddot{X}_{n-1,l} |^2\big]$) is significantly larger than one near the substructure natural frequency ω_{n0}, the power spectrum of the top story response, $\mathrm{E}\big[| \ddot{X}_{n,l} |^2\big]$, is much larger than that of the story below $\mathrm{E}\big[| \ddot{X}_{n-1,l} |^2\big]$ near the substructure natural frequency ω_{n0}. As a result, the top story response $\ddot{X}_{n,l}$ will be exclusively selected as the system input to formulate the identification problem near the substructure natural frequency ω_{n0} (the key frequency range to determine the identification errors).

Moreover, using the relation given in Equation (4.27), Equation (4.26) can be rewritten as

$$\begin{bmatrix} \theta_{kn}^{(2)} \\ \theta_{cn}^{(2)} \end{bmatrix} \approx \sum_{l=1}^{N} \mathrm{Re}\left\{ \begin{bmatrix} W_{12,l} \\ W_{22,l} \end{bmatrix} \cdot \frac{\ddot{X}_{n,l}\left[-\alpha_{n,l}\right]}{(\ddot{X}_{n,l} - \ddot{X}_{n-1,l})} \right\} \tag{4.29}$$

where the expressions of the deterministic factors $W_{12,l}$ and $W_{22,l}$ are give in Equation (3.26).

d) Comparison of the Identification Errors between TF_SUBID and FFT_SUBID methods (non-top story)

Comparing the identification errors of the TF_SUBID method for the top story parameters in Equations (4.20) and (4.29) with the corresponding identification errors of the FFT_SUBID method in Equation (3.26), it is found that the identification errors in both methods share the same weighting factors ($W_{11,l}$, $W_{21,l}$, $W_{12,l}$ and $W_{22,l}$) as well as the frequency response of interstory acceleration $(\ddot{X}_{n,l} - \ddot{X}_{n-1,l})$ in the denominator of the uncertainty terms. Therefore, the comparison of the two methods simplifies to comparing the numerator of the uncertainty terms in these two methods, $N_{j,l}$ and $\ddot{X}_{j,l}\alpha_{j,l}$ $(j = n-1, n)$. Because these two quantities are both zero-mean complex random variables, the variances of these random variables are compared by computing their ratio:

$$\mathrm{E}\left[\left|\ddot{X}_{j,l}\alpha_{j,l}\right|^2\right] \Big/ \mathrm{E}\left[\left|N_{j,l}\right|^2\right] = \alpha_{j,l}^{\ 2} \cdot \mathrm{E}\left[\left|\ddot{X}_{j,l}\right|^2\right] \Big/ \mathrm{E}\left[\left|N_{j,l}\right|^2\right] = \frac{\alpha_{j,l}^{\ 2}}{\alpha_{j,l}} = \alpha_{j,l} \tag{4.30}$$

where Equation (4.30) uses the definition of the noise-to-signal ratio (NSR), $\mathrm{E}\left[|\ddot{X}_{j,l}|^2\right] / \mathrm{E}\left[|N_{j,l}|^2\right] = 1/\alpha_{j,l}$, in Chapter 3. Since $\alpha_{j,l}$ is, in general, much smaller than unity, the variance of $\ddot{X}_{j,l}\alpha_{j,l}$ is much smaller than that of $N_{j,l}$, implying that for the top story parameter identification, the TF_SUBID method will provide much more accurate identification results than the FFT_SUBID method.

Moreover, there is a common term, the frequency response of the top story interstory acceleration $(\ddot{X}_{n,l} - \ddot{X}_{n-1,l})$, in the numerator of all uncertainty terms. Al factors $W_{ij,l}$ are significantly large near the substructure natural frequency ω_{n0}. Hence, significantly amplifying the interstory response $(\ddot{X}_{n,l} - \ddot{X}_{n-1,l})$ near the substructure natural frequency ω_{n0} will greatly improve the identification error. This is the same conclusion that was obtained for the FFT_SUBID method.

4.4.2 Non-top Story Identification Error

Similar to what has been done for the top story substructure identification problem, Equation (4.11) can be rewritten into the following three separate identification problems, each of which exclusively uses one of the three measurements in the identification process.

In the parameter identification of the i^{th} story ($i < n$), the identified parameters of the $(i+1)^{\text{th}}$ story are used; thus, the parameter identification error of the $(i+1)^{\text{th}}$ story from the previous step will inevitably affect the accuracy of the current step identification and should be included in the identification error analysis. Using the relative parameters β_{ki}

and β_{ci}, the identification problem in (4.11) that uses the first transfer function forms $\hat{g}_l^{\,1}$ exclusively could be rewritten as

$$\underset{\beta_{ki},\beta_{ci}}{\arg\min} \quad J(\beta_{ki},\beta_{ci}) = \sum_{l=1}^{N}\left\{\left|g_l(\beta_{ki},\beta_{ci}) - \hat{g}_l^{\,1}(\hat{H}_{\ddot{x}_i\ddot{x}_{i-1},l}, \hat{H}_{\ddot{x}_{i+1}\ddot{x}_{i-1},l}, \beta_{k(i+1)}, \beta_{c(i+1)})\right|^2\right\} \tag{4. 31}$$

where $g_l(k_i, c_i) = \dfrac{1}{1 - j\,c_i/(m_i\omega_l) - k_i/(m_i\omega_l^2)}$,

$$\hat{g}_l^{\,1}\left(\hat{H}_{\ddot{x}_i\ddot{x}_{i-1},l}, \hat{H}_{\ddot{x}_{i+1}\ddot{x}_{i-1},l}, \beta_{k(i+1)}, \beta_{c(i+1)}\right) = \frac{1 - \hat{H}_{\ddot{x}_i\ddot{x}_{i-1},l}}{1 + (\hat{H}_{\ddot{x}_{i+1}\ddot{x}_{i-1},l} - \hat{H}_{\ddot{x}_i\ddot{x}_{i-1},l})\left[\beta_{c(i+1)}\, j c_{i+1}/(m_i\omega_l) + \beta_{k(i+1)}\, k_{i+1}/(m_i\omega_l^2)\right]}$$

From the results of the transfer function estimation in section 4.2, it can be shown that $\hat{H}_{\ddot{x}_i\ddot{x}_{i-1},l} / H_{\ddot{x}_i\ddot{x}_{i-1},l} = \hat{H}_{\ddot{x}_{i+1}\ddot{x}_{i-1},l} / H_{\ddot{x}_{i+1}\ddot{x}_{i-1},l} = \gamma_{i-1,l}$ and $\gamma_{i-1,l} = 1/(1 + \alpha_{i-1,l})$ where $\alpha_{i-1,l} = \mathrm{E}\left[\| N_{i-1,l} |^2\right] / \mathrm{E}\left[\| \ddot{X}_{i-1,l} |^2\right]$ is the NSR of structural response $\ddot{x}_{i-1}$ at frequency ω_l. Then, identification problem (4.31) can be simplified as

$$\underset{\beta_{ki},\beta_{ci}}{\arg\min} \quad J(\beta_{ki},\beta_{ci}) = \sum_{l=1}^{N}\left\{\left|g_l(\beta_{ki},\beta_{ci}) - \hat{g}_l^{\,1}(\gamma_{i-1,l}, \beta_{k(i+1)}, \beta_{c(i+1)})\right|^2\right\} \tag{4.32}$$

where $g_l(k_i, c_i) = \dfrac{1}{1 - j\,c_i/(m_i\omega_l) - k_i/(m_i\omega_l^2)}$,

$$\hat{g}_l^{\,1}\left(\gamma_{i-1,l}, \beta_{k(i+1)}, \beta_{c(i+1)}\right) = \frac{1 - \gamma_{i-1,l} H_{\ddot{x}_i\ddot{x}_{i-1},l}}{1 + (\gamma_{i-1,l} H_{\ddot{x}_{i+1}\ddot{x}_{i-1},l} - \gamma_{i-1,l} H_{\ddot{x}_i\ddot{x}_{i-1},l})\left[\beta_{c(i+1)}\, j \cdot c_{i+1}/(m_i\omega_l) + \beta_{k(i+1)}\, k_{i+1}/(m_i\omega_l^2)\right]}$$

Similarly, the other two identification problems for identification problem (4.11), exclusively using the second and third transfer function forms, can be formulated as

$$\underset{\beta_{ki},\beta_{ci}}{\arg\min} \quad J(\beta_{ki},\beta_{ci}) = \sum_{l=1}^{N}\left\{\left|g_l(\beta_{ki},\beta_{ci}) - \hat{g}_l^{\,2}(\gamma_{i,l},\beta_{k(i+1)},\beta_{c(i+1)})\right|^2\right\} \tag{4.33}$$

where $g_l(k_i, c_i) = \dfrac{1}{1 - j\,c_i/(m_i\omega_l) - k_i/(m_i\omega_l^2)}$;

$$\hat{g}_l^{\,2}(\gamma_{i,l},\beta_{k(i+1)},\beta_{c(i+1)}) = \frac{\gamma_{i,l}H_{\ddot{x}_{i-1}\ddot{x}_i,l} - 1}{\gamma_{i,l}H_{\ddot{x}_{i-1}\ddot{x}_i,l} + (\gamma_{i,l}H_{\ddot{x}_{i+1}\ddot{x}_i,l} - 1)\left[\beta_{c(i+1)}\,j\cdot c_{i+1}/(m_i\omega_l) + \beta_{k(i+1)}\,k_{i+1}/(m_i\omega_l^2)\right]}.$$

$$\underset{\beta_{ki},\beta_{ci}}{\arg\min} \quad J(\beta_{ki},\beta_{ci}) = \sum_{l=1}^{N}\left\{\left|g_l(\beta_{ki},\beta_{ci}) - \hat{g}_l^{\,3}(\gamma_{i+1,l},\beta_{k(i+1)},\beta_{c(i+1)})\right|^2\right\} \tag{4.34}$$

where $g_l(k_i, c_i) = \dfrac{1}{1 - j\,c_i/(m_i\omega_l) - k_i/(m_i\omega_l^2)}$;

$$\hat{g}_l^{\,3}(\gamma_{i+1,l},\beta_{k(i+1)},\beta_{c(i+1)}) = \frac{\gamma_{i+1,l}(H_{\ddot{x}_{i-1}\ddot{x}_{i+1},l} - H_{\ddot{x}_i\ddot{x}_{i+1},l})}{\gamma_{i+1,l}H_{\ddot{x}_{i-1}\ddot{x}_{i+1},l} + (1 - \gamma_{i+1,l}H_{\ddot{x}_i\ddot{x}_{i+1},l})\left[\beta_{c(i+1)}\,jc_{i+1}/(m_i\omega_l) + \beta_{k(i+1)}\,k_{i+1}/(m_i\omega_l^2)\right]}.$$

Using the identification error analysis method proposed in section 3.2, the identification errors of problems (4.32) ~ (4.34) are obtained respectively.

a) The identification errors of identification problem 4.32

$$\mathbf{h}_l = \left[\frac{\partial g_l}{\partial \beta_{ki}} \quad \frac{\partial g_l}{\partial \beta_{ci}}\right]_{\beta_\bullet = 1} = \begin{bmatrix} \dfrac{k_i/(m_i\omega_l^2)}{\left[1 - j\,c_i/(m_i\omega_l) - k_i/(m_i\omega_l^2)\right]^2} \\ \dfrac{jc_i/(m_i\omega_l)}{\left[1 - j\,c_i/(m_i\omega_l) - k_i/(m_i\omega_l^2)\right]^2} \end{bmatrix}^{\mathrm{T}} \tag{4.35}$$

$$
\hat{\mathbf{h}}_l^1 = \left[\frac{\partial \hat{g}_l^1}{\partial \gamma_{i-1,l}} \quad \frac{\partial \hat{g}_l^1}{\partial \beta_{k(i+1)}} \quad \frac{\partial \hat{g}_l^1}{\partial \beta_{c(i+1)}} \right]_{\substack{\gamma_{i-1,l}=1 \\ \beta_\bullet = 1}}
= \left[\begin{array}{c}
\dfrac{-H_{\ddot{x}_i\ddot{x}_{i-1},l} - (H_{\ddot{x}_{i+1}\ddot{x}_{i-1},l} - H_{\ddot{x}_i\ddot{x}_{i-1},l})\left[jc_{i+1}/(m_i\omega_l) + k_{i+1}/(m_i\omega_l^2)\right]}{\left\{1 + (H_{\ddot{x}_{i+1}\ddot{x}_{i-1},l} - H_{\ddot{x}_i\ddot{x}_{i-1},l})\left[jc_{i+1}/(m_i\omega_l) + k_{i+1}/(m_i\omega_l^2)\right]\right\}^2} \\
\dfrac{(1 - H_{\ddot{x}_i\ddot{x}_{i-1},l})(H_{\ddot{x}_{i+1}\ddot{x}_{i-1},l} - H_{\ddot{x}_i\ddot{x}_{i-1},l})\, k_{i+1}/(m_i\omega_l^2)}{\left\{1 + (H_{\ddot{x}_{i+1}\ddot{x}_{i-1},l} - H_{\ddot{x}_i\ddot{x}_{i-1},l})\left[jc_{i+1}/(m_i\omega_l) + k_{i+1}/(m_i\omega_l^2)\right]\right\}^2} \\
\dfrac{(1 - H_{\ddot{x}_i\ddot{x}_{i-1},l})(H_{\ddot{x}_{i+1}\ddot{x}_{i-1},l} - H_{\ddot{x}_i\ddot{x}_{i-1},l})\, jc_{i+1}/(m_i\omega_l)}{\left\{1 + (H_{\ddot{x}_{i+1}\ddot{x}_{i-1},l} - H_{\ddot{x}_i\ddot{x}_{i-1},l})\left[jc_{i+1}/(m_i\omega_l) + k_{i+1}/(m_i\omega_l^2)\right]\right\}^2}
\end{array} \right]^{\mathrm{T}} \tag{4.36}
$$

Rearranging Equation (4.8) gives

$$
\begin{aligned}
&(1 - H_{\ddot{x}_i\ddot{x}_{i-1}})\left[1 - j\,c_i/(m_i\omega) - k_i/(m_i\omega^2)\right] = \\
&1 + (H_{\ddot{x}_{i+1}\ddot{x}_{i-1}} - H_{\ddot{x}_i\ddot{x}_{i-1}})\left[jc_{i+1}/(m_i\omega) + k_{i+1}/(m_i\omega^2)\right]
\end{aligned} \tag{4.37}
$$

Replacing the terms in Equation (4.36), which equal the right side of Equation (4.37), by the left side of Equation (4.37), Equation (4.36) are simplified as

$$
\hat{\mathbf{h}}_l^1 = \left[\begin{array}{c}
\dfrac{jc_i/(m_i\omega_l) + k_i/(m_i\omega_l^2)}{(1 - H_{\ddot{x}_i\ddot{x}_{i-1},l})\left[1 - j\,c_i/(m_i\omega_l) - k_i/(m_i\omega_l^2)\right]^2} \\
\dfrac{(H_{\ddot{x}_{i+1}\ddot{x}_{i-1},l} - H_{\ddot{x}_i\ddot{x}_{i-1},l})\, k_{i+1}/(m_i\omega_l^2)}{(1 - H_{\ddot{x}_i\ddot{x}_{i-1},l})\left[1 - j\,c_i/(m_i\omega_l) - k_i/(m_i\omega_l^2)\right]^2} \\
\dfrac{(H_{\ddot{x}_{i+1}\ddot{x}_{i-1},l} - H_{\ddot{x}_i\ddot{x}_{i-1},l})\, jc_{i+1}/(m_i\omega_l)}{(1 - H_{\ddot{x}_i\ddot{x}_{i-1},l})\left[1 - j\,c_i/(m_i\omega_l) - k_i/(m_i\omega_l^2)\right]^2}
\end{array} \right]^{\mathrm{T}} \tag{4.38}
$$

Using the results of the identification error analysis in Equation (3.19) as well as the relation that the true transfer function equals the ratio between the Fourier transform of the noiseless input and output signals, the identification error for problem (4.32) can be obtained as

$$\begin{bmatrix} \theta_{ki}^{(1)} \\ \theta_{ci}^{(1)} \end{bmatrix} \approx \sum_{l=1}^{N} \mathrm{Re}\left\{ \begin{bmatrix} U_{11,l} \\ U_{12,l} \end{bmatrix} \frac{\ddot{X}_{i-1,l}\left[-\alpha_{i-1,l}\right]}{(\ddot{X}_{i,l} - \ddot{X}_{i-1,l})} \right\} + \sum_{l=1}^{N} \mathrm{Re}\left\{ \begin{bmatrix} U_{14,l} & U_{15,l} \\ U_{24,l} & U_{25,l} \end{bmatrix} \cdot \begin{bmatrix} \dfrac{(\ddot{X}_{i+1,l} - \ddot{X}_{i,l})}{(\ddot{X}_{i,l} - \ddot{X}_{i-1,l})} \theta_{k(i+1)} \\ \dfrac{(\ddot{X}_{i+1,l} - \ddot{X}_{i,l})}{(\ddot{X}_{i,l} - \ddot{X}_{i-1,l})} \theta_{c(i+1)} \end{bmatrix} \right\} \tag{4.39}$$

where the expressions of factors $U_{11,l}$, $U_{21,l}$, $U_{14,l}$, $U_{24,l}$, $U_{15,l}$ and $U_{25,l}$ are given in Equation (3.32).

b) The identification errors of identification problem 4.33

$$\mathbf{h}_l = \begin{bmatrix} \dfrac{\partial g_l}{\partial \beta_{ki}} & \dfrac{\partial g_l}{\partial \beta_{ci}} \end{bmatrix}_{\beta_\bullet = 1} = \begin{bmatrix} \dfrac{k_i/(m_i\omega_l^2)}{\left[1 - j\,c_i/(m_i\omega_l) - k_i/(m_i\omega_l^2)\right]^2} \\ \dfrac{jc_i/(m_i\omega_l)}{\left[1 - j\,c_i/(m_i\omega_l) - k_i/(m_i\omega_l^2)\right]^2} \end{bmatrix}^{\mathrm{T}} \tag{4.40}$$

$$\hat{\mathbf{h}}_l^2 = \begin{bmatrix} \dfrac{\partial \hat{g}_l^2}{\partial \gamma_{i,l}} & \dfrac{\partial \hat{g}_l^2}{\partial \beta_{k(i+1)}} & \dfrac{\partial \hat{g}_l^2}{\partial \beta_{c(i+1)}} \end{bmatrix}_{\substack{\gamma_{i-1,l}=1 \\ \beta_\bullet = 1}}$$

$$= \begin{bmatrix} \dfrac{H_{\ddot{x}_{i-1}\ddot{x}_i,l} + (H_{\ddot{x}_{i+1}\ddot{x}_i,l} - H_{\ddot{x}_{i-1}\ddot{x}_i,l})\left[jc_{i+1}/(m_i\omega_l) + k_{i+1}/(m_i\omega_l^2)\right]}{\left\{H_{\ddot{x}_{i-1}\ddot{x}_i,l} + (H_{\ddot{x}_{i+1}\ddot{x}_i,l} - 1)\left[jc_{i+1}/(m_i\omega_l) + k_{i+1}/(m_i\omega_l^2)\right]\right\}^2} \\ \dfrac{(H_{\ddot{x}_{i-1}\ddot{x}_i,l} - 1)(H_{\ddot{x}_{i+1}\ddot{x}_i,l} - 1)\,k_{i+1}/(m_i\omega_l^2)}{\left\{H_{\ddot{x}_{i-1}\ddot{x}_i,l} + (H_{\ddot{x}_{i+1}\ddot{x}_i,l} - 1)\left[jc_{i+1}/(m_i\omega_l) + k_{i+1}/(m_i\omega_l^2)\right]\right\}^2} \\ \dfrac{(H_{\ddot{x}_{i-1}\ddot{x}_i,l} - 1)(H_{\ddot{x}_{i+1}\ddot{x}_i,l} - 1)\,j \cdot c_{i+1}/(m_i\omega_l)}{\left\{H_{\ddot{x}_{i-1}\ddot{x}_i,l} + (H_{\ddot{x}_{i+1}\ddot{x}_i,l} - 1)\left[jc_{i+1}/(m_i\omega_l) + k_{i+1}/(m_i\omega_l^2)\right]\right\}^2} \end{bmatrix}^{\mathrm{T}} \tag{4.41}$$

Rearranging Equation (4.9) gives

$$\begin{aligned} &(H_{\ddot{x}_{i-1}\ddot{x}_i} - 1)\left[1 - j\,c_i/(m_i\omega) - k_i/(m_i\omega^2)\right] = \\ &H_{\ddot{x}_{i-1}\ddot{x}_i} + (H_{\ddot{x}_{i+1}\ddot{x}_i} - 1)\left[jc_{i+1}/(m_i\omega) + k_{i+1}/(m_i\omega^2)\right] \end{aligned} \tag{4.42}$$

Replacing the terms in Equation (4.41), which equals the right side of Equation (4.42), by the left side of Equation (4.42), Equation (4.31) are simplified as

$$\hat{\mathbf{h}}_l^2 = \begin{bmatrix} \dfrac{1 - j(c_{i+1}+c_i)/(m_i\omega_l) - (k_{i+1}+k_i)/(m_i\omega_l^2)}{(H_{\ddot{x}_{i-1}\ddot{x}_i,l}-1)\left[1 - j\,c_i/(m_i\omega_l) - k_i/(m_i\omega_l^2)\right]^2} \\ \dfrac{(H_{\ddot{x}_{i+1}\ddot{x}_i,l}-1)\,k_{i+1}/(m_i\omega_l^2)}{(H_{\ddot{x}_{i-1}\ddot{x}_i,l}-1)\left[1 - j\,c_i/(m_i\omega_l) - k_i/(m_i\omega_l^2)\right]^2} \\ \dfrac{(H_{\ddot{x}_{i+1}\ddot{x}_i,l}-1)\,jc_{i+1}/(m_i\omega)}{(H_{\ddot{x}_{i-1}\ddot{x}_i,l}-1)\left[1 - j\,c_i/(m_i\omega_l) - k_i/(m_i\omega_l^2)\right]^2} \end{bmatrix}^{\mathrm{T}} \tag{4.43}$$

Using the result of the identification error analysis in Equation (3.19) as well as the relation that the true transfer function equals the ratio between the Fourier transform of the noiseless input and output signals, the identification error for the problem (4.33) can be obtained as

$$\begin{bmatrix} \theta_{ki}^{(2)} \\ \theta_{ci}^{(2)} \end{bmatrix} \approx \sum_{l=1}^{N} \mathrm{Re}\left\{ \begin{bmatrix} U_{21,l} \\ U_{22,l} \end{bmatrix} \frac{\ddot{X}_{i,l}\left[-\alpha_{i,l}\right]}{(\ddot{X}_{i,l} - \ddot{X}_{i-1,l})} \right\} + \sum_{l=1}^{N} \mathrm{Re}\left\{ \begin{bmatrix} U_{14,l} & U_{15,l} \\ U_{24,l} & U_{25,l} \end{bmatrix} \cdot \begin{bmatrix} \dfrac{(\ddot{X}_{i+1,l} - \ddot{X}_{i,l})}{(\ddot{X}_{i,l} - \ddot{X}_{i-1,l})}\theta_{k(i+1)} \\ \dfrac{(\ddot{X}_{i+1,l} - \ddot{X}_{i,l})}{(\ddot{X}_{i,l} - \ddot{X}_{i-1,l})}\theta_{c(i+1)} \end{bmatrix} \right\} \tag{4.44}$$

where the expressions of factors $U_{12,l}$, $U_{22,l}$, $U_{14,l}$, $U_{24,l}$, $U_{15,l}$ and $U_{25,l}$ are given in Equation (3.32).

c) *The identification errors of identification problem 4.34*

$$\mathbf{h}_l = \begin{bmatrix} \dfrac{\partial g_l}{\partial \beta_{ki}} & \dfrac{\partial g_l}{\partial \beta_{ci}} \end{bmatrix}_{\beta_\bullet = 1} = \begin{bmatrix} \dfrac{k_i/(m_i\omega_l^2)}{\left[1 - j\,c_i/(m_i\omega_l^2) - k_i/(m_i\omega_l^2)\right]^2} \\ \dfrac{jc_i/(m_i\omega_l^2)}{\left[1 - j\,c_i/(m_i\omega_l^2) - k_i/(m_i\omega_l^2)\right]^2} \end{bmatrix}^{\mathrm{T}} \tag{4.45}$$

$$
\hat{\mathbf{h}}_l^3 = \left[\frac{\partial \hat{g}_l^3}{\partial \gamma_{i+1,l}} \quad \frac{\partial \hat{g}_l^3}{\partial \beta_{k(i+1)}} \quad \frac{\partial \hat{g}_l^3}{\partial \beta_{c(i+1)}} \right]_{\substack{\gamma_{i-1,l}=1 \\ \beta_\bullet=1}}
$$

$$
= \begin{bmatrix} \dfrac{(H_{\ddot{x}_{i-1}\ddot{x}_{i+1},l} - H_{\ddot{x}_i\ddot{x}_{i+1},l})\left[jc_{i+1}/(m_i\omega_l) + k_{i+1}/(m_i\omega_l^2)\right]}{\left\{H_{\ddot{x}_{i-1}\ddot{x}_{i+1},l} + (1-H_{\ddot{x}_i\ddot{x}_{i+1},l})\left[jc_{i+1}/(m_i\omega_l) + k_{i+1}/(m_i\omega_l^2)\right]\right\}^2} \\ \dfrac{(H_{\ddot{x}_{i-1}\ddot{x}_{i+1},l} - H_{\ddot{x}_i\ddot{x}_{i+1},l})(H_{\ddot{x}_i\ddot{x}_{i+1},l} - 1)\,k_{i+1}/(m_i\omega_l^2)}{\left\{H_{\ddot{x}_{i-1}\ddot{x}_{i+1},l} + (1-H_{\ddot{x}_i\ddot{x}_{i+1},l})\left[jc_{i+1}/(m_i\omega_l) + k_{i+1}/(m_i\omega_l^2)\right]\right\}^2} \\ \dfrac{(H_{\ddot{x}_{i-1}\ddot{x}_{i+1},l} - H_{\ddot{x}_i\ddot{x}_{i+1},l})(H_{\ddot{x}_i\ddot{x}_{i+1},l} - 1)\; jc_{i+1}/(m_i\omega_l)}{\left\{H_{\ddot{x}_{i-1}\ddot{x}_{i+1},l} + (1-H_{\ddot{x}_i\ddot{x}_{i+1},l})\left[jc_{i+1}/(m_i\omega_l) + k_{i+1}/(m_i\omega_l^2)\right]\right\}^2} \end{bmatrix}^{\mathrm{T}} \tag{4.46}
$$

Rearranging Equation (4.10) gives

$$
\begin{aligned} &(H_{\ddot{x}_{i-1}\ddot{x}_{i+1}} - H_{\ddot{x}_i\ddot{x}_{i+1}})\left[1 - j\cdot c_i/(m_i\omega) - k_i/(m_i\omega^2)\right] = \\ &H_{\ddot{x}_{i-1}\ddot{x}_{i+1}} + (1-H_{\ddot{x}_i\ddot{x}_{i+1}})\left[j\cdot c_{i+1}/(m_i\omega) + k_{i+1}/(m_i\omega^2)\right] \end{aligned} \tag{4.47}
$$

Replacing the terms in Equation (4.46), which equals the right side of Equation (4.47), by the left side of Equation (4.47), Equation (4.46) are simplified as

$$
\hat{\mathbf{h}}_l^3 = \begin{bmatrix} \dfrac{1 - j(c_{i+1} + c_i)/(m_i\omega_l) - (k_{i+1} + k_i)/(m_i\omega_l^2)}{(H_{\ddot{x}_{i-1}\ddot{x}_{i+1},l} - H_{\ddot{x}_i\ddot{x}_{i+1},l})\left[1 - j\,c_i/(m_i\omega_l) - k_i/(m_i\omega_l^2)\right]^2} \\ \dfrac{(H_{\ddot{x}_i\ddot{x}_{i+1},l} - 1)\,k_{i+1}/(m_i\omega_l^2)}{(H_{\ddot{x}_{i-1}\ddot{x}_{i+1},l} - H_{\ddot{x}_i\ddot{x}_{i+1},l})\left[1 - j\,c_i/(m_i\omega_l) - k_i/(m_i\omega_l^2)\right]^2} \\ \dfrac{(H_{\ddot{x}_i\ddot{x}_{i+1},l} - 1)\; jc_{i+1}/(m_i\omega)}{(H_{\ddot{x}_{i-1}\ddot{x}_{i+1},l} - H_{\ddot{x}_i\ddot{x}_{i+1},l})\left[1 - j\,c_i/(m_i\omega_l) - k_i/(m_i\omega_l^2)\right]^2} \end{bmatrix}^{\mathrm{T}} \tag{4.48}
$$

Using the results of the identification error analysis in Equation (3.19) as well as the relation that the true transfer function equals the ratio between the Fourier transform of the noiseless input and output signals, the identification error for the problem (4.34) can be obtained as

$$\begin{bmatrix} \theta_{ki}^{(3)} \\ \theta_{ci}^{(3)} \end{bmatrix} \approx \sum_{l=1}^{N} \mathrm{Re}\left\{ \begin{bmatrix} U_{31,l} \\ U_{32,l} \end{bmatrix} \frac{\ddot{X}_{i+1,l}\left[-\alpha_{i+1,l}\right]}{(\ddot{X}_{i,l} - \ddot{X}_{i-1,l})} \right\} + \sum_{l=1}^{N} \mathrm{Re}\left\{ \begin{bmatrix} U_{14,l} & U_{15,l} \\ U_{24,l} & U_{25,l} \end{bmatrix} \cdot \begin{bmatrix} \dfrac{(\ddot{X}_{i+1,l} - \ddot{X}_{i,l})}{(\ddot{X}_{i,l} - \ddot{X}_{i-1,l})} \theta_{k(i+1)} \\ \dfrac{(\ddot{X}_{i+1,l} - \ddot{X}_{i,l})}{(\ddot{X}_{i,l} - \ddot{X}_{i-1,l})} \theta_{c(i+1)} \end{bmatrix} \right\} \tag{4.49}$$

where the expressions of factors $U_{13,l}$, $U_{23,l}$, $U_{14,l}$, $U_{24,l}$, $U_{15,l}$ and $U_{25,l}$ are given in Equation (3.32).

d) *Comparison of the Identification Errors between TF_SUBID and FFT_SUBID methods (non-top story)*

Comparing the identification errors of the TF_SUBID method for the non-top story parameters (in Equations (4.39), (4.44) and (4.49)) with the corresponding identification errors of the FFT_SUBID method (in Equation (3.32)), it is found that the second part of the identification errors of the TF_SUBID method, due to the estimation errors of the $(i+1)^{\text{th}}$ story parameter, is same as that of the FFT_SUBID method. This suggests that the TF_SUBID method does not reduce the identification errors propagated from errors in the parameter estimates for the story above.

However, if the first part of the identification errors for both methods are compared, which are due to the measurement noise of structural responses, the TF_SUBID method does improve the identification accuracy for the same reason as discussed in the analysis of the top story parameter identification. Furthermore, all measurement uncertainty terms in the transfer function based method share the same denominator terms, $(\ddot{X}_{i,l} - \ddot{X}_{i-1,l})$, and all factors $U_{ij,l}$ are significantly large only near the substructure natural frequency ω_{i0}; therefore, significantly amplifying the interstory response, $(\ddot{X}_{i,l} - \ddot{X}_{i-1,l})$, near the substructure natural frequency ω_{i0} will greatly improve the identification error. This is the same conclusion that was obtained for the FFT_SUBID method.

4.5 Illustrative Examples

The same 5-story shear structure used in Chapter 3 is used again here to demonstrate the effectiveness of the TF_SUBID method. The parameters of the structure are m_i=1×10^5 kg, c_i=8×10^5 N·sec/m, k_i=16×10^7 N/m (i=1…5).

4.5.1 Substructure Identification with Undamaged Structure

The TF_SUBID method requires long stationary structural responses to calculate the transfer functions used to formulate the identification problems. Thus, 1800 second structural responses, with a sampling rate of 200Hz, are simulated to calculate the transfer functions between different structural responses. The 1800 second responses are divided into many shorter response segments, each of which is 60 seconds in length. Welch's method (see section 5.2 for detailed information about this method) is applied to compute the power spectral densities of the responses, which is in turn used to calculate the transfer functions needed for the substructure identification. The MATLAB® routines *pwelch* and *cpsd* are used to calculate the power spectral densities of the structural responses; Hamming windows are applied to filter the structural response with a 25% overlap between the adjacent frames of the response.

Since it is expected, according to the identification error analysis, that the TF_SUBID method will provide much more accurate results than the FFT_SUBID method, larger levels of noise, 20% and 40%, are added to the simulated structural responses to mimic the effect of the measurement noise. 20% (or 40%) noise means that the root-mean-square (RMS) value of the measurement noise is equal to 20% (or 40%) of the RMS of the ground excitation. It is also assumed herein that the magnitude of the measurement noise of all acceleration measurement is the same. The measurement noise is modeled by a band-limited Gaussian white noise with a cut-off frequency at 100Hz. Figure 4.2 shows an example of first two second of the response of the 1st story acceleration, which demonstrates how much the structural response is distorted by the measurement noise. It is easily seen that 40% noise largely distorts the true structural response, posing a big challenge for the identification method to give accurate estimation of the structural parameters.

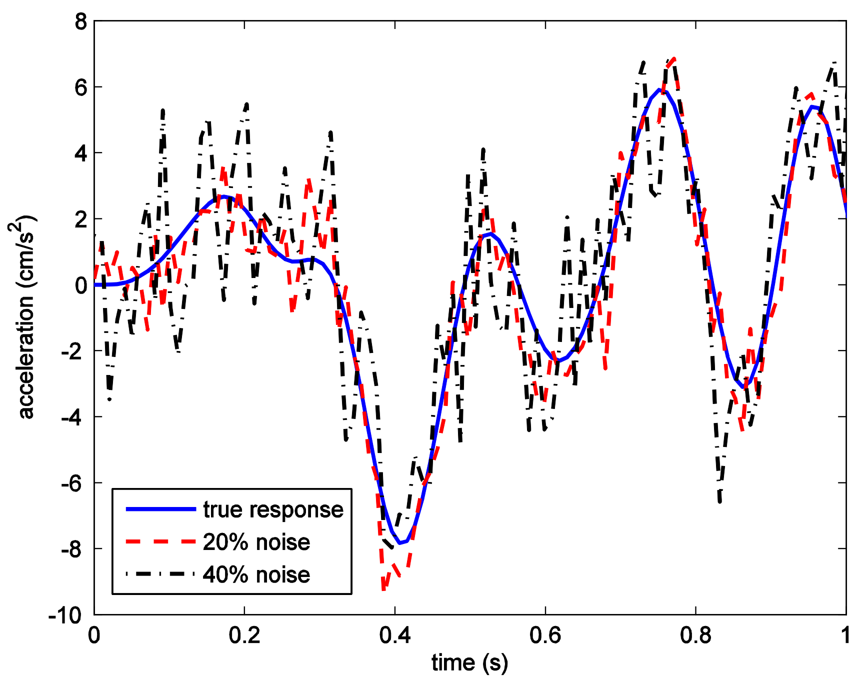

Figure 4.2 The 1st floor noisy acceleration response with and without measurement noise

Using "scenario 1" of Chapter 3, 100 independent substructure identifications via the TF_SUBID method are performed with 20% and 40% noise respectively. The statistics of the identification results are listed in Tables 4.1 and 4.2 respectively.

Compared with the identification results of the FFT_SUBID method in Table 3.4, the TF_SUBID provides much more accurate identification results: when the medium level (20%) of noise are existed in the measured structural responses, the TFF_SUBID is simply not able to give any sufficiently accurate results for damage detection tasks; while, with 20% noise disturbance the TF_SUBID method provides excellent identification results, with accuracy even better than that of the FFT_SUBID method with much smaller (5%) noise disturbance (compared Table 4.1 with Table 3.2). Moreover, even for the story damping parameters, which are much difficult to accurately identify than the story stiffness parameters, the TF_SUBID method manages to give quite accurate estimates (the maximum relative RMSE value of all damping parameters is only 3.5%). As measurement noise increases to a fairly large level (40%), the accuracy of TF_SUBID method decreases to some extent but is still able to provide acceptably good identification results.

The error analysis in section 4.4 shows that, similar to the FFT_SUBID method, the accuracy of the TF_SUBID method is largely affected by the frequency response of the interstory acceleration $(\ddot{X}_{i,l} - \ddot{X}_{i-1,l})$ $(i = 1,\ldots,n)$ near the substructure natural frequency ω_{i0}, with larger response corresponding to smaller identification errors. As shown in Chapter 3, that the third interstory acceleration is significantly smaller near its substructure natural frequency (40 rad/sec), so it is expected that the identification error of the third story parameters is much larger than that of others, which is verified by the simulation results.

Table 4.1 The statistics of the identification results with 20% noise

Story number	Story stiffness $\hat{k}_i$ ($\times 10^5$N/m)			Story damping $\hat{c}_i$ ($\times 10^5$N·sec/m)		
	mean	relative RMSE	relative STD	mean	relative RMSE	relative STD
1	1600 (0.0%)*	0.3%	0.3%	8.09 (1.2%)*	1.7%	1.2%
2	1602 (0.1%)	0.3%	0.3%	8.07 (0.9%)	1.7%	1.4%
3	1587 (-0.8%)	0.9%	0.5%	8.20 (2.5%)	3.5%	2.5%
4	1595 (-0.3%)	0.4%	0.2%	7.97 (-0.3%)	1.0%	0.9%
5	1601 (0.1%)	0.1%	0.1%	7.95 (-0.6%)	0.9%	0.6%

*: relative error for mean estimate

Table 4.2 The statistics of the identification results with 40% noise

Story number	Story stiffness $\hat{k}_i$ ($\times 10^5$N/m)			Story damping $\hat{c}_i$ ($\times 10^5$N·sec/m)		
	mean	relative RMSE	relative STD	mean	relative RMSE	relative STD
1	1597 (-0.2%)	0.7%	0.7%	8.38 (4.8%)	5.8%	3.3%
2	1604 (0.1%)	0.7%	0.7%	8.22 (2.8%)	5.3%	4.5%
3	1559 (-2.6%)	3.1%	1.8%	8.62 (7.8%)	10.4%	6.8%
4	1585 (-0.9%)	1.0%	0.5%	7.99 (-0.2%)	2.0%	2.0%
5	1604 (0.3%)	0.4%	0.3%	7.82 (-2.3%)	2.6%	1.3%

4.5.2 Effects of Structural Response Length on Identification Accuracy

Since the TF_SUBID method uses long stationary structural responses to estimate the transfer functions, needed to formulate the substructure identification problems, this section investigates the effects of the length of stationary structural responses on the accuracy of the substructure identification.

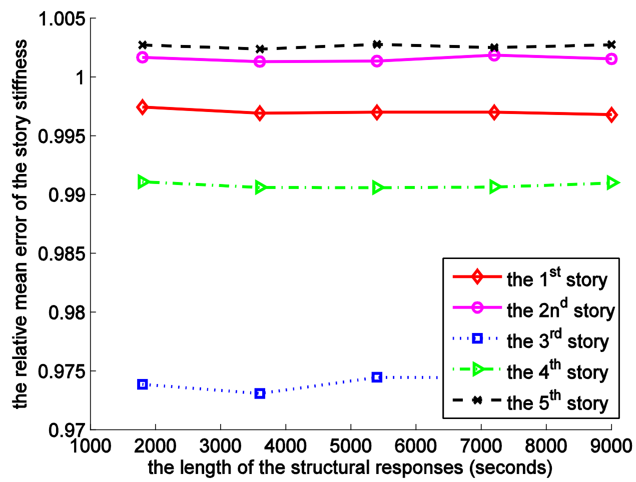

Figure 4.3 The relative mean of the estimated stiffness with different length of the structural responses

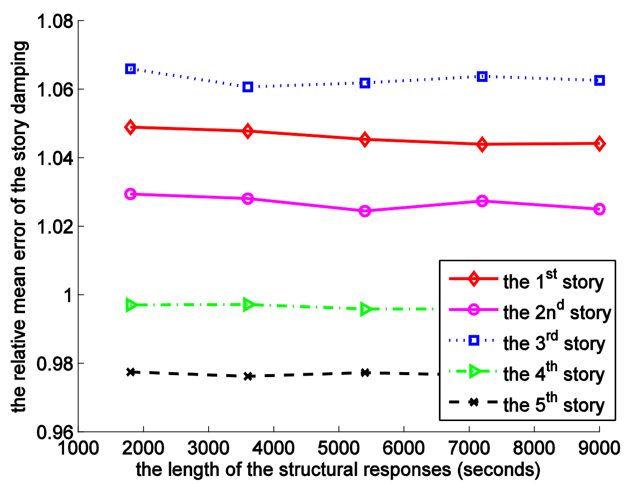

Figure 4.4 The relative mean of the estimated damping with different length of the structural responses

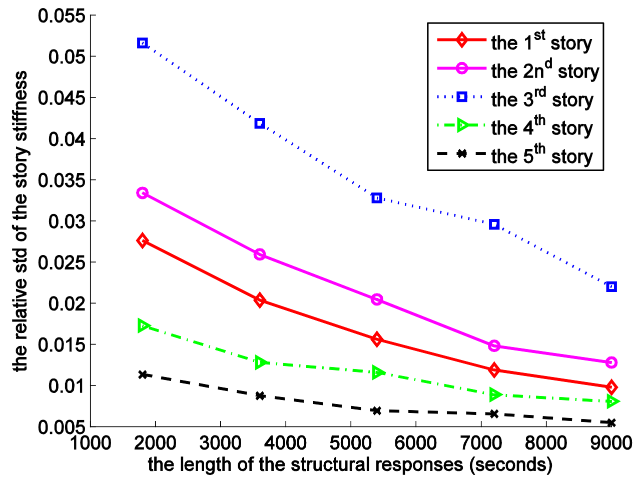

Figure 4.5 The relative standard deviation of the estimated stiffness with different length of the structural responses

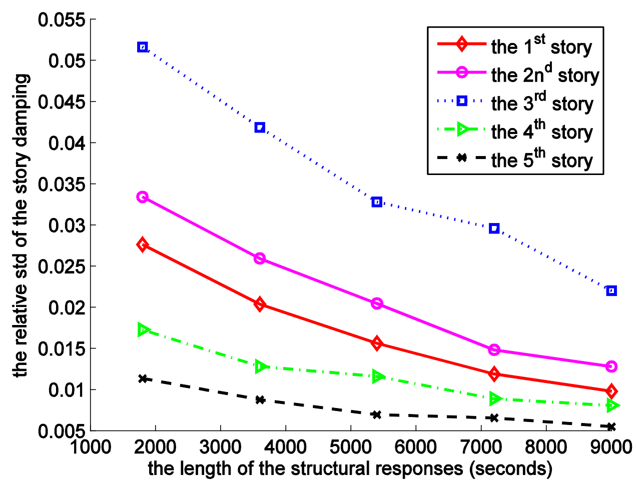

Figure 4.6 The relative standard deviation of the estimated damping with different length of the structural responses

Figures 4.3~4.6 show the changes of relative mean error and standard deviation of the estimated stiffness and damping parameters, respectively, with different length of the structural responses being used to perform the substructure identification. As longer structural responses are used, the estimated transfer functions, used in the substructure identification, have smaller variance, leading to smaller variances of the estimated structural parameters as shown in Figures 4.5 and 4.6. However, the transfer function estimation method in section 4.2 is a biased estimation method, which means that the estimated transfer function does not converge to its true value as the length of structural responses increases; thus, the TF_SUBID method is also a biased estimator for the structural parameter. This is verified by the Figures 4.3 and 4.4, showing that the mean errors of the estimated parameters do not decrease as additional structural responses are used in the identification.

4.5.3 Damage Detection Results

Applying the damage detection strategy proposed in section 3.5, damage detection tests are performed by using structural parameters estimated by the TF_SUBID method. The damage scenario of the structure is the same as that in Chapter 3: the structural damage occurs at the first, third and fifth stories, which results in a reduction of the story stiffness by 5% and an increase of the story damping by 20%. Since the TF_SUBID method is able to provide quite good estimates of the structural parameters with both 20% and 40% noise disturbance, damage detection tests are carried out at both noise levels.

In order to test the ability of the proposed damage detection strategy to correctly identify the health status of the structure, 600 independent substructure identifications using the TF_SUBID method are carried out on the damaged structure; the results are used in the hypothesis test to determine whether or not the structure is damaged. The number of the substructure identifications that each hypothesis test uses to reach the conclusion is selected as 1,3 or 5 respectively. According to the number of the tests each hypothesis test uses, the identification results of 600 tests are divided into groups and a hypothesis test is performed for each group using the method proposed in section 3.5. Since the identified structural parameters of the undamaged structure have quite small variances, a larger β value, 5, is selected in the hypothesis tests to reduce the probability of the second kind error of the hypothesis test – faulty detection. The percentage of the hypothesis tests that give the correct health status of the structure with two different levels of noise disturbance are shown in Tables 4.3 and 4.4 respectively.

Table 4.3 The percentage of the hypothesis tests which give the correct conclusion about the structural health status with 20% noise

Floor Number	n		
	1	3	5
1	100%	100%	100%
2	92%	96%	100%
3	100%	100%	100%
4	87%	96%	98%
5	100%	100%	100%

Table 4.4 The percentage of the hypothesis tests which give the correct conclusion about the structural health status with 40% noise

Floor Number	n		
	1	3	5
1	100%	100%	100%
2	91%	97%	100%
3	100%	100%	100%
4	61%	67%	73%
5	100%	100%	100%

Due to the smaller variance of the identified structural parameters of the undamaged structure, the proposed damage detection procedure perfectly accurately identifies all structural damage under both levels of noise disturbance. However, in some cases the damage detection procedure does make some mistakes of labeling the undamaged structural members as being damaged, especially when the measurement noise level is high. This is partially due to the fact that large noises in the measured structural responses cause the estimated transfer functions used in formulating the substructure identification problems to have large bias, leading to a biased estimation of the structural parameters. When structural damage occurs, structural responses will be changed according, which results in the change of the noise level relative to the structural response and, thus, leads to the migration of the bias of the estimated parameters. Such a migration may cause the misdetection of the healthy structural members.

Moreover, as the number of the identifications, *n*, that each hypothesis test uses to make the decision increases, the chances that hypothesis tests make the correct decision also increase, which verifies that the proposed hypothesis test method, using *n* identifications together to make the decision, is effective in improving the probability to make the right decision about the health status of the structure. However, the derivation of this technique in Chapter 3 observed that if the probability that the hypothesis test with one identification result is large and close to 50%, increasing the number of identification results used in each hypothesis test can only provide limited improvement in increasing the accuracy of the hypothesis test. This is verified by the hypothesis test result of the fourth story structure under 40% noise disturbance. In that case, the error probability of the hypothesis test with one identification result is quite large (100%–61%=39%); thus, using more identification results in each hypothesis test only provides quite moderate improvement of the accuracy of the hypothesis test: the error probability of the hypothesis test only decreases from 39% with one identification result to 27% with five identification results.

The results of the hypothesis test in this section imply that it is important to reduce the bias in the estimate of structural parameters in order to further improve the accuracy of hypothesis test.

Chapter 5

Cross Power Spectral Density Based Substructure Identification Method

In Chapter 3, an innovative substructure identification method (FFT_SUBID), formulated by using the Fourier transform of floor acceleration responses, is proposed to identify the parameters of a shear structure. However, due to the noisy nature of the acceleration measurements, this method cannot provide accurate results when the measurement noise is not small. To improve identification accuracy in larger noise cases, an improved transfer function based substructure method (TF_SUBID) is put forward in Chapter 4, which does greatly improve the identification accuracy. However, the implementation of the TF method requires that 1) there is only one excitation source affecting the structure, and 2) very long stationary structural responses are available. These constraints, especially the first one, severely restrain the wide application of the TF_SUBID method.

In this chapter, a new substructure identification method based on a cross power spectral density (CSD_SUBID) is derived from the differential equation governing the structural random responses. This method not only overcomes the previous constraints required by TF_SUBID method but also further improves the identification accuracy. A reference response, which is jointly wide sense stationary (WSS) with all structural responses, is introduced. The cross power spectral density (CSD) between the acceleration responses of the substructure and this reference response, calculated by averaging long stationary responses in the frequency domain, are used in formulating the new substructure method. Since the new CSD_SUBID method is just like the

FFT_SUBID method with the exchange of some structural response parameters, an identification error analysis for the CSD_SUBID method is directly obtained by accordingly modifying the results of the error analysis of the FFT_SUBID method presented in Chapter 3. Based on the error analysis of the CSD_SUBID method, a smart selecting algorithm is proposed to determine the optimal reference response candidate that can further reduce the effect of measurement noise and improve identification accuracy. Moreover, the explicit formulas to calculate the variances of the estimated parameters are derived for the CSD_SUBID method, which makes it possible for this method to provide the optimal identified parameters as well as the confidence interval of these estimates. Although the CSD_SUBID method is originally derived under the assumption that the structural responses are wide sense stationary, it is subsequently shown that, with little change, the CSD_SUBID method can be directly extended to handle the identification with non-stationary responses. Finally, the proposed CSD_SUBID method is tested on two shear structures; the results demonstrate the efficacy of this new method and verify many analysis results for this method.

5.1 Method Formulation

The dynamic equation of an *n*-story shear structure subject to ground excitation can be written for each story substructure as follows:

Top floor ($i = n$):

$$m_n \ddot{x}_n(t) + c_n[\dot{x}_n(t) - \dot{x}_{n-1}(t)] + k_n[x_n(t) - x_{n-1}(t)] = 0 \tag{5.1}$$

Middle floor ($2 \le i \le n-1$):

$$m_i \ddot{x}_i(t) + c_i[\dot{x}_i(t) - \dot{x}_{i-1}(t)] + k_i[x_i(t) - x_{i-1}(t)] \\ + c_{i+1}[\dot{x}_i(t) - \dot{x}_{i+1}(t)] + k_{i+1}[x_i(t) - x_{i-1}(t)] = 0 \tag{5.2}$$

Bottom floor (i = 1):

$$m_1 \ddot{x}_1(t) + c_1[\dot{x}_1(t) - \dot{u}_g(t)] + k_1[x_1(t) - u_g(t)] \\ + c_2[\dot{x}_1(t) - \dot{x}_2(t)] + k_2[x_1(t) - x_2(t)] = 0 \tag{5.3}$$

where m_i is the mass of the i^{th} floor; c_i and k_i are the damping coefficient and stiffness of the i^{th} story; $x_i(t)$ and $u_g(t)$ are the displacements of the i^{th} floor and ground relative to an inertial reference frame at time t; and overdots represent the derivatives with respect to time t. It is assumed here that the mass of the structure is known.

The motion of the top floor is affected only by the top story structural parameters as well as by the motion of the top two floors. Thus, the substructure identification will start with the top floor as follows. Adding $-m_n \ddot{x}_{n-1}(t)$ to both side of Equation (5.1), multiplying both sides by a reference response at an earlier time $y(t-\tau)$ and taking the expectation will give

$$m_n R_{(\ddot{x}_n - \ddot{x}_{n-1})y}(\tau) + c_n R_{(\dot{x}_n - \dot{x}_{n-1})y}(\tau) + k_n R_{(x_n - x_{n-1})y}(\tau) = -m_n R_{y\ddot{x}_{n-1}}(\tau) \tag{5.4}$$

where $R_{xy}(\tau) = \mathrm{E}[x(t)y(t-\tau)]$ is cross correlation function between the responses $y(t)$ and $x(t)$. Here it is assumed that the reference response $y(t)$ and all structural responses are jointly WSS.

When $y(t)$ and $x(t)$ are joint WSS process, their cross correlation function satisfies the following equation (Bendat *et al.*, 2000)

$$R_{x^{(m)}y}(\tau) = R_{xy}^{(m)}(\tau) \tag{5.5}$$

Let $x^{(m)}$ denote the m^{th} derivative of random process $x(t)$ with respect to time, and $R_{xy}^{(m)}(\tau)$ denotes the m^{th} derivative of the correlation function $R_{xy}(\tau)$ with respect to τ. If the mean square derivatives exist, Equation (5.4) can be rewritten as

$$m_n \ddot{R}_{(x_n - x_{n-1})y}(\tau) + c_n \dot{R}_{(x_n - x_{n-1})y}(\tau) + k_n R_{(x_n - x_{n-1})y}(\tau) = -m_n \ddot{R}_{x_{n-1}y}(\tau) \tag{5.6}$$

Taking a two sided Fourier transform of both sides of (5.6), rearranging the order of the terms and exploiting the property $F(\ddot{R}) = (j\omega)^2 F(R)$ (where F denotes the Fourier transform operator and $j^2 = -1$) gives

$$\frac{1}{1 - j c_n/(m_n \omega) - k_n/(m_n \omega^2)} = \frac{S_{\ddot{x}_{n-1}y} - S_{\ddot{x}_n y}}{S_{\ddot{x}_{n-1}y}} \tag{5.7}$$

where $S_{\ddot{x}_j y} = S_{\ddot{x}_j y}(j\omega)$, the Fourier transform of the cross correlation function $R_{\ddot{x}_j y}(\tau)$, is the cross power spectral density (CSD) function between the reference response y and the structural acceleration response $\ddot{x}_j$ (herein, $j\omega$ is often omitted for notational simplicity).

Since the right side of Equation (5.7) only involves the CSD between the structural acceleration responses and the reference response, all of which can be calculated directly from the measurements, the structural parameters $[k_n \;\; c_n]^{\mathrm{T}}$ can be identified by solving the following optimization problem that minimizes the difference between the two sides of Equation (5.7) over all frequencies.

$$\arg\min_{k_n, c_n} \quad J(k_n, c_n) = \sum_{l=1}^{N} \left| f_l(k_n, c_n) - \hat{f}_l(\hat{S}_{\ddot{x}_n y, l}, \hat{S}_{\ddot{x}_{n-1} y, l}) \right|^2 \tag{5.8}$$

where $f_l(k_n, c_n) = \dfrac{1}{1 - j\,c_n/(m_n\omega_l) - k_n/(m_n\omega_l^2)}$, $\hat{f}_l(\hat{S}_{\ddot{x}_n y,l}, \hat{S}_{\ddot{x}_{n-1} y,l}) = \dfrac{\hat{S}_{\ddot{x}_{n-1} y,l} - \hat{S}_{\ddot{x}_n y,l}}{\hat{S}_{\ddot{x}_{n-1} y,l}}$.

and where $\hat{S}_{\ddot{x}_i y,l} = \hat{S}_{\ddot{x}_i y}(j\omega_l)$ (i=1,…,n) stands for the CSD at frequency ω_l between the i^{th} floor acceleration $\ddot{x}_i$ and the reference response y as estimated from the measured (noise contaminated) responses; $\omega_l = l \cdot \Delta\omega$ $(l = 1,..., N)$ are discrete frequencies at which the CSD are calculated and $\Delta\omega$ is the frequency interval.

After $[k_n \;\; c_n]^{\mathrm{T}}$ have been identified, the following induction method can be used to identify structural parameters of other stories in the following manner. Adding $-m_i\ddot{x}_{i-1}$ to both sides of Equation (5.2) and following a similar procedure as in the top story parameter identification gives

$$\frac{1}{1 - j\,c_i/(m_i\omega) - k_i/(m_i\omega^2)} = \frac{S_{\ddot{x}_{i-1} y} - S_{\ddot{x}_i y}}{S_{\ddot{x}_{i-1} y} + (S_{\ddot{x}_{i+1} y} - S_{\ddot{x}_i y})[\,jc_{i+1}/(m_i\omega) + k_{i+1}/(m_i\omega^2)]} \tag{5.9}$$

Assuming that structural parameters $[k_{i+1} \;\; c_{i+1}]^{\mathrm{T}}$ in Equation (5.9) are known, the right side of the equation can be directly calculated from the measured acceleration responses. Then, a similar optimization problem, shown in Equation (5.10), is formulated to identify the structural parameters $[k_i \;\; c_i]^{\mathrm{T}}$ on the left side of Equation (5.9):

$$\underset{k_i, c_i}{\arg\min} \quad J(k_i, c_i) = \sum_{l=1}^{N} \left| g_l(k_i, c_i) - \hat{g}_l(\hat{S}_{\ddot{x}_{i-1} y,l}, \hat{S}_{\ddot{x}_i y,l}, \hat{S}_{\ddot{x}_{i+1} y,l}) \right|^2 \tag{5.10}$$

where $g_l(k_i, c_i) = \dfrac{1}{1 - j\,c_i/(m_i\omega_l) - k_i/(m_i\omega_l^2)}$,

$$\hat{g}_l(\hat{S}_{\ddot{x}_{i-1} y,l}, \hat{S}_{\ddot{x}_i y,l}, \hat{S}_{\ddot{x}_{i+1} y,l}) = \frac{\hat{S}_{\ddot{x}_{i-1} y,l} - \hat{S}_{\ddot{x}_i y,l}}{\hat{S}_{\ddot{x}_{i-1} y,l} + (\hat{S}_{\ddot{x}_{i+1} y,l} - \hat{S}_{\ddot{x}_i y,l})[\,jc_{i+1}/(m_i\omega_l) + k_{i+1}/(m_i\omega_l^2)]}.$$

Since the identification problem (5.10) is applicable to the parameter identification of every story in the structure except for the top (n^{th}) story, an induction identification step is essentially established by Equation (5.10) in which the parameters of any i^{th} story $[k_i \;\; c_i]^{\mathrm{T}}$ can be identified if the parameters of the story above (the $(i+1)^{\text{th}}$ story) $[k_{i+1} \;\; c_{i+1}]^{\mathrm{T}}$ are known. The top story structural parameters $[k_n \;\; c_n]^{\mathrm{T}}$ identified from optimization problem (5.8) are already available to initiate the above induction identification process. Thus, all structural parameters $[k_i \;\; c_i]^{\mathrm{T}}$ (i=1,…,n) can be identified iteratively by following the identification procedure in Equation (5.10). Note that when the parameters of the first story are to be identified, a simple replacement of $\hat{S}_{\ddot{x}_{i-1}y}$ with $\hat{S}_{\ddot{u}_g y}$ is needed in Equation (5.10).

5.1.1 Relation to the FFT_SUBID Method

Comparing the two key identifications in the CSD_SUBID method, Equation (5.8) for the top story substructure and Equation (5.10) for the non-top story substructure, with the corresponding key identification equations, Equation (3.8) and (3.10), of the FFT_SUBID method, it is found that the CSD_SUBID method looks like the FFT_SUBID method with the replacement of all Fourier transforms of the responses $\ddot{X}_j$ by the cross power spectral density $S_{\ddot{x}_j y}$. This observation provides an easy way to analyze the properties (*i.e.*, the identification error analysis) of the new CSD_SUBID method by reutilizing the analysis results from the FFT_SUBID method with the simple change of corresponding terms from the Fourier transform of the responses to their corresponding cross power spectral densities with the reference response $y(t)$.

5.1.2 Relation to the TF_SUBID Method

In addition to the estimation method of a transfer function describe in the section 4.2, Equation (5.11) shows another way of calculating the deterministic transfer function from structural response $\ddot{x}_i$ to response $\ddot{x}_j$, assuming that such a transfer function exists:

$$H_{\ddot{x}_j\ddot{x}_i} = \ddot{X}_j \big/ \ddot{X}_i = (\ddot{X}_j Y^*) \big/ (\ddot{X}_i Y^*) = \mathrm{E}\left[\ddot{X}_j Y^*\right] \big/ \mathrm{E}\left[\ddot{X}_i Y^*\right] = S_{\ddot{x}_j y} \big/ S_{\ddot{x}_i y} \tag{5.11}$$

where $\ddot{X}_i$ and $\ddot{X}_j$ are the Fourier transforms of the responses $\ddot{x}_i$ and $\ddot{x}_j$, respectively; Y is the Fourier transform of an arbitrary reference response y, which is wide sense stationary with the responses $\ddot{x}_i$ and $\ddot{x}_j$; "*" denotes the complex conjugate; E[·] is the ensemble average operator; $S_{\ddot{x}_i y}$ and $S_{\ddot{x}_j y}$ are the cross power spectral density between the structural acceleration responses $\ddot{x}_i$ and $\ddot{x}_j$, respectively, and the reference response y.

If the reference response y is selected as the response $\ddot{x}_i$, then the transfer function estimation method in Equation (5.11) is the same as used in section 4.2. In this sense, the TF_SUBID method is just a special case of CSD_SUBID method in which the reference response $y(t)$ is fixed as a specific response.

However, it is worth mentioning that the derivation of the CSD_SUBID method does not have the restriction that there must be one excitation source in the structure as the TF_SUBID method did, which greatly extends the applicability of this new identification method.

5.2 Estimation of Cross Power Spectral Density: Welch Method

Since the cross power spectral density between structural responses and reference $y(t)$ are needed in the CSD_SUBID method, a power spectrum estimation method, the Welch average periodogram method (Welch, 1967) is introduced for calculating the cross power spectra.

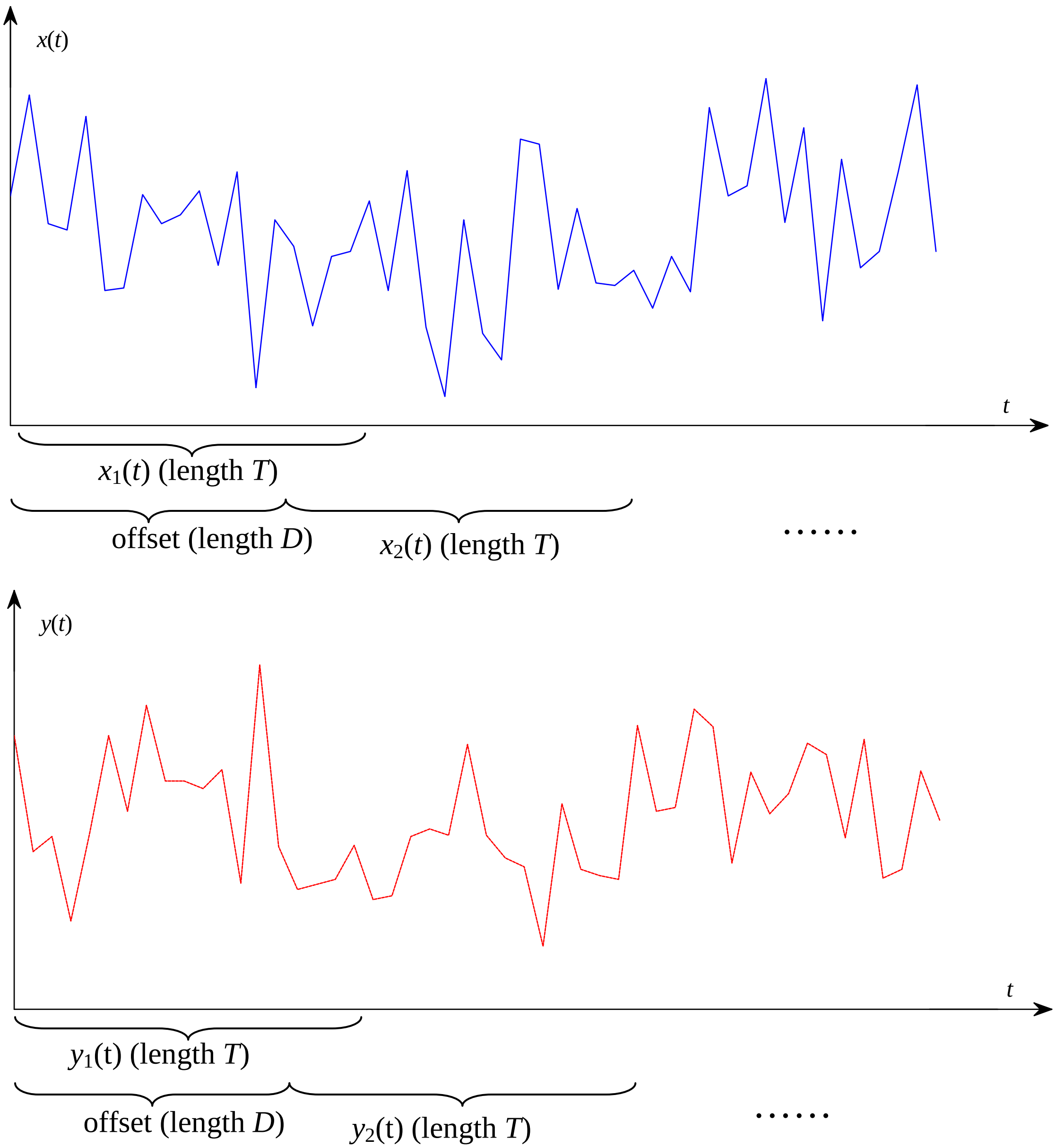

Figure 5.1 Partition responses x(t) and $y(t)$ into overlapped short segments

Let $x(t)$ and $y(t)$ be two continuous stationary signals. As shown in Figure 5.1, $x(t)$ and $y(t)$ are partitioned into Q overlapping short segments of the same length T, $x_i(t)$ and $y_i(t)$, and the successive segments are offset by D ($D \leq T$).

$$\begin{matrix} x_i(t) = x(D \times i + t) \\ y_i(t) = y(D \times i + t) \end{matrix} \begin{pmatrix} t \in [0, T] \\ i = 0,1,\ldots,Q-1 \end{pmatrix} \tag{5.12}$$

To reduce the leakage problem, sometimes the segment signals are multiplied by a window function, such as hanning window, before being used to calculate the cross power spectrum. The expression of a hanning window of length T is given in Equation (5.13).

$$w(t) = 0.5\left(1 - \cos\frac{2\pi \cdot t}{T}\right),\ t \in [0, T] \tag{5.13}$$

Then the Welch method calculates the cross power spectral density by averaging the cross power spectral density of the windowed segments signals as follows,

$$\hat{S}_{xy}\left(e^{j\omega}\right) = \frac{1}{QTU}\sum_{i=1}^{Q}\left[\int_0^T w(t)x_i(t)e^{j\omega \cdot t}dt\right]\left[\int_o^T w(t)y_i(t)e^{-j\omega \cdot t}dt\right] \tag{5.14}$$

where $U = \frac{1}{T}\int_0^T |w(t)|^2 dt$.

One of the important properties of the Welch average periodogram method is that as the length of each segment L and the number of segments Q tend to infinity, the Welch method becomes an asymptotically unbiased and consistent estimator of the cross power spectrum (Hayes, 1996).

5.3 Identification Error Analysis

As stated in section 5.1, the CSD_SUBID method is like the FFT_SUBID method with the simple replacements of the Fourier transforms of structural responses by the corresponding cross power spectral densities; thus, the identification errors of the CSD_SUBID method can be easily obtained by using the identification error analysis results of the Fourier transform based method with similar replacements.

5.3.1 Top Story Identification Case

The parameter identification error of the top story identification in the CSD_SUBID method can be written as

$$\begin{bmatrix} \theta_{kn} \\ \theta_{cn} \end{bmatrix} \approx \sum_{l=1}^{N} \mathrm{Re}\left\{ \begin{bmatrix} W_{11,l} & W_{12,l} \\ W_{21,l} & W_{22,l} \end{bmatrix} \cdot \begin{bmatrix} N_{\ddot{x}_{n-1}y,l} \big/ S_{(\ddot{x}_n - \ddot{x}_{n-1})y,l} \\ N_{\ddot{x}_n y,l} \big/ S_{(\ddot{x}_n - \ddot{x}_{n-1})y,l} \end{bmatrix} \right\} \tag{5.15}$$

where θ_{kn} and θ_{cn} are the relative identification errors of the n^{th} story parameters k_n and c_n, respectively; $N_{\ddot{x}_i y,l} = \hat{S}_{\ddot{x}_i y,l} - S_{\ddot{x}_i y,l}$ $(i = 1,\ldots,n)$ are the measurement uncertainties of the CSD estimation, which equals the difference between the CSD estimated from the noise-contaminated measured responses and the CSD of the true (noiseless) responses at frequency ω_l; $S_{(\ddot{x}_n - \ddot{x}_{n-1})y,l}$ is the CSD between the interstory acceleration of the i^{th} story $(\ddot{x}_i - \ddot{x}_{i-1})$ and the reference response $y(t)$; $W_{ij,l}$ are the same factors in Equation (3.26).

All factors $W_{ij,l}$ are significantly large near the natural frequency of the n^{th} story substructure ω_{n0} $(\omega_{n0} = \sqrt{k_n / m_n})$, and very small when far away from this frequency; thus, the uncertainty measurement terms, $N_{\ddot{x}_{n-1}y,l} \big/ S_{(\ddot{x}_n - \ddot{x}_{n-1})y,l}$ and $N_{\ddot{x}_n y,l} \big/ S_{(\ddot{x}_n - \ddot{x}_{n-1})y,l}$, near the substructure natural frequency ω_{n0} play a dominant role in determining the parameter identification accuracy; dramatically reducing these values can significantly improve the identification accuracy.

Since both numerator and denominator of the measurement uncertain terms, $N_{\ddot{x}_{n-1}y,l} \big/ S_{(\ddot{x}_n - \ddot{x}_{n-1})y,l}$ and $N_{\ddot{x}_n y,l} \big/ S_{(\ddot{x}_n - \ddot{x}_{n-1})y,l}$, are related to the reference $y(t)$, selecting different responses as the reference will lead to different measurement uncertainty and, thus, different accuracy of the identified parameters. Therefore, the CSD_SUBID method, compared with the FFT_SUBID method, provides an opportunity to improve the identification accuracy by choosing an appropriate reference (see section 5.4 for more detailed information).

5.3.2 Non-top Story Identification Case

The parameter identification errors of the i^{th} non-top story of the CSD_SUBID method can be written as

$$\begin{bmatrix}\theta_{ki}\\ \theta_{ci}\end{bmatrix} \approx \sum_{l=1}^{N} \mathrm{Re}\left\{\begin{bmatrix}U_{11,l} & U_{12,l} & U_{13,l}\\ U_{21,l} & U_{22,l} & U_{23,l}\end{bmatrix} \cdot \begin{bmatrix} N_{\ddot{x}_{i-1}y,l} \big/ S_{(\ddot{x}_i - \ddot{x}_{i-1})y} \\ N_{\ddot{x}_i y,l} \big/ S_{(\ddot{x}_i - \ddot{x}_{i-1})y} \\ N_{\ddot{x}_{i+1}y,l} \big/ S_{(\ddot{x}_i - \ddot{x}_{i-1})y} \end{bmatrix}\right\} + \sum_{l=1}^{N} \mathrm{Re}\left\{\begin{bmatrix}U_{14,l} & U_{15,l}\\ U_{24,l} & U_{25,l}\end{bmatrix} \cdot \begin{bmatrix} \dfrac{S_{(\ddot{x}_{i+1} - \ddot{x}_i)y}}{S_{(\ddot{x}_i - \ddot{x}_{i-1})y}} \theta_{k(i+1)} \\ \dfrac{S_{(\ddot{x}_{i+1} - \ddot{x}_i)y}}{S_{(\ddot{x}_i - \ddot{x}_{i-1})y}} \theta_{c(i+1)} \end{bmatrix}\right\} \tag{5.16}$$

where $\theta_{k(i+1)}$ and $\theta_{c(i+1)}$ are the relative identification errors of the $(i+1)^{\text{th}}$ story parameters k_{i+1} and c_{i+1}, respectively. $U_{ij,l}$ are the same factors as in Equation (3.32).

The identification errors of the i^{th} story parameters $[\theta_{ki} \quad \theta_{ci}]^{\text{T}}$ in Equation (5.16) consist of two kinds of errors: the errors (the first part of the right side) directly related to the measurement uncertainty of the structural responses ($N_{\ddot{x}_{i-1}y} \big/ S_{(\ddot{x}_i - \ddot{x}_{i-1})y}$, $N_{\ddot{x}_i y} \big/ S_{(\ddot{x}_i - \ddot{x}_{i-1})y}$ and $N_{\ddot{x}_{i+1}y} \big/ S_{(\ddot{x}_i - \ddot{x}_{i-1})y}$) and the accumulation errors (the second part) due to the uncertainty in the identified structural parameters of the story above ($\theta_{k(i+1)} S_{(\ddot{x}_{i+1}-\ddot{x}_i)y} \big/ S_{(\ddot{x}_i-\ddot{x}_{i-1})y}$ and $\theta_{c(i+1)} S_{(\ddot{x}_{i+1}-\ddot{x}_i)y} \big/ S_{(\ddot{x}_i-\ddot{x}_{i-1})y}$). All factors $U_{ij,l}$ are significantly large in magnitude near the natural frequency of the i^{th} story substructure natural frequency $\omega_{i0} = \sqrt{k_i / m_i}$ and decay very fast when moving to lower and higher frequencies. Therefore, both the measurement uncertainties and the upper story parameter uncertainties near the substructure natural frequency ω_{i0} play an important in determining error; significantly reducing their values can greatly reduce identification errors.

Another interesting observation of this result is that the magnitudes of both kinds of uncertainties are not only related to the sources of these uncertainties – the measurement uncertainties ($N_{\ddot{x}_{i-1}y}$, $N_{\ddot{x}_i y}$ and $N_{\ddot{x}_{i+1}y}$) and the identification errors of the upper story parameters ($\theta_{k(i+1)}$ and $\theta_{c(i+1)}$) – but also are affected by two important structural responses: $S_{(\ddot{x}_i-\ddot{x}_{i-1})y}$ and $S_{(\ddot{x}_{i+1}-\ddot{x}_i)y} \big/ S_{(\ddot{x}_i-\ddot{x}_{i-1})y}$. Since $S_{(\ddot{x}_i-\ddot{x}_{i-1})y}$ serves as the common denominator for all three measurement uncertainty terms, amplifying $S_{(\ddot{x}_i-\ddot{x}_{i-1})y}$ near the substructure natural frequency ω_{i0} will lead to smaller measurement uncertainties and, in turn, smaller identification errors. Similarly, reducing the cross power spectral density ratio $S_{(\ddot{x}_{i+1}-\ddot{x}_i)y} \big/ S_{(\ddot{x}_i-\ddot{x}_{i-1})y}$ near the frequency ω_{i0} will result in smaller upper story parameter uncertainties and, thus, smaller identification errors.

5.4 Selection of the Reference Response

The choice of the reference $y(t)$ affects the accuracy of the identification. From the error analysis results of the previous section, it becomes obvious that the best reference response should be the one that minimizes both kinds of uncertainties near the substructure natural frequency. In order to make the reference selection procedure simpler, three assumptions are made herein:

1. The measurement noise of structural responses is zero-mean and independent of the true (noiseless) structural response.
2. The noises of different structural response measurements are mutually independent.
3. There is only one excitation source in the structure.

Based on the third assumption, it can easily be shown that the cross power spectral density ratio $S_{(\ddot{x}_{i+1}-\ddot{x}_i)y} \big/ S_{(\ddot{x}_i-\ddot{x}_{i-1})y}$, which affects the accumulation error of the substructure identification, is not changed by selecting different reference responses. That is, the accumulation error will be independent of the selection of the reference response. Therefore, the selection of the reference response only needs to focus on minimizing the measurement uncertainty near the substructure natural frequency. If the third assumption is relaxed, the selection of reference signal $y(t)$ can still be made but the process is somewhat more complicated and may not give the global optimum.

From the error analysis results in the previous section, the measurement uncertainty for the i^{th} story parameter identification will have the general form of $N_{\ddot{x}_j y} \big/ S_{(\ddot{x}_i-\ddot{x}_{i-1})y}$ where $j \in \{i-1, i\}$ if $i = n$ (top story identification) or $j \in \{i-1, i, i+1\}$ if $i \neq n$ (for non-top story identification). To make this ratio small, the reference response $y(t)$ should be chosen such that the numerator of this ratio is small and, simultaneously, the denominator is large. The numerator of this ratio can be evaluated as

$$
\begin{aligned}
N_{\ddot{x}_j y} &= \hat{S}_{\ddot{x}_j y} - S_{\ddot{x}_j y} \\
&= \mathrm{E}[(\ddot{X}_j + N_{\ddot{x}_j})(Y + N_y)^*] - \mathrm{E}[\ddot{X}_j Y^*] = \mathrm{E}[Y^* N_{\ddot{x}_j}] + \mathrm{E}[N_y^* \ddot{X}_j] + \mathrm{E}[N_y^* N_{\ddot{x}_j}] \\
&= \mathrm{E}[Y^*]\mathrm{E}[N_{\ddot{x}_j}] + \mathrm{E}[N_y^*]\mathrm{E}[\ddot{X}_j] + \mathrm{E}[N_y^* N_{\ddot{x}_j}] = \mathrm{E}[N_y^* N_{\ddot{x}_j}]
\end{aligned}
\qquad (5.17)
$$

where Y and $\ddot{X}_j$ are the Fourier transforms of the responses $y(t)$ and $\ddot{x}_j(t)$, respectively; and N_y and $N_{\ddot{x}_j}$ are the Fourier transforms of the measurement noises of $y(t)$ and $\ddot{x}_j(t)$, respectively. The third and the fourth equality in Equation (5.17) are obtained by using the first and second assumption given previously. It is obvious that if the response $y(t)$ is not the structural response $\ddot{x}_j(t)$, $N_{\ddot{x}_j y}$ becomes zero. Therefore, the first rule for selecting the response $y(t)$ is that $y(t)$ should not be any of the structural responses involved in this step of the substructure identification. More specifically, $y(t)$ is not none of the following: $\ddot{x}_{i-1}(t)$, $\ddot{x}_i(t)$ and, for the non-top story, $\ddot{x}_{i+1}(t)$. By choosing $y(t)$ using this principle, the numerators of all measurement uncertainty terms will be zeros. However, it is worth emphasizing that the expected value in Equation (5.17) requires, theoretically, infinite long structural responses; in practice, the measurements are always of finite duration and, thus, the expected value in Equation (5.17) calculated from finite responses will usually be small but not zero. So the denominator of the measurement uncertainty, $S_{(\ddot{x}_i - \ddot{x}_{i-1})y}$, still needs to be considered to further reduce the measurement uncertainty.

Since the goal of reference response selection is to minimize the measurement uncertainty near the substructure natural frequency ω_{i0}, the denominator of the measurement uncertainty should be maximized near ω_{i0}. Define a performance function for the k^{th} candidate reference response y_k.

$$J[y_k] = \int_0^\infty \left| W(j\omega)\frac{1}{S_{(\ddot{x}_i - \ddot{x}_{i-1})y_k}} \right|^2 d\omega \tag{5.18}$$

where $W(j\omega)$ is a frequency weighting function, having the following expression,

$$W(j\omega) = \frac{-k_i/(m_i\omega^2)}{[1 - jc_i/(m_i\omega) - k_i/(m_i\omega^2)]^2}$$

As shown in Figure 5.2, the magnitude of the frequency weighting function peaks around frequency ω_{i0} and quickly vanishes when further away. Hence, the reference y_k minimizing the performance function in Equation (5.18) will minimize measurement uncertainty $N_{\ddot{x}_j y}/S_{(\ddot{x}_i - \ddot{x}_{i-1})y}$ near the substructure frequency ω_{i0}.

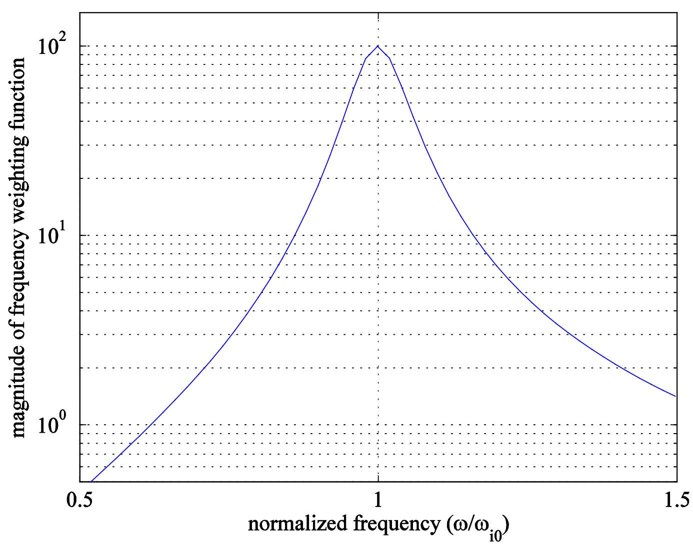

Figure 5.2 Magnitude of frequency weighting function *W*(*jω*)

To summarize the selection rules of the reference response $y(t)$: $y(t)$ will be selected among all possible structural responses that are not involved in this step of the substructure identification and which gives the smallest value of Equation (5.18).

5.5 Statistical Moment Estimation for Identification Error

In practice, it is of great value to provide some kind of uncertainty measurement for the identified parameters. Such information plays an important role in the case of structural damage detection, helping to determine if the change of the estimated parameters is caused by structural damage or simply by the inherent randomness of the estimation results. In this section, an approach to approximately estimate the first two statistical moments (mean and variance) of the identification error is proposed based on the results of identification error analysis developed in a prior section. The result of this analysis not only helps provide better comprehension of the performance of the proposed substructure method in real uncertain circumstances, but also provides some important suggestions to further improve its accuracy.

5.5.1 Top Story Identification Case

From the result of Equation (5.15), the identification errors of the top story parameters are influenced by three kinds of terms: 1) the measurement uncertainty of the cross power spectral density estimations $N_{\ddot{x}_j y,l}, \quad j \in \{n-1, n\}$; 2) the cross power spectral density between the n^{th} interstory acceleration and the reference response $S_{(\ddot{x}_n - \ddot{x}_{n-1})y,l}$; and 3) factors $W_{ij,l}$. The $W_{ij,l}$ are only related to the structural parameters of the top story and, thereby, have deterministic values for a given structure; in contrast, the measurement noise terms and the structural response terms change from one identification to another and are considered to be random variables.

For notational simplicity, two sets of complex random variables are defined as:

$$\begin{bmatrix} \varepsilon_{kn,l} \\ \varepsilon_{cn,l} \end{bmatrix} = \begin{bmatrix} W_{11,l} & W_{12,l} \\ W_{21,l} & W_{22,l} \end{bmatrix} \cdot \begin{bmatrix} N_{\ddot{x}_{n-1}y,l} \big/ S_{(\ddot{x}_n-\ddot{x}_{n-1})y,l} \\ N_{\ddot{x}_n y,l} \big/ S_{(\ddot{x}_n-\ddot{x}_{n-1})y,l} \end{bmatrix} \tag{5.19}$$

Using these newly defined random variables, the relative identification errors of the top story parameters in Equation (5.15) can be expressed as

$$\begin{bmatrix} \theta_{kn} \\ \theta_{cn} \end{bmatrix} \approx \sum_{l=1}^{N} \frac{1}{2} \begin{bmatrix} \varepsilon_{kn,l} + \varepsilon_{kn,l}{}^{*} \\ \varepsilon_{cn,l} + \varepsilon_{cn,l}{}^{*} \end{bmatrix} \tag{5.20}$$

Four assumptions are made in this moment estimation:

1. The measurement noise and the true structural response are statistically independent.
2. The measurement noise is a zero-mean white Gaussian process and the measurement noises of different structural responses are statistically independent.
3. The true structural responses can be modeled as one or several independent zero-mean white Gaussian processes passing through a linear time invariant system.
4. When calculating cross power spectrum densities by the Welch average periodogram method, there is on overlap between two adjacent short segments (*i.e.*, $D \geq T$); therefore, the measurement noise in different segments are independent one another. If the segments overlap, the noise from one segment and the noise histories from the previous or following segments – or several previous or following segments if the overlap is significant – now overlap,

causing their Fourier transforms to possibly be correlated. As a result, it becomes very difficult to estimate the variance of the parameter estimates in Equations (5.21) and in Equations (5.24) and (5.25). Thus, only for the estimation of the statistical moments, it is assumed that the segments do not overlap; this assumption does not restrict the substructure identification base on the cross power spectral density, which can be used with non-overlapping segments.

Based on above four assumptions, the following properties of random variables $\varepsilon_{kn,l}$ and $\varepsilon_{cn,l}$ can be obtained as:

$$\mathrm{E}\left[\varepsilon_{kn,l}\right]=0 \quad \text{for } \forall l,\, l=1\ldots N \tag{5.21a}$$

$$\mathrm{E}\left[\varepsilon_{cn,l}\right]=0 \quad \text{for } \forall l,\, l=1\ldots N \tag{5.21b}$$

$$\mathrm{E}\left[\varepsilon_{kn,l}\varepsilon_{kn,m}\right]=0 \quad \text{for } \forall l,m \in Z[1,N] \text{ and } l \neq m \tag{5.21c}$$

$$\mathrm{E}\left[\varepsilon_{kn,l}\varepsilon^{*}_{kn,m}\right]=\delta_{lm}\left\{\begin{aligned}&\left|W_{11,l}\right|^2 \mathrm{E}\left[\left|N_{\ddot{x}_{n-1}y,l}\right|^2 \Big/ \left|S_{(\ddot{x}_n-\ddot{x}_{n-1})y,l}\right|^2\right]\\ &+\left|W_{12,l}\right|^2 \mathrm{E}\left[\left|N_{\ddot{x}_{n}y,l}\right|^2 \Big/ \left|S_{(\ddot{x}_n-\ddot{x}_{n-1})y,l}\right|^2\right]\end{aligned}\right\} \quad \text{for } \forall l,m \in Z[1,N] \tag{5.21d}$$

$$\mathrm{E}\left[\varepsilon_{cn,l}\varepsilon_{cn,m}\right]=0 \quad \text{for } \forall l,m \in Z[1,N] \text{ and } l \neq m \tag{5.21e}$$

$$\mathrm{E}\left[\varepsilon_{cn,l}\varepsilon^{*}_{cn,m}\right]=\delta_{lm}\left\{\begin{aligned}&\left|W_{21,l}\right|^2 \mathrm{E}\left[\left|N_{\ddot{x}_{n-1}y,l}\right|^2 \Big/ \left|S_{(\ddot{x}_n-\ddot{x}_{n-1})y,l}\right|^2\right]\\ &+\left|W_{22,l}\right|^2 \mathrm{E}\left[\left|N_{\ddot{x}_{n}y,l}\right|^2 \Big/ \left|S_{(\ddot{x}_n-\ddot{x}_{n-1})y,l}\right|^2\right]\end{aligned}\right\} \quad \text{for } \forall l,m \in Z[1,N] \tag{5.21f}$$

$$\mathrm{E}\left[\varepsilon_{kn,l}\varepsilon_{cn,m}\right]=0 \quad \text{for } \forall l,m \in Z[1,N] \text{ and } l \neq m \tag{5.21g}$$

$$\mathrm{E}\left[\varepsilon_{kn,l}\varepsilon_{cn,m}^{*}\right]=\delta_{lm}\left\{\begin{array}{l}W_{11,l}W_{21,l}^{*}\mathrm{E}\left[\left|N_{\ddot{x}_{n\text{-}1}y,l}\right|^{2}\Big/\left|S_{(\ddot{x}_n-\ddot{x}_{n-1})y,l}\right|^{2}\right]\\+W_{21,l}W_{22,l}^{*}\mathrm{E}\left[\left|N_{\ddot{x}_n y,l}\right|^{2}\Big/\left|S_{(\ddot{x}_n-\ddot{x}_{n-1})y,l}\right|^{2}\right]\end{array}\right\}\quad \text{for } \forall l,m\in Z[1,N] \tag{5.21h}$$

$$\mathrm{E}\left[\varepsilon_{kn,l}^{*}\varepsilon_{cn,m}\right]=\delta_{lm}\left\{\begin{array}{l}W_{11,l}^{*}W_{21,l}\mathrm{E}\left[\left|N_{\ddot{x}_{n\text{-}1}y,l}\right|^{2}\Big/\left|S_{(\ddot{x}_n-\ddot{x}_{n-1})y,l}\right|^{2}\right]\\+W_{21,l}^{*}W_{22,l}\mathrm{E}\left[\left|N_{\ddot{x}_n y,l}\right|^{2}\Big/\left|S_{(\ddot{x}_n-\ddot{x}_{n-1})y,l}\right|^{2}\right]\end{array}\right\}\quad \text{for } \forall l,m\in Z[1,N] \tag{5.21i}$$

where Z[1,N] denotes a set containing natural numbers from 1 to N; δ_{lm} is Kronecker delta function. $\delta_{lm}=\begin{cases}1 & \text{if } l=m\\ 0 & \text{if } l\neq m\end{cases}$

The proofs of Equation (5.21a)~(5.21i) are given in Appendix B. Using the results from Equation (5.21a)~(5.21i), the mean and the variance of the identification error for the top story structural parameters $[k_n \;\; c_n]^{\mathrm{T}}$ can be calculated as

$$\mathrm{E}\left[\theta_{kn}\right]\approx 0 \tag{5.22}$$

$$\mathrm{E}\left[\theta_{cn}\right]\approx 0 \tag{5.23}$$

$$\mathrm{VAR}\left[\theta_{kn}\right]=\frac{1}{2}\sum_{l=1}^{N}\left\{\left|W_{11,l}\right|^{2}\mathrm{E}\left[\frac{\left|N_{\ddot{x}_{n-1}y,l}\right|^{2}}{\left|S_{(\ddot{x}_n-\ddot{x}_{n-1})y,l}\right|^{2}}\right]+\left|W_{12,l}\right|^{2}\mathrm{E}\left[\frac{\left|N_{\ddot{x}_n y,l}\right|^{2}}{\left|S_{(\ddot{x}_n-\ddot{x}_{n-1})y,l}\right|^{2}}\right]\right\} \tag{5.24}$$

$$\mathrm{VAR}\left[\theta_{cn}\right]=\frac{1}{2}\sum_{l=1}^{N}\left\{\left|W_{21,l}\right|^{2}\mathrm{E}\left[\frac{\left|N_{\ddot{x}_{n-1}y,l}\right|^{2}}{\left|S_{(\ddot{x}_n-\ddot{x}_{n-1})y,l}\right|^{2}}\right]+\left|W_{22,l}\right|^{2}\mathrm{E}\left[\frac{\left|N_{\ddot{x}_n y,l}\right|^{2}}{\left|S_{(\ddot{x}_n-\ddot{x}_{n-1})y,l}\right|^{2}}\right]\right\} \tag{5.25}$$

$$\mathrm{COV}\left[\theta_{kn}\theta_{cn}\right]=0 \tag{5.26}$$

The proofs of Equations (5.22)~(5.26) are given in Appendix C. The results in Equations (5.22) ~ (5.23) show that the CSD_SUBID method is an approximately unbiased estimator of structural parameters with finite length structural responses.

The values of $\mathrm{E}\{|N_{\ddot{x}_j y,l}|^2 \big/ |S_{(\ddot{x}_n-\ddot{x}_{n-1})y,l}|^2\}$ $(j=n-1,n)$, needed for the calculation of the identification error variances in Equations (5.24)~(5.25), are computed using the following approximation: the random variable $|N_{\ddot{x}_j y,l}|^2 \big/ |S_{(\ddot{x}_n-\ddot{x}_{n-1})y,l}|^2$ is first expanded into a Taylor series up to the second order with respect to the mean value $\mathrm{E}\{|N_{\ddot{x}_j y,l}|^2\}$ and $\mathrm{E}\{|S_{(\ddot{x}_n-\ddot{x}_{n-1})y,l}|^2\}$; then, take the expectation of this Taylor expansion to obtain the following result.

$$\begin{aligned}\mathrm{E}\left\{\frac{\left|N_{\ddot{x}_j y,l}\right|^2}{\left|S_{(\ddot{x}_n-\ddot{x}_{n-1})y,l}\right|^2}\right\} \approx \frac{\mathrm{E}\left\{\left|N_{\ddot{x}_j y,l}\right|^2\right\}}{\mathrm{E}\left\{\left|S_{(\ddot{x}_n-\ddot{x}_{n-1})y,l}\right|^2\right\}} - \frac{\mathrm{COV}\left\{\left|N_{\ddot{x}_j y,l}\right|^2, \left|S_{(\ddot{x}_n-\ddot{x}_{n-1})y,l}\right|^2\right\}}{\mathrm{E}\left\{\left|S_{(\ddot{x}_n-\ddot{x}_{n-1})y,l}\right|^2\right\}^2} \\ + \frac{\mathrm{E}\left\{\left|N_{\ddot{x}_j y,l}\right|^2\right\}\mathrm{VAR}\left\{\left|S_{(\ddot{x}_n-\ddot{x}_{n-1})y,l}\right|^2\right\}}{\mathrm{E}\left\{\left|S_{(\ddot{x}_n-\ddot{x}_{n-1})y,l}\right|^2\right\}^2}\end{aligned} \tag{5.27}$$

Due to the difficulty in directly evaluating the covariance term $\mathrm{COV}\{|N_{\ddot{x}_j y,l}|^2, |S_{(\ddot{x}_n-\ddot{x}_{n-1})y,l}|^2\}$, the upper bound values of $\mathrm{E}\{|N_{\ddot{x}_j y,l}|^2 \big/ |S_{(\ddot{x}_n-\ddot{x}_{n-1})y,l}|^2\}$, calculated via inequality relation shown in Equation (5.28), are used to calculate the variances of identification errors in Equations (5.24) & (5.25).

$$-1 \le \mathrm{COV}\left\{\left|N_{y\ddot{x}_j,l}\right|^2, \left|S_{y(\ddot{x}_n-\ddot{x}_{n-1}),l}\right|^2\right\} \Big/ \sqrt{\mathrm{VAR}\left\{\left|N_{y\ddot{x}_j,l}\right|^2\right\}\mathrm{VAR}\left\{\left|S_{y(\ddot{x}_n-\ddot{x}_{n-1}),l}\right|^2\right\}} \le 1 \tag{5.28}$$

$$\begin{aligned}\mathrm{E}\left\{\frac{\left|N_{\ddot{x}_j y,l}\right|^2}{\left|S_{(\ddot{x}_n-\ddot{x}_{n-1})y,l}\right|^2}\right\} \le \frac{\mathrm{E}\left\{\left|N_{\ddot{x}_j y,l}\right|^2\right\}}{\mathrm{E}\left\{\left|S_{(\ddot{x}_n-\ddot{x}_{n-1})y,l}\right|^2\right\}} + \frac{\sqrt{\mathrm{VAR}\left\{\left|N_{\ddot{x}_j y,l}\right|^2\right\}\mathrm{VAR}\left\{\left|S_{(\ddot{x}_n-\ddot{x}_{n-1})y,l}\right|^2\right\}}}{\mathrm{E}\left\{\left|S_{(\ddot{x}_n-\ddot{x}_{n-1})y,l}\right|^2\right\}^2} \\ + \frac{\mathrm{E}\left\{\left|N_{\ddot{x}_j y,l}\right|^2\right\}\mathrm{VAR}\left\{\left|S_{(\ddot{x}_n-\ddot{x}_{n-1})y,l}\right|^2\right\}}{\mathrm{E}\left\{\left|S_{(\ddot{x}_n-\ddot{x}_{n-1})y,l}\right|^2\right\}^2}\end{aligned} \tag{5.29}$$

The values of $E\{|N_{\ddot{x}_j y,l}|^2\}$, $E\{|S_{(\ddot{x}_n-\ddot{x}_{n-1})y,l}|^2\}$, $VAR\{\left|S_{(\ddot{x}_n-\ddot{x}_{n-1})y,l}\right|^2\}$ and $E\{|S_{(\ddot{x}_n-\ddot{x}_{n-1})y,l}|^2\}$ needed for the computation of Equation (5.29) can be evaluated as follows.

$$
\begin{aligned}
N_{\ddot{x}_j y,l} &= \frac{1}{Q}\sum_{p=1}^{Q}\left[(Y_l^{(p)} + N_{y,l}^{(p)})^*(\ddot{X}_{j,l}^{(p)} + N_{\ddot{x}_j,l}^{(p)})\right] - \frac{1}{Q}\sum_{p=1}^{Q}\left[Y_l^{(p)^*} X_{j,l}^{(p)}\right] \\
&= \frac{1}{Q}\sum_{p=1}^{Q}\left[Y_l^{(p)^*} N_{\ddot{x}_j,l}^{(p)} + N_{y,l}^{(p)^*}\ddot{X}_{j,l}^{(p)} + N_{y,l}^{(p)^*} N_{\ddot{x}_j,l}^{(p)}\right]
\end{aligned}
\tag{5.30}
$$

According to the central limit theorem for weakly dependent random variables (Billingsley, 1995), as Q – the number of the structural response segments used in calculating power spectral in Welch method – becomes large, the probability distribution of $N_{y\ddot{x}_j,l}$ is approximated by a complex Gaussian distribution with the mean $E[Y_l^* N_{\ddot{x}_j,l} + N_{y,l}^*\ddot{X}_{j,l} + N_{y,l}^* N_{\ddot{x}_j,l}]$ and the variance $VAR[Y_l^* N_{\ddot{x}_j,l} + N_{y,l}^*\ddot{X}_{j,l} + N_{y,l}^* N_{\ddot{x}_j,l}]/Q$. (The superscript p is dropped here due to the stationary condition for both the structural responses and the measurement noise. Note that the variance need not include covariance between segments as the noises in non-overlapping segments are independent.) Similarly, as Q becomes large, the probability distribution of $S_{(\ddot{x}_n-\ddot{x}_{n-1})y,l}$ can be approximated by a complex Gaussian distribution with the mean $E[(\ddot{X}_{n,l} - \ddot{X}_{n-1,l})Y_l^*]$ and the variance $VAR[(\ddot{X}_{n,l} - \ddot{X}_{n-1,l})Y_l^*]/Q$. The means and variances of $N_{\ddot{x}_j y,l}$ and $S_{(\ddot{x}_n-\ddot{x}_{n-1})y,l}$, which completely define the probability distribution functions of these Gaussian random variables, can be evaluated from the statistics of the structural response and the measurement noise. Therefore, all values of $E\{|N_{\ddot{x}_j y,l}|^2\}$, $E\{|S_{(\ddot{x}_n-\ddot{x}_{n-1})y,l}|^2\}$,

$\mathrm{VAR}\{|N_{\ddot{x}_j y,l}|^2\}$ and $\mathrm{VAR}\{|S_{(\ddot{x}_n-\ddot{x}_{n-1})y,l}|^2\}$ needed in Equation (5.29) can be then calculated from the probability distribution functions of $N_{\ddot{x}_j y,l}$ and $S_{(\ddot{x}_n-\ddot{x}_{n-1})y,l}$.

Since the variances $\mathrm{VAR}\{|N_{\ddot{x}_j y,l}|^2\}$ and $\mathrm{VAR}\{|S_{(\ddot{x}_n-\ddot{x}_{n-1})y,l}|^2\}$ vanishes in the Welch average periodogram method as Q tends to infinity. The limit of Equation (5.29), as Q tends to infinity, becomes

$$\lim_{Q\to\infty}\mathrm{E}\left\{\frac{\left|N_{\ddot{x}_j y,l}\right|^2}{\left|S_{(\ddot{x}_n-\ddot{x}_{n-1})y,l}\right|^2}\right\}\approx\frac{\lim_{Q\to\infty}\mathrm{E}\left\{\left|N_{\ddot{x}_j y,l}\right|^2\right\}}{\lim_{Q\to\infty}\mathrm{E}\left\{\left|S_{(\ddot{x}_n-\ddot{x}_{n-1})y,l}\right|^2\right\}}=\frac{\mathrm{E}\left\{\lim_{Q\to\infty}\left[\left|N_{\ddot{x}_j y,l}\right|^2\right]\right\}}{\mathrm{E}\left\{\lim_{Q\to\infty}\left[\left|S_{(\ddot{x}_n-\ddot{x}_{n-1})y,l}\right|^2\right]\right\}}=0 \tag{5.31}$$

The last step in Equation (5.31) is due to the facts that $N_{\ddot{x}_j y,l}$ is a zero-mean complex random variable with infinite small variance (as $Q\to\infty$) and $S_{(\ddot{x}_n-\ddot{x}_{n-1})y,l}$ is a non zero-mean complex random variable with infinite small variance (as $Q\to\infty$). Thus, the limit in Equation (5.31) becomes the ratio of the magnitude square of the complex random variables $N_{\ddot{x}_j y,l}$ and $S_{(\ddot{x}_n-\ddot{x}_{n-1})y,l}$, which obviously equal zero.

Thus, as Q tends to infinity, the values of $\mathrm{E}\{|N_{\ddot{x}_j y,l}|^2 \big/ |S_{(\ddot{x}_n-\ddot{x}_{n-1})y,l}|^2\}$ $(j=n-1,n)$ converge to zero, implying that the variance of estimated structural parameters converge to zero. Therefore, the CSD_SUBID method is also an asymptotically consistent estimator for the top story structural parameters.

5.5.2 Non-top Story Identification Case

As suggested by Equation (5.16), the identification errors for the i^{th} (non-top) story substructures $[\theta_{k(i+1)}\ \ \theta_{c(i+1)}]^{\mathrm{T}}$ equal the combination of two kinds of identification errors.

$$\begin{bmatrix}\theta_{ki}\\ \theta_{ci}\end{bmatrix} \approx \begin{bmatrix}\theta_{ki}{}^{(1)}\\ \theta_{ci}{}^{(1)}\end{bmatrix} + \begin{bmatrix}\theta_{ki}{}^{(2)}\\ \theta_{ci}{}^{(2)}\end{bmatrix} \tag{5.32}$$

where $[\theta_{ki}{}^{(1)}\ \ \theta_{ci}{}^{(1)}]^{\mathrm{T}}$ are the identification errors caused by the measurement uncertainty of the cross power spectral density as defined in Equation (5.33); and $[\theta_{ki}{}^{(2)}\ \theta_{ci}{}^{(2)}]^{\mathrm{T}}$ are the identification errors due to the uncertainty of the structural parameters of the story above as defined in Equation (5.34).

$$\begin{bmatrix}\theta_{ki}{}^{(1)}\\ \theta_{ci}{}^{(1)}\end{bmatrix} = \sum_{l=1}^{N} \mathrm{Re}\left\{ \begin{bmatrix} U_{11,l} & U_{12,l} & U_{13,l}\\ U_{21,l} & U_{22,l} & U_{23,l}\end{bmatrix} \cdot \begin{bmatrix} N_{\ddot{x}_{i-1}y,l} / S_{(\ddot{x}_i-\ddot{x}_{i-1})y,l}\\ N_{\ddot{x}_i y,l} / S_{(\ddot{x}_i-\ddot{x}_{i-1})y,l}\\ N_{\ddot{x}_{i+1}y,l} / S_{(\ddot{x}_i-\ddot{x}_{i-1})y,l}\end{bmatrix} \right\} \tag{5.33}$$

$$\begin{bmatrix}\theta_{ki}{}^{(2)}\\ \theta_{ci}{}^{(2)}\end{bmatrix} = \sum_{l=1}^{N} \mathrm{Re}\left\{ \begin{bmatrix} U_{14,l} & U_{15,l}\\ U_{24,l} & U_{25,l}\end{bmatrix} \cdot \begin{bmatrix} \dfrac{S_{(\ddot{x}_{i+1}-\ddot{x}_i)y,l}}{S_{(\ddot{x}_i-\ddot{x}_{i-1})y,l}}\theta_{k(i+1)}\\ \dfrac{S_{(\ddot{x}_{i+1}-\ddot{x}_i)y,l}}{S_{(\ddot{x}_i-\ddot{x}_{i-1})y,l}}\theta_{c(i+1)}\end{bmatrix} \right\} \tag{5.34}$$

Since the identification error $[\theta_{k(i+1)}\ \theta_{c(i+1)}]^{\mathrm{T}}$ is a real-value vector, Equation (5.34) can be further simplified as

$$\begin{bmatrix}\theta_{ki}{}^{(2)}\\ \theta_{ci}{}^{(2)}\end{bmatrix} = \begin{bmatrix} \sum_{l=1}^{N}\mathrm{Re}\left[U_{14,l}\Delta_{(i+1)i,l}\right] & \sum_{l=1}^{N}\mathrm{Re}\left[U_{15,l}\Delta_{(i+1)i,l}\right]\\ \sum_{l=1}^{N}\mathrm{Re}\left[U_{24,l}\Delta_{(i+1)i,l}\right] & \sum_{l=1}^{N}\mathrm{Re}\left[U_{25,l}\Delta_{(i+1)i,l}\right]\end{bmatrix} \cdot \begin{bmatrix}\theta_{k(i+1)}\\ \theta_{c(i+1)}\end{bmatrix} \tag{5.35}$$

where $\Delta_{(i+1)i,l} = S_{(\ddot{x}_{i+1}-\ddot{x}_i)y,l} / S_{(\ddot{x}_i-\ddot{x}_{i-1})y,l}$.

Following derivations, similar to those in subsection 5.5.1, it can be easily shown that the statistical moments of the error $[\theta_{ki}{}^{(1)}\ \ \theta_{ci}{}^{(1)}]^{\mathrm{T}}$ in Equation (5.33) can be evaluated as,

$$\mathrm{E}\left[\theta_{ki}{}^{(1)}\right] \approx 0 \tag{5.36a}$$

$$\mathrm{E}\left[\theta_{ci}{}^{(1)}\right] \approx 0 \tag{5.36b}$$

$$\mathrm{VAR}\left[\theta_{ki}{}^{(1)}\right] \approx \frac{1}{2}\sum_{l=1}^{N}\left\{\begin{aligned} & \left|U_{11,l}\right|^2 \mathrm{E}\left[\left|N_{\ddot{x}_{i-1}y,l}\right|^2 \Big/ \left|S_{(\ddot{x}_i-\ddot{x}_{i-1})y,l}\right|^2\right] \\ & + \left|U_{12,l}\right|^2 \mathrm{E}\left[\left|N_{\ddot{x}_i y,l}\right|^2 \Big/ \left|S_{(\ddot{x}_i-\ddot{x}_{i-1})y,l}\right|^2\right] \\ & + \left|U_{13,l}\right|^2 \mathrm{E}\left[\left|N_{\ddot{x}_{i+1}y,l}\right|^2 \Big/ \left|S_{(\ddot{x}_i-\ddot{x}_{i-1})y,l}\right|^2\right] \end{aligned}\right\} \tag{5.36c}$$

$$\mathrm{VAR}\left[\theta_{ci}{}^{(1)}\right] \approx \frac{1}{2}\sum_{l=1}^{N}\left\{\begin{aligned} & \left|U_{21,l}\right|^2 \mathrm{E}\left[\left|N_{\ddot{x}_{i-1}y,l}\right|^2 \Big/ \left|S_{(\ddot{x}_i-\ddot{x}_{i-1})y,l}\right|^2\right] \\ & + \left|U_{22,l}\right|^2 \mathrm{E}\left[\left|N_{\ddot{x}_i y,l}\right|^2 \Big/ \left|S_{(\ddot{x}_i-\ddot{x}_{i-1})y,l}\right|^2\right] \\ & + \left|U_{23,l}\right|^2 \mathrm{E}\left[\left|N_{\ddot{x}_{i+1}y,l}\right|^2 \Big/ \left|S_{(\ddot{x}_i-\ddot{x}_{i-1})y,l}\right|^2\right] \end{aligned}\right\} \tag{5.36d}$$

$$\mathrm{COV}\left[\theta_{ki}{}^{(1)}\theta_{ci}{}^{(1)}\right] \approx 0 \tag{5.36e}$$

The proofs for Equations (5.36a)~(5.36e), which are similar to those of Equations (5.22) ~ (5.26), are omitted here.

Due to the third assumption in the choice of reference selection in section 5.4 that there is only one excitation source in the structure, the terms $\Delta_{(i+1)i,l} = S_{(\ddot{x}_{i+1}-\ddot{x}_i)y,l} \big/ S_{(\ddot{x}_i-\ddot{x}_{i-1})y,l}$ become deterministic values. Then, the mean of the second kind of identification errors $[\theta_{ki}{}^{(2)}\ \ \theta_{ci}{}^{(2)}]^{\mathrm{T}}$ are calculated as follows

$$\mathrm{E}\begin{bmatrix}\theta_{ki}{}^{(2)} \\ \theta_{ci}{}^{(2)}\end{bmatrix} = \mathbf{T}\cdot\mathrm{E}\begin{bmatrix}\theta_{k(i+1)} \\ \theta_{c(i+1)}\end{bmatrix} \tag{5.37}$$

where $\mathbf{T} = \begin{bmatrix} \sum_{l=1}^{N}\mathrm{Re}\left[U_{14,l}\Delta_{(i+1)i,l}\right] & \sum_{l=1}^{N}\mathrm{Re}\left[U_{15,l}\Delta_{(i+1)i,l}\right] \\ \sum_{l=1}^{N}\mathrm{Re}\left[U_{24,l}\Delta_{(i+1)i,l}\right] & \sum_{l=1}^{N}\mathrm{Re}\left[U_{25,l}\Delta_{(i+1)i,l}\right] \end{bmatrix}$.

Combining the results from Equation (5.36a), (5.36b) and (5.37), the mean of the identification error for the i^{th} story parameters becomes

$$\mathrm{E}\begin{bmatrix}\theta_{ki}\\ \theta_{ci}\end{bmatrix} \approx \mathrm{E}\begin{bmatrix}\theta_{ki}{}^{(1)}\\ \theta_{ci}{}^{(2)}\end{bmatrix} + \mathrm{E}\begin{bmatrix}\theta_{ki}{}^{(2)}\\ \theta_{ci}{}^{(2)}\end{bmatrix} = \mathbf{T}\cdot\mathrm{E}\begin{bmatrix}\theta_{k(i+1)}\\ \theta_{c(i+1)}\end{bmatrix} \quad (i = 1\ldots n-1) \tag{5.38}$$

Given that the mean of the identification errors of the top story parameters $[\theta_{kn} \;\; \theta_{cn}]^{\mathrm{T}}$ are zero as shown in Equations (5.25a) and (5.25b), the mean of the identification errors of other story parameters all (approximately) become zero.

$$\mathrm{E}\begin{bmatrix}\theta_{ki}\\ \theta_{ci}\end{bmatrix} \approx \begin{bmatrix}0\\ 0\end{bmatrix} \quad (i = 1\ldots n) \tag{5.39}$$

Putting the result of Equation (5.39) back to Equation (5.37), the covariance matrix of the second kind identification error $[\theta_{ki}{}^{(2)} \; \theta_{ci}{}^{(2)}]^{\mathrm{T}}$ becomes

$$\begin{aligned}\mathrm{COV}\begin{bmatrix}\theta_{ki}{}^{(2)}\\ \theta_{ci}{}^{(2)}\end{bmatrix} &= \begin{bmatrix}\mathrm{VAR}\left[\theta_{ki}{}^{(2)}\right] & \mathrm{COV}\left[\theta_{ki}{}^{(2)},\theta_{ci}{}^{(2)}\right]\\ \mathrm{COV}\left[\theta_{ki}{}^{(2)},\theta_{ci}{}^{(2)}\right] & \mathrm{VAR}\left[\theta_{ci}{}^{(2)}\right]\end{bmatrix}\\ &\approx \mathbf{T}\cdot\begin{bmatrix}\mathrm{VAR}\left[\theta_{k(i+1)}\right] & \mathrm{COV}\left[\theta_{k(i+1)},\theta_{c(i+1)}\right]\\ \mathrm{COV}\left[\theta_{k(i+1)},\theta_{c(i+1)}\right] & \mathrm{VAR}\left[\theta_{c(i+1)}\right]\end{bmatrix}\cdot\mathbf{T}^{\mathrm{T}}\end{aligned} \tag{5.40}$$

Then, the covariance matrix of the identification errors $[\theta_{ki} \;\; \theta_{ci}]^{\mathrm{T}}$ are evaluated as shown in Equation (5.41).

$$\begin{aligned}\mathrm{COV}\begin{bmatrix}\theta_{ki}\\ \theta_{ci}\end{bmatrix} \approx &\begin{bmatrix}\mathrm{VAR}\left[\theta_{ki}{}^{(1)}\right] & \mathrm{COV}\left[\theta_{ki}{}^{(1)},\theta_{ci}{}^{(1)}\right]\\ \mathrm{COV}\left[\theta_{ki}{}^{(1)},\theta_{ci}{}^{(1)}\right] & \mathrm{VAR}\left[\theta_{ci}{}^{(1)}\right]\end{bmatrix}\\ &+\begin{bmatrix}\mathrm{VAR}\left[\theta_{ki}{}^{(2)}\right] & \mathrm{COV}\left[\theta_{ki}{}^{(2)},\theta_{ci}{}^{(2)}\right]\\ \mathrm{COV}\left[\theta_{ki}{}^{(2)},\theta_{ci}{}^{(2)}\right] & \mathrm{VAR}\left[\theta_{ci}{}^{(2)}\right]\end{bmatrix}\\ &+2\begin{bmatrix}\mathrm{COV}\left[\theta_{ki}{}^{(1)},\theta_{ki}{}^{(2)}\right] & \mathrm{COV}\left[\theta_{ki}{}^{(1)},\theta_{ci}{}^{(2)}\right]\\ \mathrm{COV}\left[\theta_{ki}{}^{(2)},\theta_{ci}{}^{(1)}\right] & \mathrm{COV}\left[\theta_{ci}{}^{(1)},\theta_{ci}{}^{(2)}\right]\end{bmatrix}\end{aligned} \tag{5.41}$$

Since the two kinds of the identification error – $[\theta_{ki}^{(1)}\ \ \theta_{ci}^{(1)}]^{\mathrm{T}}$ and $[\theta_{ki}^{(2)}\ \ \theta_{ci}^{(2)}]^{\mathrm{T}}$ – are all related to some common structural responses (*e.g.*, $S_{(\ddot{x}_i-\ddot{x}_{i-1})y,l}$), they are generally correlated; thus, the covariance matrix between the two kinds of the identification error – the third term in Equation (5.40) – is not a zero matrix. However, due to the great complexity involved in obtaining the analytical expression for this covariance matrix, two alternative methods are discussed herein to evaluate the third term in Equation (5.41). The first method simply assumes that the two kinds of identification error are uncorrelated. Then the third matrix on the right of Equation (5.41) equals a zero matrix and the covariance matrix in Equation (5.41) is further simplified as Equation (5.42). But such an assumption may sometimes lead to an under-estimation of the identification error variance, which is undesirable in real applications.

$$\begin{aligned}\mathrm{COV}\begin{bmatrix}\theta_{ki}\\ \theta_{ci}\end{bmatrix} &\approx \begin{bmatrix}\mathrm{VAR}\left[\theta_{ki}^{(1)}\right] & \mathrm{COV}\left[\theta_{ki}^{(1)},\theta_{ci}^{(1)}\right]\\ \mathrm{COV}\left[\theta_{ki}^{(1)},\theta_{ci}^{(1)}\right] & \mathrm{VAR}\left[\theta_{ci}^{(1)}\right]\end{bmatrix}\\ &+\begin{bmatrix}\mathrm{VAR}\left[\theta_{ki}^{(2)}\right] & \mathrm{COV}\left[\theta_{ki}^{(2)},\theta_{ci}^{(2)}\right]\\ \mathrm{COV}\left[\theta_{ki}^{(2)},\theta_{ci}^{(2)}\right] & \mathrm{VAR}\left[\theta_{ci}^{(2)}\right]\end{bmatrix}\end{aligned} \tag{5.42}$$

The second method utilizes the inequality in Equation (5.43).

$$\begin{aligned}&\begin{bmatrix}\mathrm{VAR}\left[\theta_{ki}^{(1)}\right] & \mathrm{COV}\left[\theta_{ki}^{(1)},\theta_{ci}^{(1)}\right]\\ \mathrm{COV}\left[\theta_{ki}^{(1)},\theta_{ci}^{(1)}\right] & \mathrm{VAR}\left[\theta_{ci}^{(1)}\right]\end{bmatrix}+\begin{bmatrix}\mathrm{VAR}\left[\theta_{ki}^{(2)}\right] & \mathrm{COV}\left[\theta_{ki}^{(2)},\theta_{ci}^{(2)}\right]\\ \mathrm{COV}\left[\theta_{ki}^{(2)},\theta_{ci}^{(2)}\right] & \mathrm{VAR}\left[\theta_{ci}^{(2)}\right]\end{bmatrix}\\ &\geq 2\begin{bmatrix}\mathrm{COV}\left[\theta_{ki}^{(1)},\theta_{ki}^{(2)}\right] & \mathrm{COV}\left[\theta_{ki}^{(1)},\theta_{ci}^{(2)}\right]\\ \mathrm{COV}\left[\theta_{ki}^{(2)},\theta_{ci}^{(1)}\right] & \mathrm{COV}\left[\theta_{ci}^{(1)},\theta_{ci}^{(2)}\right]\end{bmatrix}\end{aligned} \tag{5.43}$$

where "≥" denotes the semi-positiveness of the matrix relationship.

Then, the upper bound values of the covariance matrix of the identification errors $[\theta_{ki}\ \ \theta_{ci}]^{\mathrm{T}}$ are evaluated as

$$\mathrm{COV}\begin{bmatrix}\theta_{ki}\\ \theta_{ci}\end{bmatrix} \leq 2\begin{bmatrix}\mathrm{VAR}\left[\theta_{ki}{}^{(1)}\right] & \mathrm{COV}\left[\theta_{ki}{}^{(1)},\theta_{ci}{}^{(1)}\right]\\ \mathrm{COV}\left[\theta_{ki}{}^{(1)},\theta_{ci}{}^{(1)}\right] & \mathrm{VAR}\left[\theta_{ci}{}^{(1)}\right]\end{bmatrix} + 2\begin{bmatrix}\mathrm{VAR}\left[\theta_{ki}{}^{(2)}\right] & \mathrm{COV}\left[\theta_{ki}{}^{(2)},\theta_{ci}{}^{(2)}\right]\\ \mathrm{COV}\left[\theta_{ki}{}^{(2)},\theta_{ci}{}^{(2)}\right] & \mathrm{VAR}\left[\theta_{ci}{}^{(2)}\right]\end{bmatrix} \tag{5.44}$$

where "≤" denotes the semi-negative nature of the matrix.

However, if Equation (5.44) is adopted to calculate the variance of the parameter identification error, the variances are over-estimated. Moreover, the over-estimated variances will propagate to the variance estimation of the identification error of the lower story parameters. Therefore, Equation (5.44) will lead to large over-estimation of the identification error variance for the structural parameters in the lower stories, which, of course, is also undesired. In this study, Equation (5.42), assuming the two errors are uncorrelated, will still be used to calculate the variance of the identification error; Equation (5.44), assuming the two errors are fully correlated, is only treated as the conservative upper bound for the variance estimation.

5.6 CSD_SUBID with Non-stationary Response

The derivation of the CSD_SUBID method in section 5.1 requires that the structural responses are wide sense stationary. In order to achieve accurate identification results when the noise level in the measurements is large, very long stationary structural responses are usually needed by the CSD_SUBID method. However, since most ambient excitation sources, *e.g.*, micro ground tremor, are not wide sense stationary in the long run, the structural responses due to ambient excitations are, strictly speaking, not stationary. Can CSD_SUBID method be used to identify the structural parameter when the structure is subject to ambient excitations? In this section, it will be shown that, with little modification, the CSD_SUBID method can be applied to perform the identification with non-stationary structural responses.

Assume that there are Q groups of the structural responses available, each of which contains the structural acceleration responses $\ddot{x}_i(t)\ (i=1,...,n)$ and a reference response $y(t)$ of the same duration T. The structural responses in these Q groups are not necessarily stationary; they can be obtained by partitioning a set of long structural response records into Q non-overlapped/overlapped segments or by recording the structural responses of the same duration T at Q different times.

5.6.1 Top Story Identification

Since the structural responses in each group satisfy the dynamic equations of the structure, these responses are also governed by the dynamic equation of the top story substructure as follows,

$$m_n \ddot{x}_n^{(q)} + c_n(\dot{x}_n^{(q)} - \dot{x}_{n-1}^{(q)}) + k_n(x_n^{(q)} - x_{n-1}^{(q)}) = 0 \tag{5.45}$$

where $\ddot{x}_i^{(q)}\ (i=1,...,N)$ is the i^{th} floor displacement response relative to an inertial reference frame in the q^{th} group responses; the superscript q (q=1,…,Q) denotes the number of group responses. Adding $-m_n \ddot{x}_{n-1}^{(q)}$ to both sides of Equation (5.45) gives

$$m_n\left(\ddot{x}_n^{(q)} - \ddot{x}_{n-1}^{(q)}\right) + c_n\left(\dot{x}_n^{(q)} - \dot{x}_{n-1}^{(q)}\right) + k_n\left(x_n^{(q)} - x_{n-1}^{(q)}\right) = -m_n \ddot{x}_{n-1}^{(q)} \tag{5.46}$$

Take Fourier transform of Equation (5.46)

$$m_n\left(\ddot{X}_n^{(q)} - \ddot{X}_{n-1}^{(q)}\right) + c_n\left(\dot{X}_n^{(q)} - \dot{X}_{n-1}^{(q)}\right) + k_n\left(X_n^{(q)} - X_{n-1}^{(q)}\right) = -m_n \ddot{X}_{n-1}^{(q)} \tag{5.47}$$

where $X_i^{(q)}, \dot{X}_i^{(q)}, \ddot{X}_i^{(q)}$ are the Fourier transforms (or the frequency responses) of the displacement, velocity and acceleration responses of the i^{th} floor $x_i^{(q)}, \dot{x}_i^{(q)}, \ddot{x}_i^{(q)}$ in the q^{th} group, respectively. Using the rule of integration by parts, it can be shown that $X_i^{(q)}, \dot{X}_i^{(q)}$ and $\ddot{X}_i^{(q)}$ have the following relations.

$$\dot{X}_i^{(q)} = x_i^{(q)}(t)e^{-j\omega t}\Big|_{t=T}^{t=0} + (j\omega)X_i^{(q)} \tag{5.48}$$

$$\ddot{X}_i^{(q)} = \dot{x}_i^{(q)}(t)e^{-j\omega t}\Big|_{t=T}^{t=0} + (j\omega)x_i^{(q)}(t)e^{-j\omega t}\Big|_{t=T}^{t=0} + (j\omega)^2 X_i^{(q)} \tag{5.49}$$

Substituting the results of Equations (5.48) & (5.49) back to Equation (5.47) leads to

$$\left(\ddot{X}_n^{(q)} - \ddot{X}_{n-1}^{(q)}\right)\left(m_n + \frac{c_n}{j\omega} + \frac{k_n}{(j\omega)^2}\right) = -m_n\ddot{X}_{n-1}^{(q)} + F_n^{(q)} \tag{5.50}$$

where $F_n^{(q)} = \Delta_{x_n}^{(q)} e^{-j\omega t}\Big|_{t=T}^{t=0} \dfrac{k_n}{(j\omega)} + \dot{\Delta}_{x_n}^{(q)} e^{-j\omega t}\Big|_{t=T}^{t=0}\left[\dfrac{c_n}{(j\omega)} + \dfrac{k_n}{(j\omega)^2}\right]$;

$\Delta_{x_n}^{(q)} = x_n^{(q)}(t) - x_{n-1}^{(q)}(t)$; $\dot{\Delta}_{x_n}^{(q)} = \dot{x}_n^{(q)}(t) - \dot{x}_{n-1}^{(q)}(t)$.

Rearrange the order of Equation (5.50).

$$\frac{1}{1 - j\,c_n/(m_n\omega) - k_n/(m_n\omega^2)} = \frac{\ddot{X}_{n-1}^{(q)} - \ddot{X}_n^{(q)}}{\ddot{X}_{n-1}^{(q)} - F_n^{(q)}/m_n} \tag{5.51}$$

Multiply both the numerator and denominator of the right side of Equation (5.51) by the conjugate of the Fourier transform of the reference response $y^{(q)}$. It is worth pointing out here that there is not any specific requirement for the reference response, as opposed to the CSD_SUBID method which requires the reference response be wide sense stationary with respect to other structural responses.

$$\frac{1}{1-j\,c_n/(m_n\omega)-k_n/(m_n\omega^2)}=\frac{(\ddot{X}_{n-1}{}^{(q)}-\ddot{X}_n{}^{(q)})Y^{(q)^*}}{(\ddot{X}_{n-1}{}^{(q)}-F_n{}^{(q)}/m_n)Y^{(q)^*}} \tag{5.52}$$

An identity in fraction number analysis is shown in Equation (5.53),

$$\frac{A}{B}=\frac{C}{D}\Rightarrow\frac{A}{B}=\frac{C}{D}=\frac{A+C}{B+D} \tag{5.53}$$

where A/B and C/D are two fraction numbers.

Since Equation (5.52) is true for any q (q=1,…,Q), by using the equality in Equation (5.53), Equation (5.52) can be rewritten into a new equation, whose right side involves all Q groups of structural responses together.

$$\frac{1}{1-j\,c_n/(m_n\omega)-k_n/(m_n\omega^2)}=\frac{\sum_{q=1}^{Q}\left(\ddot{X}_{n-1}{}^{(q)}-\ddot{X}_n{}^{(q)}\right)Y^{(q)^*}}{\sum_{q=1}^{Q}\left(\ddot{X}_{n-1}{}^{(q)}-F_n{}^{(q)}/m_n\right)Y^{(q)^*}} \tag{5.54}$$

Divide the numerator and denominator of the right side of Equation (5.54) by QT.

$$\frac{1}{1-j\,c_n/(m_n\omega)-k_n/(m_n\omega^2)}=\frac{P_{\ddot{x}_{n-1}y}-P_{\ddot{x}_n y}}{P_{\ddot{x}_{n-1}y}-P_{f_n y}} \tag{5.55}$$

where $P_{\ddot{x}_i y}=\frac{1}{QT}\sum_{q=1}^{Q}\ddot{X}_i{}^{(q)}Y^{(q)^*}\quad(i=1,\ldots,n)$; $\qquad P_{f_n y}=\frac{1}{QT}\sum_{q=1}^{Q}F_n{}^{(q)}Y^{(q)^*}/m_n$.

Then, an identification problem can be formulated by minimizing the second norm of the difference between the two sides of Equation (5.55) over all possible frequencies, in which the structural parameters of the top story $[k_n\ \ c_n]^{\mathrm{T}}$ are identified.

$$\underset{k_n,c_n}{\arg\min}\quad J(k_n,c_n)=\sum_{l=1}^{N}\left|f_l(k_n,c_n)-\hat{f}_l(\hat{P}_{\ddot{x}_n y},\hat{P}_{\ddot{x}_{n-1}y},\hat{P}_{f_n y})\right|^2 \tag{5.56}$$

where $f_l(k_n, c_n) = \dfrac{1}{1 - j\,c_n/(m_n\omega_l) - k_n/(m_n\omega_l^2)}$, $\hat{f}_l(\hat{P}_{\ddot{x}_n y}, \hat{P}_{\ddot{x}_{n-1} y}, \hat{P}_{f_n y}) = \dfrac{\hat{P}_{\ddot{x}_{n-1} y} - \hat{P}_{\ddot{x}_n y}}{\hat{P}_{\ddot{x}_{n-1} y} - \hat{P}_{f_n y}}$;

$\hat{P}_{y\ddot{x}_i}$ and $\hat{P}_{f_n y}$ are the variables $P_{\ddot{x}_i y}$ and $P_{f_n y}$ in Equation (5.55), respectively, calculated from the noise contaminated measurements.

5.6.2 Non-top Story Identification

After the structural parameters of the top story $[k_n\ c_n]^{\mathrm{T}}$ have been identified, a similar induction method as in the CSD_SUBID method is established to identify structural parameters of other stories in the following manner.

The dynamic equation of the i^{th} ($i<n$) story substructure can be written as

$$\begin{aligned} m_i\ddot{x}_i^{(q)} &+ c_i(\dot{x}_i^{(q)} - \dot{x}_{i-1}^{(q)}) + k_i(x_i^{(q)} - x_{i-1}^{(q)}) \\ &+ c_{i+1}(\dot{x}_i^{(q)} - \dot{x}_{i+1}^{(q)}) + k_{i+1}(x_i^{(q)} - x_{i+1}^{(q)}) = 0 \end{aligned} \tag{5.57}$$

where $\ddot{x}_i^{(q)}$ $(i = 1,..., N-1)$ is the i^{th} floor displacement response relative to an inertial reference frame in the q^{th} group responses; the superscript q (q=1,…,Q) denotes the group response number. Adding $-m_i\ddot{x}_{i-1}^{(q)}$ to both sides of Equation (5.57) and taking the Fourier transformation gives

$$\begin{aligned} m_i(\ddot{X}_i^{(q)} - \ddot{X}_{i-1}^{(q)}) &+ c_i(\dot{X}_i^{(q)} - \dot{X}_{i-1}^{(q)}) + k_i(X_i^{(q)} - X_{i-1}^{(q)}) \\ &+ c_{i+1}(\dot{X}_i^{(q)} - \dot{X}_{i+1}^{(q)}) + k_{i+1}(X_i^{(q)} - X_{i+1}^{(q)}) = -m_i\ddot{X}_{i-1}^{(q)} \end{aligned} \tag{5.58}$$

Using the relations between $X_i^{(q)}, \dot{X}_i^{(q)}$ and $\ddot{X}_i^{(q)}$, shown in Equations (5.48) and (5.49), the following equation is obtained

$$\left(\ddot{X}_i^{(q)} - \ddot{X}_{i-1}^{(q)}\right)\left(m_i + \frac{c_i}{j\omega} + \frac{k_i}{(j\omega)^2}\right)$$
$$= -m_i \ddot{X}_{i-1}^{(q)} + \left(\ddot{X}_{i+1}^{(q)} - \ddot{X}_i^{(q)}\right)\left(\frac{c_{i+1}}{j\omega} + \frac{k_{i+1}}{(j\omega)^2}\right) + F_i^{(q)} \tag{5.59}$$

where
$$F_i^{(q)} = \Delta_{x_i}^{(q)} e^{-j\omega t}\Big|_{t=T}^{t=0} \frac{k_i}{j\omega} + \dot{\Delta}_{x_i}^{(q)} e^{-j\omega t}\Big|_{t=T}^{t=0}\left[\frac{c_i}{j\omega} + \frac{k_i}{(j\omega)^2}\right]$$
$$- \Delta_{x_{i+1}}^{(q)} e^{-j\omega t}\Big|_{t=T}^{t=0} \frac{k_{i+1}}{j\omega} - \dot{\Delta}_{x_{i+1}}^{(q)} e^{-j\omega t}\Big|_{t=T}^{t=0}\left[\frac{c_{i+1}}{j\omega} + \frac{k_{i+1}}{(j\omega)^2}\right];$$

$\Delta_{x_i}^{(q)} = x_i^{(q)}(t) - x_{i-1}^{(q)}(t)$; $\dot{\Delta}_{x_i}^{(q)} = \dot{x}_i^{(q)}(t) - \dot{x}_{i-1}^{(q)}(t)$; $\Delta_{x_{i+1}}^{(q)} = x_{i+1}^{(q)}(t) - x_i^{(q)}(t)$;

$\dot{\Delta}_{x_{i+1}}^{(q)} = \dot{x}_{i+1}^{(q)}(t) - \dot{x}_i^{(q)}(t)$. Rearrange the order of Equation (5.59) to get.

$$\frac{1}{1 - j c_i/(m_i\omega) - k_i/(m_i\omega^2)}$$
$$= \frac{\ddot{X}_{i-1}^{(q)} - \ddot{X}_i^{(q)}}{-\ddot{X}_{i-1}^{(q)} + (\ddot{X}_{i+1}^{(q)} - \ddot{X}_i^{(q)})\left[jc_{i+1}/(m_i\omega) + k_{i+1}/(m_i\omega^2)\right] - F_i^{(q)}/m_i} \tag{5.60}$$

Multiplying both the numerator and denominator of the right side of Equation (5.60) by the conjugate of the Fourier transform of the reference response $y^{(q)}$ and using the equality condition of fraction numbers given in Equation (5.52), the following equation is obtained

$$\frac{1}{1 - j c_i/(m_i\omega) - k_i/(m_i\omega^2)}$$
$$= \frac{\sum_{q=1}^{Q}\left(\ddot{X}_{i-1}^{(q)} - \ddot{X}_i^{(q)}\right)Y^{(q)*}}{\sum_{q=1}^{Q}\left\{-\ddot{X}_{i-1}^{(q)} + \left(\ddot{X}_{i+1}^{(q)} - \ddot{X}_i^{(q)}\right)\left[jc_{i+1}/(m_i\omega) + k_{i+1}/(m_i\omega^2)\right] + F_i^{(q)}/m_i\right\}Y^{(q)*}} \tag{5.61}$$

Divide the numerator and denominator of the right side of Equation (5.61) by *QT*.

$$\frac{1}{1-j\,c_i/(m_i\omega)-k_i/(m_i\omega^2)} = \frac{P_{\ddot{x}_{i-1}y}-P_{\ddot{x}_iy}}{P_{\ddot{x}_{i-1}y}+(P_{\ddot{x}_{i+1}y}-P_{\ddot{x}_iy})[jc_{i+1}/(m_i\omega)+k_{i+1}/(m_i\omega^2)]-P_{f_iy}} \tag{5.62}$$

where $P_{\ddot{x}_iy}=\frac{1}{QT}\sum_{q=1}^{Q}\ddot{X}_i^{(q)}Y^{(q)^*}$ $(i=1,\ldots,n)$; $P_{f_iy}=\frac{1}{QT}\sum_{q=1}^{Q}F_i^{(q)}Y^{(q)^*}\Big/m_i$ $(i=1,\ldots,n-1)$.

Assuming that the structural parameters of the $(i+1)^{\text{th}}$ story are known, an identification problem can be formulated to identify the structural parameters of the non-top story $[k_i\ \ c_i]^{\mathrm{T}}$, which minimizes the difference between two sides of Equation (5.61) over all possible frequencies.

$$\underset{k_i,c_i}{\arg\min}\quad J(k_i,c_i)=\sum_{l=1}^{N}\left|g_l(k_i,c_i)-\hat{g}_l(\hat{P}_{\ddot{x}_{i-1}y,l},\hat{P}_{\ddot{x}_iy,l},\hat{P}_{\ddot{x}_{i+1}i,l},\hat{P}_{f_iy,l})\right|^2 \tag{5.63}$$

where $g_l(k_i,c_i)=\dfrac{1}{1-j\,c_i/(m_i\omega_l)-k_i/(m_i\omega_l^2)}$;

$$\hat{g}_l(\hat{P}_{\ddot{x}_{i-1}y,l},\hat{P}_{\ddot{x}_iy,l},\hat{P}_{\ddot{x}_{i+1}y,l},\hat{P}_{f_iy,l})=\frac{\hat{P}_{\ddot{x}_{i-1}y,l}-\hat{P}_{\ddot{x}_iy,l}}{\hat{P}_{\ddot{x}_{i-1}y,l}+(\hat{P}_{\ddot{x}_{i+1}y,l}-\hat{P}_{\ddot{x}_iy,l})[jc_{i+1}/(m_i\omega_l)+k_{i+1}/(m_i\omega_l^2)]-\hat{P}_{f_iy,l}}$$

Since the identification parameters of the top story have been identified from the previous step, which can be used to initiate the induction identification process described in this section, by repeating the identification problem (5.63), the structural parameters of all stories can be identified from top to bottom iteratively.

5.6.3 Comparison of CSD_SUBID Method with Stationary and Non-stationary Responses

Comparing the CSD_SUBID method using non-stationary structural responses, shown in Equations (5.57)&(5.63), with the method using stationary structural responses, shown in Equations (5.8)&(5.10), it is found that the two identification problems differ in the following two aspects:

1. The terms $P_{\ddot{x}_i y}$, used in the identification with non-stationary responses, replace the cross power spectral $S_{\ddot{x}_i y}$ used in the identification with stationary responses.
2. There are new terms $P_{f_i y}$ involved into the identification with non-stationary responses, which does not exist in the identification with stationary responses.

The terms $P_{\ddot{x}_i y}$ can be considered a pseudo cross power spectral density between the structural response $\ddot{x}_i(t)$ and the reference responses $y(t)$, estimated by the Welch average periodogram method without window function as introduced in section 5.2. If the structural responses $\ddot{x}_i(t)$ and the reference response $y(t)$ are jointly wide sense stationary, $P_{\ddot{x}_i y}$ just becomes the cross power spectrum $S_{\ddot{x}_i y}$ in the original derivation of the CSD_SUBID method.

The terms $P_{f_i y}$ are introduced into the identification process due to the fact that the structural displacement and velocity may not be zero at the beginning (t=0) and the ending (t=T) in the recorded responses. Next, it will be shown that if the structural responses $\ddot{x}_i(t)$ and the reference response $y(t)$ are jointly wide sense stationary, $\hat{P}_{f_i y}$ will converge to zero as the number of group responses Q and the length of the responses T tends to infinity. For simplicity, only the proof of the top story substructure case (i=n) will be given below; the proof for other story substructures (i≠n) can be easily obtained by following a similar procedure.

$$\lim_{Q,T\to\infty} P_{f_n y} = \lim_{Q,T\to\infty} \frac{1}{QT}\sum_{q=1}^{Q} F_n^{(q)} Y^{(q)^*} \Big/ m_n = \mathrm{E}\left[\lim_{T\to\infty}\frac{1}{T} F_n Y^* \Big/ m_n\right]$$

$$= \frac{k_n}{m_n(j\omega)} \lim_{T\to\infty}\frac{1}{T}\mathrm{E}\left\{\Delta_{x_n} e^{-j\omega t}\Big|_{t=T}^{t=0} Y^*\right\} + \left[\frac{c_n}{j\omega} + \frac{k_n}{(j\omega)^2}\right] \lim_{T\to\infty}\frac{1}{T}\mathrm{E}\left[\dot{\Delta}_{x_n} e^{-j\omega t}\Big|_{t=T}^{t=0} Y^*\right] \tag{5.64}$$

Now, show that $\lim_{T\to\infty}\frac{1}{T}\mathrm{E}[\Delta_{x_n} e^{-j\omega t}\Big|_{t=T}^{t=0} Y^*] = 0$:

$$\lim_{T\to\infty}\frac{1}{T}\mathrm{E}\left\{\Delta_{x_n} e^{-j\omega t}\Big|_{t=T}^{t=0} Y^*\right\} = \lim_{T\to\infty}\frac{1}{T}\mathrm{E}\left\{\left[\Delta_{x_n}(T)e^{-j\omega\cdot T} - \Delta_{x_n}(0)\right]\int_0^T y(t)e^{j\omega\cdot t}dt\right\}$$

$$= \lim_{T\to\infty}\frac{1}{T}e^{-j\omega\cdot T}\int_0^T \mathrm{E}\left[\Delta_{x_n}(T)y(t)\right]e^{j\omega\cdot t}dt \text{ - } \lim_{T\to\infty}\frac{1}{T}\int_0^T \mathrm{E}\left[\Delta_{x_n}(0)y(t)\right]e^{j\omega\cdot t}dt$$

$$= \lim_{T\to\infty}\frac{-1}{T}\int_0^T R_{(\ddot{x}_n-\ddot{x}_{n-1})y}(T-t)e^{-j\omega\cdot(T-t)}d(T-t) - \lim_{T\to\infty}\frac{1}{T}\int_0^T R_{(\ddot{x}_n-\ddot{x}_{n-1})y}(-t)e^{j\omega\cdot t}dt \tag{5.65}$$

$$= \lim_{T\to\infty}\frac{1}{T}\int_0^T R_{(\ddot{x}_n-\ddot{x}_{n-1})y}(t)e^{-j\omega\cdot t}dt - \lim_{T\to\infty}\frac{1}{T}\int_{-T}^0 R_{(\ddot{x}_n-\ddot{x}_{n-1})y}(t)e^{-j\omega\cdot t}dt = 0$$

The last step in the proof uses the results that the terms $\lim_{T\to\infty}\int_0^T R_{(\ddot{x}_n-\ddot{x}_{n-1})y}(t)e^{-j\omega\cdot t}dt$ and $\lim_{T\to\infty}\int_{-T}^0 R_{(\ddot{x}_n-\ddot{x}_{n-1})y}(t)e^{-j\omega\cdot t}dt$ are finite in the general wide sense stationary cases.

A similar proof can be given to show that $\lim_{T\to\infty}\frac{1}{T}\mathrm{E}[\dot{\Delta}_{x_n} e^{-j\omega t}\Big|_{t=T}^{t=0} Y^*] = 0$. Therefore, it is proved that $P_{f_n y} = 0$ as both Q and T tend to infinity.

The above proof provides some insightful information about the CSD_SUBID method with non-stationary responses:

1. When the structural responses are stationary, the pseudo cross power spectrum terms $P_{\ddot{x}_i y}$ become the cross power spectrum $S_{\ddot{x}_i y}$; thus, the new CSD_SUBID method using non-stationary structural responses, in Equations (5.56) and (5.63), converges to the original method in Equations (5.8) and (5.10) with a little

modification, which accounts for the effect that the structural responses are not zero at the beginning (t=0) and the ending (t=T) in the recorded responses.

2. Since, in most practical cases, the structural displacement and velocity are not measured, the terms $P_{f_i y}$ become unknown and have to be omitted in the formulation of the identification. Under such a situation, elongating the length of the measurements T will reduce the identification errors caused by neglecting the terms $P_{f_i y}$ in the identification.

5.6.4 Identification Error of CSD_SUBID with Non-stationary Response

Applying the identification error analysis method in section 3.2, the identification error of the CSD_SUBID method with non-stationary structural responses for both top n^{th} story and the non-top i^{th} story can be obtained as

$$\begin{bmatrix}\theta_{kn}\\ \theta_{cn}\end{bmatrix} \approx \sum_{l=1}^{N}\mathrm{Re}\left\{\begin{bmatrix}W_{11,l} & W_{12,l}\\ W_{21,l} & W_{22,l}\end{bmatrix}\cdot\begin{bmatrix}N_{\ddot{x}_{n-1}y,l}\big/P_{(\ddot{x}_n-\ddot{x}_{n-1})y,l}\\ N_{\ddot{x}_n y,l}\big/P_{(\ddot{x}_n-\ddot{x}_{n-1})y,l}\end{bmatrix}+\begin{bmatrix}W_{13,l}\\ W_{23,l}\end{bmatrix}\frac{N_{f_n y,l}}{P_{(\ddot{x}_n-\ddot{x}_{n-1})y,l}}\right\} \tag{5.66}$$

$$\begin{aligned}\begin{bmatrix}\theta_{ki}\\ \theta_{ci}\end{bmatrix} \approx &\sum_{l=1}^{N}\mathrm{Re}\left\{\begin{bmatrix}U_{11,l} & U_{12,l} & U_{13,l}\\ U_{21,l} & U_{22,l} & U_{23,l}\end{bmatrix}\cdot\begin{bmatrix}N_{\ddot{x}_{i-1}y,l}\big/P_{(\ddot{x}_i-\ddot{x}_{i-1})y,l}\\ N_{\ddot{x}_i y,l}\big/P_{(\ddot{x}_i-\ddot{x}_{i-1})y,l}\\ N_{\ddot{x}_{i+1}y,l}\big/P_{(\ddot{x}_i-\ddot{x}_{i-1})y,l}\end{bmatrix}+\begin{bmatrix}U_{16,l}\\ U_{26,l}\end{bmatrix}\frac{N_{f_i y,l}}{P_{(\ddot{x}_i-\ddot{x}_{i-1})y,l}}\right\}\\ &+\sum_{l=1}^{N}\mathrm{Re}\left\{\begin{bmatrix}U_{14,l} & U_{15,l}\\ U_{24,l} & U_{25,l}\end{bmatrix}\cdot\begin{bmatrix}\dfrac{P_{(\ddot{x}_{i+1}-\ddot{x}_i)y,l}}{P_{(\ddot{x}_i-\ddot{x}_{i-1})y,l}}\theta_{k(i+1)}\\ \dfrac{P_{(\ddot{x}_{i+1}-\ddot{x}_i)y,l}}{P_{(\ddot{x}_i-\ddot{x}_{i-1})y,l}}\theta_{c(i+1)}\end{bmatrix}\right\}\end{aligned} \tag{5.67}$$

where $N_{f_i y,l}=\hat{P}_{f_i y,l}-P_{f_i y,l}$. The proofs of Equations (5.66) and (5.67) are given in Appendix D. It is worth pointing out that all factors $W_{ij,l}$ and $U_{ij,l}$ in the above two equations are the same factors in Equation (5.15) and (5.16) (the identification errors of the CSD_SUBID method with stationary responses), except for the four factors $(W_{16,l}, W_{26,l}, U_{16,l}\ and\ U_{26,l})$ that do not exist in Equations (5.15) and (5.16).

It is interesting that the identification errors of CSD_SUBID method with non-stationary responses and with stationary responses are so similar that the only difference is the additional error terms caused by the introduction of the extra uncertainty terms $N_{f_i y,l}$ in the case of non-stationary responses. Thus, many results of error analysis of the CSD_SUBID method using stationary structural responses can be conveniently re-utilized.

As shown in Figures 5.3 and 5.4, the magnitude of all factors $W_{ij,l}$ and $U_{ij,l}$ in Equations (5.66) and (5.67) are significantly large near the story substructure natural frequency and decay very fast when moving to lower and higher frequencies. Therefore, the parameter identification errors are mainly determined by the uncertainty terms in Equations (5.66) and (5.67) near the substructure natural frequency; largely reducing the uncertainty terms near the substructure natural frequency can significantly improve the identification accuracy.

Moreover, all uncertainty terms in Equation (5.66) and (5.67) are also related to two important structural responses: $P_{(\ddot{x}_i-\ddot{x}_{i-1})y,l}$ and $P_{(\ddot{x}_{i+1}-\ddot{x}_i)y,l} \big/ P_{(\ddot{x}_i-\ddot{x}_{i-1})y,l}$. Since $P_{(\ddot{x}_i-\ddot{x}_{i-1})y,l}$ serves as the common denominator for all measurement uncertainty terms, larger $P_{(\ddot{x}_i-\ddot{x}_{i-1})y,l}$ leads to smaller measurement uncertainties and, in turn, smaller identification errors. The terms including $P_{(\ddot{x}_{i+1}-\ddot{x}_i)y,l} \big/ P_{(\ddot{x}_i-\ddot{x}_{i-1})y,l}$ are proportional to the uncertainty of the upper story parameters; smaller $P_{(\ddot{x}_{i+1}-\ddot{x}_i)y,l} / P_{(\ddot{x}_i-\ddot{x}_{i-1})y,l}$ will result in smaller upper story parameter uncertainties and, thus, smaller identification error.

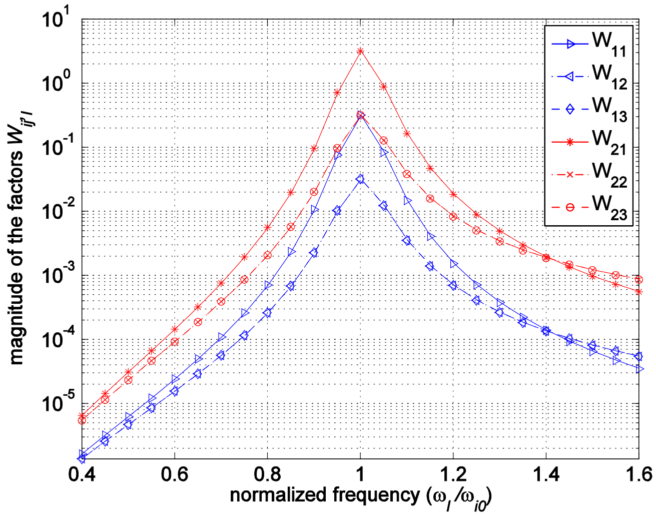

Figure 5.3 Magnitude of the factors $W_{ij,l}$

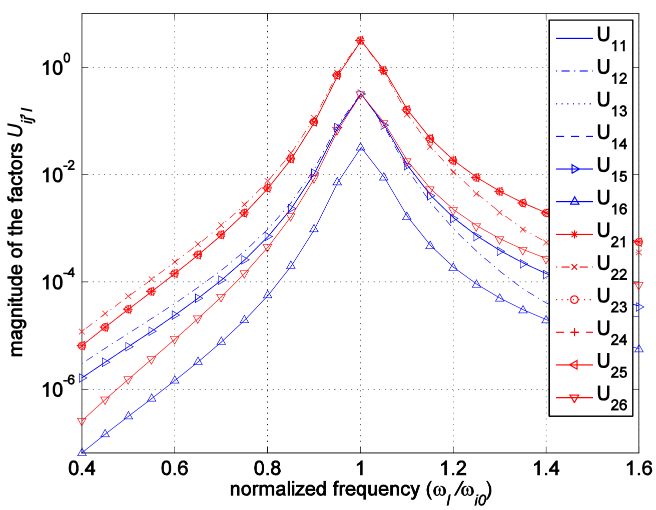

Figure 5.4 Magnitude of the factors $U_{ij,l}$

5.7 Illustrative Examples

5.7.1 CSD_SUBID Method with Stationary Response

In this section, the CSD_SUBID method is first tested on the same 5-story shear structure used in the third and fourth chapters with stationary structural responses. Then, a large 10-story uniform shear structure is used to check if the CSD_SUBID method can be scaled well to deal with larger shear structures. The parameters of the 10-story shear structures are picked as $m_i=1\times10^5$ kg, $c_i=8\times10^5$ N·sec/m, $k_i=16\times10^7$ N/m (i=1,…,10). It is assumed that both structures are subject to ground excitation only.

The ground excitation $\ddot{u}_g$ is modeled by a Gaussian random pulse process passing through a 4th order band-pass Butterworth filter with 1Hz low cut-off frequency and 12 Hz high cut-off frequency. 3600-second ground and floor acceleration responses, sampled at 200Hz, are simulated to perform the identification with the CSD_SUBID method. The Welch average periodogram method is applied to calculate the cross power spectral densities needed to formulate the identification problem: the 3600-second long structural responses are partitioned into short segments of 30 seconds each. A Hanning window is applied to each segment response to reduce the effect of leakage. To increase the number of averages and reduce the variance of the estimated power spectral, two adjacent segments are overlapped by 25% of the frame length. The measurement noise is also assumed to be band-limited Gaussian white noise with the cut-off frequency at 100Hz. To test the effectiveness of the proposed method as would be typical with only ambient excitation sources, fairly large measurement noise is added to the true structural response. It is assumed herein that the magnitude of the measurement noise of all acceleration responses is the same, with root-mean-square (RMS) value equal to 50% of the RMS value of the ground excitation. Figure 5.5 shows an example of the first two seconds of response of the 5th story acceleration, which demonstrates how significantly the measurements are distorted by the added noise.

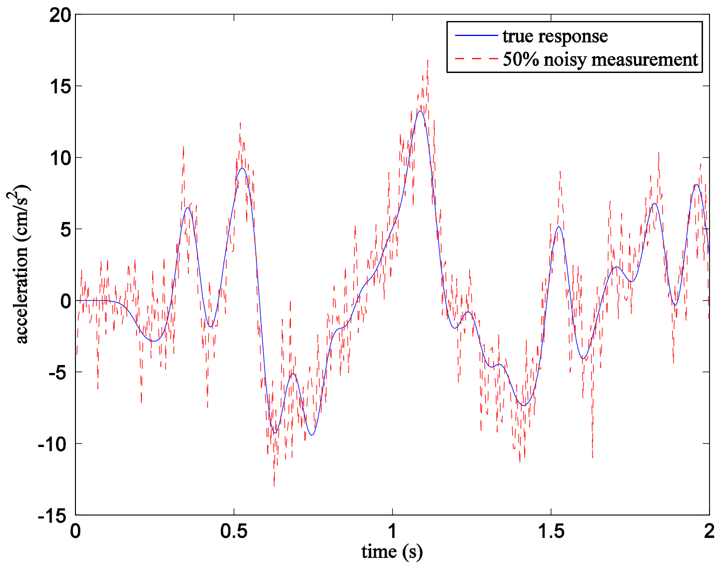

Figure 5.5 The 5th floor acceleration response with and without measurement noise

To examine the effect of choosing different reference responses $y(t)$ on the identification accuracy, two scenarios are considered here: 1) for each step of substructure identification the reference $y(t)$ is selected among the measured floor accelerations and ground acceleration, using the reference selection rules in section 5.4; and 2) The reference $y(t)$ is fixed as the top floor acceleration for all story substructure identification, chosen because the top floor acceleration has the largest response in terms of RMS value among all floor acceleration responses.

a) Identification Results

100 identification tests, using the CSD_SUBID method, are performed on the 5-story and 10-story structures. The statistics of the identification errors of the 5-story structure in both scenarios are listed in Tables 5.1 and 5.2.

Table 5.1 shows that the CSD_SUBID method, coupled with the proposed reference response selection rule, provides excellent identification results: *i*) the means of the identification errors of both stiffness and damping parameters are all very close to zero even with quite large (50%) noise disturbance, which verifies the analysis result that the CSD_SUBID method is an asymptotically unbiased estimator for structural parameters. *ii*) the CSD_SUBID method can still provide very consistently accurate results under the disturbance of quite large measurement noise (50%). The largest relative root-mean-square-error (RMSE) of all story stiffnessees is just 1.1%; even for damping parameters, usually difficult to accurately identify, the largest relative RMSE is only 5.3%.

However, the results in Table 5.2 show that if the top story acceleration response is chosen to be the reference response for all substructure identifications in scenario 2, the identification accuracy decreases drastically. As shown in section 5.4, if the reference response is one of the structural responses involved in the substructure identification process, the expected values of measurement uncertainty terms will no longer be zeros, which leads to the biased estimation of structural parameters. Moreover, the noisier the reference and structural responses are, the larger the biased estimation will be. Since the story acceleration $\ddot{x}_5$ is involved in the identification of the 4th and 5th story parameters and the measured structural responses are quite noisy in this case (50%), using $\ddot{x}_5$ as the reference in that identification results in large identification error for the 4th and 5th story parameters, which consequently causes the large identification errors for the structural parameters in lower stories due to error accumulation.

Table 5.3 shows the statistics of the identification results of the 10-story structure using the optimal reference selection rules in the section 5.4, which demonstrates results similar to the 5-story structure. For the larger 10-story structure, the CSD_SUBID method is still able to provide very accurate identification results when subject to a quite high level of noise disturbance: the largest relative RMSE of all stiffness estimates is only 2.1% and the largest relative RMSE of all damping estimates is only 9.2%.

Table 5.1 The identification result statistics of the 5-story structure with 50% noise (scenario 1: using the optimally selected responses as the references)

Story number	$y(t)$	Story stiffness $\hat{k}_i$ ($\times 10^5$N/m)			Story damping $\hat{c}_i$ ($\times 10^5$N·sec/m)		
		mean	relative RMSE	relative STD	mean	relative RMSE	relative STD
1	$\ddot{x}_5$	1601 (0.1%)*	0.5%	0.5%	8.03 (0.4%)*	2.7%	2.7%
2	$\ddot{x}_g$	1600 (0.0%)	0.5%	0.5%	8.02 (0.3 %)	2.4%	2.4%
3	$\ddot{x}_g$	1597 (-0.2%)	1.1%	1.1%	7.97 (-0.3%)	5.3%	5.3%
4	$\ddot{x}_2$	1600 (0.0%)	0.4%	0.4%	7.99 (-0.1%)	1.5%	1.5%
5	$\ddot{x}_2$	1600 (0.0%)	0.2%	0.2%	8.00 (0.0%)	1.1%	1.1%

*: relative error for mean estimate

Table 5.2 The identification result statistics of the 5-story structure with 50% noise (scenario 2: using the top the story accelerations as the references)

Story number	$y(t)$	Story stiffness $\hat{k}_i$ ($\times 10^5$N/m)			Story damping $\hat{c}_i$ ($\times 10^5$N·sec/m)		
		mean	relative RMSE	relative STD	mean	relative RMSE	relative STD
1	$\ddot{x}_5$	1551 (-3.1%)*	3.3%	1.2%	8.48 (5.9%)*	8.6%	6.3%
2	$\ddot{x}_5$	1539 (-3.8%)	4.1%	1.4%	7.59 (-5.1%)	8.7%	7.1%
3	$\ddot{x}_5$	1634 (2.1%)	3.7%	3.1%	4.61 (-42.4%)	44.6%	14.0%
4	$\ddot{x}_5$	1683 (5.2%)	5.2%	0.4%	7.97 (-0.3%)	1.9%	1.9%
5	$\ddot{x}_5$	1609 (0.6%)	0.6%	0.2%	7.72 (-3.3%)	3.5%	1.0%

Table 5.3The identification result statistics of the 10-story structure with 50% noise (scenario 1: using the optimally selected responses as the references)

Story number	$y(t)$	Story stiffness $\hat{k}_i$ ($\times 10^5$N/m)			Story damping $\hat{c}_i$ ($\times 10^5$N·sec/m)		
		mean	relative RMSE	relative STD	mean	relative RMSE	relative STD
1	$\ddot{x}_5$	1598 (0.1%)	0.8%	0.8%	7.97 (-0.3%)	3.9%	3.9%
2	$\ddot{x}_g$	1600 (-0.1%)	0.8%	0.8%	7.91 (-1.1 %)	4.2%	4.0%
3	$\ddot{x}_1$	1601 (-0.1%)	0.8%	0.8%	7.97 (-0.3%)	4.0%	4.0%
4	$\ddot{x}_1$	1602 (0.1%)	0.8%	0.8%	8.01 (0.1%)	4.4%	4.4%
5	$\ddot{x}_1$	1601 (0.1%)	1.1%	1.1%	8.05 (0.6%)	5.3%	5.3%
6	$\ddot{x}_1$	1598 (-0.1%)	0.8%	0.8%	8.05 (0.6%)	4.7%	4.7%
7	$\ddot{x}_1$	1598 (-0.1%)	0.9%	0.9%	8.02 (0.3%)	4.8%	4.8%
8	$\ddot{x}_1$	1599 (-0.1%)	2.1%	2.1%	7.84 (-1.9%)	9.2%	9.0%
9	$\ddot{x}_1$	1600 (0.0%)	0.5%	0.5%	8.00 (0.1%)	2.5%	2.5%
10	$\ddot{x}_1$	1600 (0.1%)	0.4%	0.4%	8.00 (0.0%)	1.8%	1.8%

Similar to the 5-story structure, if the top floor (the 10th floor) acceleration response is chosen to be the reference response for all substructure identifications as in scenario 2, the CSD_SUBID method will no longer provide accurate identification results, which is verified by the identification results in Table 5.4.

Table 5.4 The identification result statistics of the 10-story structure with 50% noise (scenario 2: using the top the story accelerations as the references)

Story number	$y(t)$	Story stiffness $\hat{k}_i$ ($\times 10^5$N/m)			Story damping $\hat{c}_i$ ($\times 10^5$N·sec/m)		
		mean	relative RMSE	relative STD	mean	relative RMSE	relative STD
1	$\ddot{x}_{10}$	1570 (-1.8%)	1.9%	0.4%	741 (-7.4%)	8.0%	3.1%
2	$\ddot{x}_{10}$	1609 (0.6%)	0.9%	0.7%	690 (-13.8%)	14.0%	2.2%
3	$\ddot{x}_{10}$	1643 (2.7%)	2.7%	0.6%	764 (-4.5%)	5.3%	2.9%
4	$\ddot{x}_{10}$	1643 (2.6%)	2.7%	0.4%	868 (8.5%)	9.4%	4.2%
5	$\ddot{x}_{10}$	1587 (-0.8%)	1.4%	1.1%	970 (21.2%)	21.4%	2.8%
6	$\ddot{x}_{10}$	1543 (-3.6%)	3.6%	0.7%	848 (6.0%)	7.0%	3.6%
7	$\ddot{x}_{10}$	1530 (-4.4%)	4.4%	0.7%	745 (-6.9%)	8.6%	5.2%
8	$\ddot{x}_{10}$	1647 (2.9%)	3.7%	2.2%	416 (-47.9%)	48.3%	5.7%
9	$\ddot{x}_{10}$	1688 (5.5%)	5.5%	0.4%	803 (0.4%)	2.5%	1.9%
10	$\ddot{x}_{10}$	1607 (0.4%)	0.5%	0.2%	772 (-3.5%)	3.6%	0.9%

b) Variance Estimation of the Identification Errors

In section 5.6, the formulae to calculate the variances of the identification errors for the identified parameters were developed. To test the accuracy of these formulae in predicting the variances of the identification errors of the structural parameters, the results of the relative standard deviation of the identification errors in the last section simulations were compared with that calculated from the formulae given in section 5.6 (Equations (5.24), (5.25) and (5.41)).

As pointed out in section 5.6, the identification errors of the structural parameters for a non-top story substructure are the combination of two kinds of errors: the errors due to the measurement uncertainty and the errors caused by the uncertainty in the estimated structural parameters of the story above. Strictly speaking, these two errors are correlated. However, due to the complexity in directly obtaining the explicit expression for the covariance matrix between two errors, it is assumed that these two errors are uncorrelated when calculating the variance. But such an assumption may sometimes lead to the underestimation of the error variances, which is not desirable in real application. Thus, an upper bound of the error variance is calculated by assuming the two errors are fully correlated. In addition, this example uses segments that overlap by 25% of their lengths; since the approximate formulae for the variances of the parameter estimations were derived assuming no segment overlap and no correlation between segments, the predicted variance might differ a bit from the actual variance.

Figures 5.6 and 5.7 show comparisons of the relative standard deviations of the estimated story stiffness and damping parameter errors for the 5-story structure, respectively. It is found that the formulae provide reasonably good prediction of the relation standard deviation of the estimated structural parameters, while the upper bound predictions significantly over-estimate the standard deviation of the identification error in the lower stories.

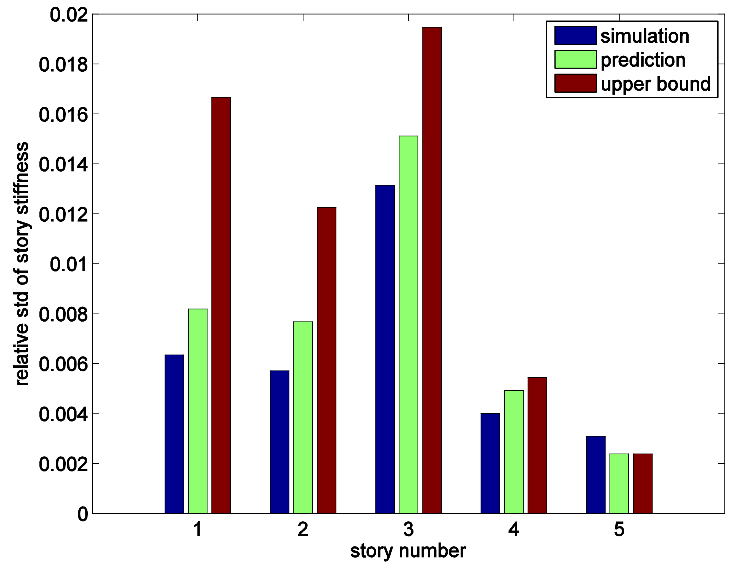

Figure 5. 6 The comparison of the relative standard deviation of the stiffness parameters for the 5-story structure

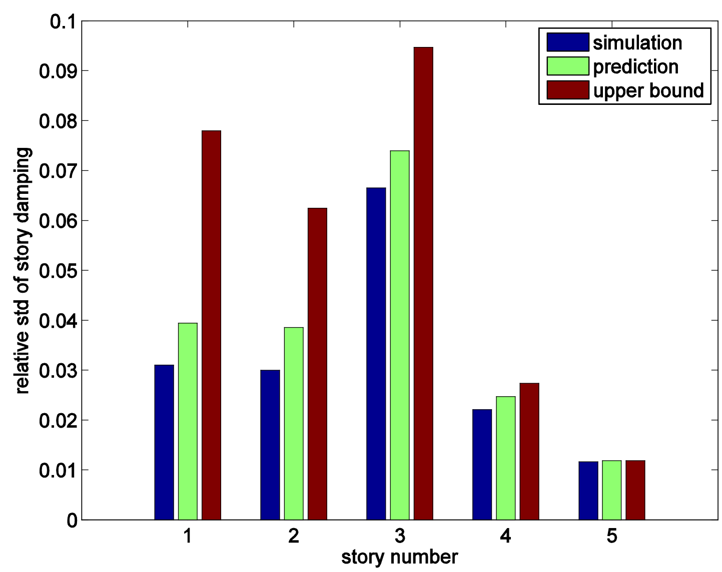

Figure 5.7 The comparison of the relative standard deviation of the damping parameters for the 5-story structure

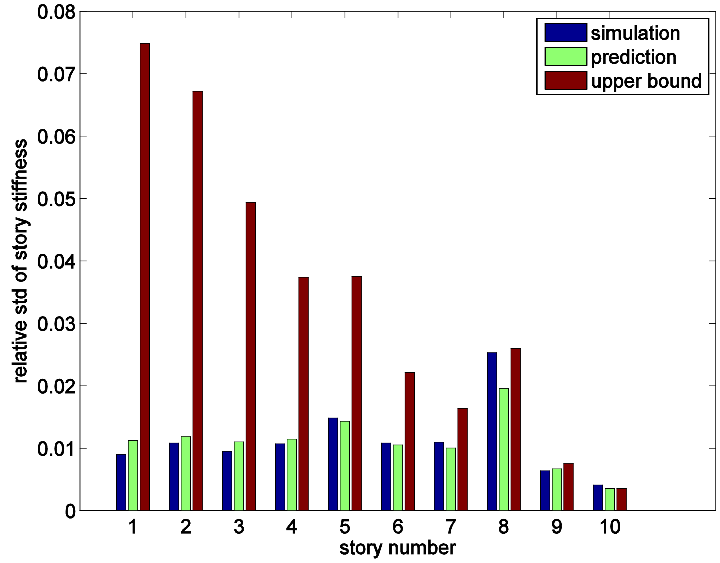

Figure 5.8 The comparison of the relative standard deviation of the stiffness parameters for the 10-story structure

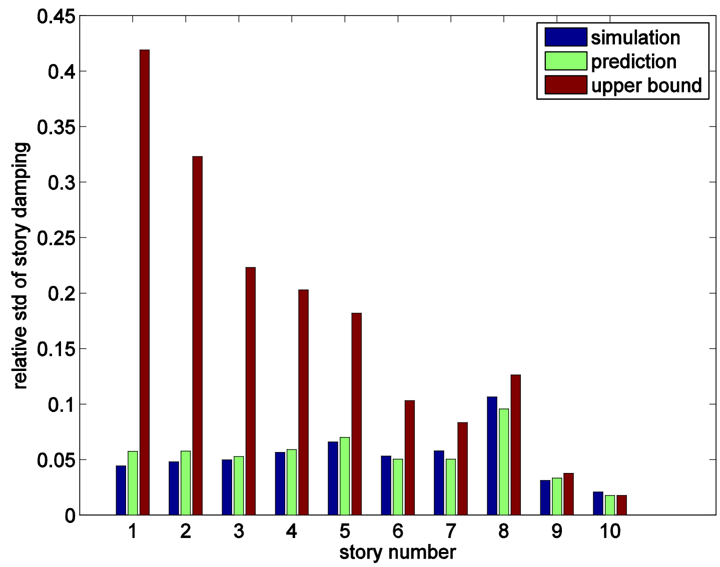

Figure 5.9 The comparison of the relative standard deviation of the damping parameters for the 10-story structure

Similar results with the relative standard deviations of the estimated parameter errors in the 10-story structure are shown in Figures 5.8 and 5.9. It is worth pointing out that there are some cases (*i.e.*, the 8th story parameters) that the predicted standard deviations are less than that obtained from the simulation, though the differences are not very large. This does recall the aforementioned concern that the assumption of no correlation between the two kinds of errors may lead to the underestimation of the variance of some structural parameters. However, overall, the assumption of no correlation between the two errors provides reasonably good prediction of the standard deviation of the identification errors.

Another important observation is that the factors $W_{ij,l}$ and $U_{ij,l}$ in the formulae of the identification error variances are functions of the structural parameters $[k_i\ c_i]^T$ and $[k_{i+1}\ c_{i+1}]^T$, whose values, of course, are unknown at the time of the variance estimation; thus, the formulae of the identification error variance could not be directly calculated. However, since the estimated structural parameters by the CSD_SUBID method are unbiased estimations of the structural parameters, it is recommended in practice to use the estimated values of the structural parameters to calculate the factors $W_{ij,l}$ and $U_{ij,l}$, which then can be used to calculate the variance of the identification errors.

c) Damage Detection

Applying the damage detection strategy proposed in section 3.5, damage detection tests are carried out on the 5-story structure by using structural parameters estimated by the CSD_SUBID method. The damage scenario of the structure stays the same as in the third and fourth chapters: the structural damage occurs at the first, third and fifth stories, which results in the reduction of story stiffness by 5% and the increase of story damping by 20%. Damage detection tests are carried out with 50% noise (in terms of RMS).

In order to test the ability of the proposed damage detection strategy to correctly identify the health status of the structure, 600 independent substructure identifications using the CSD_SUBID method are carried out on the damaged structure; these results are used in the hypothesis test to determine whether or not the structure is damaged. The number of the substructure identifications that each hypothesis test uses to reach the conclusion is selected as 1, 3 and 5, respectively. According to the number of the tests each hypothesis test uses, the identification results of 600 tests are divided into groups and a hypothesis test is performed for each group using the majority vote method proposed in section 3.5. Since the identified structural parameters of the undamaged structure have quite small variances, a larger β value, 6, is selected in the hypothesis tests to reduce the probability of the second kind of error of the hypothesis test – faulty detection. The percentage of the hypothesis tests which give the corrected health status of the structure are shown in Table 5.5.

Table 5.5 The percentage of the hypothesis tests which give the corrected conclusion about the structural health status

Floor Number	*n*		
	1	3	5
1	100%	100%	100%
2	96%	100%	100%
3	100%	100%	100%
4	72%	79%	88%
5	100%	100%	100%

Due to the smaller variances of the identified structural parameters of the undamaged structure, the proposed damage detection procedure 100 percentage accurately picks out all structural damage. However, in some cases the damage detection procedure does make some mistakes of labeling the undamaged structural members as being damaged. This is partially due to the fact that the occurrence of structural damage changes the structural responses, resulting in the change of the variances of the identified parameters.

5.7.2 CSD_SUBID Method with Non-stationary Response

As shown in section 5.6, the CSD_SUBID method can be used to perform identification with non-stationary structural responses by replacing the cross power spectral density of the stationary responses by the pseudo cross power spectral density of the non-stationary responses. To verify this result, an ensemble of the structural responses due to many small earthquakes is used to carry out the identification.

It is assumed that the ground excitation during earthquakes can be modeled by a band-pass Gaussian random process times a time variant envelop function $a(t)$ (Amin *et al.*, 1968). The band-pass Gaussian random process is assumed to be a white Gaussian process passing through an 4^{th} order Butterworth filter with 1Hz low cut-off frequency and 12 Hz high cut-off frequency. The expression of the envelop function $a(t)$ is given in Equation (5.65) and its shape is shown in Figure 5.10. The nominal values of the parameters in the envelop function are selected as A=1, B=1/7, t_1=3 and t_2=9. To simulate the variations among different earthquakes, the parameter values of the envelop function for each earthquake is assumed to be the nominal parameter values multiplied by some random variables which are uniformly distributed from 0.9 to 1.1.

100 identification tests are performed on the 5-story and 10-story structures. For each test, 120 micro-tremor excitations and the corresponding structural responses are simulated to perform the identification via the CSD_SUBID method and the length of the responses is 30 second. It is assumed that the magnitudes of the measurement noises of all acceleration responses are the same, with root-mean-square (RMS) value equal to 50% of the RMS of the ground excitation.

$$a(t) = \begin{cases} A \times (t/t_1) & t \le t_1 \\ A & t_1 < t \le t_2 \\ A \times \exp[-B(t - t_2)] & t_2 < t \end{cases} \tag{5.65}$$

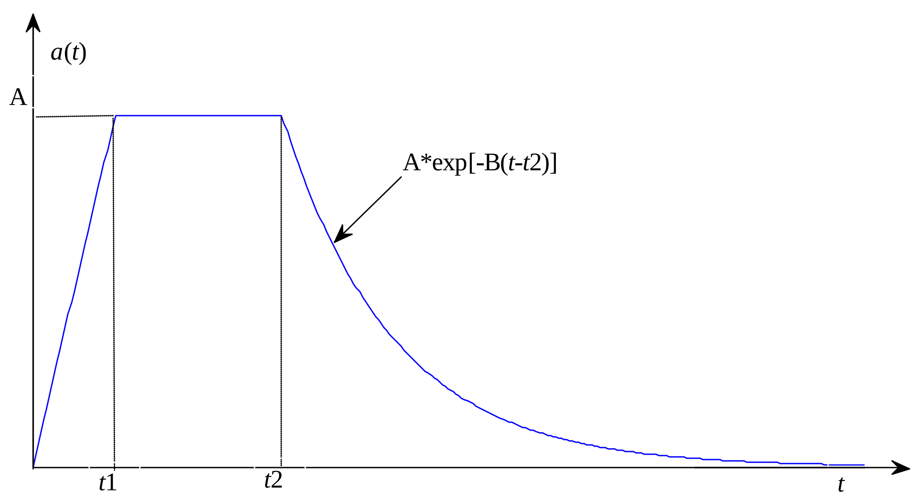

Figure 5.10 The envelop function *a*(*t*) for earthquake excitations

The statistics of the identification results of the 5-story and the 10-story structures are listed in Tables 5.6 and 5.7, respectively.

Table 5.6 The identification result statistics of the 5-story structure with non-stationary structural responses and 50% noise

Story number	$y(t)$	Story stiffness $\hat{k}_i$ (×10^5N/m)			Story damping $\hat{c}_i$ (×10^5N·sec/m)		
		mean	relative RMSE	relative STD	mean	relative RMSE	relative STD
1	$\ddot{x}_5$	1604 (0.3%)	0.6%	0.5%	7.96 (-0.4%)	2.5%	2.5%
2	$\ddot{x}_g$	1604 (0.3%)	0.6%	0.5%	7.81 (-2.3 %)	3.6%	2.8%
3	$\ddot{x}_g$	1618 (1.1%)	2.6%	2.4%	8.17 (2.1%)	8.7%	8.5%
4	$\ddot{x}_2$	1602 (0.1%)	0.6%	0.6%	7.97 (-0.4%)	2.8%	2.8%
5	$\ddot{x}_2$	1601 (0.1%)	0.3%	0.3%	7.81 (-2.3%)	3.0%	1.9%

The identification results in Tables 5.6 and 5.7 show that the CSD_SUBID method is able to provide very accurate results with non-stationary structural responses, which numerically verifies that the CSD_SUBID method is applicable to non-stationary structural responses, though with a bit less accurate than stationary cases.

Table 5.7 The identification result statistics of the 10-story structure with non-stationary responses and 50% noise

Story number	$y(t)$	Story stiffness $\hat{k}_i$ ($\times 10^5$N/m)			Story damping $\hat{c}_i$ ($\times 10^5$N·sec/m)		
		mean	relative RMSE	relative STD	mean	relative RMSE	relative STD
1	$\ddot{x}_5$	1608 (0.5%)	0.8%	0.6%	7.89 (-1.4%)	3.5%	3.2%
2	$\ddot{x}_g$	1606 (0.3%)	0.8%	0.7%	7.90 (-1.1 %)	3.0%	2.7%
3	$\ddot{x}_1$	1605 (0.3%)	0.6%	0.5%	7.96 (-0.5%)	2.8%	2.8%
4	$\ddot{x}_1$	1606 (0.4%)	0.8%	0.7%	7.85 (-1.8%)	4.2%	3.8%
5	$\ddot{x}_1$	1607 (0.5%)	1.2%	1.1%	7.89 (-1.4%)	6.4%	6.3%
6	$\ddot{x}_1$	1604 (0.2%)	0.9%	0.8%	7.95 (-0.6%)	3.7%	3.7%
7	$\ddot{x}_1$	1604 (0.3%)	1.0%	1.0%	7.79 (-2.5%)	5.4%	4.7%
8	$\ddot{x}_1$	1617 (1.0%)	4.4%	4.3%	8.63 (7.9%)	17.3%	15.5%
9	$\ddot{x}_1$	1601 (0.0%)	0.9%	0.9%	8.00 (0.0%)	4.7%	4.7%
10	$\ddot{x}_1$	1603 (0.2%)	0.6%	0.5%	7.82 (-2.3%)	3.5%	2.7%

Chapter 6

Controlled Substructure Identification for Shear Structures

Due to the great potential to improve structural safety and reliability as well as to lower structural maintenance cost, many researchers have studied global vibration-based structural health monitoring (SHM) methods to detect (and localize and quantify) damage, often by examining changes in the identified structural parameters or modal properties. The identification process inherent in such approaches often suffers from difficulties, such as insufficient excitation energy at high frequency, sensor noise, lower sensitivity of the measurements to structural damage, ill conditioning in the inverse problem to be solved, and so forth.

In order to overcome some of these difficulties, some researchers attempted to utilize structural control (SC) systems to improve the accuracy of the damage detection. Many reasons are behind this trend: first, the SC system and the SHM system contain many similar components that can be shared by both systems, such as sensors, data acquisition systems, central computers and so forth. The synergy of the two systems fully utilizes these components and, thus, makes the whole system more cost-efficient. Second, generally the SC system is designed and implemented to mitigate large structural vibrations caused by strong earthquakes or high speed winds. However, due to the infrequent occurrence of such natural hazards compared with the whole service life of the structure, actually the SC system remains in idle status most of the time. Incorporating SHM functions into the SC system not only makes the SC system more cost-effective by providing important structural health information but also has the potential to improve the SC performance of reducing structure vibration (because SHM provides the SC system with a more accurate structural model which facilitates the design of efficient control algorithms). Third, the SC system is capable of intentionally changing the structural responses and/or other features (*e.g.*, natural frequency and mode shape etc.) in some specific ways such that the structural damage can be more accurately detected from the modified structural responses and/or features.

Recently, many new techniques have been developed to use SC systems to improve the accuracy of SHM. These techniques can be classified into two categories: multiple configuration and sensitivity improvement. For multiple configuration methods, different control algorithms are often used in SC systems to tune the structural modal properties of the original structure to different configurations. Since the controlled structure in each configuration contains some information about the uncontrolled structure, combining the information from the controlled structure in all configurations provides much more information about the uncontrolled structure, which helps to solve rank deficiency problem in SHM identification (Lew *et al.*, 2002) and, thus, improves the identification accuracy. Sensitivity improvement methods (Koh *et al.*, 2004) utilize some specially designed control algorithms to shift structural modal properties and make these properties more sensitive to structural damage; therefore, structural damage can be more accurately identified.

However, there is a problem often ignored by the above methods: how will the imperfections in the control system affect the identification results? Some control system error always exists, such as time delay for computation, unmodeled actuator dynamics, measurement noise in feedback and so forth. Since SC systems are deeply involved in the system identification procedure in the above methods, it is inevitable that the control system errors will affect their identification accuracy, possibly even eliminating the identification benefits of using control. Moreover, because of the complexity of the closed-loop control system, the effects of control system error on the identification accuracy usually become extremely difficult to analyze and predict. Thus, it would be beneficial to develop some new approaches in which control improves the identification accuracy but the identification results are robust to errors in the control forces.

In the third, fourth and fifth chapters, three interrelated substructure identification methods have been proposed for shear structures. The error analyses for these identification methods demonstrate that the identification errors are closely related to two important structural responses: 1) the frequency responses of the interstory acceleration of the story being identified and 2) the frequency response ratio between two adjacent interstory accelerations, the story being identified and the story above it. The accuracy of these substructure identification methods can be improved by significantly changing these two responses accordingly near the substructure natural frequency. This result provides an easy way to make use of control systems to change structural responses and improve the identification accuracy.

In this chapter, two kinds of structural control (SC) systems, an active mass driver (AMD) system and a semi-active interstory brace system, are used to induce the aforementioned structural response changes and to improve the accuracy of the substructure identification methods. The accuracy of the substructure identification method proposed in the previous chapters does not directly depend on the SC system but only indirectly on the performance of SC system, that is, the response of the closed-loop controlled structure; any control system errors (such as feedback measurement noise, time delay and so forth) that do not significantly deteriorate this performance of the designed control system should not have a large side effect on the accuracy of the controlled identification. Therefore, the proposed substructure controlled identification should be quite robust to the possible control system errors.

This chapter is organized as follows: first the identification error analyses of the proposed three substructure identification methods are reviewed. Then, based on the results of the error analyses, some optimization problems are formulated, in which the optimal parameters of two control systems are obtained. Next, a three-stage structural control system design strategy is proposed to overcome the difficulty that the true structural parameters are unknown when designing the control system for the identification purpose. Moreover, a study is carried out to demonstrate that the proposed controlled substructure identification method is very robust to one very common uncertainty in the control system – measurement noise. Finally, several numerical examples demonstrate that both control methods greatly improve the identification accuracy and are robust to fairly large feedback measurement noise.

6.1 Review of Identification Error Analysis Results of Three Substructure Identification Methods

In this section, the results of the identification error analysis of the previously proposed three substructure identification methods are briefly reviewed, which provides the foundation as to how to design structural control systems to change structural responses and improve the identification accuracy. As shown in Figure (6.1), the top (n^{th}) story substructure can be considered a special case of the general non-top (i^{th}) story substructure in which the fictitious upper (n+1$^{\text{th}}$) structural parameters $[k_{n+1}\ c_{n+1}]^{\mathrm{T}}$ and the fictitious upper structural responses $\ddot{x}_{n+1}$ are all zero. Therefore, only the identification error of the general non-top (i^{th}) will be reviewed; the results of the identification error analysis of the top story can be easily derived based on the results of the non-top substructure and the simple substitution.

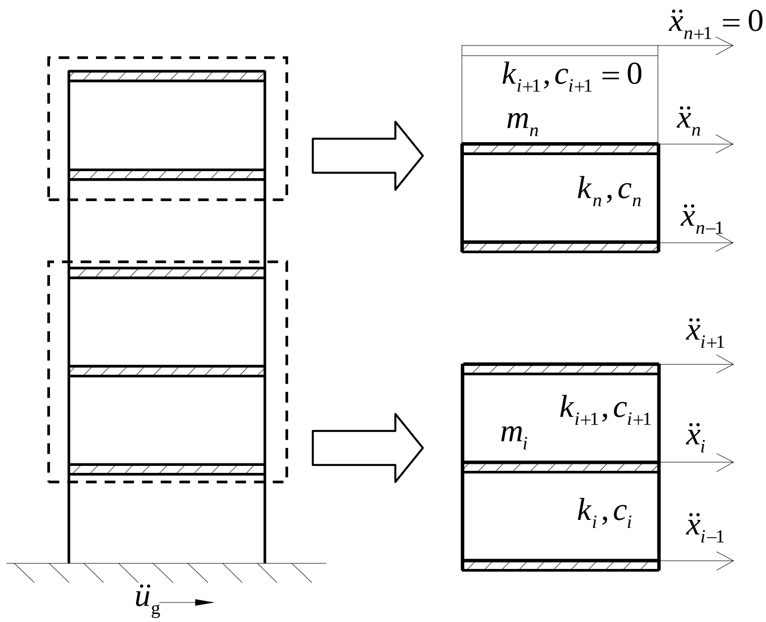

Figure 6.1 Comparison of top story substructure and non-top story substructure

6.1.1 Identification Error of FFT_SUBID Method

As stated in section 3.3.2, the relative identification errors of the i^{th} non-top story parameters $[k_i \quad c_i]^{\mathrm{T}}$ in FFT_SUBID method can be obtained as,

$$\begin{bmatrix}\theta_{ki}\\ \theta_{ci}\end{bmatrix} \approx \sum_{l=1}^{N}\mathrm{Re}\left\{\begin{bmatrix}U_{11,l} & U_{12,l} & U_{13,l}\\ U_{21,l} & U_{22,l} & U_{23,l}\end{bmatrix}\cdot\begin{bmatrix}N_{i-1,l}\big/(\ddot{X}_{i,l}-\ddot{X}_{i-1,l})\\ N_{i,l}\big/(\ddot{X}_{i,l}-\ddot{X}_{i-1,l})\\ N_{i+1,l}\big/(\ddot{X}_{i,l}-\ddot{X}_{i-1,l})\end{bmatrix}\right\}$$
$$+\sum_{l=1}^{N}\mathrm{Re}\left\{\begin{bmatrix}U_{14,l} & U_{15,l}\\ U_{24,l} & U_{25,l}\end{bmatrix}\cdot\begin{bmatrix}\dfrac{(\ddot{X}_{i+1,l}-\ddot{X}_{i,l})}{(\ddot{X}_{i,l}-\ddot{X}_{i-1,l})}\theta_{k(i+1)}\\ \dfrac{(\ddot{X}_{i+1,l}-\ddot{X}_{i,l})}{(\ddot{X}_{i,l}-\ddot{X}_{i-1,l})}\theta_{c(i+1)}\end{bmatrix}\right\} \tag{6.1}$$

where $\theta_{k(i+1)}$ and $\theta_{k(i+1)}$ are the relative identification errors of the $(i+1)^{\text{th}}$ story parameters k_{i+1} and c_{i+1}, respectively; the expression of all factors $U_{ij,l}$ are given in Equation (3.32).

As shown in section 3.3.2, the magnitude of all factors $U_{ij,l}$ are significantly large near the i^{th} story substructure natural frequency ω_{i0} and decay very fast when the frequency moves to both lower and higher frequency; hence, the uncertainty terms near the substructure natural frequency dominate the identification errors.

Moreover, the frequency response of the i^{th} interstory acceleration $(\ddot{X}_{i,l} - \ddot{X}_{i-1,l})$ is in the denominator of all measurement uncertainty terms and the frequency response ratio between the two adjacent interstory accelerations, $(\ddot{X}_{i+1,l} - \ddot{X}_{i,l})\big/(\ddot{X}_{i,l} - \ddot{X}_{i-1,l})$, multiplies the uncertainty terms related to the errors in the $(i+1)^{\text{th}}$ story parameters; therefore, the identification errors of the i^{th} story parameters can be reduced by (a) maximizing the frequency response of the i^{th} interstory acceleration $(\ddot{X}_{i,l} - \ddot{X}_{i-1,l})$ in a frequency range around the i^{th} substructure natural frequency ω_{i0}, which will reduce the identification error due to measurement uncertainty; (b) minimizing the frequency response ratio between the $(i+1)^{\text{th}}$ interstory acceleration and the i^{th} interstory acceleration, $(\ddot{X}_{i+1,l} - \ddot{X}_{i,l})\big/(\ddot{X}_{i,l} - \ddot{X}_{i-1,l})$, in the same frequency range, which reduces the error caused by the parameter estimate errors from the $(i + 1)^{\text{th}}$ story.

6.1.2 Identification Error of TF_SUBID Method

As analyzed in section 4.4.2, the relative identification errors of the i^{th} non-top story parameters $\begin{bmatrix} k_i & c_i \end{bmatrix}^{\mathrm{T}}$ in the TF_SUBID method should be less than the following three identification errors, each of which assumes that only one of floor acceleration responses is used as the pseudo input to calculate the transfer functions needed in the identification process.

$$\begin{bmatrix} \theta_{ki}^{(1)} \\ \theta_{ci}^{(1)} \end{bmatrix} \approx \sum_{l=1}^{N} \mathrm{Re}\left\{ \begin{bmatrix} U_{11,l} \\ U_{12,l} \end{bmatrix} \cdot \frac{\ddot{X}_{i-1,l}\left[-\alpha_{i-1,l}\right]}{(\ddot{X}_{i,l} - \ddot{X}_{i-1,l})} \right\} + \sum_{l=1}^{N} \mathrm{Re}\left\{ \begin{bmatrix} U_{14,l} & U_{15,l} \\ U_{24,l} & U_{25,l} \end{bmatrix} \cdot \begin{bmatrix} \dfrac{(\ddot{X}_{i+1,l} - \ddot{X}_{i,l})}{(\ddot{X}_{i,l} - \ddot{X}_{i-1,l})}\theta_{k(i+1)} \\ \dfrac{(\ddot{X}_{i+1,l} - \ddot{X}_{i,l})}{(\ddot{X}_{i,l} - \ddot{X}_{i-1,l})}\theta_{c(i+1)} \end{bmatrix} \right\} \tag{6.2}$$

$$\begin{bmatrix} \theta_{ki}^{(2)} \\ \theta_{ci}^{(2)} \end{bmatrix} \approx \sum_{l=1}^{N} \mathrm{Re}\left\{ \begin{bmatrix} U_{21,l} \\ U_{22,l} \end{bmatrix} \cdot \frac{\ddot{X}_{i,l}\left[-\alpha_{i,l}\right]}{(\ddot{X}_{i,l} - \ddot{X}_{i-1,l})} \right\} + \sum_{l=1}^{N} \mathrm{Re}\left\{ \begin{bmatrix} U_{14,l} & U_{15,l} \\ U_{24,l} & U_{25,l} \end{bmatrix} \cdot \begin{bmatrix} \dfrac{(\ddot{X}_{i+1,l} - \ddot{X}_{i,l})}{(\ddot{X}_{i,l} - \ddot{X}_{i-1,l})}\theta_{k(i+1)} \\ \dfrac{(\ddot{X}_{i+1,l} - \ddot{X}_{i,l})}{(\ddot{X}_{i,l} - \ddot{X}_{i-1,l})}\theta_{c(i+1)} \end{bmatrix} \right\} \tag{6.3}$$

$$\begin{bmatrix} \theta_{ki}^{(3)} \\ \theta_{ci}^{(3)} \end{bmatrix} \approx \sum_{l=1}^{N} \mathrm{Re}\left\{ \begin{bmatrix} U_{31,l} \\ U_{32,l} \end{bmatrix} \cdot \frac{\ddot{X}_{i+1,l}\left[-\alpha_{i+1,l}\right]}{(\ddot{X}_{i,l} - \ddot{X}_{i-1,l})} \right\} + \sum_{l=1}^{N} \mathrm{Re}\left\{ \begin{bmatrix} U_{14,l} & U_{15,l} \\ U_{24,l} & U_{25,l} \end{bmatrix} \cdot \begin{bmatrix} \dfrac{(\ddot{X}_{i+1,l} - \ddot{X}_{i,l})}{(\ddot{X}_{i,l} - \ddot{X}_{i-1,l})}\theta_{k(i+1)} \\ \dfrac{(\ddot{X}_{i+1,l} - \ddot{X}_{i,l})}{(\ddot{X}_{i,l} - \ddot{X}_{i-1,l})}\theta_{c(i+1)} \end{bmatrix} \right\} \tag{6.4}$$

As in the FFT_SUBID method, in the TF_SUBID method, the frequency response $(\ddot{X}_{i,l} - \ddot{X}_{i-1,l})$ shows up in the denominator of all measurement uncertainty terms and the frequency response ratio $(\ddot{X}_{i+1,l} - \ddot{X}_{i,l})/(\ddot{X}_{i,l} - \ddot{X}_{i-1,l})$ multiplies the uncertainty terms related to the errors of the upper $(i+1)^{\text{th}}$ story parameters; hence, largely maximizing the frequency response $(\ddot{X}_{i,l} - \ddot{X}_{i-1,l})$ and minimizing the frequency response ratio $(\ddot{X}_{i+1,l} - \ddot{X}_{i,l})/(\ddot{X}_{i,l} - \ddot{X}_{i-1,l})$ in a frequency range around the i^{th} substructure natural frequency ω_{i0} can significantly reduce of the identification errors of the TF_SUBID method.

6.1.3 Identification Error of CSD_SUBID Method

As analyzed in section 5.3.2, the relative identification errors of the i^{th} non-top story parameters $[k_i \quad c_i]^{\mathrm{T}}$ in the CSD_SUBID method can be expressed as,

$$\begin{bmatrix}\theta_{ki}\\ \theta_{ci}\end{bmatrix} \approx \sum_{l=1}^{N} \mathrm{Re}\left\{\begin{bmatrix}U_{11,l} & U_{12,l} & U_{13,l}\\ U_{21,l} & U_{22,l} & U_{23,l}\end{bmatrix}\cdot\begin{bmatrix}N_{\ddot{x}_{i-1}y,l}\big/S_{(\ddot{x}_i-\ddot{x}_{i-1})y,l}\\ N_{\ddot{x}_i y,l}\big/S_{y(\ddot{x}_i-\ddot{x}_{i-1})y,l}\\ N_{\ddot{x}_{i+1}y,l}\big/S_{y(\ddot{x}_i-\ddot{x}_{i-1})y,l}\end{bmatrix}\right\}+ \tag{6.5}$$

$$\sum_{l=1}^{N}\mathrm{Re}\left\{\begin{bmatrix}U_{14,l} & U_{15,l}\\ U_{24,l} & U_{25,l}\end{bmatrix}\cdot\begin{bmatrix}\dfrac{S_{(\ddot{x}_{i+1}-\ddot{x}_i)y,l}}{S_{(\ddot{x}_i-\ddot{x}_{i-1})y,l}}\theta_{k(i+1)}\\ \dfrac{S_{(\ddot{x}_{i+1}-\ddot{x}_i)y,l}}{S_{(\ddot{x}_i-\ddot{x}_{i-1})y,l}}\theta_{c(i+1)}\end{bmatrix}\right\}$$

Since the identification errors of the CSD_SUBID method has a format similar to that of the FFT_SUBID method, a similar conclusion about how to change the structural responses to improve the identification accuracy is obtained: the identification errors of the CSD_SUBID method can be reduced by maximizing the cross power spectral density, $S_{(\ddot{x}_i-\ddot{x}_{i-1})y,l}$, and minimizing the cross power spectral density ratio, $S_{(\ddot{x}_{i+1}-\ddot{x}_i)y,l}\big/S_{(\ddot{x}_i-\ddot{x}_{i-1})y,l}$, in a frequency range around the i^{th} substructure natural frequency ω_{i0}.

If it is assumed that there is only one excitation source (*e.g.*, ground excitation $\ddot{u}_g$) forcing in the structure, then the cross power spectral density ratio, $S_{(\ddot{x}_{i+1}-\ddot{x}_i)y}\big/S_{(\ddot{x}_i-\ddot{x}_{i-1})y}$, will become independent of the selection of the reference response $y(t)$ and can be simplified as

$$\frac{S_{(\ddot{x}_{i+1}-\ddot{x}_i)y}}{S_{(\ddot{x}_i-\ddot{x}_{i-1})y}} = \frac{H^*_{y\ddot{u}_g}H_{(\ddot{x}_{i+1}-\ddot{x}_i)\ddot{u}_g}S_{\ddot{u}_g}}{H^*_{y\ddot{u}_g}H_{(\ddot{x}_i-\ddot{x}_{i-1})\ddot{u}_g}S_{\ddot{u}_g}} = \frac{H_{(\ddot{x}_{i+1}-\ddot{x}_i)\ddot{u}_g}}{H_{(\ddot{x}_i-\ddot{x}_{i-1})\ddot{u}_g}} = \frac{\ddot{X}_{i+1}-\ddot{X}_i}{\ddot{X}_i-\ddot{X}_{i-1}} \tag{6.7}$$

where $H_{y\ddot{u}_g}$ is the transfer function from the ground excitation $\ddot{u}_g$ to the reference response $y(t)$; $H_{(\ddot{x}_i-\ddot{x}_{i-1})\ddot{u}_g}$ is the transfer function from the ground excitation $\ddot{u}_g$ to the i^{th} interstory acceleration $(\ddot{x}_i-\ddot{x}_{i-1})$; $H_{(\ddot{x}_{i+1}-\ddot{x}_i)\ddot{u}_g}$ is the transfer function from the ground excitation $\ddot{u}_g$ to the $(i+1)^{\text{th}}$ interstory acceleration $(\ddot{x}_{i+1}-\ddot{x}_i)$. Therefore, in the case of one excitation, the cross power spectral density ratio $S_{(\ddot{x}_{i+1}-\ddot{x}_i)y} \big/ S_{(\ddot{x}_i-\ddot{x}_{i-1})y}$ equals the frequency response ratio $(\ddot{X}_{i+1,l}-\ddot{X}_{i,l})\big/(\ddot{X}_{i,l}-\ddot{X}_{i-1,l})$.

If the structure is only subjected to the ground excitation, the magnitude of the cross power spectral density $S_{(\ddot{x}_i-\ddot{x}_{i-1})y}$ can be evaluated as

$$\begin{aligned}\left|S_{(\ddot{x}_i-\ddot{x}_{i-1})y}\right| &= \sqrt{S_{(\ddot{x}_i-\ddot{x}_{i-1})y}S^{*}_{(\ddot{x}_i-\ddot{x}_{i-1})y}} = \sqrt{\left|H_{y\ddot{u}_g}\right|^2\left|H_{(\ddot{x}_{i+1}-\ddot{x}_i)\ddot{u}_g}\right|^2 S^2_{\ddot{u}_g}} \\ &= \sqrt{S_y \cdot S_{(\ddot{x}_i-\ddot{x}_{i-1})}}\end{aligned} \tag{6.8}$$

Equation (6.8) shows that the magnitude of the cross power spectrum – $\left|S_{y(\ddot{x}_i-\ddot{x}_{i-1})}\right|$ – is closely related to the power spectrum density of the i^{th} interstory acceleration $S_{(\ddot{x}_i-\ddot{x}_{i-1})}$, larger $S_{(\ddot{x}_i-\ddot{x}_{i-1})}$ leads to larger $\left|S_{y(\ddot{x}_i-\ddot{x}_{i-1})}\right|$ and, thus, more accurate identification results of the CSD_SUBID method. Moreover, since $S_{(\ddot{x}_i-\ddot{x}_{i-1})} = \mathrm{E}\left[\left|\ddot{X}_{i,l}-\ddot{X}_{i-1,l}\right|^2\right]$, large $S_{(\ddot{x}_i-\ddot{x}_{i-1})}$ implies larger average frequency response $(\ddot{X}_i-\ddot{X}_{i-1})$.

6.2 Design for Controlled Substructure Identification Systems

Based on the error analysis results of all three substructure identification methods, it becomes obvious that the goal of an identification-focused control system is to increase the frequency response of the interstory acceleration $(\ddot{X}_i - \ddot{X}_{i-1})$ and simultaneously to reduce the frequency responses ratio $(\ddot{X}_{i+1} - \ddot{X}_i)/(\ddot{X}_i - \ddot{X}_{i-1})$ near the story substructure natural frequency ω_{i0} as much as possible.

To achieve the goal of improving the parameter identification accuracy, two structural control systems are studied: a semi-active brace system and an active mass damper system (AMD). Figure 6.2 shows an example of the active AMD system and the semi-active brace system. New control algorithms for these two systems are designed to attain the desired structural response changes previously mentioned so that the structural parameters can be more accurately identified. It is worth emphasizing that the proposed identification-facilitated control algorithm will be implemented with a fail-safe mechanism, that is, if excessive excitation is detected the control system will immediately switch back to the original control algorithm that is designed to mitigate the structural vibration. Therefore, the new algorithm will not weaken the main function of the control system, vibration mitigation, but add extra value to the installed control system.

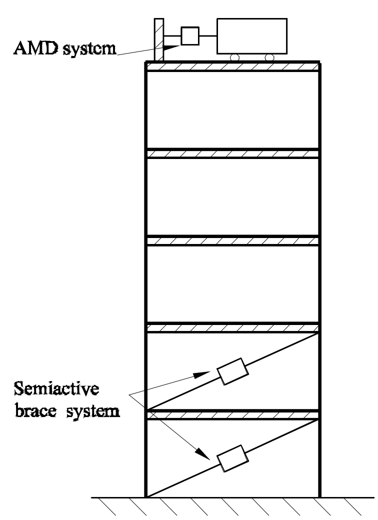

Figure 6.2 Illustration of semi-active brace systems and AMD system

For the simplicity of designing control algorithms to improve substructure identification accuracy, it is assumed herein that

1. The structure is excited only by the ground motion in addition to the control system force(s).
2. The control system is ideal and no control system errors (such as feedback measurement noise, actuator time delay and so forth) exist.

Based on these assumptions, it can be easily shown that 1) the frequency response ratio $(\ddot{X}_{i+1} - \ddot{X}_i)/(\ddot{X}_i - \ddot{X}_{i-1})$ equals the transfer function from the i^{th} interstory acceleration response to the $(i+1)^{\text{th}}$ interstory acceleration response and does not change with different ground excitation inputs, and 2) the frequency response of the interstory acceleration $(\ddot{X}_i - \ddot{X}_{i-1})$ is equal to the frequency response of the ground excitation multiplied by the closed-loop transfer function from ground excitation to the i^{th} interstory acceleration. Hence, instead of directly utilizing the frequency response of the interstory acceleration, which is random in nature due to the random ground excitation, the control system is designed by using the deterministic transfer functions of the closed-loop controlled structure, as shown subsequently in Equations (6.9), (6.11) and (6.12).

The control systems need to simultaneously achieve two goals: amplifying $(\ddot{X}_i - \ddot{X}_{i-1})$ and reducing $(\ddot{X}_{i+1} - \ddot{X}_i)/(\ddot{X}_i - \ddot{X}_{i-1})$ near the story substructure natural frequency, which may be competing goals in some situations; to overcome this problem, the above two-objective optimization problem is converted into a single objective optimization problem by assigning some importance weighting factors for each goal as shown in Equations (6.9), (6.11) and (6.12). Moreover, the goal of amplifying response

$(\ddot{X}_i - \ddot{X}_{i-1})$ is replaced by an equivalent goal of reducing the inverse of the response, $1/(\ddot{X}_i - \ddot{X}_{i-1})$.

6.2.1 AMD System

The linear state-feedback control method is adopted for designing the active AMD system to improve the parameter identification accuracy. Let **L** denote the state feedback gain matrix of the AMD system. The optimal **L** matrix can be obtained by solving the following optimization problem in Equation (6.9). Since the AMD control system has the potential to destabilize the controlled structure system, a stability constraint is imposed on the optimization problem to require that the damping ratio of the closed-loop controlled system be greater than a given threshold.

$$\arg\min_{\mathbf{L}} J(\mathbf{L}) = \alpha \int_{\omega_l}^{\omega_u} \left| W(j\omega) \cdot 1/H_{(\ddot{x}_i - \ddot{x}_{i-1})\ddot{u}_g} \right|^2 d\omega + (1-\alpha) \int_{\omega_l}^{\omega_u} \left| W(j\omega) H_{(\ddot{x}_{i+1} - \ddot{x}_i)(\ddot{x}_i - \ddot{x}_{i-1})} \right|^2 d\omega \tag{6.9}$$
$$\text{subject to } \xi_k \ge \xi_0 > 0,\ k = 1, 2, \cdots, 2n$$

where $H_{(\ddot{x}_i - \ddot{x}_{i-1})\ddot{u}_g}$ and $H_{(\ddot{x}_{i+1} - \ddot{x}_i)(\ddot{x}_i - \ddot{x}_{i-1})}$ are the closed-loop transfer functions from the ground excitation $\ddot{u}_g$ to the i^{th} interstory acceleration response $(\ddot{x}_i - \ddot{x}_{i-1})$ and from the i^{th} interstory acceleration response $(\ddot{x}_i - \ddot{x}_{i-1})$ to the $(i+1)^{\text{th}}$ interstory acceleration response $(\ddot{x}_{i+1} - \ddot{x}_i)$, respectively; ξ_k is the damping ratio of the k^{th} root of the closed-loop system and ξ_0 is a positive real number, taking the value of 0.02 in the following numerical examples; ω_l and ω_u are the lower and upper frequency bounds of the integration, herein taken to be $0.8\omega_{i0}$ and $1.2\omega_{i0}$; α is a weighting factor that balances the role of the SC system in achieving the two possibly competing control goals of changing structural responses; α takes the value of 0.8 in the following examples. $W(j\omega)$ is a frequency weighting function

$$W(j\omega)=\frac{k_i/(m_i\omega^2)}{\left[1-jc_i/(m_i\omega)-k_i/(m_i\omega^2)\right]^2} \tag{6.10}$$

As shown in Figure 6.3, the magnitude of $W(j\omega)$ peaks at around the i^{th} story substructure natural frequency ω_{i0} and quickly vanishes when further away. The role of this frequency weighting function is to implicitly force the control system to focus on changing the two interested structural responses, $(\ddot{X}_i-\ddot{X}_{i-1})$ and $(\ddot{X}_{i+1}-\ddot{X}_i)/(\ddot{X}_i-\ddot{X}_{i-1})$, only around the substructure natural frequency ω_{i0}, so that the identification error can be greatly reduced.

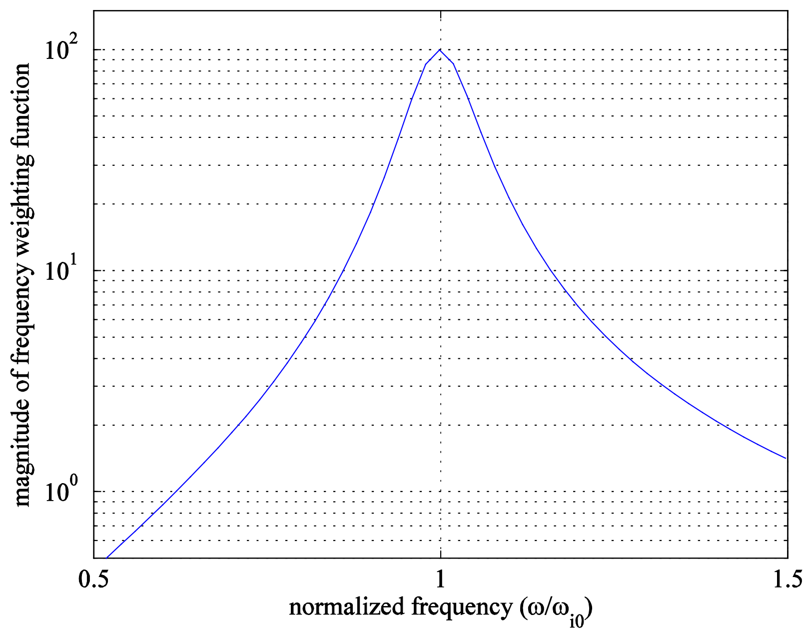

Figure 6.3 Magnitude of frequency weighting function *W(jω)*

6.2.2 VSDD Brace System

Two kinds of control strategies to design a variable stiffness damping device (VSDD) brace system are studied herein. First, the VSDD braces are used as passive devices that add fixed stiffness and damping to the structure. Second, in a semiactive strategy, the VSDD braces try to mimic, as closely as possible, the control force trajectory of an optimally designed active control system.

a) Passive Control Algorithm Design

Let $\boldsymbol{\theta} = [\theta_1 \ \ldots \ \theta_p]^{\mathrm{T}}$ be a vector composed of the stiffness and damping parameters of the semiactive braces. The following optimization problem is posed to minimize the inverse of the frequency ith interstory acceleration $1/(\ddot{X}_i - \ddot{X}_{i-1})$ as well as the frequency ratio $(\ddot{X}_{i+1} - \ddot{X}_i)/(\ddot{X}_i - \ddot{X}_{i-1})$ near the i^{th} story substructure natural frequency ω_{i0}.

$$\arg\min_{\boldsymbol{\theta}} J(\boldsymbol{\theta}) = \alpha \int_{\omega_l}^{\omega_u} \left| W(j\omega) \cdot 1/H_{(\ddot{x}_i - \ddot{x}_{i-1})\ddot{u}_g} \right|^2 d\omega + (1-\alpha) \int_{\omega_l}^{\omega_u} \left| W(j\omega) H_{(\ddot{x}_{i+1} - \ddot{x}_i)(\ddot{x}_i - \ddot{x}_{i-1})} \right|^2 d\omega \qquad (6.11)$$
$$\text{subject to } \theta_k^{\max} \geq \theta_k \geq 0, k = 1,2,\cdots,p$$

where ω_l and ω_u are the lower and upper limit of the integration frequency range, respectively; $\theta_k^{\max}$ $(k = 1,2,\cdots,p)$ are the upper limit of the corresponding stiffness or damping parameters of the braces; all design variables θ_k should be non-negative due to the passive nature of the devices; p is the number of the braces; and α and $W(j\omega)$ are the same as given in Equation (6.9).

b) Semiactive Control Algorithm Design

A clipped optimal control strategy (Dyke *et al.*, 1996; Ramallo *et al.*, 2002) is used to design a semiactive algorithm to enhance the identification accuracy. The clipped optimal control is composed of two controllers in series: the primary controller is designed by a linear state feedback control algorithm assuming that the actuators are fully active, and a clipping algorithm is used as a secondary controller to make the semiactive brace mimic the control force commanded by the primary controller.

Due to the dissipative nature of semiactive braces, a semiactive brace cannot always provide the exact control force as calculated by the primary controller. The performance of the clipped optimal control system, compared with the corresponding fully active system, is largely dependent on the dissipativity of the control forces from the primary controller (Johnson *et al*., 2007). Therefore, a dissipativity constraint for the primary controller is integrated into the optimization procedure of the algorithm design (6.12) to assure that the control forces applied to the structure are dissipative during most of the time history, so that the semiactive system effectively tracks the active system.

Let **G** be the state feedback gain matrix of the primary controller in a clipped optimal semiactive control system. An approximate optimal semiactive strategy can be found by solving for an active primary controller state feedback gain subject to a constraint that it be dissipative much of the time

$$\arg\min_{\mathbf{G}} J(\mathbf{G}) = \alpha\int_{\omega_l}^{\omega_u} \left|W(j\omega)\cdot 1/H_{(\ddot{x}_i-\ddot{x}_{i-1})\ddot{u}_g}\right|^2 d\omega + (1-\alpha)\int_{\omega_l}^{\omega_u} \left|W(j\omega)H_{(\ddot{x}_{i+1}-\ddot{x}_i)(\ddot{x}_i-\ddot{x}_{i-1})}\right|^2 d\omega \qquad (6.12)$$
$$\text{subject to } \rho_{u_l v_l} \le \varepsilon < 0, k = 1,2,\cdots,p$$

where $\rho_{u_l v_l}$ is the correlation coefficient between the control force u_l and the velocity v_l across the l^{th} semi-active brace; ε is a negative number between 0 and –1, with smaller ε requiring the control force be more dissipative; ε is chosen to be –0.5 in the numerical examples herein. The weighting function $W(j\omega)$ is the same as given in Equation (6.9).

After the primary controller is designed, a secondary clipped optimal controller is concatenated afterward to form the full controller, where desired control force $u_l(t)$ is exerted at time t if $u_l(t) \cdot v_l(t) \leq 0$ for velocity $v_l(t)$ across the l^{th} device (i.e., if it is dissipative), and zero force otherwise.

Since the accuracy of substructure identification does not directly depend on the SC system but only indirectly on the performance of the SC system – the ability to change the structural response – any control system errors, like feedback measurement noise, which do not significantly weaken this performance of the designed control system will not have a large side effect on the final identification results. Therefore, the proposed controlled substructure identification should be quite robust to the possible control system errors.

6.3 Control System Design with Unknown Structural Parameters

To optimally design a control system, the exact structural parameters are required to accurately evaluate the performance of the closed-loop controlled system. However, the whole purpose for designing control systems herein is to improve parameter identification; thus, these parameter values, at least their exact values, should not be available for control design. To overcome this difficulty, a three-stage design strategy can be adopted. Figure 6.4 shows the flowchart of this three-stage design method. At the first stage, several substructure identifications with no control forces are performed to initially estimate structural parameters. In the second stage, a probabilistic model for the structural parameters will be constructed from the previous step identification results to describe the uncertainty of the structural parameters. Given the limited number of identification results from the first stage, only the first two statistical moments (mean and variance) of structural parameters can be computed accurately. Thus, based on the maximum entropy theorem (Jaynes, 1968), a Gaussian probability model is selected in this study to keep the maximum uncertainty of the random parameters when only their means and variances are given. The parameters (statistics) of this Gaussian model are estimated from the previous step identification results. Based on the probability model of the structural parameters, a sampling technique is applied to generalize many realizations of the structural parameters, each of which is used to create a structure model. In the final stage, instead of using the best guess model of the structure, whose parameters are the mean estimates of the structural parameters, to design the control system, all structural models generated by the sampling are used together to evaluate both the objective function and the constraints in the optimization.

Let $\mathbf{L}$ denote the design parameters of the control system, which is the state feedback gain matrix for the AMD system or the added story stiffness and damping for semiactive brace system; let $\boldsymbol{\theta} = [k_1 \ \dots \ k_n \quad c_1 \ \dots \ c_n]^{\mathrm{T}}$ be the uncertain structural parameter vector with probability distribution obtained in the second stage. The optimization problem used to design control system with uncertain structural parameters can be written as,

$$\begin{aligned} &\arg\min_{\mathbf{L}} J(\mathbf{L}) = \alpha \int_{\omega_l}^{\omega_u} \mathrm{E}_{\boldsymbol{\theta}}\left[\left|W(j\omega) / H_{(\ddot{x}_i - \ddot{x}_{i-1})\ddot{u}_g}\right|^2\right] d\omega + (1-\alpha)\int_{\omega_l}^{\omega_u} \mathrm{E}_{\boldsymbol{\theta}}\left[\left|W(j\omega) H_{(\ddot{x}_{i+1} - \ddot{x}_i)(\ddot{x}_i - \ddot{x}_{i-1})}\right|^2\right] d\omega \\ &\qquad \text{subject to } \mathrm{E}_{\boldsymbol{\theta}}\left[c(\boldsymbol{\theta})\right] + 2\sigma_{\boldsymbol{\theta}}\left[c(\boldsymbol{\theta})\right] < 0, k = 1,2,\cdots, p \end{aligned} \tag{6.13}$$

where subscript $\boldsymbol{\theta}$ denotes that the expectation operator is taken with respect to the uncertain structural parameters; $\mathrm{E}_{\boldsymbol{\theta}}\left[c(\boldsymbol{\theta})\right]$ stands for the mean value of the constraint function $c(\boldsymbol{\theta})$, whose value must be less than zero (i.e., $c(\boldsymbol{\theta}) < 0$) in the original control system design with deterministic structural parameters; $\sigma_{\boldsymbol{\theta}}[c(\boldsymbol{\theta})]$ denotes the standard deviation of the constraint function $c(\boldsymbol{\theta})$ due to the uncertainty in the structural parameters. The factor of 2 in front of $\sigma_{\boldsymbol{\theta}}[\cdot]$ is used to ensure that the constraint is satisfied most of the time (larger values than 2 would be used to ensure a higher likelihood of satisfying the constraint).

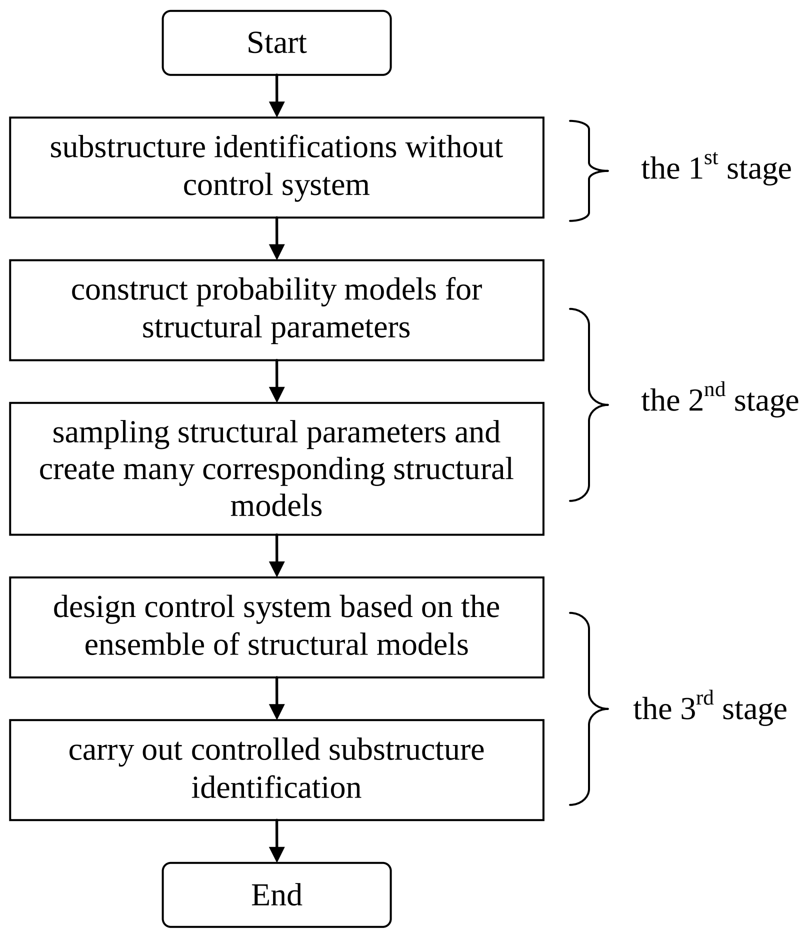

Figure 6.4 Flowchart of three stage control system design strategy

6.4 Effect of Feedback Measurement Noise on Controlled Substructure Identification

Using structural control systems to amplify the response $(\ddot{X}_i - \ddot{X}_{i-1})$ and reduce the response ratio $(\ddot{X}_{i+1} - \ddot{X}_i)/(\ddot{X}_i - \ddot{X}_{i-1})$ near the story substructure natural frequency can significantly improve substructure identification accuracy. Further, since each step of the substructure identification method only involves the dynamic response of a certain floor substructure, a control force applied on one floor will not enter into most of the identification steps and, thus, the error in control force will not directly affect the accuracy of these identifications and the side effect of the control system error is minimized. Moreover, because the control system error affects the identification accuracy by diverting the controlled structural responses from the optimally designed responses, the effect of the control system error can be easily analyzed and predicted by observing the responses of the controlled structure. Therefore, the proposed controlled substructure identification methods will improve identification accuracy and also be robust to the errors in the control forces.

The control algorithm in the previous section is designed on the assumption of an ideal control system. However, some control system errors always exist and will inevitably affect, more or less, the performance of the designed control system to improve identification accuracy. In this section, an analysis is made to examine how one of the common control system errors, feedback measurement noise, will affect the performance of the control system. Since the identification accuracy of substructure identification directly depends on two closed-loop substructure responses, $(\ddot{X}_i - \ddot{X}_{i-1})$

and $(\ddot{X}_{i+1} - \ddot{X}_i)/(\ddot{X}_i - \ddot{X}_{i-1})$, the effect of feedback measurement noise on the accuracy of the substructure identification can be analyzed by examining how the noise will change these responses from what was originally designed.

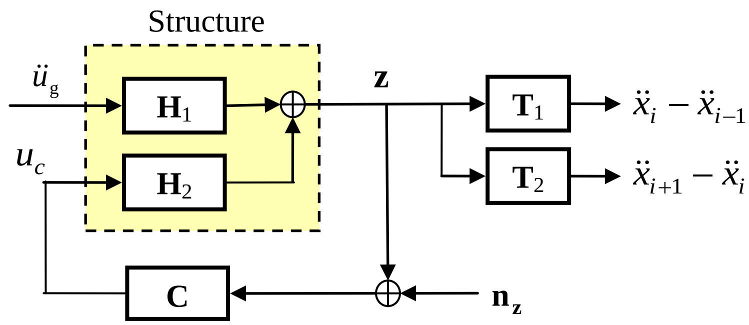

Figure 6.5 Control system with state feedback measurement noise

It can be shown that both active AMD and semiactive brace systems can be represented by the flowchart in Figure 6.4, where $\ddot{u}_g$ is the ground excitation; u_c are the control system force(s) applied on the structure; $\mathbf{z}$ represents the structural state-space response vector, containing the displacement and velocity responses of all floors; $\mathbf{n}_\mathbf{z}$ is the measurement noise vector of the state space response, assumed to be band-limited Gaussian random processes; $\mathbf{H}_1$ and $\mathbf{H}_2$ are the structure transfer functions from ground excitation and control forces to the structural state-space responses respectively; $\mathbf{C}$ is the designed controller; $\mathbf{T}_1$ and $\mathbf{T}_2$ are the linear matrices that link the state-space response to the i^{th} and $(i+1)^{th}$ interstory acceleration respectively.

Assuming that the controller $\mathbf{C}$ is a linear controller, the closed-loop controlled structure is a linear time invariant (LTI) system. By applying the superposition principal to the output of this system in the frequency domain, the frequency response of the i^{th}

interstory acceleration $(\ddot{X}_i - \ddot{X}_{i-1})$ and the $(i+1)^{\text{th}}$ interstory acceleration $(\ddot{X}_{i+1} - \ddot{X}_i)$, can be calculated as

$$\ddot{X}_i - \ddot{X}_{i-1} = \mathbf{T}_1(\mathbf{I} - \mathbf{H}_2\mathbf{C})^{-1}\mathbf{H}_1\ddot{U}_\mathrm{g} + \mathbf{T}_1(\mathbf{I} - \mathbf{H}_2\mathbf{C})^{-1}\mathbf{H}_2\mathbf{C}\mathbf{N}_\mathrm{y} = R_i + \Delta R_i \tag{6.14}$$

$$\ddot{X}_{i+1} - \ddot{X}_i = \mathbf{T}_2(\mathbf{I} - \mathbf{H}_2\mathbf{C})^{-1}\mathbf{H}_1\ddot{U}_\mathrm{g} + \mathbf{T}_2(\mathbf{I} - \mathbf{H}_2\mathbf{C})^{-1}\mathbf{H}_2\mathbf{C}\mathbf{N}_\mathrm{y} = R_{i+1} + \Delta R_{i+1} \tag{6.15}$$

where $\ddot{X}_{i-1}, \ddot{X}_i, \ddot{X}_{i+1}, \ddot{U}_\mathrm{g}, \mathbf{N}_\mathbf{z}$ are the frequency response of the corresponding time domain responses of $\ddot{x}_{i-1}, \ddot{x}_i, \ddot{x}_{i+1}, \ddot{u}_\mathrm{g}, \mathbf{n}_\mathbf{z}$, respectively. The responses in Equations (6.14) and (6.15) contain two parts: the first part is due to the ground excitation, which is just equal to the responses from the ideally controlled system without feedback noise; the second part is the responses contributed by the feedback noise. For notational simplicity, new variables R_i, ΔR_i, R_{i+1}, ΔR_{i+1} are introduced to represent these response, respectively.

a) Feedback Noise Effect on Response $(\ddot{X}_i - \ddot{X}_{i-1})$

In order to perform an analysis, it is assumed that feedback measurement noises $\mathbf{n}_\mathbf{z}$ are independent of the ground excitation $\ddot{u}_\mathrm{g}$. Therefore, the variance of the frequency response of the i^{th} closed-loop controlled interstory acceleration can be calculated as

$$\mathrm{E}\left[\left|\ddot{X}_i - \ddot{X}_{i-1}\right|^2\right] = \mathrm{E}\left[\left|\mathbf{T}_1(\mathbf{I} - \mathbf{H}_2\mathbf{C})^{-1}\mathbf{H}_1\ddot{U}_\mathrm{g}\right|^2\right] + \mathrm{E}\left[\left|\mathbf{T}_1(\mathbf{I} - \mathbf{H}_2\mathbf{C})^{-1}\mathbf{H}_2\mathbf{C}\mathbf{N}_\mathrm{y}\right|^2\right] \tag{6.16}$$

The variance in Equation (6.16) consists of two parts: the first part is due to ground excitation, which just equals the variance of the responses from the ideally controlled system without feedback noise; the second part is contributed by the feedback noise variance. Since the second part is always greater than zero, the variance of the responses from the non-ideally controlled system (with feedback noise) will be larger than that from the ideally controlled system; this indicates that from the response $(\ddot{X}_i - \ddot{X}_{i-1})$ point of view, the feedback noise does not deteriorate but rather ***improves*** the performance of the control system to amplify the frequency response of the i^{th} interstory acceleration $(\ddot{X}_i - \ddot{X}_{i-1})$ and , thus, enhance the final identification accuracy.

b) Feedback Noise Effect on Response $(\ddot{X}_{i+1} - \ddot{X}_i)/(\ddot{X}_i - \ddot{X}_{i-1})$

Using the results from Equations (6.14) and (6.15), the frequency response ratio $(\ddot{X}_{i+1} - \ddot{X}_i)/(\ddot{X}_i - \ddot{X}_{i-1})$ under feedback noise can be calculated as

$$\frac{\ddot{X}_{i+1} - \ddot{X}_i}{\ddot{X}_i - \ddot{X}_{i-1}} = \frac{R_{i+1} + \Delta R_{i+1}}{R_i + \Delta R_i} \tag{6.16}$$

Treating the variables ΔR_i and ΔR_{i+1} as the increment of the variables R_i and R_{i+1} respectively and applying a first order Taylor expansion with respect to variables R_i and R_{i+1}, the response in Equation (6.16) can be approximated by

$$\frac{\ddot{X}_{i+1} - \ddot{X}_i}{\ddot{X}_i - \ddot{X}_{i-1}} \approx \frac{R_{i+1}}{R_i} - \frac{R_{i+1}}{R_i}\frac{\Delta R_i}{R_i} + \frac{\Delta R_{i+1}}{R_i} = H_{(\ddot{x}_{i+1}-\ddot{x}_i)(\ddot{x}_i-\ddot{x}_{i-1})}\left(1 - \frac{\Delta R_i}{R_i}\right) + \frac{\Delta R_{i+1}}{R_i} \tag{6.17}$$

The ratio R_{i+1}/R_i is equal to the closed-loop transfer function from the i^{th} interstory acceleration to the $(i+1)^{\text{th}}$ interstory acceleration $H_{(\ddot{x}_{i+1}-\ddot{x}_i)(\ddot{x}_i-\ddot{x}_{i-1})}$ of an ideally-controlled structure, which is designed to be small near the substructure natural frequency. Therefore, if the i^{th} and $(i+1)^{\text{th}}$ interstory acceleration ΔR_i and ΔR_{i+1} caused by the feedback noise are small compared with the i^{th} interstory acceleration R_i due to the ground excitation, the frequency response ratio $(\ddot{X}_{i+1} - \ddot{X}_i)/(\ddot{X}_i - \ddot{X}_{i-1})$ with feedback noise will not be largely amplified compared with that from the ideally-controlled system (without feedback noise). Moreover, the R_i response, equal to the i^{th} interstory acceleration $(\ddot{X}_i - \ddot{X}_{i-1})$ in ideally control system, is originally designed to be large near the substructure natural frequency; thus, generally, the frequency response ratio $(\ddot{X}_{i+1} - \ddot{X}_i)/(\ddot{X}_i - \ddot{X}_{i-1})$ should not be largely amplified near the substructure natural frequency by the introduction of feedback noise.

Combining the conclusions from (a) and (b) regarding the feedback noise effect on response $(\ddot{X}_i - \ddot{X}_{i-1})$, it can be concluded that the proposed control-facilitated identification method designed under ideal conditions (without feedback noise) are quite robust to the side effect of the existence of feedback noise and may even have a potential to provide more accurate identification results with feedback noise because the noise amplifies the structural response $(\ddot{X}_i - \ddot{X}_{i-1})$.

6.5 A Numerical Example

The same 5-story shear structure used in the third, fourth and fifth chapters is reused here to illustrate the effectiveness of utilizing the control systems to improve the accuracy of the structural parameter identification. The parameters of the shear structure are $m_i = 1\times10^5$ kg, $c_i = 8\times10^5$ N·sec/m and $k_i = 16\times10^7$ N/m ($i = 1,\ldots,5$). The structure is subject to ground excitation $\ddot{u}_g$, which is modeled by a Gaussian random pulse process passing through a 4-th order band pass Butterworth filter with 1Hz low cut-off frequency and 12 Hz high cut-off frequency.

Two control systems, an AMD system installed on the roof (the fifth floor) and a VSDD brace system implemented in the first and second stories, are considered respectively. The state feedback control strategy is used to design the AMD system; the passive and the pseudo-active state feedback control strategies are applied to design the

VSDD brace system. The optimal parameters of the control systems are obtained by solving the optimization methods proposed in section 6.2. Then, the designed control systems are then used to control the structural response when the controlled substructure identifications are performed.

To test the performance of the newly designed control systems in improving the parameter identification accuracy, 100 substructure identification tests, via the FFT_SUBID method, are carried out for the structure without control, with VSDD brace and AMD control systems respectively. It is assumed in the simulation that there is noise in the measurements of floor accelerations and control forces, but the control systems works ideally and there is no noise in the state feedback measurement.

Figures 6.6 and 6.7 demonstrate an example of how the control systems change the structural responses to improve the parameter identification accuracy. Figure 6.6 shows the transfer functions from the ground excitation to the 1st interstory acceleration of the uncontrolled and the controlled structures; Figure 6.7 shows the frequency response ratio $(\ddot{X}_2 - \ddot{X}_1)/(\ddot{X}_1 - \ddot{U}_g)$ between the two adjacent interstory responses of the uncontrolled and the controlled structures. It can be seen that two control systems – passive VSDD system and AMD system – amplify the 1st interstory acceleration responses, which controls the identification error of the 1st story parameters $[k_1 \quad c_1]^T$ due to the measurement noise, and reduce the frequency response ratio $(\ddot{X}_2 - \ddot{X}_1)/(\ddot{X}_1 - \ddot{U}_g)$, which controls the identification error related to the error propagation effect; thus, it is expected that the control systems will improve the accuracy of the substructure identifications.

Note that the transfer functions of the VSDD system using pseudo-active control strategy are not included in the figures because this control system is not a linear system.

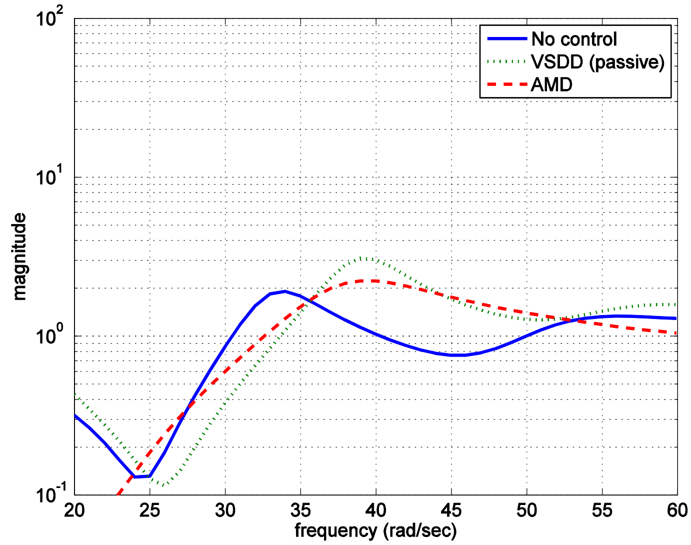

Figure 6. 6 The transfer functions from ground excitation to the 1st interstory acceleration of uncontrolled and controlled structure

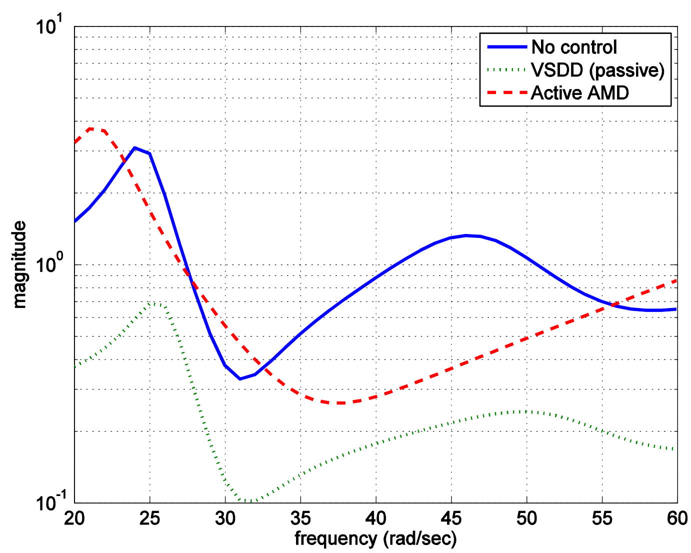

Figure 6.7 The frequency response ratio between the 2nd interstory acceleration and the 1st interstory acceleration

In each substructure identification test, 180-second ground and floor acceleration responses, with sampling rate 200 Hz, are calculated to carry out the identification. It is assumed that the magnitudes of the measurement noises of all acceleration responses $\ddot{x}_i$ are the same, with root-mean-square (RMS) value equal 5% of the RMS of the ground excitation; the measurement of the control force (in controlled identification case) is also contaminated by 5% noise, that is, the RMS of the measurement noise of the control force is equal to 5% of the RMS of the corresponding control force.

The relative RMS errors (RMSE) of the identified parameters (in percentage) are listed in Table 6.1. From the result, it is clearly seen that all control systems do greatly improve the parameter identification accuracy. Taking the third story parameter as an example, the RMSEs of stiffness and damping parameter estimates are reduced by a factor of 4.7 and 5.4 for the passive control method (VSDD system), by a factor of 3.3 and 3.9 for the pseudo-active control method (VSDD system), and by a factor of 8.3 and 11.9 for the active control method (AMD system).

Table 6.1 Relative (percentage) RMSE of identification results without control and with ideally passive, pseudo-active and active control

floor #	No control		VSDD (passive)		VSDD (pseudo-active)		AMD	
	k_i	c_i	k_i	c_i	k_i	c_i	k_i	c_i
1	1.40	3.85	0.22	1.92	0.29	0.99	0.26	2.01
2	1.90	4.65	0.42	2.18	0.47	1.41	0.41	2.36
3	2.33	20.59	0.49	3.83	0.71	5.33	0.28	1.73
4	0.63	6.64	0.20	1.12	0.21	1.17	0.17	1.16
5	0.39	3.31	0.19	0.78	0.15	0.63	0.19	1.29

Table 6.2 Relative (percentage) RMSE of identification result of passive and active control with 20% feedback noise

floor #	VSDD (passive)		VSDD (pseudo-active)		AMD	
	k_i	c_i	k_i	c_i	k_i	c_i
1	0.38	2.76	0.31	1.05	0.22	1.72
2	0.46	1.96	0.42	1.23	0.36	1.95
3	0.54	4.76	0.63	5.46	0.23	1.50
4	0.19	1.02	0.21	1.46	0.20	1.05
5	0.16	0.59	0.14	0.70	0.13	0.67

The analyses in section 6.4 show that the proposed control-identification methods are robust to the feedback measurement noise and it is possible that the noise may even enhance the identification accuracy. To test this conclusion, fairly large 20% Gaussian white control feedback noise is added into the structural state feedback; that is, the RMS of noise $\mathbf{n_z}$ is equal to 20% of the RMS of the corresponding state response. Similarly, 100 identification tests are performed with the noise-contaminated passive and active control systems. The results of these tests are shown in Table 6.2.

By comparing the corresponding results between Tables 6.1 and 6.2, it is observed that there is no obvious deterioration of the identification accuracy due to the addition of 20% state feedback noise; on the contrary, the identification results for most story parameters with feedback noise become more accurate than those without noise. This simulation result partially verifies the previous analysis that the controlled identification systems are robust to the state feedback noise and the noise may even help to improve the identification accuracy via amplifying structural response $(\ddot{X}_i - \ddot{X}_{i-1})$. However, there are some cases that the identification results deteriorate slightly. This may be due to two reasons: 1) the introduction of feedback noise may also amplify the response ratio $(\ddot{X}_{i+1} - \ddot{X}_i)/(\ddot{X}_i - \ddot{X}_{i-1})$ compared with the ideally-controlled case, which in turn deteriorates the accuracy. 2) The uncertainty of the measured control forces may contribute to the increase of the identification errors. Taking the AMD system as an example, the control force (from the actuator) is directly applied on the 5th floor of the structure; thus, the measured control force is needed for the identification of the 5th story parameters. In the non-ideal control case, the measured control force is also assumed to be noise contaminated; thus, the uncertainty in the measured control force will inevitably increase the identification error for the 5th story parameters and also affect the identification accuracy of other parameters through the error accumulation effect.

In summary, although the estimates of some parameters with feedback noise deteriorates slightly compared with an ideally-controlled case, both control systems do still provide quite large improvements for the identification accuracy under fairly large feedback noise, compared to uncontrolled identification results. These simulation results reconfirm the conclusion of the analysis that the proposed control-identification methods are quite robust to the feedback measurement noise.

Chapter 7

Loop Substructure Identification Method

In the third, fourth and fifth chapters, three substructure identification methods have been proposed to identify the structural parameters of a shear structure. These identification methods essentially establish an induction identification problem, in which the parameters of the whole structure are identified iteratively from top to bottom. However, there are two limitations of these substructure identification methods. First, the induction process in these methods requires *a priori* information of the structural floor masses. But the structural mass may not be always known in reality, which prevents the application of the substructure identification methods. Second, in some cases, such as post-earthquake damage evaluation of building structures, people may only care about the structural parameters of a few stories where structural damage is most likely to occur (*e.g.*, the lower stories). However, to identify the parameters of a lower story in the substructure identification methods, the structural parameters of all stories have to be first identified in the induction identification process, which requires installation of accelerometers on every floor above the story being identified; this may result in prohibitive costs for the SHM system if the building has tens of stories. Therefore, it is of practical interest to develop some methods that can identify the parameters of any story in the structure by only measuring a few structural responses related to that part of the structure.

In this chapter, a new substructure identification method, the LOOP_SUBID method, is proposed to address the aforementioned limitations of substructure identification methods in Chapters 3~5: how can one perform the identification with unknown structural mass and with only a few measurements in the structure. Different from the previous substructure identification methods, in the new LOOP_SUBID method only the dynamic equation of one non-top story substructure, containing the story whose parameters are to be identified, is used in formulating the identification problem. Two substructure identification problems, each of which identifies the parameters of one story in the substructure given that the parameters of another story in the substructure are known, are alternately used to establish a sequence of loop identification problems, in which all four structural parameters $[k_i \quad c_i \quad k_{i+1} \quad c_{i+1}]^{\mathrm{T}}$ are identified all together once. Moreover, the new method does not need the absolute value of the story mass m_i in the identification if the mass normalized structural parameters $[k_i/m_i \quad c_i/m_i \quad k_{i+1}/m_i \quad c_{i+1}/m_i]^{\mathrm{T}}$ are identified.

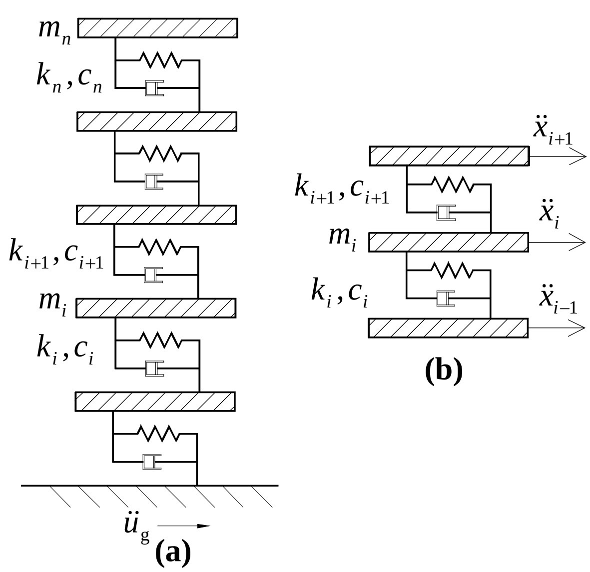

Figure 7.1 (a) A shear story (b) two-story standard substructure

This chapter is organized as follows. First is to examine how to make use of the dynamic equation of one story substructure to formulate the loop identification problems in the LOOP_SUBID method. Then, the convergence behavior of the LOOP_SUBID method is studied and a numerical example is used to verify the convergence; the results show that not all identification estimates of the LOOP_SUBID method converge. Next, an analysis is made to explain why the LOOP_SUBID method fails to converge, leading to the proposal of a modification of the LOOP_SUBID method to fix the problem by using two sets of special structural responses in formulating the loop identification problems. Moreover, a method of designing some control system is proposed to change structural responses so that the convergence of the loop identification in the LOOP_SUBID method can be achieved. Finally, the same 5-story example is used to show that by utilizing the specially designed control systems, the LOOP_SUBID method is able to achieve converged identification results.

7.1 Method Formulation

Figure 7.1a shows an *n*-story shear structure; Figure 7.1b shows a standard two-story substructure that will be used in formulating the LOOP_SUBID method. The dynamic equation of a middle floor of this substructure can be written as

$$m_i \ddot{x}_i(t) + c_i\left[\dot{x}_i(t) - \dot{x}_{i-1}(t)\right] + k_i\left[x_i(t) - x_{i-1}(t)\right] + c_{i+1}\left[\dot{x}_i(t) - \dot{x}_{i+1}(t)\right] + k_{i+1}\left[x_i(t) - x_{i+1}(t)\right] = 0 \tag{7.1}$$

where m_i is the mass of the i^{th} floor; c_i and k_i are the damping coefficient and stiffness of the i^{th} story; x_i is the displacement of the i^{th} floor relative to an inertial reference frame.

Adding $-m_i\ddot{x}_{i-1}(t)$ to both side of Equation (7.1), pre-multiplying both sides by a reference response at an earlier time $y(t-\tau)$ and taking the expectation will give

$$m_i R_{(\ddot{x}_i-\ddot{x}_{i-1})y} + c_i R_{(\dot{x}_i-\dot{x}_{i-1})y} + k_i R_{(x_i-x_{i-1})y} + c_{i+1} R_{(\dot{x}_i-\dot{x}_{i+1})y} + k_{i+1} R_{(x_i-x_{i+1})y} = -m_i R_{\ddot{x}_{i-1}y} \tag{7.2}$$

where $R_{xy}(\tau) = \mathrm{E}\left[x(t)y(t-\tau)\right]$ is cross correlation function between the responses $x(t)$ and $y(t)$. It is assumed here that the reference response $y(t)$ and all structural responses are jointly wide sense stationary (WSS). When $y(t)$ and $x(t)$ are joint WSS process, their cross correlation function satisfies the following equation (Bendal *et al.*, 2000)

$$R_{x^{(m)}y}(\tau) = R_{xy}^{(m)}(\tau) \tag{7.3}$$

Let $x^{(m)}$ denote the m^{th} derivative of the random process $x(t)$ with respect to time, and $R_{xy}^{(m)}(\tau)$ denote the m^{th} derivative of the correlation function $R_{xy}(\tau)$ with respect to τ. If the mean square derivatives exist, Equation (7.2) can be rewritten as

$$m_i \ddot{R}_{(x_i-x_{i-1})y} + c_i \dot{R}_{(x_i-x_{i-1})y} + k_i R_{(x_i-x_{i-1})y} + c_{i+1} \dot{R}_{(x_i-x_{i+1})y} + k_{i+1} R_{(x_i-x_{i+1})y} = -m_i \ddot{R}_{x_{i-1}y} \tag{7.4}$$

Taking a two sided Fourier transform of both sides, rearranging the order of the equation and exploiting the property of $F(\ddot{R}) = (j\omega)^2 F(R)$ (where F denotes Fourier transform operator and j^2=−1) gives

$$\frac{1}{1 - j\,c_i/(m_i\omega) - k_i/(m_i\omega^2)} = \frac{S_{\ddot{x}_{i-1}y} - S_{\ddot{x}_i y}}{S_{\ddot{x}_{i-1}y} + (S_{\ddot{x}_{i+1}y} - S_{\ddot{x}_i y})[\,jc_{i+1}/(m_i\omega) + k_{i+1}/(m_i\omega^2)]} \tag{7.5}$$

where $S_{\ddot{x}_j y}$, the Fourier transform of the cross correlation function $R_{\ddot{x}_j y}(\tau)$, is the cross power spectral density function between the structural acceleration response $\ddot{x}_j$ and the reference response y.

If the structural parameters of the $(i+1)^{\text{th}}$ story $[k_{i+1}\ c_{i+1}]^T$ are known, then the right side of Equation (7.5) can be calculated from the measured structural responses and the following the optimization problem is formulated to identify the parameters of the i^{th} story $[k_i\ \ c_i]^T$.

$$\underset{k_i, c_i}{\arg\min} \quad J(k_i, c_i) = \sum_{l=1}^{N} \left| g_l(k_i, c_i) - \hat{g}_l(\hat{S}_{\ddot{x}_{i-1}y}, \hat{S}_{\ddot{x}_i y}, \hat{S}_{\ddot{x}_{i+1}y}) \right|^2 \tag{7.6}$$

where $g_l(k_i, c_i) = \dfrac{1}{1 - j c_i/(m_i \omega_l) - k_i/(m_i \omega_l^2)}$,

$$\hat{g}_l(\hat{S}_{\ddot{x}_{i-1}y,l}, \hat{S}_{\ddot{x}_i y,l}, \hat{S}_{\ddot{x}_{i+1}y,l}) = \frac{\hat{S}_{\ddot{x}_{i-1}y,l} - \hat{S}_{\ddot{x}_i y,l}}{\hat{S}_{\ddot{x}_{i-1}y,l} + (\hat{S}_{\ddot{x}_{i+1}y,l} - \hat{S}_{\ddot{x}_i y,l})[jc_{i+1}/(m_i \omega_l) + k_{i+1}/(m_i \omega_l^2)]}$$

(The derivation in Equations (7.1)~(7.6) is nothing but a duplication of the derivation of the non-top story identification in the CSD_SUBID method in section 5.1). In order to solve the optimization problem (7.6), the value of the $(i+1)^{\text{th}}$ story parameters $[k_{i+1}\ c_{i+1}]^T$ have to be known. To identify parameters $[k_{i+1}\ \ c_{i+1}]^T$, the CSD_SUBID method in Chapter 5 uses the dynamic equation of the $(i+1)^{\text{th}}$ floor shown in Equation (7.7), which results in the establishment of an induction identification problem.

$$m_{i+1}\ddot{x}_{i+1} + c_{i+1}(\dot{x}_{i+1} - \dot{x}_i) + k_{i+1}(x_{i+1} - x_i) + c_{i+2}(\dot{x}_{i+1} - \dot{x}_{i+2}) + k_{i+2}(x_{i+1} - x_{i+2}) = 0 \tag{7.7}$$

Unlike the CSD_SUBID method, the LOOP-SUBID method utilizes a different approach to identify the parameters $[k_{i+1}\ c_{i+1}]^T$, one based on the dynamic equation of the i^{th} floor, Equation (7.1), rather than that of the $(i+1)^{\text{th}}$ floor.

One interesting property of Equation (7.1) is that the equation remains unchanged with the structural parameters swapped (k_i, c_i $\Leftrightarrow$ k_{i+1}, c_{i+1}) and structural responses swapped ($x_{i-1}, \dot{x}_{i-1}, \ddot{x}_{i-1} \Leftrightarrow x_{i+1}, \dot{x}_{i+1}, \ddot{x}_{i+1}$), which implies that the i^{th} story substructure and

$(i+1)^{\text{th}}$ story substructure have some symmetry in the identification process. This symmetry provides a way of developing a symmetric identification method similar to that of Equation (7.6), in which that the parameters of the $(i+1)^{\text{th}}$ story $[k_{i+1} \;\; c_{i+1}]^{\mathrm{T}}$ can be identified given that the parameters of the i^{th} story $[k_i \;\; c_i]^{\mathrm{T}}$ are known. This symmetric identification method is developed as follows,

Adding the term $-m_i \ddot{x}_{i+1}$ to both sides of Equation (7.1) and following a procedure similar to that in Equations (7.2)~(7.5), another key equation can be obtained as follows

$$\frac{1}{1 - j\, c_{i+1}/(m_i \omega) - k_{i+1}/(m_i \omega^2)} = \frac{S_{\ddot{x}_{i+1}y} - S_{\ddot{x}_i y}}{S_{\ddot{x}_{i+1}y} + (S_{\ddot{x}_{i-1}y} - S_{\ddot{x}_i y})[\, jc_i/(m_i \omega) + k_i/(m_i \omega^2)]} \tag{7.8}$$

If the structural parameters of the i^{th} story $[k_i \;\; c_i]^{\mathrm{T}}$ are known, then the right side of Equation (7.8) can be calculated from the measured structural responses and the following the optimization problem can be formulated to identify the parameters of the $(i+1)^{\text{th}}$ story $[k_{i+1} \;\; c_{i+1}]^{\mathrm{T}}$.

$$\underset{k_{i+1}, c_{i+1}}{\arg\min} \quad J(k_{i+1}, c_{i+1}) = \sum_{l=1}^{N} \left| h_l(k_{i+1}, c_{i+1}) - \hat{h}_l(\hat{S}_{\ddot{x}_{i-1}y,l}, \hat{S}_{\ddot{x}_i y,l}, \hat{S}_{\ddot{x}_{i+1}y,l}) \right|^2 \tag{7.9}$$

where $h_l(k_{i+1}, c_{i+1}) = \dfrac{1}{1 - j\, c_{i+1}/(m_i \omega_l) - k_{i+1}/(m_i \omega_l^2)}$,

$$\hat{h}_l(\hat{S}_{\ddot{x}_{i-1}y,l}, \hat{S}_{\ddot{x}_i y,l}, \hat{S}_{\ddot{x}_{i+1}y,l}) = \frac{\hat{S}_{\ddot{x}_{i+1}y,l} - \hat{S}_{\ddot{x}_i y,l}}{\hat{S}_{\ddot{x}_{i+1}y,l} + (\hat{S}_{\ddot{x}_{i-1}y,l} - \hat{S}_{\ddot{x}_i y,l})[\, jc_i/(m_i \omega_l) + k_i/(m_i \omega_l^2)]} \; .$$

Thus far, two identification problems, Equation (7.6) and (7.9), for the two-story substructure in Figure 7.1b are established, each of which can identify the parameters of one story in the two-story substructure by using the parameters of the other. By connecting these two identification problem in a loop as shown in Figure (7.2), a loop identification sequence is established in which all four structural parameters $\begin{bmatrix} k_i & c_i & k_{i+1} & c_{i+1} \end{bmatrix}^{\mathrm{T}}$ are identified once together. It is worth pointing out here that although the LOOP-SUBID method is developed by using the cross power spectral densities between structural acceleration responses and the reference response, it can also be formulated by using the Fourier transform of structural responses or using the transfer functions among different structural responses as in Chapter 3 or 4.

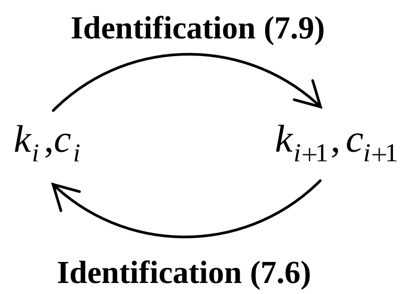

Figure 7.2 Loop identification sequence in the LOOP_SUBID method

Compared with the previous substructure identification methods, the LOOP_SUBID method has several advantages.

1. Different from the previous substructure identification methods which require of measuring the structural responses of all floors above the story being identified, the LOOP_SUBID method only needs four structural responses to formulate the identification problems: three floor accelerations and one reference response. This may greatly reduce of the costs of SHM systems, especially in the case that the structure has many stories but only the health status of a few lower stories are of interest.

2. The LOOP_SUBID method essentially forms a loop identification sequence as shown in Figure 7.2. It can be imagined that if the parameter identification errors for each step in the sequence are *small enough*, the sequence of identifications will perform like a contraction mapping such that after a sufficient number of steps, the sequence will always give the identification near their true values no matter what the initial structural parameters are.
3. If the mass normalized structural parameters $[k_i/m_i \;\; c_i/m_i \;\; k_{i+1}/m_i \;\; c_{i+1}/m_i]^T$ are treated as the variables to be identified in the optimization problems (7.6) and (7.9), the value of the i^{th} floor mass is no longer needed in the identification, which means that the LOOP_SUBID can be performed without structural mass information.
4. If the LOOP_SUBID identification is carried out twice, once on each of the two adjacent two-story substructures, *i.e.*, the i^{th} and $(i+1)^{th}$ floor substructures, two sets of mass normalized parameters $[k_i/m_i \;\; c_i/m_i \;\; k_{i+1}/m_i \;\; c_{i+1}/m_i]^T$ and $[k_{i+1}/m_{i+1} \;\; c_{i+1}/m_{i+1} \;\; k_{i+2}/m_{i+1} \;\; c_{i+2}/m_{i+1}]^T$ will be identified. The mass ratio m_i/m_{i+1} between these two floors can be calculated by using these identified parameters as shown in Equation (7.10); hence, the results of LOOP_SUBID identification is also able to provide information about the relative distribution of structural mass on different floors.

$$m_{i+1}/m_i = (k_{i+1}/m_i)/(k_{i+1}/m_{i+1}) \tag{7.10}$$

Even though the LOOP_SUBID method possesses many attractive features, how to implement it to ensure the convergence of the identification sequence is still a big challenge. In the next section, the condition under which the identification sequence will converge near true structural parameters is first studied.

7.2 Convergence Condition of LOOP_SUBID Method

Comparing the two identification problems, (7.6) and (7.9), involved in the identification sequence of the LOOP_SUBID method, it is found that these two problems are essentially the same with the structural parameters swapped ($k_i, c_i \Leftrightarrow k_{i+1}, c_{i+1}$) and structural responses swapped ($S_{y\ddot{x}_{i-1}} \Leftrightarrow S_{y\ddot{x}_{i+1}}$); thus, all identification analysis results of (7.6), developed in the fifth chapter, can be also applied to that of (7.9) with the same variable exchange.

According to the results of identification error analysis of the CSD_SUBID method in the fifth chapter, following Equations (5.37) and (5.38), the relative parameter identification errors of identification problem (7.6) can be approximated as,

$$\boldsymbol{\theta}_i \approx \boldsymbol{\varepsilon}_i + \mathbf{T}_1 \cdot \boldsymbol{\theta}_{i+1} \tag{7.11}$$

where $\boldsymbol{\theta}_i = [\theta_{ki} \;\; \theta_{ci}]^{\mathrm{T}}$ and $\boldsymbol{\theta}_{i+1} = [\theta_{k(i+1)} \;\; \theta_{c(i+1)}]^{\mathrm{T}}$; θ_{ki} and θ_{ci} are the relative errors of the i^{th} story parameters $[k_i \;\; c_i]^{\mathrm{T}}$; $\theta_{k(i+1)}$ and $\theta_{c(i+1)}$ are the relative errors of the $(i+1)^{\text{th}}$ story parameters $[k_{i+1} \;\; c_{i+1}]^{\mathrm{T}}$; the first term on the right side of Equation (7.11), $\boldsymbol{\varepsilon}_i = [\varepsilon_{ki} \;\; \varepsilon_{ci}]^{\mathrm{T}}$, is the identification error due to the measurement uncertainty of the structural responses, calculated by Equation (7.12); the second term on the right side of Equation (7.11), $\mathbf{T}_1 \cdot \boldsymbol{\theta}_{i+1}$, is the identification errors caused by the propagation of parameter errors of the $(i+1)^{\text{th}}$ story parameters. The expression of the matrix $\mathbf{T}_1$ is shown in Equation (7.13).

$$\boldsymbol{\varepsilon}_i = \begin{bmatrix} \varepsilon_{ki} \\ \varepsilon_{ci} \end{bmatrix} = \sum_{l=1}^{N} \mathrm{Re}\left\{ \begin{bmatrix} U_{11,l} & U_{12,l} & U_{13,l} \\ U_{21,l} & U_{22,l} & U_{23,l} \end{bmatrix} \cdot \begin{bmatrix} N_{\ddot{x}_{i-1}y,l} \big/ S_{(\ddot{x}_i-\ddot{x}_{i-1})y,l} \\ N_{\ddot{x}_i y,l} \big/ S_{(\ddot{x}_i-\ddot{x}_{i-1})y,l} \\ N_{\ddot{x}_{i+1}y,l} \big/ S_{(\ddot{x}_i-\ddot{x}_{i-1})y,l} \end{bmatrix} \right\} \tag{7.12}$$

$$\mathbf{T}_1 = \begin{bmatrix} \sum_{l=1}^{N} \mathrm{Re}\left[U_{14,l}\Delta_{(i+1)i,l}\right] & \sum_{l=1}^{N} \mathrm{Re}\left[U_{15,l}\Delta_{(i+1)i,l}\right] \\ \sum_{l=1}^{N} \mathrm{Re}\left[U_{24,l}\Delta_{(i+1)i,l}\right] & \sum_{l=1}^{N} \mathrm{Re}\left[U_{25,l}\Delta_{(i+1)i,l}\right] \end{bmatrix} \tag{7.13}$$

where $\Delta_{(i+1)i,l} = S_{(\ddot{x}_{i+1}-\ddot{x}_i)y,l} \big/ S_{(\ddot{x}_i-\ddot{x}_{i-1})y,l}$; the expressions of factors $U_{ij,l}$ are given in Equation (3.32).

Using the structural parameter and response swap previously mentioned, the identification error of identification problem (7.9) can be written as

$$\boldsymbol{\theta}_{i+1} \approx \boldsymbol{\varepsilon}_{i+1} + \mathbf{T}_2 \cdot \boldsymbol{\theta}_i \tag{7.14}$$

where $\boldsymbol{\varepsilon}_{i+1} = [\varepsilon_{k(i+1)} \;\; \varepsilon_{c(i+1)}]^{\mathrm{T}}$ is the identification error due to the measurement uncertainty of the structural responses, calculated by Equation (7.15). The expression of the matrix $\mathbf{T}_2$ is shown in Equation (7.16).

$$\boldsymbol{\varepsilon}_{i+1} = \begin{bmatrix} \varepsilon_{k(i+1)} \\ \varepsilon_{c(i+1)} \end{bmatrix} = \sum_{l=1}^{N} \mathrm{Re}\left\{ \begin{bmatrix} \tilde{U}_{11,l} & \tilde{U}_{12,l} & \tilde{U}_{13,l} \\ \tilde{U}_{21,l} & \tilde{U}_{22,l} & \tilde{U}_{23,l} \end{bmatrix} \cdot \begin{bmatrix} N_{y\ddot{x}_{i-1},l} \big/ S_{(\ddot{x}_i-\ddot{x}_{i+1})y,l} \\ N_{y\ddot{x}_i,l} \big/ S_{(\ddot{x}_i-\ddot{x}_{i+1})y,l} \\ N_{y\ddot{x}_{i+1},l} \big/ S_{(\ddot{x}_i-\ddot{x}_{i+1})y,l} \end{bmatrix} \right\} \tag{7.15}$$

$$\mathbf{T}_2 = \begin{bmatrix} \sum_{l=1}^{N} \mathrm{Re}\left[\tilde{U}_{14,l}\Delta_{i(i+1),l}\right] & \sum_{l=1}^{N} \mathrm{Re}\left[\tilde{U}_{15,l}\Delta_{i(i+1),l}\right] \\ \sum_{l=1}^{N} \mathrm{Re}\left[\tilde{U}_{24,l}\Delta_{i(i+1),l}\right] & \sum_{l=1}^{N} \mathrm{Re}\left[\tilde{U}_{25,l}\Delta_{i(i+1),l}\right] \end{bmatrix} \tag{7.16}$$

where factors $\tilde{U}_{ij,l}$ has the same expression as factors $U_{ij,l}$ (in Equation 3.32) with the structural parameter swap ($k_i, c_i \Leftrightarrow k_{i+1}, c_{i+1}$); $\Delta_{i(i+1),l} = S_{(\ddot{x}_{i-1}-\ddot{x}_i)y,l} \big/ S_{(\ddot{x}_i-\ddot{x}_{i+1})y,l} = 1 \big/ \Delta_{(i+1)i,l}$.

To start the sequence of identifications in the LOOP_SUBID method, an initial guess of the parameters of one of the two stories, $[k_i \;\; c_i]^{\mathrm{T}}$ or $[k_{i+1} \;\; c_{i+1}]^{\mathrm{T}}$, is needed. It is assumed herein that an initial guess of the $(i+1)^{\mathrm{th}}$ story parameters is given and used to start the loop identification sequence. Let $\boldsymbol{\theta}_{i+1}{}^{(0)}$ denote the relative error of the initial guess of the $(i+1)^{\mathrm{th}}$ story parameters. The superscript (0) standards for the step number in the loop sequence identification. It is also assume herein that only one set of structural responses is used in performing the sequence identifications in the LOOP_SUBID method. Therefore, $\boldsymbol{\varepsilon}_i$ and $\boldsymbol{\varepsilon}_{i+1}$, the identification errors due to the measurement uncertainty, are unchanged during the whole sequence identification process. Moreover, the matrices $\mathbf{T}_1$ and $\mathbf{T}_2$ are also unchanged during the whole identification process.

Utilizing the relative parameter identification error in each step of the sequence identification can be expressed by the following two equations,

$$\boldsymbol{\theta}_i{}^{(2q+1)} = \boldsymbol{\varepsilon}_i + \mathbf{T}_1 \cdot \boldsymbol{\theta}_{i+1}{}^{(2q)} \tag{7.17}$$

$$\boldsymbol{\theta}_{i+1}{}^{(2q+2)} = \boldsymbol{\varepsilon}_{i+1} + \mathbf{T}_2 \cdot \boldsymbol{\theta}_i{}^{(2q+1)} \tag{7.18}$$

where q=0,1,2,3,…. Substituting Equation (7.17) into (7.18), a difference equation in the relative identification errors of the $(i+1)^{\mathrm{th}}$ story parameters $\boldsymbol{\theta}_{i+1}$ is established.

$$\boldsymbol{\theta}_{i+1}{}^{(2q+2)} = \mathbf{T}_2\mathbf{T}_1 \cdot \boldsymbol{\theta}_{i+1}{}^{(2q)} + \boldsymbol{\varepsilon}_{i+1} + \mathbf{T}_2\boldsymbol{\varepsilon}_i \tag{7.19}$$

Similarly, a difference equation in the relative identification error of the i^{th} story parameters $\boldsymbol{\theta}_i$ can also be obtained as

$$\boldsymbol{\theta}_i{}^{(2q+3)} = \mathbf{T}_1\mathbf{T}_2 \cdot \boldsymbol{\theta}_i{}^{(2q+1)} + \boldsymbol{\varepsilon}_i + \mathbf{T}_1\boldsymbol{\varepsilon}_{i+1} \tag{7.20}$$

The initial conditions of these two difference equations are $\boldsymbol{\theta}_{i+1}{}^{(0)}$ and $\boldsymbol{\theta}_i{}^{(1)} = \boldsymbol{\varepsilon}_i + \mathbf{T}_1 \cdot \boldsymbol{\theta}_{i+1}{}^{(0)}$, respectively.

Difference equation (7.19) can be solved as follows

$$\begin{aligned}\boldsymbol{\theta}_{i+1}{}^{(2q+2)} &= \mathbf{T}_2\mathbf{T}_1 \cdot \boldsymbol{\theta}_{i+1}{}^{(2q)} + \boldsymbol{\varepsilon}_{i+1} + \mathbf{T}_2\boldsymbol{\varepsilon}_i \\ &= (\mathbf{T}_2\mathbf{T}_1)^2 \cdot \boldsymbol{\theta}_{i+1}{}^{(2q-2)} + (\mathbf{T}_2\mathbf{T}_1)(\boldsymbol{\varepsilon}_{i+1} + \mathbf{T}_2\boldsymbol{\varepsilon}_i) + (\boldsymbol{\varepsilon}_{i+1} + \mathbf{T}_2\boldsymbol{\varepsilon}_i) \\ &= \cdots \\ &= (\mathbf{T}_2\mathbf{T}_1)^{q+1} \cdot \boldsymbol{\theta}_{i+1}{}^{(0)} + \sum_{l=0}^{q} (\mathbf{T}_2\mathbf{T}_1)^l \cdot (\boldsymbol{\varepsilon}_{i+1} + \mathbf{T}_2\boldsymbol{\varepsilon}_i)\end{aligned} \tag{7.21}$$

The value of $S = \sum_{l=0}^{q} (\mathbf{T}_2\mathbf{T}_1)^l$ can be further evaluated as follows

$$(\mathbf{I} - \mathbf{T}_2\mathbf{T}_1)S = \sum_{l=0}^{q} (\mathbf{T}_2\mathbf{T}_1)^l - \sum_{l=1}^{q+1} (\mathbf{T}_2\mathbf{T}_1)^l = \mathbf{I} - (\mathbf{T}_2\mathbf{T}_1)^{q+1} \tag{7.22}$$

where $\mathbf{I}$ is the identity matrix of the same size as the matrix $\mathbf{T}_2\mathbf{T}_{1.}$ Assuming that matrix ($\mathbf{I}$-$\mathbf{T}_2\mathbf{T}_1$) is invertible,

$$S = \sum_{l=0}^{q} (\mathbf{T}_2\mathbf{T}_1)^l = (\mathbf{I} - \mathbf{T}_2\mathbf{T}_1)^{-1}[\mathbf{I} - (\mathbf{T}_2\mathbf{T}_1)^{q+1}] \tag{7.23}$$

Therefore, the final solution to the difference equation (7.19) is obtained by substituting Equation (7.23) into Equation (7.24) to give

$$\boldsymbol{\theta}_{i+1}{}^{(2q+2)} = (\mathbf{T}_2\mathbf{T}_1)^{q+1} \cdot \boldsymbol{\theta}_{i+1}{}^{(0)} + (\mathbf{I} - \mathbf{T}_2\mathbf{T}_1)^{-1}[\mathbf{I} - (\mathbf{T}_2\mathbf{T}_1)^{q+1}] \cdot (\boldsymbol{\varepsilon}_{i+1} + \mathbf{T}_2\boldsymbol{\varepsilon}_i) \tag{7.24}$$

Similarly, assuming that matrix ($\mathbf{I}$–$\mathbf{T}_1\mathbf{T}_2$) is invertible, the solution to difference equation (7.20) can be written

$$\boldsymbol{\theta}_i{}^{(2q+3)} = (\mathbf{T}_1\mathbf{T}_2)^{q+1} \cdot \boldsymbol{\theta}_i{}^{(1)} + (\mathbf{I} - \mathbf{T}_1\mathbf{T}_2)^{-1}[\mathbf{I} - (\mathbf{T}_1\mathbf{T}_2)^{q+1}] \cdot (\boldsymbol{\varepsilon}_i + \mathbf{T}_1\boldsymbol{\varepsilon}_{i+1}) \tag{7.25}$$

The results of the identification errors in Equation (7.24) and (7.25) clearly indicate that the identification errors $\boldsymbol{\theta}_i{}^{(2q+2)}$ and $\boldsymbol{\theta}_{i+1}{}^{(2q+3)}$ converge as q goes to infinity if the following two conditions are satisfied,

$$\lim_{q\to\infty}(\mathbf{T}_1\mathbf{T}_2)^q = 0\,,\quad \lim_{q\to\infty}(\mathbf{T}_2\mathbf{T}_1)^q = 0 \tag{7.26}$$

From linear algebra (Wylie *et al.*, 1982), the conditions (7.26) hold if the maximum eigenvalues of both matrices, $\mathbf{T}_1\mathbf{T}_2$ and $\mathbf{T}_2\mathbf{T}_1$, have magnitudes less than unity.

Since $\mathbf{T}_1$ and $\mathbf{T}_2$ are 2×2 square matrices, the products of these matrices, $\mathbf{T}_1\mathbf{T}_2$ and $\mathbf{T}_2\mathbf{T}_1$, are also 2×2 square matrices. By directly solving for the eigenvalue of the matrix $\mathbf{T}_1\mathbf{T}_2$ and $\mathbf{T}_2\mathbf{T}_1$ symbolically via the matlab® Symbolic Math Toolbox, it can be proven that the eigenvalue of these two square matrices are equal. As a result, the identification sequence in the LOOP_SUBID method converges to the values near the true structural parameters if the magnitude of the maximum eigenvalue of the matrix $\mathbf{T}_1\mathbf{T}_2$ is less than unity.

If the magnitude of the maximum eigenvalue of the matrix $\mathbf{T}_1\mathbf{T}_2$ is less than unity, after a sufficiently large number of loop identifications have been carried out, the identification errors of the structural parameters in the identification sequence, the solutions to difference equations (7.24) and (7.25), will converge to

$$\lim_{q\to\infty}\boldsymbol{\theta}_i^{(2q+2)} = (\mathbf{I}-\mathbf{T}_1\mathbf{T}_2)^{-1}\cdot(\boldsymbol{\varepsilon}_i+\mathbf{T}_1\boldsymbol{\varepsilon}_{i+1}) \tag{7.27}$$

$$\lim_{q\to\infty}\boldsymbol{\theta}_{i+1}^{(2q+3)} = (\mathbf{I}-\mathbf{T}_2\mathbf{T}_1)^{-1}\cdot(\boldsymbol{\varepsilon}_{i+1}+\mathbf{T}_2\boldsymbol{\varepsilon}_i) \tag{7.28}$$

Thus, it becomes clear that the key to the success of the LOOP_SUBID method, the convergence of the identification sequence, is that the magnitude of the maximum eigenvalue of the matrix $\mathbf{T}_1\mathbf{T}_2$ in the identification needs to be less than unity.

Matrices $\mathbf{T}_1$ and $\mathbf{T}_2$ are related to the structural response $\Delta_{i(i+1),l} = S_{y(\ddot{x}_{i-1}-\ddot{x}_i),l} \big/ S_{y(\ddot{x}_i-\ddot{x}_{i+1}),l}$ as well as deterministic factors $U_{ij,l}$ and $\tilde{U}_{ij,l}$, which are the functions of structural parameters. If there is only one excitation, response $\Delta_{i(i+1),l}$ will be independent of the excitation and become a function of structural parameters only. Under such a circumstance, matrices $\mathbf{T}_1$ and $\mathbf{T}_2$ become deterministic functions of the structural parameters and can be directly evaluated. In the following subsection, the 5-story shear structure used in the previous chapters is reutilized to check if the LOOP_SUBID method will lead to converged identification results for that structure.

7.2.1 An Illustrative Example

The parameters of the 5-story shear structure are m_i=1×10^5 kg, c_i=8×10^5 N·sec/m, k_i=16×10^7 N/m (i=1,…,5). The structure is only subject to ground excitation which is modeled as a Gaussian random pulse process passing through a 4th order band-pass Butterworth filter with 1Hz low cut-off frequency and 12 Hz high cut-off frequency.

In this 5-story structure, four standard two-story substructures can be formulated, each of which uses one of the non-top story floors as the middle floor in the standard two-story substructure. The maximum eigenvalues of the matrix $\mathbf{T}_1\mathbf{T}_2$ for the four substructures are calculated and listed in Table 7.1. All four eigenvalues are larger than unity, indicating that the identification using the LOOP_SUBID method will not converge for any of these substructures.

Table 7.1 Maximum eigenvalue of the matrix $\mathbf{T}_1\mathbf{T}_2$ of each substructure

Number of middle floor in the two-story substructure	1	2	3	4
Largest magnitude eigenvalue of matrix $\mathbf{T}_1\mathbf{T}_2$	1.97	1.22	1.18	1.41

To verify this conclusion, the LOOP_SUBID method is carried out for all four substructures. In the simulation, it is assumed that a set of 1800-second long structural responses, sampled at 200Hz, are used to perform the loop identification. The Welch average periodogram method is applied to calculate the cross power spectral densities needed in the identification: the 1800-second long structural responses are partitioned into short segments of 30 seconds each. Adjacent segments are overlapped by 25% of the segment length to increase the number of CSDs averaged. The magnitudes of the measurement noises of all acceleration responses are assumed to be the same, with RMS equal to 50% of the RMS of the ground excitation.

Figures (7.3)~(7.7) show how the relative errors of the identified parameters change as the loop identification progresses. It is easily seen that the identified parameters do not converge to near their true values in all four identification cases, consistent with expectations from the eigenvalue analysis.

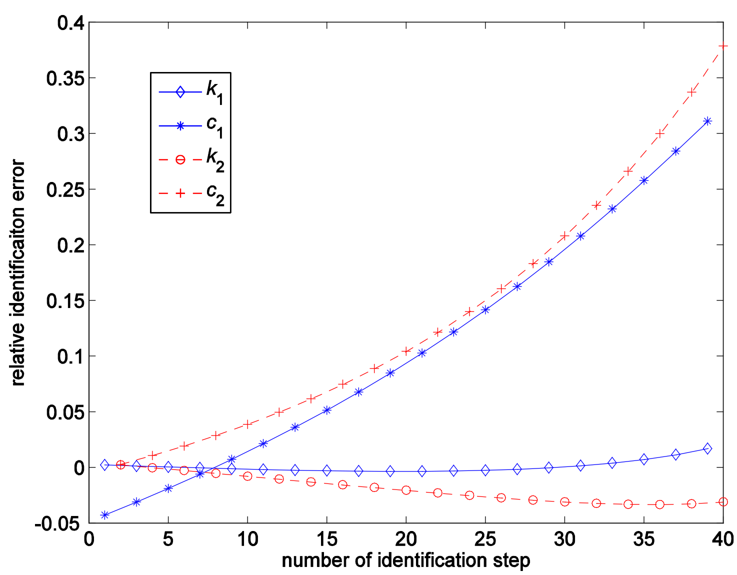

Figure 7.3 Relative identification errors of loop identification for the 1st floor substructure

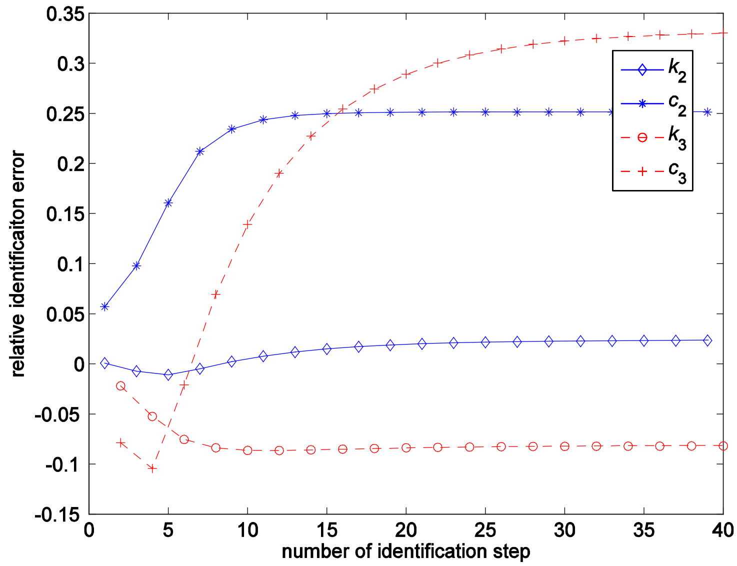

Figure 7.4 Relative identification errors of loop identification for the 2nd floor substructure

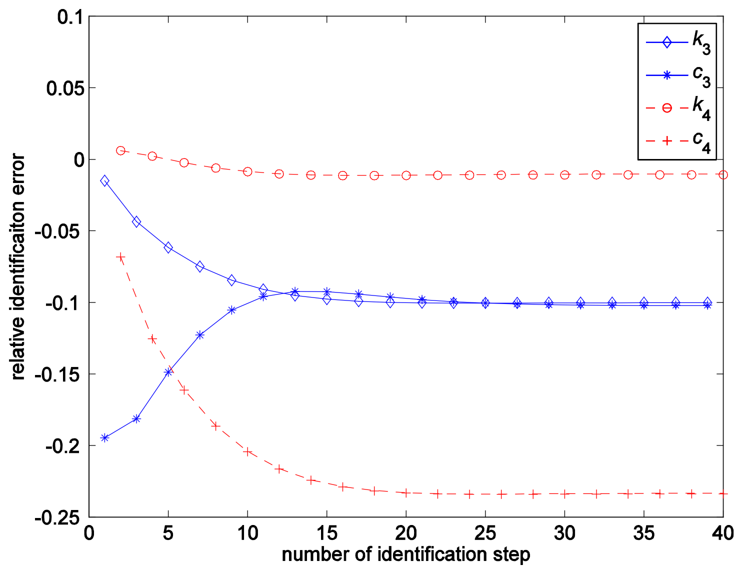

Figure 7.5 Relative identification errors of loop identification for the 3rd floor substructure

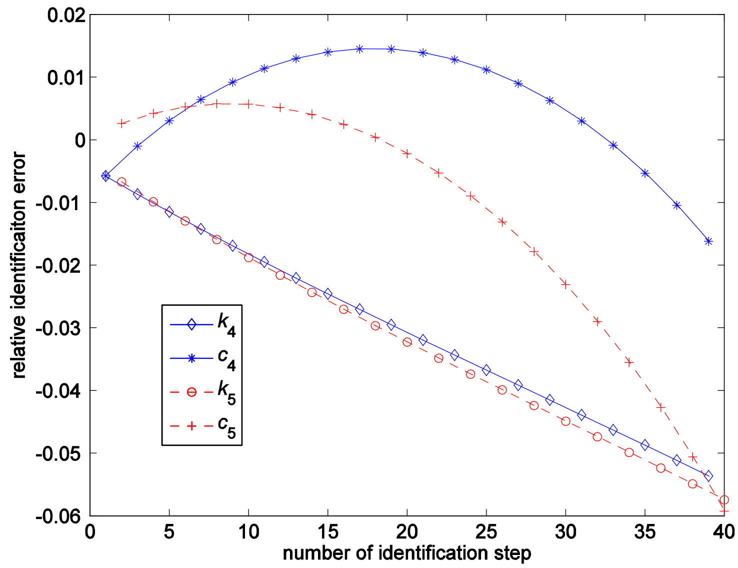

Figure 7.6 Relative identification errors of loop identification for the 4th floor substructure

In the next subsection, the reason that the LOOP_SUBID fails to provide converged results is analyzed. Based on that result, a new measure is proposed to modify the LOOP_SUBID method so that the loop identification sequence converges to near the true structural parameters.

7.2.2 Analysis of the Identification Results of LOOP_SUBID Method

In the previous subsection, the simulation results show that the LOOP_SUBID method fails to give corrected identification results for all four substructures. In this subsection, a qualitative explanation of this result is provided which reveals the in-depth reason behind the failure of the LOOP_SUBID method.

The LOOP_SUBID method consists of two basic identification steps. Each step identifies the parameters of one story in the two-story substructure given the parameter values of the other story. The identification errors of these two steps are composed of two parts as shown in Equations (7.11) and (7.14): the first part is due to the measurement uncertainty of structural responses; the second part is related to the parameter errors of the other story. The analysis in section 7.2 also demonstrates that if the second part converges to zero as the loop identification is continuously carried out, the loop identification sequence will converge. Therefore, to simplify the analysis of the lack of the convergence, assume that the first part of the identification error (from measurement uncertainty) is just zero. Then, the identification error in each step is only from the error accumulation.

For the step which identifies the i^{th} story parameters $[k_i \;\; c_i]^{\mathrm{T}}$, it has been shown in the fifth chapter that the second part of the identification error is significantly affected by the ratio of two cross power spectral densities, $\Delta_{(i+1)i,l} = S_{y(\ddot{x}_{i+1}-\ddot{x}_i),l} \big/ S_{y(\ddot{x}_i-\ddot{x}_{i-1}),l}$, near the substructure natural frequency $\sqrt{k_i/m_i}$. If this ratio is very small near frequency $\sqrt{k_i/m_i}$, the identification error of the parameters $[k_i \;\; c_i]^{\mathrm{T}}$ in this identification step will be much smaller than the identification error of the parameters $[k_{i+1} \;\; c_{i+1}]^{\mathrm{T}}$ in the previous identification step.

Since the step to identify parameters $[k_{i+1} \;\; c_{i+1}]^{\mathrm{T}}$ is identical to the step for identifying parameters $[k_i \;\; c_i]^{\mathrm{T}}$ with the structural parameters swapped ($k_i, c_i \Leftrightarrow k_{i+1}, c_{i+1}$) and structural responses swapped ($S_{y\ddot{x}_{i-1}} \Leftrightarrow S_{y\ddot{x}_{i+1}}$), a similar conclusion as to the identification error can be obtained: the second part of the identification error is greatly affected by the cross power spectral density ratio $\Delta_{i(i+1),l} = S_{y(\ddot{x}_{i-1}-\ddot{x}_i),l} \big/ S_{y(\ddot{x}_i-\ddot{x}_{i+1}),l}$ near the substructure natural frequency $\sqrt{k_{i+1}/m_i}$. If this ratio is very small near the frequency $\sqrt{k_{i+1}/m_i}$, the identification errors of the parameters $[k_{i+1}\ \ c_{i+1}]^{\mathrm{T}}$ in this identification step will be much smaller than the identification error of the parameters $[k_i\ \ c_i]^{\mathrm{T}}$ in the previous identification step.

Since the shear structure used in the illustrative example has uniform stiffness along the height of the structure, the two substructure natural frequencies, $\sqrt{k_i/m_i}$ and $\sqrt{k_{i+1}/m_i}$, are equal. Therefore, to make the identification error in the two identification steps both small, the two cross power spectral ratios, $\Delta_{(i+1)i,l}$ and $\Delta_{i(i+1),l}$, must be small near the same frequency $\sqrt{k_i/m_i}$ (or $\sqrt{k_{i+1}/m_i}$). However, since only one set of structural responses are used in formulating the loop identification sequence, $\Delta_{(i+1)i,l}$ and $\Delta_{i(i+1),l}$ are inverses of each other; that is, if one of them is small near the frequency $\sqrt{k_i/m_i}$, the other will be large near the same frequency. Hence, there exists a conflicting relation between the identification errors in the two identification steps: if one of them is smaller, then the other will be large. It is impossible to make the identification errors in the two steps both small simultaneously. This conflict leads to the failure of the LOOP_SUBID method in the example.

As previously analyzed, the key to making the loop identification sequence converge is to simultaneously reduce two cross power spectral ratio, $\Delta_{(i+1)i,l}$ and $\Delta_{i(i+1),l}$, near the same substructure natural frequency $\sqrt{k_i/m_i}$ (or $\sqrt{k_{i+1}/m_i}$). In order to achieve this goal, some modifications to the original LOOP_SUBID method are needed. In the original method, one set of structural responses is used repeatedly to carry out the loop identification, leading to the problem that the two responses $\Delta_{(i+1)i,l}$ and $\Delta_{i(i+1),l}$ cannot both be very small in the same frequency range (because they are inverse of each other). In the modified LOOP_SUBID method, two sets of structural responses are required: one in which key response ratio $\Delta_{(i+1)i,l}$ is small and the other in which $\Delta_{i(i+1),l}$ is small near the substructure natural frequency. These two sets of responses are used in an alternating order to formulate the two identification steps in the loop identification sequence. Since both response ratios, $\Delta_{(i+1)i,l}$ and $\Delta_{i(i+1),l}$, are very small in their own identification step, the identification error of the loop identification sequence is guaranteed to continuously decrease until it converges.

Clearly, the success of the modified LOOP_SUBID depends on finding two sets of structural responses in which the key response ratios, $\Delta_{(i+1)i,l}$ or $\Delta_{i(i+1),l}$, are very small near the substructure natural frequency in one of them. However, in the illustrative example it is assumed that there is only one excitation source (ground excitation); therefore, the two key response ratios, $\Delta_{(i+1)i,l}$ and $\Delta_{i(i+1),l}$, are independent of the excitation and become functions of the structural parameters only; that is, $\Delta_{(i+1)i,l}$ and $\Delta_{i(i+1),l}$ will not change due to changes in the single excitation. In order to change $\Delta_{(i+1)i,l}$ and $\Delta_{i(i+1),l}$, some effects from an outside system (*e.g.*, control systems) must be applied to the structure.

In the next section, an AMD control system (assumed to be installed on the top floor) is utilized to change structural responses so that two sets of structural responses can be achieved, in which $\Delta_{(i+1)i,l}$ and $\Delta_{i(i+1),l}$ are very small near the substructure natural frequency in one of them.

7.3 Controlled LOOP_SUBID Method

As stated in the last section, to ensure the convergence of the loop identification sequence in LOOP_SUBID method, two control algorithms are needed to be designed, each of which makes one of the response ratios $\Delta_{(i+1)i,l}$ and $\Delta_{i(i+1),l}$ as small as possible near the corresponding frequencies $\sqrt{k_i/m_i}$ and $\sqrt{k_{i+1}/m_i}$, respectively. However, the convergence of the loop identification sequence does not necessarily mean that the converged identified parameters are accurate. As shown in Equations (7.17) and (7.18), the identification errors of the converged identified parameters are related to $\boldsymbol{\varepsilon}_i$ and $\boldsymbol{\varepsilon}_{i+1}$, the part of the identification errors due to the measurement uncertainties. It has been shown in section 7.2 that $\boldsymbol{\varepsilon}_i$ and $\boldsymbol{\varepsilon}_{i+1}$ are mainly determined by two structural responses $S_{(\ddot{x}_i-\ddot{x}_{i-1})y}$ and $S_{(\ddot{x}_i-\ddot{x}_{i+1})y}$: the larger these two responses near the substructure natural frequencies $\sqrt{k_i/m_i}$ and $\sqrt{k_{i+1}/m_i}$, the smaller the measurement uncertainties will be; leading to smaller identification errors. Therefore, in addition to reducing the response ratios $\Delta_{(i+1)i,l}$ and $\Delta_{i(i+1),l}$, a control system must also amplify the two structural responses $S_{y(\ddot{x}_i-\ddot{x}_{i-1})}$ and $S_{y(\ddot{x}_i-\ddot{x}_{i+1})}$ near the frequencies $\sqrt{k_i/m_i}$ and $\sqrt{k_{i+1}/m_i}$, respectively.

In the sixth chapter, an optimization method is proposed to design the control systems to achieve two similar goals of changing structural responses. That method assigns the importance weighting factors for each of the objective functions in the optimization and converts a multi-objective optimization problem into a single-objective optimization problem. In this chapter, a different approach is proposed to design the control system to achieve the two goals of simultaneously changing the response ratio $\Delta_{(i+1)i,l}$ (or $\Delta_{i(i+1),l}$) and the response $S_{y(\ddot{x}_i-\ddot{x}_{i-1})}$ (or $S_{y(\ddot{x}_i-\ddot{x}_{i+1})}$) in favor of more accurate parameter identification.

Since the two identification steps involved in the LOOP_SUBID are essentially the same, only the control to improve the identification accuracy of the i^{th} story parameters $[k_i \;\; c_i]^{\mathrm{T}}$ is introduced. The key equation to identify parameters $[k_i \;\; c_i]^{\mathrm{T}}$ is Equation (7.5), repeated here:

$$\frac{1}{1-jc_i/(m_i\omega)-k_i/(m_i\omega^2)}=\frac{S_{\ddot{x}_{i-1}y}-S_{\ddot{x}_iy}}{S_{\ddot{x}_{i-1}y}+(S_{\ddot{x}_{i+1}y}-S_{\ddot{x}_iy})[jc_{i+1}/(m_i\omega)+k_{i+1}/(m_i\omega^2)]} \tag{7.29}$$

Introduce a new variable $H_{(\ddot{x}_{i+1}-\ddot{x}_i)\ddot{x}_{i-1}}$ as

$$H_{(\ddot{x}_{i+1}-\ddot{x}_i)\ddot{x}_{i-1}}=(S_{y\ddot{x}_{i+1}}-S_{y\ddot{x}_i})\big/S_{y\ddot{x}_{i-1}}=S_{y(\ddot{x}_{i+1}-\ddot{x}_i)}\big/S_{y\ddot{x}_{i-1}} \tag{7.30}$$

If there is only one independent excitation, the newly defined variable $H_{(\ddot{x}_{i+1}-\ddot{x}_i)\ddot{x}_{i-1}}$ can be interpreted as the transfer function from the response $\ddot{x}_{i-1}$ to the response $(\ddot{x}_{i+1}-\ddot{x}_i)$ in either uncontrolled or controlled structural systems. Using the newly defined variable, key identification equation (7.29) is rewritten as

$$\frac{1}{1-jc_i/(m_i\omega)-k_i/(m_i\omega^2)}=\frac{S_{\ddot{x}_{i-1}y}-S_{\ddot{x}_iy}}{S_{\ddot{x}_{i-1}y}\{1+H_{(\ddot{x}_{i+1}-\ddot{x}_i)\ddot{x}_{i-1}}[jc_{i+1}/(m_i\omega)+k_{i+1}/(m_i\omega^2)]\}} \tag{7.31}$$

Assuming that 1) the magnitude of $H_{(\ddot{x}_{i+1}-\ddot{x}_i)\ddot{x}_{i-1}}$ is far less than unity in a narrow frequency range around $\sqrt{k_i/m_i}$ and 2) the structure has uniform story stiffness and damping coefficient (*i.e.*, $k_i = k_{i+1}$ and $c_i = c_{i+1}$), then Equation (7.31) near the frequency $\sqrt{k_i/m_i}$ is approximated by

$$\frac{1}{1 - j\,c_i/(m_i\omega) - k_i/(m_i\omega^2)} \approx \frac{S_{\ddot{x}_{i-1}y} - S_{\ddot{x}_i y}}{S_{\ddot{x}_{i-1}y}} = \frac{-S_{(\ddot{x}_i-\ddot{x}_{i-1})y}}{S_{\ddot{x}_{i-1}y}} \tag{7.32}$$

Since the magnitude of the transfer function on the left side of the equation is large near the frequency $\sqrt{k_i/m_i}$, the structural response $S_{y(\ddot{x}_i-\ddot{x}_{i-1})}$, which is closely related to the measurement uncertainties in the identification, will not be small near the frequency $\sqrt{k_i/m_i}$ as long as the response $S_{y\ddot{x}_{i-1}}$ is not very small near the same frequency. Therefore, largely reducing the magnitude of the transfer function $H_{(\ddot{x}_{i+1}-\ddot{x}_i)\ddot{x}_{i-1}}$ to some very small value (by control systems) near the frequency $\sqrt{k_i/m_i}$ has some potential for amplifying the structural response $S_{(\ddot{x}_i-\ddot{x}_{i-1})y}$ near the frequency $\sqrt{k_i/m_i}$, which controls the identification errors due to the measurement uncertainties. (It is assumed that the control systems do not significantly reducing the response $S_{\ddot{x}_{i-1}y}$ near the frequency $\sqrt{k_i/m_i}$.)

Moreover, another key component of controlling the identification errors of $[k_i \;\; c_i]^{\mathrm{T}}$, $\Delta_{(i+1)i} = S_{y(\ddot{x}_{i+1}-\ddot{x}_i)} \big/ S_{y(\ddot{x}_i-\ddot{x}_{i-1})}$, can also be changed in favor of more accurate parameter identification by greatly reducing the magnitude of the transfer function $H_{(\ddot{x}_{i+1}-\ddot{x}_i)\ddot{x}_{i-1}}$ near the frequency $\sqrt{k_i/m_i}$. Rewrite the response ratio $\Delta_{(i+1)i}$ in a different way

$$\Delta_{(i+1)i} = S_{(\ddot{x}_{i+1}-\ddot{x}_i)y} \Big/ S_{(\ddot{x}_i-\ddot{x}_{i-1})y} = \frac{S_{(\ddot{x}_{i+1}-\ddot{x}_i)y}}{S_{\ddot{x}_{i-1}y}} \cdot \frac{S_{\ddot{x}_{i-1}y}}{S_{(\ddot{x}_i-\ddot{x}_{i-1})y}} \tag{7.33}$$

Using the definition of $H_{(\ddot{x}_{i+1}-\ddot{x}_i)\ddot{x}_{i-1}}$ and the approximate relation in Equation (7.32), Equation (7.33) becomes

$$\Delta_{(i+1)i} \approx -H_{(\ddot{x}_{i+1}-\ddot{x}_i)\ddot{x}_{i-1}} \cdot [1 - j\,c_i \big/ (m_i\omega) - k_i \big/ (m_i\omega^2)] \tag{7.34}$$

Since both $H_{(\ddot{x}_{i+1}-\ddot{x}_i)\ddot{x}_{i-1}}$ and $[1 - j\,c_i \big/ (m_i\omega) - k_i \big/ (m_i\omega^2)]$ are very small near the frequency $\sqrt{k_i/m_i}$, $\Delta_{(i+1)i}$ becomes very small near the frequency $\sqrt{k_i/m_i}$.

In summary, greatly reducing the (closed-loop) transfer function $H_{(\ddot{x}_{i+1}-\ddot{x}_i)\ddot{x}_{i-1}}$ near the frequency $\sqrt{k_i/m_i}$ by some control system will lead to small response ratio $\Delta_{(i+1)i}$ and large response $S_{(\ddot{x}_i-\ddot{x}_{i-1})y}$. Hence, it becomes clear that the ultimate goal the control system is to minimize the (closed-loop) transfer function $H_{(\ddot{x}_{i+1}-\ddot{x}_i)\ddot{x}_{i-1}}$ near the substructure natural frequency.

7.3.1 AMD System

In order to implement the controlled LOOP_SUBID method, an active mass damper (AMD) control system, installed at the top floor of the shear structure, is used in this study. For each standard two-story substructure, two control system algorithms are designed: one is to minimize transfer function $H_{(\ddot{x}_{i+1}-\ddot{x}_i)\ddot{x}_{i-1}}$ near the frequency $\sqrt{k_i/m_i}$;

the other is to minimize transfer function $H_{(\ddot{x}_{i-1}-\ddot{x}_i)\ddot{x}_{i+1}}$ near the frequency $\sqrt{k_{i+1}/m_i}$. It is assumed herein that 1) only the three floor acceleration responses, related to the two-story substructure being identified, and the control force of the AMD system are measured; 2) the three measured floor acceleration responses are used as the feedback signals to design the linear feedback algorithms, which are to achieve the previously mentioned goal of changing the closed-loop transfer functions of the structure. The optimal gain matrices of the two control systems, $\mathbf{L}_1$ and $\mathbf{L}_2$, are obtained by solving the following two optimization problems respectively.

$$\begin{gathered}\arg\min_{\mathbf{L}_1} J(\mathbf{L}_1) = \int_{\omega_l}^{\omega_u} \left| W_1(j\omega) H_{(\ddot{x}_{i+1}-\ddot{x}_i)\ddot{x}_{i-1}} \right|^2 d\omega \\ \text{subject to } \xi_k \geq \xi_0 > 0, k = 1,2,\cdots,2n\end{gathered} \quad (7.35)$$

$$\begin{gathered}\arg\min_{\mathbf{L}_2} J(\mathbf{L}_2) = \int_{\omega_l}^{\omega_u} \left| W_2(j\omega) H_{(\ddot{x}_{i-1}-\ddot{x}_i)\ddot{x}_{i+1}} \right|^2 d\omega \\ \text{subject to } \xi_k \geq \xi_0 > 0, k = 1,2,\cdots,2n\end{gathered} \quad (7.36)$$

where $H_{(\ddot{x}_{i+1}-\ddot{x}_i)\ddot{x}_{i-1}}$ is the closed-loop transfer function from the (i-1)th floor acceleration $\ddot{x}_{i-1}$ to the (i+1)th interstory acceleration response $(\ddot{x}_{i+1}-\ddot{x}_i)$; $H_{(\ddot{x}_{i-1}-\ddot{x}_i)\ddot{x}_{i+1}}$ is the closed-loop transfer functions from (i+1)th floor acceleration $\ddot{x}_{i+1}$ to the ith interstory acceleration response $(\ddot{x}_i-\ddot{x}_{i+1})$; ξ_k is the damping ratio of the kth root of the closed-loop system and ξ_0 is a positive real number, taking the value of 0.02 in the following numerical examples; ω_l and ω_u are the lower and upper frequency bounds of the integration, herein taken to be 0.8 and 1.2 times the corresponding substructure frequencies respectively; and $W_1(j\omega)$ and $W_2(j\omega)$ are frequency weighting functions

$$W_1(j\omega) = \frac{k_i/(m_i\omega^2)}{\left[1 - jc_i/(m_i\omega) - k_i/(m_i\omega^2)\right]^2} \tag{7.37}$$

$$W_2(j\omega) = \frac{k_{i+1}/(m_i\omega^2)}{\left[1 - jc_{i+1}/(m_i\omega) - k_{i+1}/(m_i\omega^2)\right]^2} \tag{7.38}$$

The magnitudes of $W_1(j\omega)$ and $W_2(j\omega)$ are very large only near the frequencies $\sqrt{k_i/m_i}$ and $\sqrt{k_{i+1}/m_i}$, respectively, and quickly vanish when departing from these frequencies. The role of these frequency weighting functions is to implicitly force the control systems to focus on changing the transfer functions, $H_{(\ddot{x}_{i+1}-\ddot{x}_i)\ddot{x}_{i-1}}$ and $H_{(\ddot{x}_{i-1}-\ddot{x}_i)\ddot{x}_{i+1}}$, only around the frequencies $\sqrt{k_i/m_i}$ and $\sqrt{k_{i+1}/m_i}$.

7.3.2 Revisit the Illustrative Example

The 5-story shear structure in subsection 7.2.2 is used to demonstrate the effectiveness of the controlled LOOP_SUBID method. It is assumed that there is an AMD system installed on the fifth floor of the structure. As in the illustrative example, the structure is only subject to ground excitation in addition to the control force from the AMD system. The ground excitation is modeled as a Gaussian random pulse process passing through a 4th order band-pass Butterworth filter with 1Hz low cut-off frequency and 12 Hz high cut-off frequency.

In this 5-story structure, four standard two-story substructures can be formulated, each of which uses one of the non-top story floors as its middle floor in the standard two-story substructure. For each two-story substructure, the two optimal feedback gain matrices of the control system are designed by utilizing the optimization methods proposed in the previous subsection. One is to minimize transfer function $H_{(\ddot{x}_{i+1}-\ddot{x}_i)\ddot{x}_{i-1}}$ near the frequency $\sqrt{k_i/m_i}$; the other is to minimize transfer function $H_{(\ddot{x}_{i-1}-\ddot{x}_i)\ddot{x}_{i+1}}$ near the frequency $\sqrt{k_{i+1}/m_i}$. The matrices $\mathbf{T}_1$ and $\mathbf{T}_2$ from Equations (7.13) and (7.16) for the corresponding closed-loop controlled structure are calculated. The largest eigenvalue magnitudes of the matrix $\mathbf{T}_1\mathbf{T}_2$ of the four controlled structures are calculated and listed in Table 7.2. All are smaller than unity, indicating that the identification using the controlled LOOP_SUBID method will converge for all these substructures.

Table 7.2 Largest magnitude eigenvalues of the matrix T_1T_2 of each controlled substructure

Number of middle floor in the two-story substructure	1	2	3	4
Largest magnitude eigenvalue of matrix $\mathbf{T}_1\mathbf{T}_2$	-0.05	-0.0006	-0.6×10^{-6}	-2×10^{-6}

To verify this conclusion, controlled LOOP_SUBID method is carried out for the all four substructures. In the simulation, it is assumed that a set of 3600-second long structural responses, sampled at 200Hz, are used to perform the loop identification. The Welch average periodogram method is applied to calculate the cross power spectral densities needed in the identification: the 3600-second long structural responses are partitioned into short segments of 30 seconds each. Adjacent segments are overlapped by 25% of the segment length to increase the number of CSDs in the average. The magnitudes of the measurement noises of all acceleration responses are assumed to be the same, with RMS equal to 50% of the RMS of the ground excitation.

Figures 7.7~7.10 show how the relative errors of the identified parameters change as the loop identification progresses. When choosing the initial values of the parameters $[k_{i+1} \ c_{i+1}]^T$ to start the loop identification sequence, very large errors are given: the initial value of the stiffness parameter k_{i+1} is 150% of its true value and the initial value of the damping parameter c_{i+} is 50% of its true value. It is easily seen that, even with such large errors in initial parameter values in the loop identification, the identified parameters still quickly converge as expected from the eigenvalue analysis.

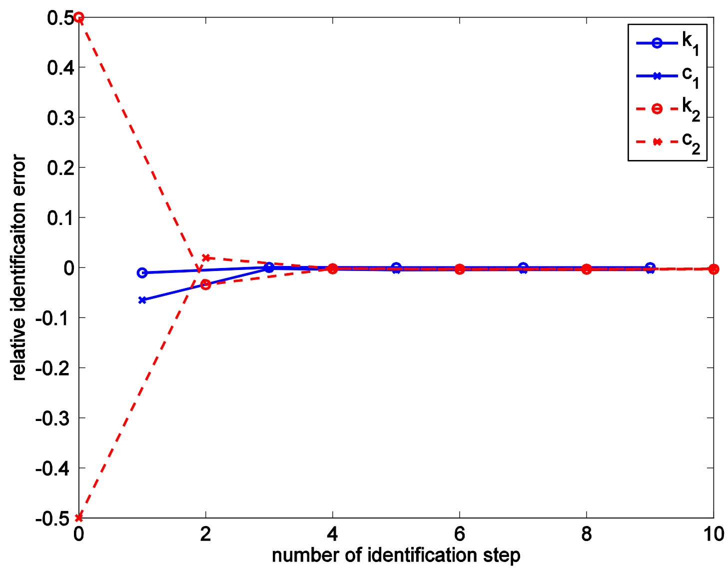

Figure 7.7 Relative identification errors of loop identification for the 1st floor substructure with control

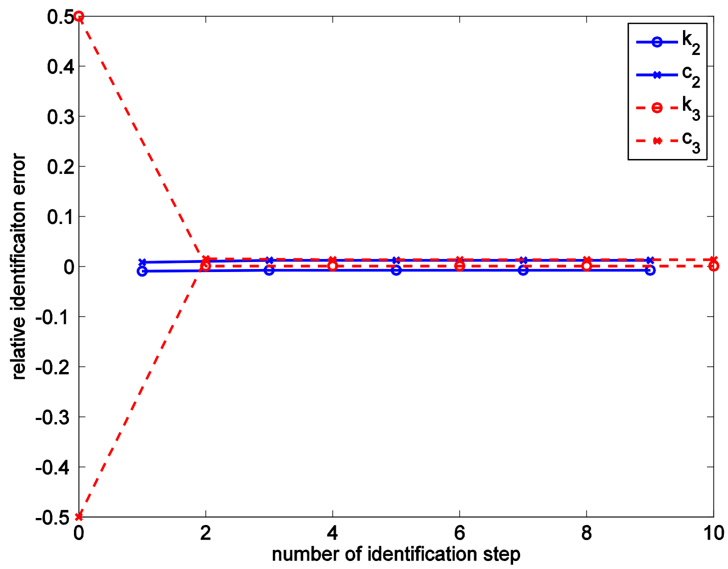

Figure 7.8 Relative identification errors of loop identification for the 2nd floor substructure with control

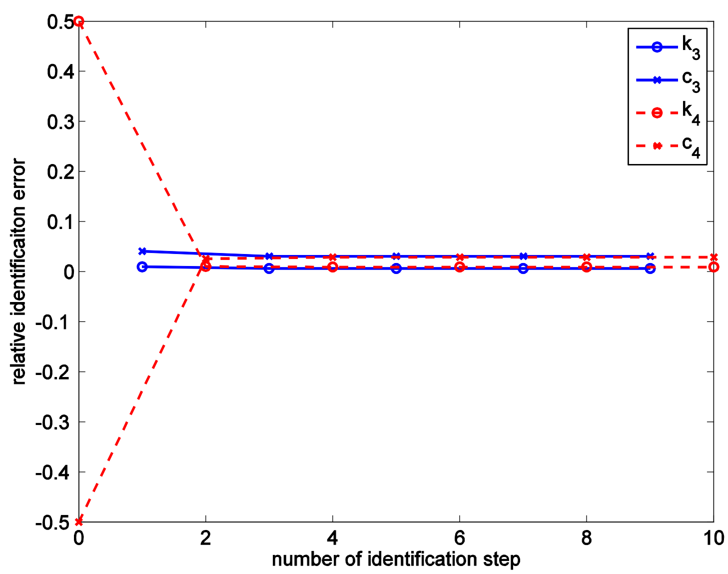

Figure 7.9 Relative identification errors of loop identification for the 3rd floor substructure with control

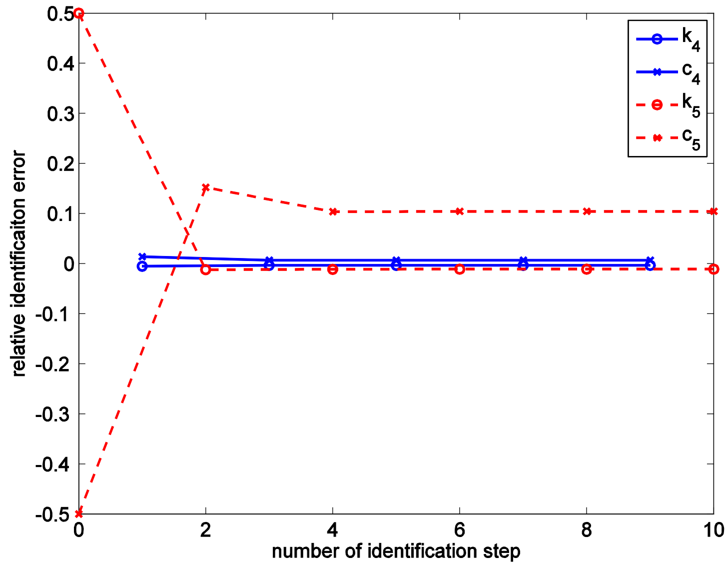

Figure 7.10 Relative identification errors of loop identification for the 4th floor substructure with control

To evaluate the identification accuracy of the proposed controlled LOOP_SUBID method, 100 similar controlled identification tests are carried out. The statistics of the identification errors of the converged identified parameters, relative mean estimate error and relative root-mean-square-error (RMSE), are calculated and listed in Tables 7.3 ~ 7.6.

Table 7.3 The statistics of the identification errors of the 1st floor substructure

	$\hat{k}_1$	$\hat{c}_1$	$\hat{k}_2$	$\hat{c}_2$
relative mean error	0.0%	0.0%	-0.1%	0.2%
relative RMSE	0.1%	0.3%	0.3%	1.2%

Table 7.4 The statistics of the identification errors of the 2nd floor substructure

	$\hat{k}_2$	$\hat{c}_2$	$\hat{k}_3$	$\hat{c}_3$
relative mean error	0.0%	0.5%	0.1%	0.6%
relative RMSE	0.3%	2.0%	0.1%	0.6%

Table 7.5 The statistics of the identification errors of the 3rd floor substructure

	$\hat{k}_3$	$\hat{c}_3$	$\hat{k}_4$	$\hat{c}_4$
relative mean error	-0.1%	0.0%	0.0%	0.1%
relative RMSE	0.4%	1.9%	0.5%	1.8%

Table 7.6 The statistics of the identification errors of the 4th floor substructure

	$\hat{k}_4$	$\hat{c}_4$	$\hat{k}_5$	$\hat{c}_5$
relative mean error	0.0%	0.1%	0.2%	0.1%
relative RMSE	0.3%	1.3%	1.5%	7.8%

As shown in Equations (7.27) and (7.28), the relative errors of the converged identified parameters are related to $\boldsymbol{\varepsilon}_i$ and $\boldsymbol{\varepsilon}_{i+1}$, the parts of the identification errors due to the measurement uncertainties. Since it has been shown in the fifth chapter that $\boldsymbol{\varepsilon}_i$ and $\boldsymbol{\varepsilon}_{i+1}$ are zero-mean random variables, the means of the parameter identification errors in the controlled LOOP_SUBID method are zeros, verified by the simulation results here. The controlled LOOP_SUBID method provides very accurate identification results under the inference of fairly large measurement noise: in most cases the relative RMSE of the stiffness estimates are far less than 1% and the relative RMSE of the damping estimates are around 1~2%.

Chapter 8

Substructure Identification for Frame Structures

The substructure identification methods and controlled substructure identification methods in the previous five chapters are based on a fundamental assumption that the identified structure is a shear model structure. Although the shear model is widely used to model the dynamic behavior of building structures, it is only a simplification of real complex structures. As shown in Figure 8.1, a simple one-bay n-story frame structure has three times as many DOFs as an n-story shear model structure; the dynamic behaviors of the frame structure will be different from that of the shear structure. Furthermore, finding damage in real complex structures, like the frame structure in Figure 8.1, is of much more practical interest than just identifying the parameter values in a shear model structure (Yan *et al.*, 2006). However, directly performing identification in a complex structure to find damage is often fruitless due to the greater complexity of the search space.

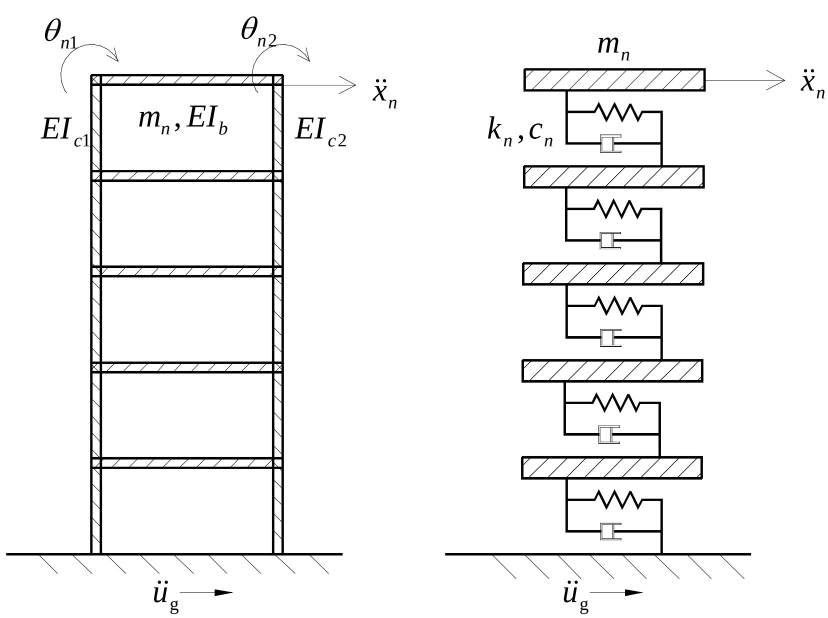

Figure 8.1 A frame structure vs. a shear structure

In this chapter, a new approach is proposed, using substructure identification methods, to locate and quantify damage in complex frame structures. First, a direct method is attempted in section 8.1 simply treating the frame structure as a shear model structure and directly applying the substructure identification method (for shear structures) to identify story stiffness k_i from the floor acceleration measured on the frame structure. However, it is found that this method only works when the beam-to-column stiffness ratio of the frame structure is very large and the frame structure essentially behaves like a shear structure. If the beam-to-column stiffness ratio is not very large, which is typical for real frame structures, the rotation of the beam-column joints in the frame structure will lead to significant errors in the identification and the direct method will not give accurate results. In order to overcome this difficulty and extend the substructure identification methods to frame structures with moderate or small beam-to-column stiffness ratios, a new substructure identification method for frame structures is proposed in section 8.2. This new method utilizes the exact dynamic equation of one floor substructure of a frame structure to formulate the identification problem, in which the equivalent story stiffness of the frame structure is identified. The "equivalent" story stiffness here refers to the story stiffness of the frame structure when fictitious constraints are added such that all rotational responses at beam-to-column joints vanish. This stiffness can also be thought as the story stiffness of a frame structure when its beam-to-column ratio is infinite or, or in other words, the frame structure approaches a shear structure. The new substructure method transforms the frame structure into a beam-like structure. Then, the substructure identification method developed for shear structures is modified and used to identify the equivalent story stiffness of this beam-like structure.

8.1 Directly Apply Substructure Identification Method for Shear Structures to Frame Structures

The substructure identification method for shear structures is derived based on the dynamic Equation (8.1) of one floor substructure in a shear structure. Various transformations result in key identification Equation (8.2) for the substructure identification.

$$m_i\ddot{x}_i + c_i(\dot{x}_i - \dot{x}_{i-1}) + k_i(x_i - x_{i-1}) + c_{i+1}(\dot{x}_i - \dot{x}_{i+1}) + k_{i+1}(x_i - x_{i+1}) = 0 \tag{8.1}$$

$$\frac{1}{1 - j\,c_i/(m_i\omega) - k_i/(m_i\omega^2)} = \frac{\ddot{X}_{i-1} - \ddot{X}_i}{\ddot{X}_{i-1} + \left(\ddot{X}_{i+1} - \ddot{X}_i\right)\left[jc_{i+1}/(m_i\omega) + k_{i+1}/(m_i\omega^2)\right]} \tag{8.2}$$

where x_i is the i^{th} floor displacement relative to an inertial reference frame; the overdots denote derivatives with respect to time; and $\ddot{X}_i$ denotes the Fourier transform of the i^{th} floor acceleration.

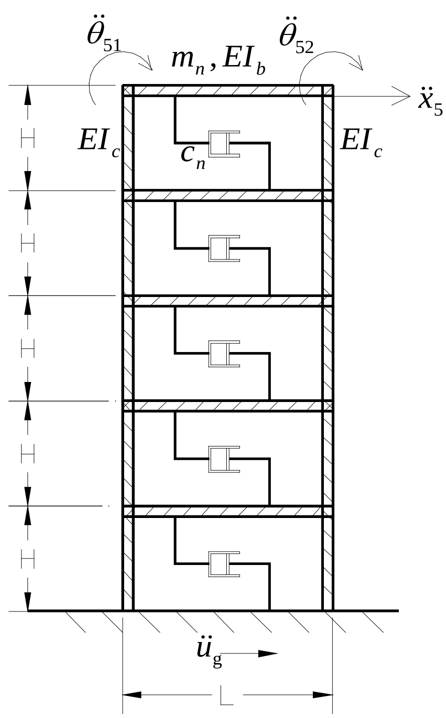

Figure 8.2 A five-story one-bay frame structure

When a frame structure replaces the shear structure, the equilibrium condition in Equation (8.1) no longer holds true, nor does Equation (8.2). However, if the difference between the two sides of Equation (8.2) is small, Equation (8.2) perhaps can still be used to form the substructure identification optimization. Therefore, this section will focus on testing how well the equilibrium of Equation (8.2) is satisfied for a frame structure.

A simple 5-story one-bay uniform frame structure, shown in Figure 8.2, is used as a test. It is assumed herein that the axial rigidities of the columns and floor labs are infinite and the mass of both columns and beams are negligible relative to the mass of the floor slabs. Therefore, there are 3 DOFs for each floor, two rotation and one horizontal translation, for total of 3*n* DOFs for the whole structure. The parameters of the frame structure are set as follows: the height of each story of the structure is H=3m; the span of the bay is L=3m; the mass of each floor slab is $m_i=1\times10^5$ kg; and the flexural rigidity of each column $EI_c= 18\times10^7$ N·m^2. If the frame structure moves in pure shear, the equivalent story stiffness would be $k_i=2\times12\mathrm{EI}_c/\mathrm{H}^3=16\times10^7$ N/m, which is the same as the story stiffness of the 5-story structure used elsewhere herein; the floor mass is also the same in this frame structure as in the shear structure example. It is assumed that the damping of the frame structure is the same as the damping of the previous 5-story shear structure (*i.e.*, $c_i=8\times10^5$ N·sec/m). The flexural rigidity of each beam is $EI_b=\beta EI_c$, where β is the beam-to-column stiffness ratio. It is well known that stiffness ratio β greatly affects how well the frame structure behaves like a shear structure; larger β value implies that the frame structure behave more like a shear structure. Three scenarios, corresponding to different levels of the relative stiffness of the beams, are studied herein: 1) the beams and the columns have the same flexural rigidity (β=1); 2) the beams have large flexural rigidity relative to that of the columns (β=10), but not rigid enough that its flexibility can be neglected; 3) the flexural rigidity of the beams is very large (β=100).

Figures 8.3~8.7 show the magnitudes of the right side of the key identification equation (8.2) of the five story substructures with three different beam-to-column stiffness ratios β. The magnitude of the left side of Equation (8.2) is also shown in the plots with red solid lines for comparison. The stiffness and damping parameters in the left side of Equation (8.2) are the "equivalent" story stiffness and damping of the frame structure, defined as the story stiffness and damping when the frame structure behave like a pure shear structure (when the beam-to-column stiffness ratio is infinite).

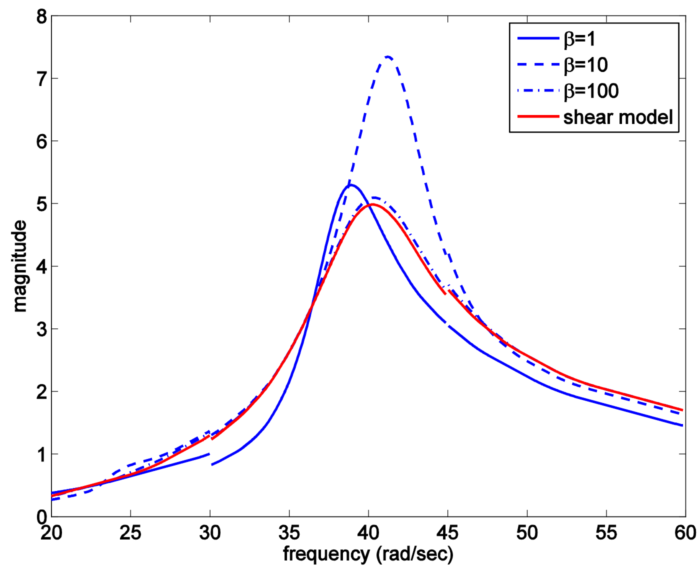

Figure 8.3 Magnitude plot comparison for the 1st story substructure

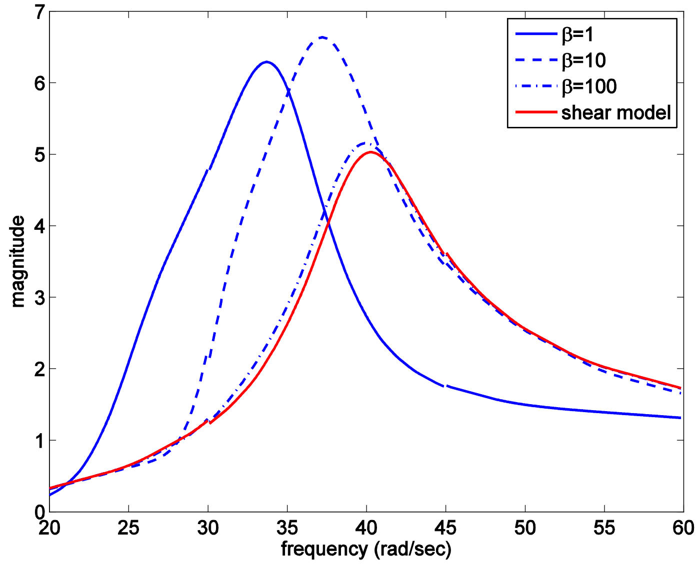

Figure 8.4 Magnitude plot comparison for the 2nd story substructure

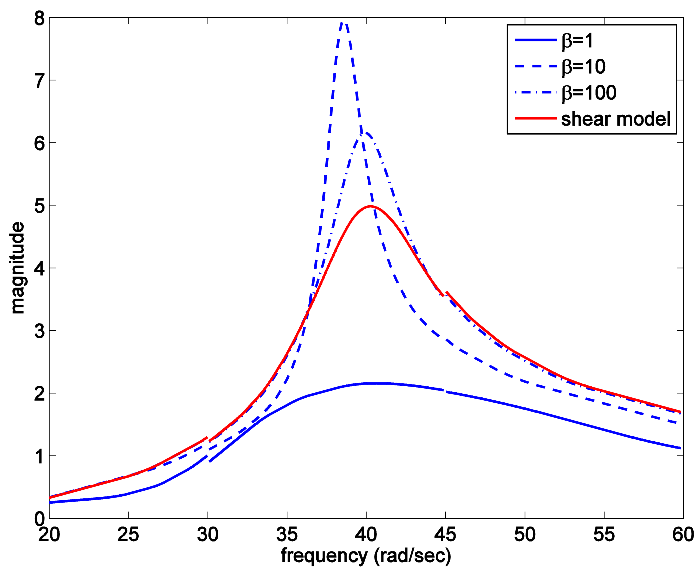

Figure 8.5 Magnitude plot comparison for the 3rd story substructure

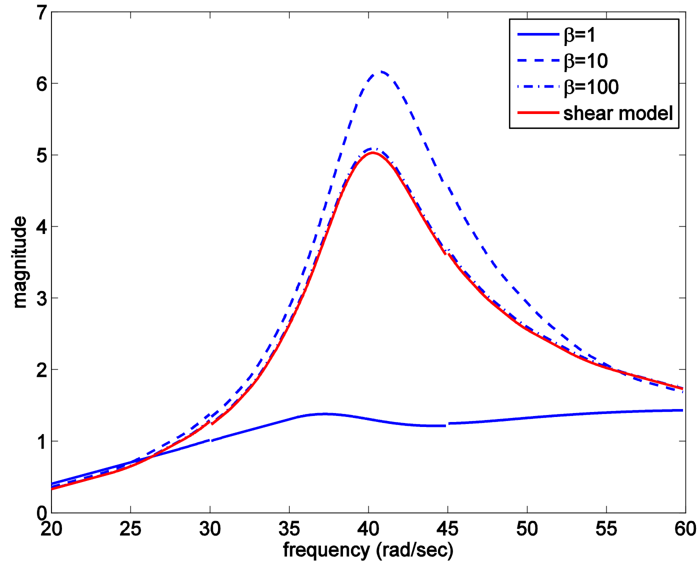

Figure 8.6 Magnitude plot comparison for the 4th story substructure

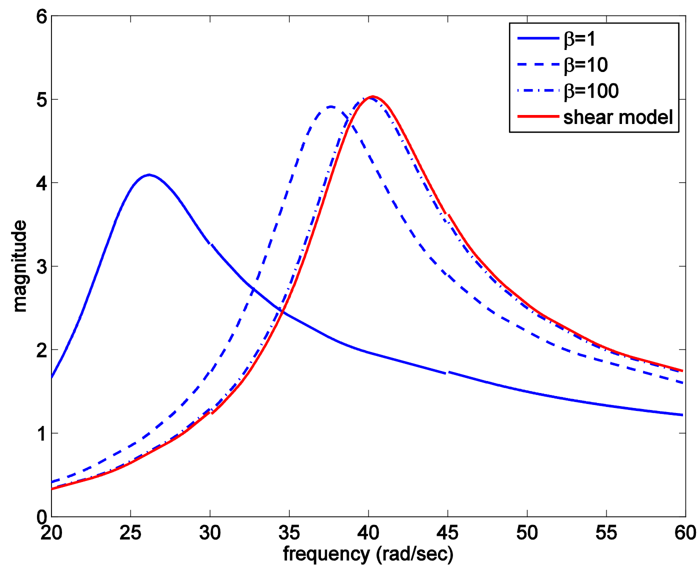

Figure 8.7 Magnitude plot comparison for the 5th story substructure

A good match between the magnitudes of the left and right sides of Equation (8.2) indicates that the substructure identification methods for shear structures can be applied to the identification of the frame structure; on the contrary, a bad match indicates that the substructure identification methods for shear structures are not suitable for the identification of the frame structures.

Several important observations can be made from Figures 8.3~8.7.1) For structures with small and moderate beam-to-column stiffness ratios (β=1 and β=10), the magnitudes of the two sides of Equation (8.2) do not match very well, indicating that the substructure identification methods for shear structures are not applicable to these frame structures. 2) For a structure with a quite large beam-to-column ratio (β=100), the magnitude plots match very well in most cases. However, there are some exceptional cases (*e.g.*, for the magnitudes of the 3rd story substructure terms). Thus, even though it seems reasonable that the substructure identification methods for shear structures can be directly applied to the frame structures with very large beam-to-column ratios, unexpected identification errors will likely occur in some cases.

8.2 Substructure Identification Method for Frame Structures

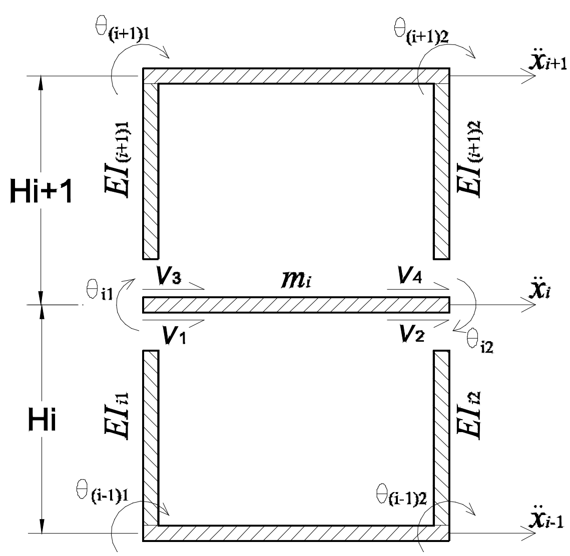

Figure 8.8 The two-story substructure of a non-top floor in a frame structure

As demonstrated in section 8.1, directly applying the substructure identification methods of shear structures to frame structures is infeasible unless the beam-to-column ratio of the frame structure is extremely large. However, the beam-to-column ratio of most real frame structures is far from what can be considered extreme large. Therefore, some modifications must be made to the original substructure identification methods for shear structures so that they can be applied to most frame structures. In this section, a new substructure identification method for frame structures is proposed, derived based on the dynamic equation of one floor substructure in a frame structure. In order to make the illustration simpler, a simple *n*-story one-bay structure is used to demonstrate how to formulate the substructure identification for frame structures.

Figure 8.8 shows a standard two-story substructure of the frame structure. According to Lagrenge-d'Alembert's principle, the dynamic equation of the i^{th} floor in the horizontal translational direction can be written as

$$m_i \ddot{x}_i = V_1 + V_2 + V_3 + V_4 \tag{8.3}$$

where V_1, V_2, V_3 and V_4 are the elastic restoring shear forces that the columns in the i^{th} and $(i+1)^{\text{th}}$ stories apply on the i^{th} floor. From structural analysis, these shear forces at the ends of the column elements can be calculated as

$$V_1 = -\frac{12EI_{i1}}{H_i^3}(x_i - x_{i-1}) - \frac{6EI_{i1}}{H_i^2}(\theta_{i1} + \theta_{(i-1)1}) \tag{8.4}$$

$$V_2 = -\frac{12EI_{i2}}{H_i^3}(x_i - x_{i-1}) - \frac{6EI_{i2}}{H_i^2}(\theta_{i2} + \theta_{(i-1)2}) \tag{8.5}$$

$$V_3 = -\frac{12EI_{(i+1)1}}{H_{i+1}^3}(x_i - x_{i+1}) + \frac{6EI_{(i+1)1}}{H_{i+1}^2}(\theta_{i1} + \theta_{(i+1)1}) \tag{8.6}$$

$$V_4 = -\frac{12EI_{(i+1)2}}{H_{i+1}^3}(x_i - x_{i+1}) + \frac{6EI_{(i+1)2}}{H_{i+1}^2}(\theta_{i2} + \theta_{(i+1)2}) \tag{8.7}$$

where EI_{i1}, EI_{i2}, $EI_{(i+1)1}$ and $EI_{(i+1)2}$ are flexural rigidities of the columns in the i^{th} and (i+1)$^{\text{th}}$ stories; and θ_{i1} and θ_{i2} (i=1,...,n) are the rotational responses of the two beam-column joints at the i^{th} floor.

Substituting Equations (8.4)~(8.7) back into Equation (8.3) gives

$$m_i \ddot{x}_i + \frac{12(EI_{i1} + EI_{i2})}{H_i^3}(x_i - x_{i-1}) + \frac{12(EI_{(i+1)1} + EI_{(i+1)2})}{H_{i+1}^3}(x_i - x_{i+1})$$
$$+ \frac{6EI_{i1}}{H_i^2}(\theta_{i1} + \theta_{(i-1)1}) + \frac{6EI_{i2}}{H_i^2}(\theta_{i2} + \theta_{(i-1)2}) - \frac{6EI_{(i+1)1}}{H_{i+1}^2}(\theta_{i1} + \theta_{(i+1)1}) - \frac{6EI_{(i+1)2}}{H_{i+1}^2}(\theta_{i2} + \theta_{(i+1)2}) = 0 \tag{8.8}$$

For the sake of notational simplicity, a reference flexural rigidity, EI, is introduced. The ratios between the flexural rigidities of the columns and the reference flexural rigidity are defined as

$$\frac{EI_{i1}}{EI} = \alpha_1, \frac{EI_{i2}}{EI} = \alpha_2, \frac{EI_{(i+1)1}}{EI} = \beta_1, \frac{EI_{(i+1)2}}{EI} = \beta_2 \tag{8.9}$$

Equation (8.8) can be transformed into

$$\begin{aligned} & m_i \ddot{x}_i + \frac{12EI}{H_i^3}(\alpha_1 + \alpha_2)(x_i - x_{i-1}) + \frac{12EI}{H_{i+1}^3}(\beta_1 + \beta_2)(x_i - x_{i+1}) \\ & \frac{6EI}{H_i^2}(\alpha_1 + \alpha_2)\left[\frac{\alpha_1}{\alpha_1 + \alpha_2}(\theta_{i1} + \theta_{(i-1)1}) + \frac{\alpha_2}{\alpha_1 + \alpha_2}(\theta_{i2} + \theta_{(i-1)2})\right] \\ & - \frac{6EI}{H_{i+1}^2}(\beta_1 + \beta_2)\left[\frac{\beta_1}{\beta_1 + \beta_2}(\theta_{i1} + \theta_{(i+1)1}) + \frac{\beta_2}{\beta_1 + \beta_2}(\theta_{i2} + \theta_{(i+1)2})\right] = 0 \end{aligned} \tag{8.10}$$

Define four new rotational responses as follows

$$\theta_{i-1}^{(2)} = \frac{\alpha_1}{\alpha_1 + \alpha_2}\theta_{(i-1)1} + \frac{\alpha_2}{\alpha_1 + \alpha_2}\theta_{(i-1)2} \tag{8.11}$$

$$\theta_{i}^{(1)} = \frac{\alpha_1}{\alpha_1 + \alpha_2}\theta_{i1} + \frac{\alpha_2}{\alpha_1 + \alpha_2}\theta_{i2} \tag{8.12}$$

$$\theta_{i}^{(2)} = \frac{\beta_1}{\beta_1 + \beta_2}\theta_{i1} + \frac{\beta_2}{\beta_1 + \beta_2}\theta_{i2} \tag{8.13}$$

$$\theta_{i+1}^{(1)} = \frac{\beta_1}{\beta_1 + \beta_2}\theta_{(i+1)1} + \frac{\beta_2}{\beta_1 + \beta_2}\theta_{(i+1)2} \tag{8.14}$$

These rotational responses are the average floor rotational responses weighted by the relative flexural rigidity of the columns in the same story. Superscripts (1) and (2) indicate which story columns are used to calculate the weighting factors: (1) for the flexural rigidity of the columns below the floor; (2) for the flexural rigidity of the columns above the floor. If the stiffness of the columns in the i^{th} and $(i+1)^{\text{th}}$ stories are the same, *i.e.*, $\alpha_1 = \beta_1$ and $\alpha_2 = \beta_2$, the two rotational responses of a floor will be equal and become one rotational response (*i.e.*, $\theta_i^{(1)} = \theta_i^{(2)}$).

Using the weighted average rotational responses, Equation (8.10) is rewritten as

$$\begin{aligned} & m_i \ddot{x}_i + \frac{12EI}{H_i^3}(\alpha_1 + \alpha_2)(x_i - x_{i-1}) + \frac{12EI}{H_{i+1}^3}(\beta_1 + \beta_2)(x_i - x_{i+1}) \\ & \frac{6EI}{H_i^2}(\alpha_1 + \alpha_2)(\theta_i^{(1)} + \theta_{i-1}^{(2)}) - \frac{6EI}{H_{i+1}^2}(\beta_1 + \beta_2)(\theta_i^{(2)} + \theta_{i+1}^{(1)}) = 0 \end{aligned} \tag{8.15}$$

Define the equivalent story stiffness of the i^{th} and $(i+1)^{\text{th}}$ stories as

$$k_i = \frac{12EI}{H_i^3}(\alpha_1 + \alpha_2) \tag{8.16}$$

$$k_{i+1} = \frac{12EI}{H_{i+1}^3}(\beta_1 + \beta_2) \tag{8.17}$$

which is just the story stiffnesses when the beam-to-column stiffness ratio of the frame structure is infinite and the frame structure behaves like a pure shear structure. Then, Equation (8.15) can be rewritten by using the equivalent story stiffness as

$$m_i \ddot{x}_i + k_i \left[x_i - x_{i-1} + \delta_i \right] + k_{i+1} \left[x_i - x_{i+1} - \delta_{i+1} \right] = 0 \tag{8.18}$$

where $\delta_i = (\theta_i^{(1)} + \theta_{i-1}^{(2)}) H_i / 2$, $\delta_{i+1} = (\theta_i^{(2)} + \theta_{i+1}^{(1)}) H_{i+1} / 2$.

If it is assumed that the damping matrix of the frame structure has a format similar to that of the stiffness matrix, the dynamic equation of the i^{th} floor, including the effects of the structural damping, can be written as

$$\begin{aligned} & m_i \ddot{x}_i + c_i \left[\dot{x}_i - \dot{x}_{i-1} + \dot{\delta}_i \right] + k_i \left[x_i - x_{i-1} + \delta_i \right] \\ & + c_{i+1} \left[\dot{x}_i - \dot{x}_{i+1} - \dot{\delta}_{i+1} \right] + k_{i+1} \left[x_i - x_{i+1} - \delta_{i+1} \right] = 0 \end{aligned} \tag{8.19}$$

where c_i and c_{i+1} are the equivalent story damping of the frame structure.

Adding the term $m_i(-\ddot{x}_{i-1} + \ddot{\delta}_i)$ to both sides of Equation (8.19), taking the Fourier transform and rearranging gives

$$\frac{1}{1 - j c_i / (m_i \omega) - k_i / (m_i \omega^2)} = \frac{\ddot{X}_{i-1} - \ddot{X}_i - \ddot{\Delta}_i}{(\ddot{X}_{i-1} - \ddot{\Delta}_i) + (\ddot{X}_{i+1} - \ddot{X}_i + \ddot{\Delta}_{i+1}) \left[j c_{i+1} / (m_i \omega) + k_{i+1} / (m_i \omega^2) \right]} \tag{8.20}$$

where $\ddot{\Delta}_i$ and $\ddot{\Delta}_{i+1}$ are the Fourier transforms of the responses $\ddot{\delta}_i$ and $\ddot{\delta}_{i+1}$, respectively; $\ddot{X}_i$ is the Fourier transform of the i^{th} floor acceleration $\ddot{x}_i$. Assuming that structural parameters $[k_{i+1} \; c_{i+1}]^{\mathrm{T}}$ in Equation (8.20) are known, the right side can be directly calculated from the measured acceleration responses. Then, an optimization problem similar to Equation (3.10) is formulated to identify structural parameters $[k_i \;\; c_i]^{\mathrm{T}}$.

$$\underset{k_i, c_i}{\arg\min} \quad J(k_i, c_i) = \sum_{l=1}^{N} |\varepsilon_l|^2 = \sum_{l=1}^{N} \left| g_l(k_i, c_i) - \hat{g}_l\left(\hat{\ddot{X}}_{i-1}, \hat{\ddot{X}}_{i}, \hat{\ddot{X}}_{i+1}, \hat{\ddot{\Delta}}_{i}, \hat{\ddot{\Delta}}_{i+1} \right) \right|^2 \qquad (8.21)$$

where $g_l(k_i, c_i) = \dfrac{1}{1 - j\, c_i/(m_i \omega_l) - k_i/(m_i \omega_l^2)}$;

$$\hat{g}_l\left(\hat{\ddot{X}}_{i-1}, \hat{\ddot{X}}_{i}, \hat{\ddot{X}}_{i+1}, \hat{\ddot{\Delta}}_{i}, \hat{\ddot{\Delta}}_{i+1} \right) = \frac{\hat{\ddot{X}}_{i-1,l} - \hat{\ddot{X}}_{i,l} - \hat{\ddot{\Delta}}_{i,l}}{(\hat{\ddot{X}}_{i-1} - \hat{\ddot{\Delta}}_{i}) + (\hat{\ddot{X}}_{i+1,l} - \hat{\ddot{X}}_{i,l} + \hat{\ddot{\Delta}}_{i+1,l})\left[j c_{i+1}/(m_i \omega_l) + k_{i+1}/(m_i \omega_l^2) \right]}.$$

Similar to the substructure identification methods for shear structures, Equation (8.21) establishes an induction identification problem which can identify the equivalent story stiffness and damping coefficient of the i^{th} story $[k_i \;\; c_i]^{\mathrm{T}}$ given that the parameters of the $(i+1)^{\mathrm{th}}$ story $[k_{i+1} \;\; c_{i+1}]^{\mathrm{T}}$ are known. Since the top-floor substructure could be considered as a special case of the general non-top two-story substructure, shown in Figure (8.8), wherein both parameters of the fictitious story $(n+1)^{\mathrm{th}}$ $[k_{n+1} \;\; c_{n+1}]^{\mathrm{T}}$ and the response of the fictitious $(n+1)^{\mathrm{th}}$ floor are zero, a simple top-story identification problem can be formulated as

$$\underset{k_n, c_n}{\arg\min} \quad J(k_n, c_n) = \sum_{l=1}^{N} \left| f_l(k_n, c_n) - \hat{f}_l\left(\hat{\ddot{X}}_{n-1}, \hat{\ddot{X}}_{n}, \hat{\ddot{\Delta}}_{n} \right) \right|^2 \qquad (8.22)$$

where $f_l(k_n, c_n) = \dfrac{1}{1 - j\, c_n/(m_n \omega) - k_n/(m_n \omega^2)}$, $\hat{f}_l\left(\hat{\ddot{X}}_{n-1}, \hat{\ddot{X}}_{n} \right) = \dfrac{\hat{\ddot{X}}_{n-1,l} - \hat{\ddot{X}}_{n,l} - \hat{\ddot{\Delta}}_{n}}{\hat{\ddot{X}}_{n-1,l} - \hat{\ddot{\Delta}}_{n}}$.

In Equation (8.22), the equivalent parameters of the n^{th} story $[k_n \;\; c_n]^{\mathrm{T}}$ are identified, which in turn can be used to start the induction identification problem in Equation (8.21). By continuously repeating the induction problem in Equation (8.21), the equivalent story parameters of the whole frame structures are identified from top to bottom iteratively.

Compared with the substructure identification method for shear structure in Chapter 3, the proposed substructure identification method for frame structure has some additional terms ($\ddot{\Delta}_i, \ddot{\Delta}_{i+1}$) that account for the effects of the rotation responses in formulating the identification problems. Moreover, although this derivation of the substructure identification method for frame structures utilizes the Fourier transform of the structural responses, it can be easily shown that, if a reference response $y(t)$ is introduced, the two key identification equations in the power spectral densities between the structural responses and the reference are

$$\frac{1}{1 - j\,c_n/(m_n\omega) - k_n/(m_n\omega^2)} = \frac{S_{\ddot{x}_{n-1}y} - S_{\ddot{x}_n y} - S_{\ddot{\Delta}_n y}}{S_{\ddot{x}_{n-1}y} - S_{\ddot{\Delta}_n y}} \tag{8.23}$$

$$\frac{1}{1 - \dfrac{jc_i}{(m_i\omega)} - \dfrac{k_i}{(m_i\omega^2)}} = \frac{S_{\ddot{x}_{i-1}y} - S_{\ddot{x}_i y} - S_{\ddot{\Delta}_i y}}{(S_{\ddot{x}_{i-1}y} - S_{\ddot{\Delta}_i y}) + (S_{\ddot{x}_{i+1}y} - S_{\ddot{x}_i y} + S_{\ddot{\Delta}_{i+1}y})\left[\dfrac{jc_{i+1}}{(m_i\omega)} + \dfrac{k_{i+1}}{(m_i\omega^2)}\right]} \tag{8.24}$$

By utilizing these two key equations, a new power spectral density based substructure identification method can be formulated as follows.

$$\underset{k_n, c_n}{\arg\min} \quad J(k_n, c_n) = \sum_{l=1}^{N} \left| f_l(k_n, c_n) - \hat{f}_l(\hat{S}_{\ddot{x}_n y}, \hat{S}_{\ddot{x}_{n-1}y}, \hat{S}_{\ddot{\Delta}_n y}) \right|^2 \tag{8.25}$$

where $f_l(k_n, c_n) = \dfrac{1}{1 - j\,c_n/(m_n\omega_l) - k_n/(m_n\omega_l^2)}$,

$$\hat{f}_l(\hat{S}_{\ddot{x}_n y}, \hat{S}_{\ddot{x}_{n-1} y},, \hat{S}_{\ddot{\Delta}_n y}) = \frac{\hat{S}_{\ddot{x}_{n-1} y,l} - \hat{S}_{\ddot{x}_n y,l} + \hat{S}_{\ddot{\Delta}_n y,l}}{\hat{S}_{\ddot{x}_{n-1} y,l} - \hat{S}_{\ddot{\Delta}_n y,l}}.$$

$$\underset{k_i, c_i}{\arg\min} \quad J(k_i, c_i) = \sum_{l=1}^{N} \left| g_l(k_i, c_i) - \hat{g}_l(\hat{S}_{\ddot{x}_{i-1} y}, \hat{S}_{\ddot{x}_i y}, \hat{S}_{\ddot{x}_{i+1} y}, \hat{S}_{\ddot{\Delta}_i y}, \hat{S}_{\ddot{\Delta}_{i+1} y}) \right|^2 \tag{8.26}$$

where $g_l(k_i, c_i) = \dfrac{1}{1 - j\,c_i/(m_i\omega_l) - k_i/(m_i\omega_l^2)}$,

$$\hat{g}_l(\hat{S}_{\ddot{x}_{i-1} y}, \hat{S}_{\ddot{x}_i y}, \hat{S}_{\ddot{x}_{i+1} y}, \hat{S}_{\ddot{\Delta}_i y}, \hat{S}_{\ddot{\Delta}_{i+1} y}) =$$
$$\frac{\hat{S}_{\ddot{x}_{i-1} y,l} - \hat{S}_{\ddot{x}_i y,l} - \hat{S}_{\ddot{\Delta}_i y,l}}{(\hat{S}_{\ddot{x}_{i-1} y,l} - \hat{S}_{\ddot{\Delta}_{i-1} y,l}) + (\hat{S}_{\ddot{x}_{i+1} y,l} - \hat{S}_{\ddot{x}_i y,l} + \hat{S}_{\ddot{\Delta}_{i+1} y,l})[\,j c_{i+1}/(m_i\omega_l) + k_{i+1}/(m_i\omega_l^2)]}.$$

The derivation of the substructure identification method for frame structures essentially converts one frame substructure, shown in Figure 8.1, into a beam-like structure, shown in Figure 8.9 with (3*n*–1) DOFs (each floor has one translation and two weighted rotation responses; the top floor is an exception which only has one rotation response). The two rotation responses of each floor are the weighted average rotation responses of all beam-column joints in the same floor; the weighting factors are determined by the relative flexural rigidities of the columns in the story above and the story below the floor being identified.

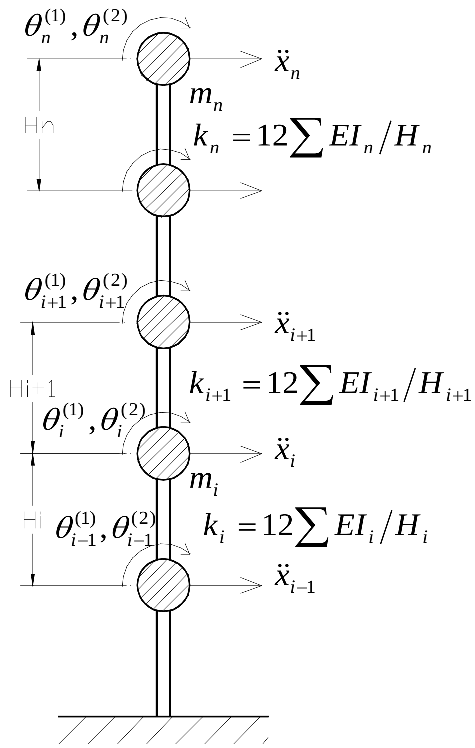

Figure 8.9 The equivalent beam-like structure for an *n*-story frame structure

Although this substructure identification method for frame structures is derived from a simple one-bay frame structure, it is easily shown that this method can be extended to more general multiple-bay frame structures by calculating the two average rotation responses from all beam-column joint rotation responses for each floor. Therefore, the proposed substructure identification method is applicable to general frame structures. However, there is one disadvantage of the newly proposed substructure identification method: it does require measuring the rotation responses of the beam-column joints in the frame structure, which may be difficult to realize. Further research, beyond the scope of this dissertation, is needed to relax this requirement and only utilize the floor acceleration responses to perform the substructure identification.

8.3 Identification Error Analysis

Utilizing the method of the identification error analysis, proposed in the third chapter, the identification errors of cross power spectrum density based method for frame structures are derived in this section.

8.3.1 Top Story Identification Case

The parameter identification error of the top story identification in the power spectral density based method (for frame structures) can be obtained as

$$\begin{bmatrix} \theta_{nk} \\ \theta_{nc} \end{bmatrix} \approx \sum_{l=1}^{N} \mathrm{Re}\left\{ \begin{bmatrix} W_{11,l} & W_{12,l} & W_{13,l} \\ W_{21,l} & W_{22,l} & W_{23,l} \end{bmatrix} \cdot \begin{bmatrix} N_{\ddot{x}_{n-1}y,l} \big/ S_{(\ddot{x}_n-\ddot{x}_{n-1}+\ddot{\Delta}_n)y,l} \\ N_{\ddot{x}_n y,l} \big/ S_{(\ddot{x}_n-\ddot{x}_{n-1}+\ddot{\Delta}_n)y,l} \\ N_{\ddot{\Delta}_n y,l} \big/ S_{(\ddot{x}_n-\ddot{x}_{n-1}+\ddot{\Delta}_n)y,l} \end{bmatrix} \right\} \tag{8.25}$$

where θ_{kn} and θ_{cn} are the relative identification errors of the n^{th} story parameters k_n and c_n, respectively; $N_{\ddot{x}_i y,l} = \hat{S}_{\ddot{x}_i y,l} - S_{\ddot{x}_i y,l}$ $(i = 1,...,n)$ is the measurement uncertainty of cross power spectrum density (CSD) estimation, given by the difference between the CSD estimated from the noise-contaminated measured responses and the CSD of the true (noiseless) responses at frequency ω_l; $S_{(\ddot{x}_n-\ddot{x}_{n-1}+\ddot{\Delta}_n)y,l}$ is the CSD between the response of the i^{th} story $(\ddot{x}_i - \ddot{x}_{i-1} + \ddot{\Delta}_i)$ and the reference response $y(t)$; the derivation of the factors $W_{ij,l}$ is given in Appendix E.

As shown in Figure 8.10, all factors $W_{ij,l}$ are significantly large near the natural frequency of the n^{th} story substructure $\omega_{n0} = \sqrt{k_n / m_n}$, and very small when far away from this frequency. Thus, the uncertainty measurement terms ($N_{\ddot{x}_{n-1}y,l} \big/ S_{(\ddot{x}_n-\ddot{x}_{n-1}+\ddot{\Delta}_n)y,l}$, $N_{\ddot{x}_n y,l} \big/ S_{(\ddot{x}_n-\ddot{x}_{n-1}+\ddot{\Delta}_n)y,l}$ and $N_{\ddot{\Delta}_n y,l} \big/ S_{(\ddot{x}_n-\ddot{x}_{n-1}+\ddot{\Delta}_n)y,l}$) near the substructure natural frequency

ω_{n0} play a dominant role in determining the parameter identification accuracy. Largely reducing these terms near the substructure natural frequency ω_{n0} will significantly reduce the identification errors and improve the identification accuracy.

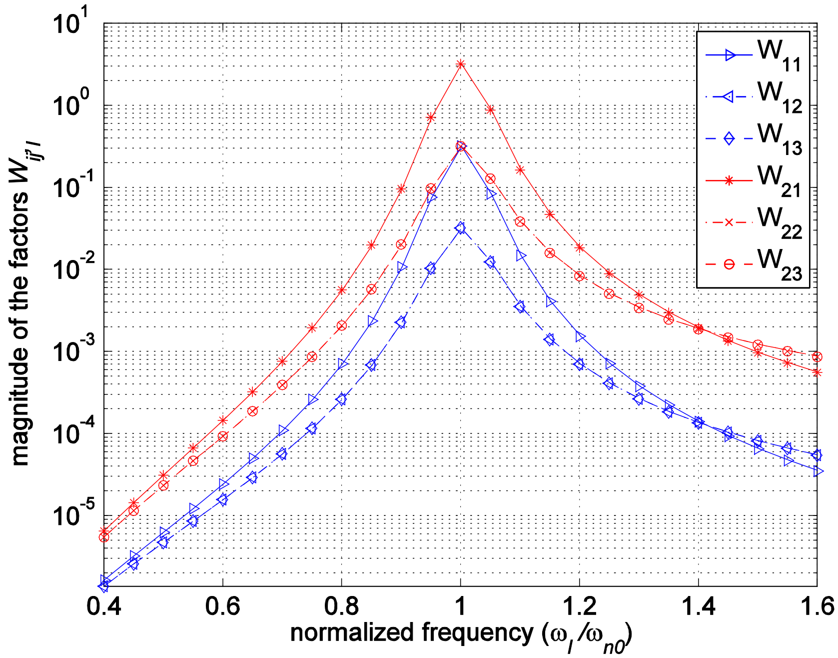

Figure 8.10 Magnitude of weighting factors $W_{ij,l}$

8.3.2 Non-top Story Identification Case

The parameter identification errors of the i^{th} non-top story in the power spectral density based method (for frame structures) can be obtained as

$$\begin{bmatrix}\theta_{ki}\\ \theta_{ci}\end{bmatrix} \approx \sum_{l=1}^{N} \mathrm{Re}\left\{\begin{bmatrix}U_{11,l} & U_{12,l} & U_{13,l} & U_{14,l} & U_{15,l}\\ U_{22,l} & U_{22,l} & U_{23,l} & U_{24,l} & U_{25,l}\end{bmatrix}\cdot\begin{bmatrix}N_{\ddot{x}_{i-1}y,l}\big/S_{(\ddot{x}_i-\ddot{x}_{i-1}+\ddot{\Delta}_i)y,l}\\ N_{\ddot{x}_iy,l}\big/S_{(\ddot{x}_i-\ddot{x}_{i-1}+\ddot{\Delta}_i)y,l}\\ N_{\ddot{x}_{i+1}y,l}\big/S_{(\ddot{x}_i-\ddot{x}_{i-1}+\ddot{\Delta}_i)y,l}\\ N_{\ddot{\Delta}_iy,l}\big/S_{(\ddot{x}_i-\ddot{x}_{i-1}+\ddot{\Delta}_i)y,l}\\ N_{\ddot{\Delta}_{i+1}y,l}\big/S_{(\ddot{x}_i-\ddot{x}_{i-1}+\ddot{\Delta}_i)y,l}\end{bmatrix}\right\}+ \tag{8.26}$$

$$\sum_{l=1}^{N} \mathrm{Re}\left\{\begin{bmatrix}U_{16,l} & U_{17,l}\\ U_{26,l} & U_{27,l}\end{bmatrix}\cdot\begin{bmatrix}\dfrac{S_{(\ddot{x}_{i+1}-\ddot{x}_i+\ddot{\Delta}_{i+1})y,l}}{S_{(\ddot{x}_i-\ddot{x}_{i-1}+\ddot{\Delta}_i)y,l}}\theta_{k(i+1)}\\ \dfrac{S_{(\ddot{x}_{i+1}-\ddot{x}_i+\ddot{\Delta}_{i+1})y,l}}{S_{(\ddot{x}_i-\ddot{x}_{i-1}+\ddot{\Delta}_i)y,l}}\theta_{c(i+1)}\end{bmatrix}\right\}$$

where $\theta_{k(i+1)}$ and $\theta_{c(i+1)}$ are the relative identification error of the $(i+1)^{\text{th}}$ story parameters k_{i+1} and c_{i+1}, respectively; the derivation of the factors $U_{ij,l}$ is given in Appendix E.

The identification errors of the i^{th} story parameters $[\theta_{ki} \quad \theta_{ci}]^{\mathrm{T}}$ in Equation (8.26) consist of two parts: the errors (the first part of the right side) directly related to the measurement uncertainty of the structural responses ($N_{\ddot{x}_{i-1}y}\big/S_{(\ddot{x}_i-\ddot{x}_{i-1}+\ddot{\Delta}_i)y}$, $N_{\ddot{x}_iy}\big/S_{(\ddot{x}_i-\ddot{x}_{i-1}+\ddot{\Delta}_1)y}$, $N_{\ddot{x}_{i+1}y}\big/S_{(\ddot{x}_i-\ddot{x}_{i-1}+\ddot{\Delta}_i)y}$, $N_{\ddot{\Delta}_iy}\big/S_{(\ddot{x}_i-\ddot{x}_{i-1}+\ddot{\Delta}_i)y}$ and $N_{\ddot{\Delta}_{i+1}y}\big/S_{(\ddot{x}_i-\ddot{x}_{i-1}+\ddot{\Delta}_i)y}$) and the accumulation errors (the second part) due to the uncertainty in the identified structural parameters of the story above ($S_{(\ddot{x}_{i+1}-\ddot{x}_i+\ddot{\Delta}_{i+1})y}\big/S_{(\ddot{x}_i-\ddot{x}_{i-1}+\ddot{\Delta}_i)y}\,\theta_{k(i+1)}$ and $S_{(\ddot{x}_{i+1}-\ddot{x}_i+\ddot{\Delta}_{i+1})y}\big/S_{(\ddot{x}_i-\ddot{x}_{i-1}+\ddot{\Delta}_i)y}\,\theta_{c(i+1)}$). As shown in Figure 8.11, all factors $U_{ij,l}$ are significantly large in magnitude near the natural frequency of the i^{th} story substructure $\omega_{i0} = \sqrt{k_i/m_i}$ and decay very fast when moving to lower and higher frequency. Therefore, both the measurement uncertainties and the upper story parameter uncertainties near the substructure natural frequency ω_{i0} play an important in determining error; significantly reducing their values can greatly reduce identification error.

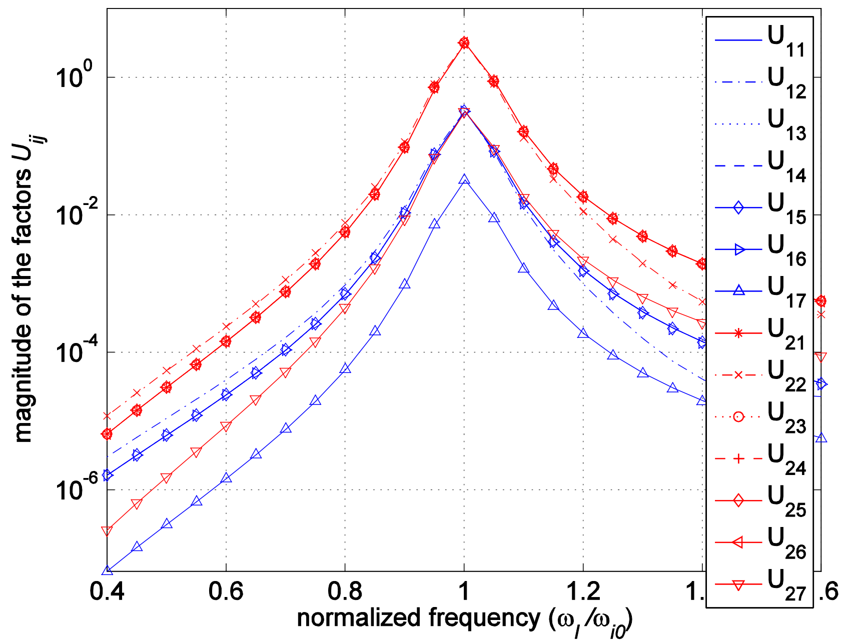

Figure 8.11 Magnitude of weighting factor $U_{ij,l}$

Another interesting observation of this result is that the magnitudes of both kinds of uncertainties are not only related to the sources of these uncertainties – the measurement uncertainties ($N_{\ddot{x}_{i-1}y}$, $N_{\ddot{x}_{i-1}y}$, $N_{\ddot{x}_{i-1}y}$, $N_{\ddot{\Delta}_i y}$ and $N_{\ddot{\Delta}_{i+1}y}$) and the identification errors of the upper story parameters ($\theta_{k(i+1)}$ and $\theta_{c(i+1)}$) – but also are affected by two important structural responses: $S_{(\ddot{x}_i-\ddot{x}_{i-1}+\ddot{\Delta}_i)y}$ and $S_{(\ddot{x}_{i+1}-\ddot{x}_i+\ddot{\Delta}_{i+1})y} \big/ S_{(\ddot{x}_i-\ddot{x}_{i-1}+\ddot{\Delta}_i)y}$. Since $S_{(\ddot{x}_i-\ddot{x}_{i-1}+\ddot{\Delta}_i)y}$ serves as the common denominator for all three measurement uncertainty terms, amplifying $S_{(\ddot{x}_i-\ddot{x}_{i-1}+\ddot{\Delta}_i)y}$ near the substructure natural frequency ω_{i0} will lead to smaller measurement uncertainties and, in turn, smaller identification errors. Similarly, reducing

$S_{y(\ddot{x}_{i+1}-\ddot{x}_i+\ddot{\Delta}_{i+1})} \Big/ S_{y(\ddot{x}_i-\ddot{x}_{i-1}+\ddot{\Delta}_i)}$ near the frequency ω_{i0} will result in smaller upper story parameter uncertainties and, thus, smaller identification errors.

8.4 An Illustrative Example

In this section, the power spectral density based substructure identification method for frame structures, shown in Equations (8.25) and (8.26), is used to identify the equivalent story stiffness and damping parameters of a simple 5-story one-bay uniform frame structure. The parameters of the test structure are picked as: the height of each story of the structure is H=3m; the span of each bay is L=3m; the mass of each floor slab is $m_i=1\times10^5$ kg (chosen so that the mass of the frame structure the same as the 5-story shear structure used in Chapters 3~7); the flexural rigidity of each column is $EI_c= 18\times10^7$ N·m^2 (which gives the same story stiffness in the frame structure as the 5-story shear structure if the beam flexibility is negligible); and the flexural rigidity of each beam is $EI_b=EI_c=18\times10^7$ N·m^2. It is assumed that the damping of the frame structure has a format similar to that of the stiffness matrix, that is,

$$[\mathbf{C}] = \alpha[\mathbf{K}] \tag{8.27}$$

where $[\mathbf{C}]$ and $[\mathbf{K}]$ are the damping and stiffness matrices of the frame structure; the coefficient α is selected such that the damping ratio of the first mode of the structure is 2% (the equivalent story damping coefficient is $c_i=8.89\times10^5$ N·sec/m). The frame structure is shaken by ground excitation $\ddot{u}_g$, modeled by a Gaussian random pulse process passing through a 4th order band-pass Butterworth filter with 1Hz low cut-off frequency and 12 Hz high cut-off frequency.

8.4.1 Estimation of Equivalent Story Stiffness and Damping Parameters

The identification results in Table 8.1 show that the largest identification error occurs at the 4th story but not at the 3rd story as would be in the shear structure (in Chapter 5) that has similar story stiffness. This result can be explained as follows. Based on the identification error analysis results previously derived in Equation (8.26), the two important substructure responses that determine the accuracy of the substructure identification method are the cross power spectral density of the modified interstory acceleration responses, $S_{(\ddot{x}_i-\ddot{x}_{i-1}+\ddot{\Delta}_i)y}$, and the ratio between the cross power spectral densities between two modified interstory acceleration responses, $S_{(\ddot{x}_{i+1}-\ddot{x}_i+\ddot{\Delta}_{i+1})y} \big/ S_{(\ddot{x}_i-\ddot{x}_{i-1}+\ddot{\Delta}_i)y}$, near the story substructure natural frequency $\omega_{i0} = \sqrt{k_i/m_i}$. As discussed in section 6.1.3, these two responses are directly related to the frequency responses $\ddot{X}_{i,l} - \ddot{X}_{i-,l} + \ddot{\Delta}_{i,l}$ and the frequency response ratio $(\ddot{X}_{i+1,l} - \ddot{X}_{i,l} + \ddot{\Delta}_{i+1,l}) \big/ (\ddot{X}_{i,l} - \ddot{X}_{i-,l} + \ddot{\Delta}_{i,l})$, respectively. The larger the first response and the smaller the second response near frequency ω_{i0}, the more accurate the identification results will be. As shown in Figure 8.12 and 8.13, the inaccurate identification results of the 4th story parameters are due to the two undesirable responses controlling the 4th story parameters identification: compared to the substructure responses related to other story identifications, the power spectral density of the modified 4th story interstory acceleration is very small near the substructure natural frequency (40 radian/sec); simultaneously, the frequency response ratio is very large near the substructure natural frequency (40 radian/sec).

Table 8.1 Statistics of relative identification errors of the 5-story frame structure

Story number	$y(t)$	Story stiffness $\hat{k}_i$			Story damping $\hat{c}_i$		
		mean error	relative RMSE	relative STD	mean	relative RMSE	relative STD
1	$\ddot{x}_5$	-0.5%	1.0%	0.9%	0.1%	4.3%	4.3%
2	$\ddot{x}_g$	0.3%	1.6%	1.6%	-3.0%	7.0%	6.3%
3	$\ddot{x}_g$	0.4%	1.0%	1.0%	0.1%	4.7%	4.7%
4	$\ddot{x}_2$	-0.3%	3.2%	3.2%	6.1%	14.6%	13.3%
5	$\ddot{x}_2$	0.0%	0.4%	0.4%	0.2%	1.7%	1.7%

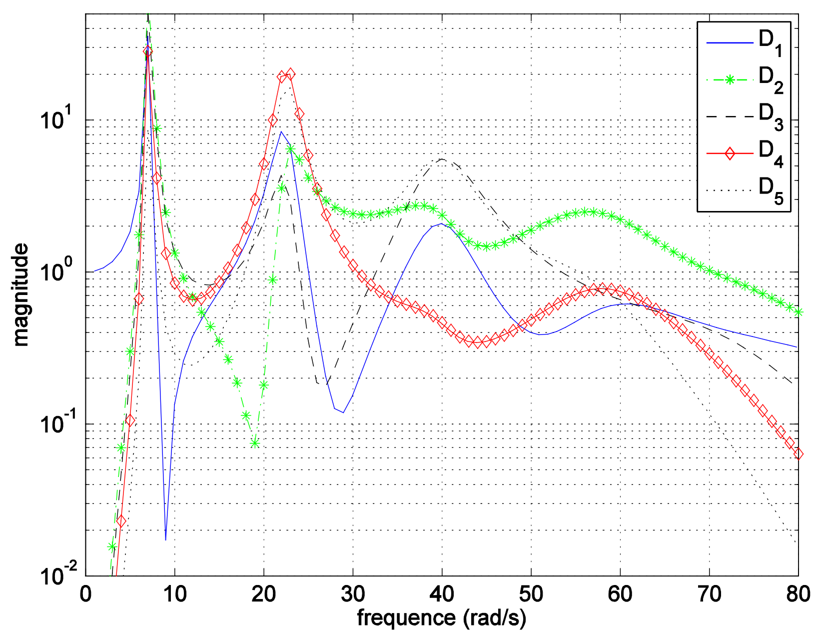

Figure 8.12 Auto power spectra of the modified interstory acceleration

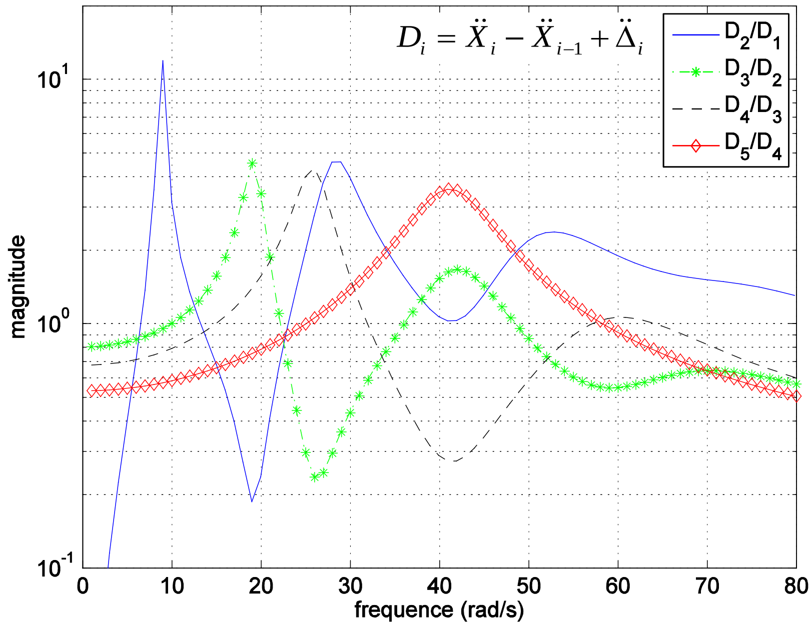

Figure 8.13 The frequency response ratio between the two modified interstory accelerations

8.4.2 Damage Detection in the Frame Structure

The proposed substructure identification method for frame structures identifies the equivalent story stiffness of the structure, which is determined by the flexural rigidity of the columns. If the occurrence of structural damage results in the decrease of a column's flexural rigidity, it will be possible for the substructure identification method to detect this change and, thus, detect the damage. In this section, the proposed substructure identification method is used to detect the damage of columns in frame structures. It is assumed that the damage occurs at the first story of the 5-story one-bay frame structure, resulting in the reduction of the flexural rigidity of one column by 10%, which is equivalent to the reduction of the equivalent story stiffness by 5%. Moreover, since it is assumed in this chapter that the damping matrix of the structure is proportional to the stiffness matrix of the structure, the equivalent damping coefficient of the 5th story is also decreased by 5%.

The damage detection method proposed in section 3.5 is used to detect the structural damage previously mentioned. The identification results of 100 tests for the undamaged structure in subsection 8.4.1 are reused to calculate the mean and variance of the identified parameters for the undamaged structure. In order to test the performance of the proposed damage detection strategy to correctly identify the health status of the structure, 300 independent substructure identification are carried out on the damaged structure; the results are used in the hypothesis test to determine whether or not the structure is damaged. The number of the substructure identifications that each hypothesis test uses to get the conclusion is selected as 1, 3 and 5. According to the number of tests each hypothesis test uses, the identification results of 300 tests are divided into groups and a hypothesis test is performed for each group using the method proposed in section 3.5. The percentages of the hypothesis tests which give the correct health status of the structure are shown in Table 8.2. The β value is selected as 5 in the hypothesis tests.

The results in Table 8.2 show that when only one identification is used in the hypothesis testing, the damage at the first story is almost 100% percent correctly identified; however, there are about a 10% chance that the undamaged stories are mistakenly reported as damaged. As the number of the identifications, n, that each hypothesis test uses to make the decision increases, the chance that hypothesis tests make the corrected decision also increase, which verifies that the proposed hypothesis test method, using n identifications together to make the decision, is effective in improving the probability to make the right decision about the health status of the structure.

Table 8.2 The percentage of the hypothesis tests which give the correct conclusion about the structural health status

Floor Number	*n*		
	1	3	5
1	99.7%	100%	100%
2	91.3%	99%	100%
3	89.3%	97%	99%
4	91.3%	99%	99%
5	87.7%	97%	100%

Chapter 9

Experimental Verification of Controlled Substructure Identification

9.1 Introduction

Figure 9.1 Small scale test system

A laboratory experiment is an important step to verify theories and the assumptions used in their derivations as well as to test how the theories work in the real world with all kinds of uncertainties. In the previous chapters, theoretical developments and simulation results have demonstrated that the proposed substructure identification methods successfully identify the parameters of shear structures and that the controlled substructure identification methods further improve the identification accuracy by changing the structural dynamic responses via specially designed structural control systems. In order to experimentally verify these results, a series of experiments are carried out on a small-scale test system, located in the SHM and Control Lab at the University of Southern California. The whole test system, shown in Figure 9.1, includes the following. a) A two-story shear building model structure, made of aluminum and plexiglass plates, serves as the test structure. b) A small-scale Quanser® uniaxial shake table provides the necessary ground excitations to the test structure. c) A small active mass driver (AMD) control system can be used to change the dynamic responses of the structure to verify the effects of the control system for improving the identification accuracy (not used in this study that only reports the results of passive control strategies; active strategies are left for future research). d) A digital controller board provides the functions of collecting measured response data and of commanding the AMD control device. e) A personal computer, installed with the software MATLAB® and QuaRC®, controls the movement of the shake table as well as the AMD device. On this test bed, several experiments are performed to test the proposed substructure identification methods as well as the controlled substructure identification methods which improve the identification accuracy by changing the structural dynamic responses via specially designed control systems.

9.2 Experiment Overview

In the area of control and SHM of civil structures, it is well recognized that experimental verification is necessary to focus research efforts in the most promising directions (Housner *et al.*, 1994; 1997). Therefore, to experimentally verify the effectiveness of the proposed substructure identification methods and controlled substructure identification methods is an essential step before these techniques can be advanced towards practical use. The goal of the experiments are 1) to check the effectiveness of the substructure identification methods for identifying the structural parameters of the 2DOF test structure and 2) to verify that the accuracy of the identified parameters can be improved by changing the structural responses via some specially designed control systems. To test the effectiveness of the substructure identification methods, the 2DOF shear structure is mounted on the shake table and excited by band-pass Gaussian white ground accelerations. The measured acceleration responses are used in the substructure identification algorithms to identify the structural parameters.

To verify the efficiency of the controlled substructure identification, using control systems to further improve the identification accuracy, some simple passive control methods are tested in this study. The effects of the control systems are replicated by changing the story stiffness via adding/removing diagonal springs installed into the structure and by changing the structure floor mass via adding/removing the additional mass attached to the structure. (The reasons that passive control methods are first adopted here are that the passive control system is easy to realize and, yet, can still serve as a first step in verifying the effectiveness of the controlled substructure identification. More advanced active control methods, implemented by the aforementioned AMD system, will be investigated in future studies.) The specially designed passive control systems are used to change the structural dynamics to improve the substructure identification accuracy. Then, the controlled structure with the passive control devices is excited by the shake table again; the measured structural acceleration responses are fed into the substructure identification algorithms to identify the structural parameters, which will be compared with the identification results of the (uncontrolled) substructure identification methods and check if the expected improved identification accuracy is achieved.

9.3 Description of Testing System

Before discussing the details of the experiments, the properties of each component in the experiments are first introduced in detail in the following subsections.

9.3.1 2DOF Test Structure

A 2DOF shear building structure, shown in Figure 9.2, is the test structure of this experiment (Quanser, 2010). The structure is composed of two vertical aluminum plates, connected with three horizontal thick plexiglass plates at the bottom, first and second story positions. The horizontal plexiglass plates and the vertical aluminum plates are fixed to each other by three UNC #8 bolts in each side at each level. The interstory height is 490 mm.

At each floor level of the experimental structure, several small aluminum plates with holes (see Figure 9.3) are attached to the structure, which allow us to change structural story stiffness by adding or removing some diagonal springs to the structure. The test structure by itself is quite soft; the first two frequencies are 1.9Hz and 5.2Hz. A pair of diagonal springs is attached to each story of the structure to increase the structural stiffness.

Prior to experimentation, the 2DOF structure was disassembled so that its dimensions and weight could be measured. An electronic scale, with measurement sensitivity 1 gm, was used to weigh each component of the structure. Table 9.1 lists the measured dimensions and masses of the structure (Elmasry, 2005). Using the lumped mass method, the equivalent floor mass of the shear model for the testing structure is calculated and shown in the Table 9.2. The calculation of the equivalent floor mass includes the mass of the springs, screws, washers, fastener plates, and accelerometers located at the corresponding level.

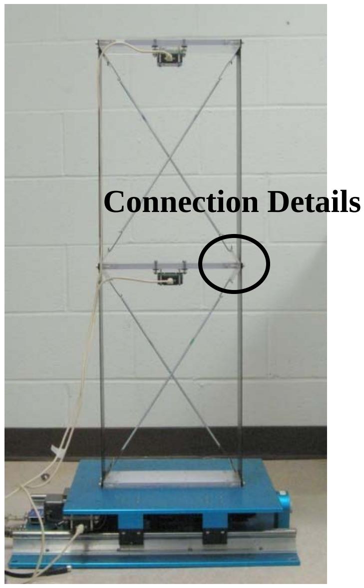

Figure 9.2 The two-story test structure

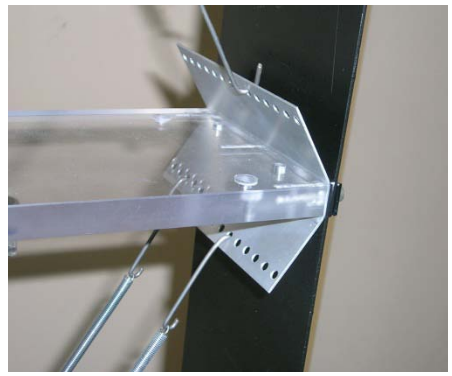

Figure 9.3 Aluminum and plexiglass connection details

Table 9.1 Dimension and mass of test structure

	Mass (kg)	Length (cm)	Width (cm)	Height (cm)
plexiglass plate at shake table level	0.654	30.48	10.80	1.24
plexiglass plate at 1st story level	0.654	30.48	10.80	1.24
plexiglass plate at 2nd story level	0.654	30.48	10.80	1.24
vertical aluminum plate in 1st story	0.236	50.17	10.80	0.18
vertical aluminum plate in 2nd story	0.236	50.17	10.80	0.18

Table 9.2 the equivalent concentrated floor mass of test structure

	m_1 (kg)	m_2 (kg)
equivalent concentrated floor mass	1.217	0.934

In order to determine the approximate "true" values of the structure story stiffness and damping coefficients, the test structure is dissembled and only one story substructure (with the pair of springs) is put on the shake table. A sine sweep test was carried out on this one story structure and the natural frequency corresponding to the maximum acceleration response was identified along with the half power bandwidth frequencies. Since the mass of this one story substructure is known (0.934 kg), the story stiffness and damping coefficient of this one story structure can be estimated to be 572 N/m and 0.29 N·sec/m, respectively, which are treated as the approximate true values of the story stiffness and damping coefficient of the original two-story test structure. Since both aluminum plates and diagonal springs are almost identical, hence, it is reasonable to assume that the story stiffness and damping coefficients of both stories in the test structure are the same, with values identified from the sine sweep test of the one-story structure.

9.3.2 Shaking Table

One of the key components of the experiments is a bench-scale shake table, shown in Figure 9.4. The shaking table is a small-scale uniaxial earthquake simulator manufactured by Quanser Consulting Inc. The table is located in the SHM and Control Lab at the University of Southern California (USC). The Quanser Shake Table is an instructional shake table device that was originally developed for the *University Consortium on Instructional Shake Tables* (UCIST). It can be used to teach structural dynamics, vibration isolation, feedback control, and various other topics for mechanical, aerospace, and civil engineers. The shake table is controlled by a personal computer with the interface software QuaRC® also provided by Quanser Consulting Inc. The design specifications of the shaking table, as supplied by the manufacturer, are shown in Table 9.3. The nominal operational frequency range of the simulator is 0–20 Hz. Because the shake table motor is inherently open loop unstable, position feedback, measured from the shake table motor, is employed to stabilize the table (Christenson *et al.*, 2003).

Table 9.3 Design specification of the shaking table

Specification	Value	Unit
Shake table system overall dimensions (L×W×H)	61×46×13	cm
Shake table system mass	27.2	kg
Table dimensions (payload area) (L×W)	46×46	cm
Maximum payload at 2.5*g*	15	kg
Peak displacement	±7.5	cm
Operational bandwidth	20	Hz
Peak acceleration	24.5	m/s^2
Accelerometer range	±49	m/s^2
Accelerometer sensitivity	1/9.81	Vs^2/m
Lead screw spread pitch	12.7	mm/rev
Brushless servo motor power	745.7	W
Maximum continuous current	12.5	A
Motor maximum torque	1.65	Nm
Linear bearing load carrying	131.5	kg
Linear bearing life expectancy (total travel)	6350	km
Lead screw encoder resolution	4096	counts/rev
	3.1	μm/count

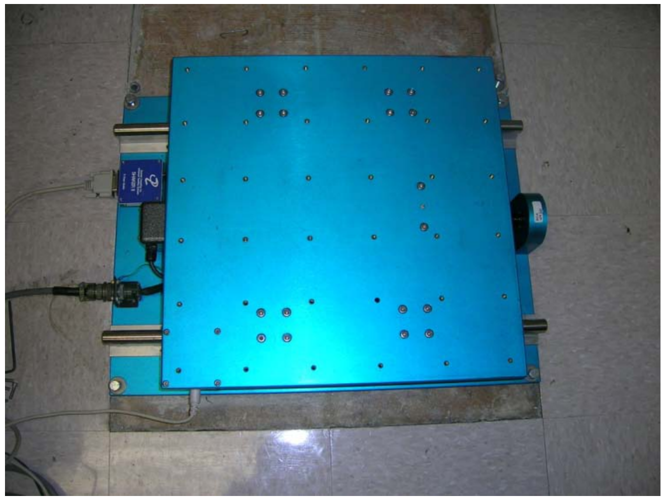

Figure 9.4 Quanser uniaxial shake table

9.3.3 Digital Control and Data Acquisition System

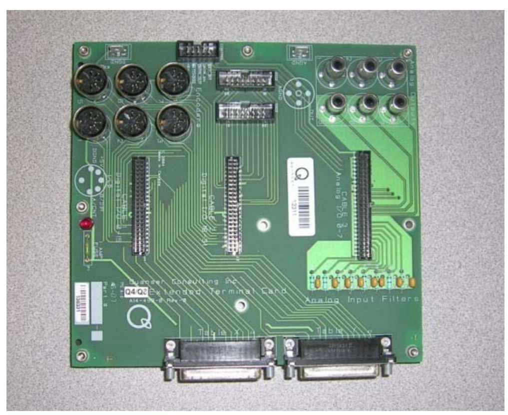

Figure 9.5 External connection board of Quanser Q4 board

The digital control and data acquisition system, used in the experiment, consists of both the hardware and the software. The main hardware of the system is Quanser Q4 hardware in the loop board (http://www.quanser.com/english/html/solutions/fs_Q4.html). This board supports 4×14 bits input analogue signal, 4×12 bits D/A analogue output, 4 quadrature encoder inputs, and 16 programmable I/O channels. It provides an ideal single-board solution for use in control system and complex measurement applications. There is another external board connecting the Quanser Q4 board via a ribbon cable to the outside input/output equipments, such as sensors, power module and electrical motor in the AMD system. The external board of the Quanser Q4 interface board, as shown in Figure 9.5, has six input and six output analog channels. Eight digital encoders are also available. The major software of this test system is the real time control software QuaRC® (http://www.quanser.com/english/html/solutions/fs_soln_software.html), also produced by Quanser Consulting Inc. QuaRC supports Matlab Simulink® models. The table control algorithm is developed using Simulink® under MATLAB 2009b and executed in real time using the QuaRC software. The Simulink code is converted to C++ code using the Real Time Workshop in MATLAB and interfaced through QuaRC® software to run the control algorithms on the CPU of the computer.

9.3.4 Accelerometer

The acceleration response of the structure during the experiment is measured by accelerometers. There are three accelerometers installed in the test systems. One is fixed to the table base level. Another two are fixed, one to each of the two stories in the middle bottom of the plexiglass plates at each floor. The range of the accelerometers is $\pm 5g$ with an output of ± 5 volts. Each accelerometer is connected via cable to the power module which is, in turn, connected to the external connection board.

Figure 9.6 the accelerometer installed at the floor level

9.4 Design of Passively Controlled Substructure Identification

9.4.1 Selection of Shake Table Excitation

During the shake table experiments, the test structure is assumed to be subject to the ambient ground excitation, induced by the shake table. The excitation of the shake table is determined by letting a white Gaussian process passing through a band-pass filter. The transfer function is shown in Equation (9.1).

$$H(s) = \frac{\omega_2^2 s^2}{(s^2 + 2\zeta_1\omega_1 s + \omega_1^2)(s^2 + 2\zeta_2\omega_2 s + \omega_2^2)} \tag{9.1}$$

where ω_1=12.6(radian/sec) and ω_2=27.7(radian/sec) are the low and high cut-off frequency of the band-pass filter respectively; ζ_1=0.6 and ζ_2=0.6 are the damper ratios of the filter. The magnitude of the ground band-pass filter is shown in Figure 9.7.

According to the previous theoretical analyses, the identification accuracy of proposed substructure identification methods is largely determined by the frequency responses of the interstory acceleration near the story substructure natural frequency.

Since the nominal values of the floor mass and story stiffness of the test structure are known, it is easy to calculate that the substructure natural frequencies of the two substructures, the first story substructure and the second story substructure, are around 21.6 (radian/sec) and 24.7 (radian/sec) respectively. The low and high cut-off frequencies of the bass-pass filter are selected such that both substructure natural frequencies are located in the pass-band frequency range of the filter. Therefore, the structural responses near the substructure natural frequencies can be fully excited, which will lead to more accurate estimation of the structural parameters.

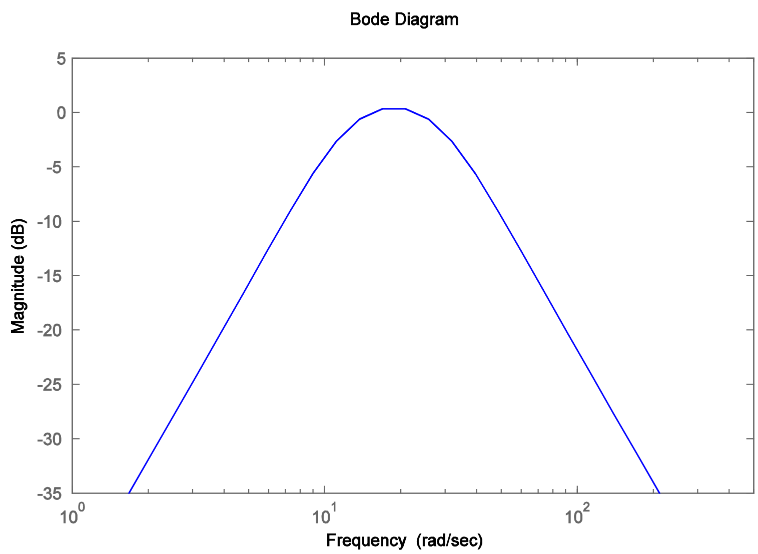

Figure 9.7 Magnitude of the band-pass filter

9.4.2 Design of Passive Control System

From the error analysis results, any control method that can amplify the interstory acceleration and minimize the interstory acceleration ratio (for non-top story identification only) near the story substructure natural frequency is theoretically able to improve the accuracy of substructure identification. Another important feature for the controlled substructure identification of a particular floor is that if the control force(s) does not directly apply on the floors being identified, the value of the control force will not be needed in the identification; as a result, the measurement error in the control force will not affects the accuracy of the controlled substructure identification and the controlled substructure identification at this floor will be very robust to such control system errors. Therefore, to ensure the robustness of the controlled identification, no control forces will be applied in the floor to be identified.

With this constraint, the possible selection of the passive control strategies that can be applied is limited in this simple structure. Three passive control system scenarios are considered in the experiments: to improve the accuracy of the second story parameter estimates, (1) the stiffness of the first story will be changed and (2) the mass of the first floor will be changed; when identifying the first story parameters, (3) the mass of the second floor will be changed. The reasons for these choices of “control” are explained above. It is worth pointing out here that, in full scale systems, these passive measures will be replaced by active or semiactive control systems, like an active mass driver (AMD) or variable stiffness and damping devices (VSDDs), which can apply similar control forces on the structure. However, in this simple study, equivalent passive methods will be used.

To guide the control system design procedure, two performance indexes are created as follows:

$$P_1(L) = \alpha \int_0^\infty \left| W_1(j\omega) \frac{1}{S_{(\ddot{x}_1 - \ddot{u}_g)y}} \right|^2 d\omega + (1-\alpha) \int_0^\infty \left| W_1(j\omega) \frac{S_{(\ddot{x}_2 - \ddot{x}_1)y}}{S_{(\ddot{x}_1 - \ddot{u}_g)y}} \right|^2 d\omega \tag{9.2}$$

$$P_2(L) = \int_0^\infty \left| W_2(j\omega) \frac{1}{S_{(\ddot{x}_2 - \ddot{x}_1)y}} \right|^2 d\omega \tag{9.3}$$

where $S_{\ddot{x}y}$ is the cross power spectral density between structural response $\ddot{x}$ and the reference y (y is fixed as the base excitation of the structure in this study); $P_i(L)$ is the performance index of the i^{th} story substructure identification, with smaller values indicating better identification accuracy; L denotes the control system parameters to be designed (here, these are the changes of the second floor mass and the first story stiffness or of the first floor mass); α is a weighting factor that balances the role of the SC system in achieving the two possible competing goals of changing structural responses, taken to be 0.8 in the following examples; and $W_i(j\omega)$ is a frequency weighting function, given as follows

$$W_i(j\omega) = \frac{-k_i}{(m_i\omega^2)\left[1 - jc_i/(m_i\omega - k_i/(m_i\omega^2)\right]^2} \tag{9.4}$$

The magnitude of this weighting function peaks around the story substructure natural frequency $\omega_{i0} = \sqrt{k_i/m_i}$ and quickly vanishes when further away. The role of this weighting function is to implicitly emphasize the importance of the structural responses $S_{(\ddot{x}_i - \ddot{x}_{i-1})y}$ and $S_{(\ddot{x}_{i+1} - \ddot{x}_i)y} / S_{(\ddot{x}_i - \ddot{x}_{i-1})y}$ around the frequency ω_{i0} and not attempt to change the response overall. Therefore, a smaller performance index corresponds to the large interstory acceleration and the small interstory acceleration ratio near its substructure natural frequency, which further corresponds to improved identification accuracy.

Figure 9.8 shows the change of the simulated performance index P_i with the change of the controlled structural parameters, more specifically the first story stiffness, the first floor mass and the second floor mass. Decreasing the first story stiffness and increasing the second story mass both decrease the performance indexes for the second and first story identification, respectively; this should result in more accurate identification. Changing the mass of the first floor has negligible effect on the performance index compared with the other two methods. Therefore, the final strategies for the control identification of the first and second story parameters are as follows. First, when identifying the second story parameters, additional stiffness will be added to the first story. Second, while identifying the second story parameters, the partial mass of the second floor will be removed. Both of these should decrease the performance index. However, in the original test structure no mass on the second floor can be taken off (since the floor mass is a solid plexiglass block and connection hardware). Therefore, an additional 0.62 kg mass is attached to the second floor of the structure. The structure with this additional mass will serve as the baseline (uncontrolled) structure. Then, when the first story parameters are to be identified, this additional mass will be removed to simulate the effect of the control systems.

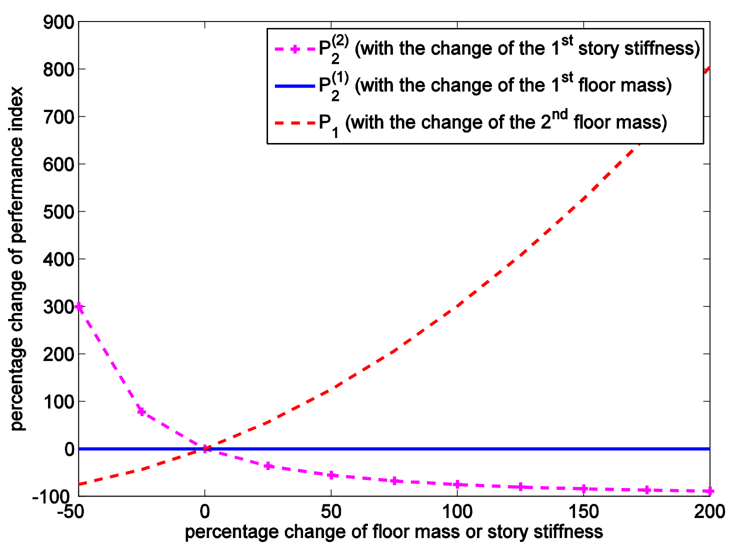

Figure 9.8 The change of the performance index

9.4.3 Experimental Procedure

The goal of this experiment is to verify that, by using several control systems, the substructure identification accuracy can be improved. Three groups of shake table experiments were performed with different configurations of the test structure.

1) Baseline structure: the original test structure with an additional mass attached on the second floor is used as the baseline (uncontrolled) structure — thus, the baseline structure has a second floor mass about 65% larger than the original test structure;
2) Control-1 structure: the additional mass on the second floor is removed (to help identify the first story parameters);
3) Control-2 structure: some additional springs are installed in the first story of the baseline structure (to help identify the second story parameters) — these newly-installed springs increase the first story stiffness by about 180%.

The baseline structure is used to identify the structural parameters of both stories, whereas the controlled structures 1 and 2 are only used to identify the first and second story parameters, respectively. For each structural configuration, ten independent shake table experiments are performed.

Tables 9.4, 9.5 and 9.6 show the (approximate) mass, stiffness and damping of the baseline, controlled 1 and controlled 2 structures respectively. Note that due to the limitation of the experiments the true values of the structure are indeed unknown; therefore, the structural parameters listed in the Tables, especially for stiffness and damping parameters, can by no means be regarded as the true parameter values of the structure. They only serve to point out the approximate range where the true structural parameters are located.

Table 9.4 The approximate structural parameter values of the baseline structure

story number	mass (kg)	stiffness (N/m)	damping (N·s/m)
1	1.217	572	0.29
2	1.549	572	0.29

Table 9.5 The approximate structural parameter values of the control-1 structure

story number	mass (kg)	stiffness (N/m)	damping (N·s/m)
1	1.217	572	0.29
2	0.934	572	0.29

Table 9.6 The approximate structural parameter values of the control-2 structure

story number	mass (kg)	stiffness (N/m)	damping (N·s/m)
1	1.217	n/a*	n/a*
2	1.549	572	0.29

* Additional springs are added to the 1st story, the exact stiffnesses of which are not measured. It is estimated that the combined stiffness of the added springs is around 180% of the story stiffness.

The commanded shake table excitation for all experiments is a white Gaussian random process passed through a band-pass filter with low-pass and high-pass cutoff frequencies at 2 Hz and 8 Hz, respectively. About 1800 seconds of structural responses, sampled at 1000 Hz, are measured and recorded. The reference response $y(t)$ is chosen to be the second floor acceleration because it has the largest responses near the substructure natural frequency of all three measurements (shaking table acceleration, the first and second floor accelerations). The MATLAB® function *cpsd* is used to calculate the power spectra of structural responses, which, in turn, are utilized to perform the substructure identification by using cross power spectral based substructure identification method.

When identifying the first story parameters, the second story parameters are required. Therefore, the mean values of the second story parameter estimates will be used in identifying the first story parameters. The statistics of the story stiffness estimates from all experiments are shown in Table 9.7.

9.5 Experimental Results

The identification error analysis of the substructure identification methods showed that the identification accuracy is closely related to the frequency response of the interstory acceleration near the story substructure natural frequency; larger response gives more accurate identification. Figures 9.9 and 9.10 show the changes of the frequency responses of the first and second interstory accelerations by the control systems.

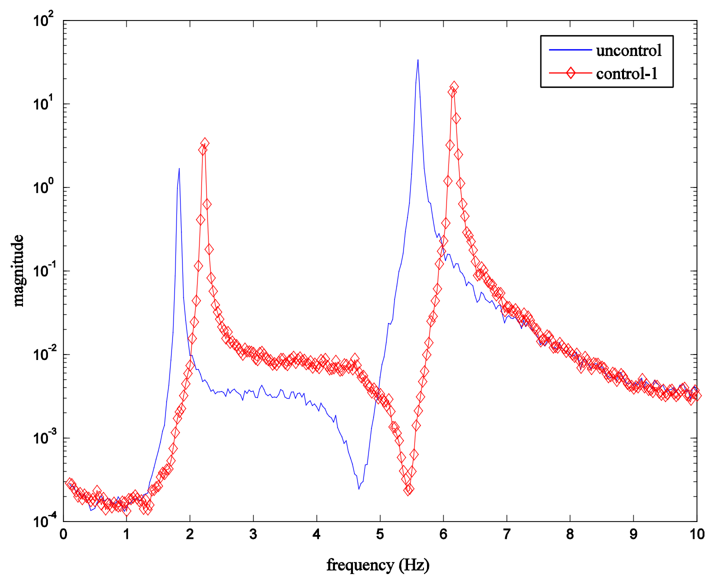

Figure 9.9 The power spectrum of the 1st interstory acceleration response of the uncontrolled and controlled structures

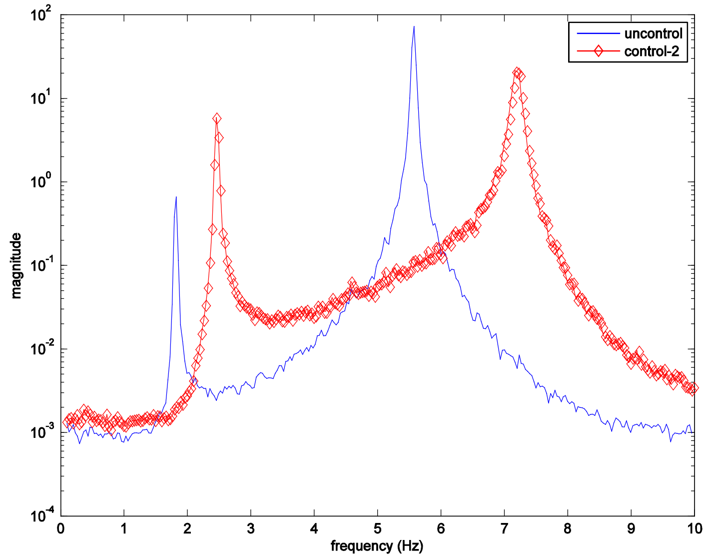

Figure 9.10 The power spectrum of the 2nd interstory acceleration response of the uncontrolled and controlled structures

Using the structural parameters of the baseline structure, it can be easily calculated that the substructure natural frequencies of the first and second story substructure are 3.4 and 3.1 Hz respectively. As shown in Figures 9.9 and 9.10, the two control systems largely amply the interstory acceleration response near those frequencies. Therefore, it is expected that the control systems will improve the identification accuracy.

Table 9.7 Statistics of the story stiffness estimates

Test Structure	k_1 [N/m]		k_2 [N/m]	
	Mean	COV	Mean	COV
baseline	660	12.7%	530	2.5%
control_1	538	2.9%	n/a	n/a
control_2	n/a	n/a	542	2.2%

COV: coefficient of variation

The results in Table 9.7 show that, compared with the baseline, the two control identification cases greatly reduce the variation in the identification results. Moreover, if the story stiffness of 572 N/m that was identified from the sine sweep excitation test is treated as an approximate true value for the stiffness of each of the two stories, the mean values of the story stiffness estimated from the controlled identification are closer to this "true" value. Therefore, the experimental results verify that the controlled substructure identification does provide more accurate estimates of the structural parameters than uncontrolled identification.

It is worth pointing out here that the passive control strategies used in these experiments, increasing the 1^{st} story stiffness by about 180% and decreasing the 2^{nd} floor mass by about 33%, do not represent feasible full scale control strategies. However, the experimental results do prove the validity of the theories of the substructure identification and the controlled substructure identification in a real application. Future experimental studies will focus on more realistic and efficient control strategies, such as using the AMD system to control the structural responses and improve the identification accuracy.

Chapter 10

Conclusion and Future Research

A shear structure, shown in Figure 10.1, is widely used to model the dynamic behaviors of building structures. Thus, developing efficient identification methods, which can accurately identify the parameters of a shear model, plays a vital role in establishing efficient and accurate SHM systems for building structures.

In this study, several innovative substructure identification and controlled substructure identification methods are proposed to accurately identify the parameters of shear structures, which form a solid foundation to design future efficient and accurate SHM system for building structures. The major achievements of this study are summarized in the following sections.

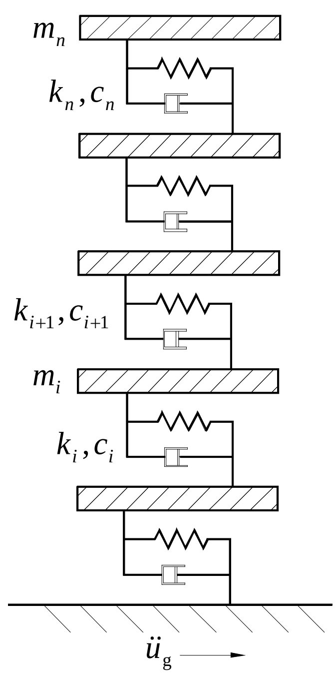

Figure 10.1 A shear structure

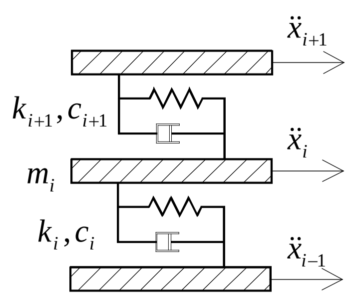

Figure 10.2 The two-story standard substructure

10.1 Summary of the Dissertation Work

10.1.1 Substructure Identification Methods for Shear Structures

Using the ‘divide and conquer’ strategy of substructure identification, a substructure identification method (FFT_SUBID) for shear structures is first developed in Chapter 3. A standard two-story substructure, shown in figure 10.2, is used to divide a large shear structure into many small substructures. An induction identification method is proposed from which the parameters of a shear structure are identified from top to bottom iteratively. In each sub-step of the identification, the Fourier transforms of two or three floor accelerations are utilized to formulate the substructure identification problem.

Due to the noisy nature of acceleration measurements, it turns out that FFT_SUBID method can provide accurate parameter estimation only when the noise level in the measurement is low. To improve the identification accuracy, a transfer function based method (TF_SUBID) is proposed in Chapter 4, which makes use of the transfer functions among different structural responses to construct the substructure identification problems. Simulation results show that the TF_SUBID method significantly improves the identification accuracy compared with the FFT_SUBID method, providing quite accurate estimates even when the measurement noise is fairly large (40% in terms of RMS value). Nonetheless, there are some shortcomings for the TF_SUBID method: 1) it requires that there be only one excitation sources in the structure. 2) The TF_SUBID method provides biased estimation of the structural parameters.

In order to further increase the identification accuracy, a new power spectrum based substructure method, the CSD_SUBID method, is proposed in Chapter 5. A reference response, wide sense stationary (WSS) with other structural responses, is introduced in this method. The cross power spectral densities are utilized to form the identification problems. Compared with previous two substructure identification methods, the CSD_SUBID method possesses some superb features. 1) It is an asymptotically unbiased and consistent estimator for the structural parameters, able to provide arbitrarily accurate estimates of the structural parameters given that enough long measurement records are available. 2) The explicit formulae to calculate the variance of the estimated parameters are developed, providing the optimal estimated parameters as well as information about their confidence range. 3) Although the CSD_SUBID method is originally developed based on the assumption that the reference and the structural responses are WSS, it is shown that the CSD_SUBID also works with non-stationary structural responses and still give very accurate estimates.

10.1.2 Controlled Substructure Identification

One of the great features of above three substructure methods is the analytical results showing how the identification error in each step is formed. The identification errors of these methods are simply controlled by two structural responses within a very narrow frequency band, centered at the substructure natural frequency of the story being identified. This important discovery gives the ability to easily improve the identification accuracy by changing the substructure responses via specially designed structural control systems.

Several controlled substructure identification methods were proposed, using different structural control systems to improve the identification accuracy of the substructure methods. Furthermore, since the accuracy of the proposed controlled substructure identification methods directly depends on the close-loop controlled structural responses rather than on the control systems themselves, it is shown that these controlled substructure identification methods are quite robust to possible control system errors; moreover, one of common control system errors, feedback measurement noise, may even have a tendency to improve the identification accuracy. The simulation results demonstrate that the structural parameters are more accurately identified by applying the controlled substructure identification methods and the identification results do not deteriorate even when large feedback measurement noise is presented.

10.1.3 Loop Substructure Identification Method

Two major difficulties of the substructure identification methods proposed in Chapters 3~5 are that 1) the structure floor mass must be known and 2) the structural responses of all floors above the story being identified must be measured. To overcome these two difficulties, a fast substructure identification method is developed in Chapter 7, which only makes use of the responses of the standard two-story standard substructure to formulate a loop-identification sequence and identify all four parameters of the substructure $[k_i \;\; c_i \;\; k_{i+1} \;\; c_{i+1}]$ once together even without knowing structural mass. This new method can directly, quickly and accurately identify any structural parameters in a large shear structure with as few as one set of substructure response data and no information about the structural mass, making it a very promising technique for many applications, such as immediate post-earthquake damage evaluation for buildings.

The analysis is carried out to find the convergence condition of the new loop-identification method; it is demonstrated that the convergence of the identified parameters cannot be achieved in the usual situation. To ensure the convergence of the loop identification, the method of controlled substructure identification is applied, in which two control systems are designed and used to control the structural response. The two controlled structural responses are alternately used in the loop identification, resulting in quick convergence of the identified parameters.

10.1.4 Substructure Identification for Frame Structures

In Chapters 3–7, the proposed substructure identification methods and their identification error analyses are all based on a fundamental assumption that the identified structure is a shear model structure. Although the shear model is widely used to model the dynamic behavior of frame structures, it is only a simplification of a complex real building structure. Furthermore, finding damage in complex real building structures is of much more practical interest than just identifying the parameter values in a shear model structure.

Using the methodology of substructuring, a substructure identification method for frame structures is successfully developed. The dynamic equilibrium of one floor substructure is used to formulate the identification problem, in which the equivalent story stiffness and damping coefficient parameters are identified. In addition to the horizontal floor responses, the rotational responses at beam-column joints are needed in the formulation of the new method. Surprisingly, the newly-formulated substructure identification method for frame structures has a format similar to the substructure identification methods for shear structures. As a consequence, the results of the identification error analysis can also be applied to the new frame substructure identification methods with some modifications. This new method can identify the structural damage occurring in the structural columns. The numerical simulation results also verify this conclusion.

10.1.5 Experiment Verification

To experimentally verify the effectiveness of the proposed substructure identification and controlled substructure identification methods, a series of experiments are carried out a bench-scale two-story shear structure model. Two substructure identification methods, FT_SUBID and PSD_SUBID, are tested on this structure. The results show that these two methods successfully identify the structural parameters. To test the effectiveness of the controlled substructure identification, some passive approaches are adopted to replicate the effects of the control system. These approaches include adding/removing the part of the floor mass and adding/removing the part of the structural story stiffness. Experimental results demonstrate that, by using the specially designed structural control systems, the identification accuracy of the structural parameters can be improved.

10.2 Future Research

Although significant improvements have been achieved in this study toward the ultimate goal of designing accurate and efficient SHM system for real building structures, there are still a lot of challenges ahead. Here are some critical areas needing further investigation.

10.2.1 Substructure Identification of Three Dimensional Shear Structures

The substructure identification methods developed in this work apply to general one dimensional shear buildings. However, real buildings are 3-dimensional; extending the substructure identification method to 3-D shear structure is a very important practical issue.

When the structure is symmetric (the center of gravity and the center of the stiffness are coincident for all floors), the structural responses can be decoupled into three independent motions (two horizontal and one rotational), and the substructure identification method can be used to identify the structural parameters in each direction separately. However, if the structure is asymmetric (by design or due to damage), the structural vibrations in the three directions will be coupled. How to decouple three substructure identifications and accurately identify the structural parameters requires further investigation.

10.2.2 Damage Detection of Frame Structures without Measuring Rotational Responses

The damage detection method for frame structures has been studied in Chapter 8 via identifying the equivalent story stiffness of the structure by using the substructure identification method. But this identification method requires that the rotational responses of all beam-column joints in the structure be measured, which is generally impractical. In practice, usually only the floor translational responses are measured. How to perform the parameter identification and damage detection in frame structures with only floor translational responses is another very important research direction.

10.2.3 Experimental Verification of Controlled Substructure Identification Using AMD Control System

In Chapter 9, the passive control approaches, changing the floor mass and the story stiffness, are tested to demonstrate that specially designed control systems can improve the accuracy of the substructure identification. However, changing the floor mass and the story stiffness does not represent a real achievable means of effecting dynamic changes in practice. In the future, more realistic control methods, such as controlling structural responses via the AMD system, should be conducted.

References

Adams RD, Cawley P, Pye CJ and Stone BJ (1978). "A vibration technique for non-destructively assessing the integrity of structures," *Journal of Mechanical Engineering Science*, **20**(2), 93−100.

Allemang RJ and Brown DL (1982). "Correlation coefficient for modal vector analysis," *Proceedings of the 1st International Modal Analysis Conference*, 110−116.

Amin M and Ang AHS (1968) "Nonstationary Stochastic Model of Earthquake Motions," *Proceedings of the American Society of Civil Engineers*, *Journal of the Engineering Mechanics Division*, **94**, 559–583.

Avitabile P and Pechinsky F (1994). "Coordinate Orthogonality Check (CORTHOG)," *Proceedings of International Modal Analysis Conference of sound and vibration*, 753−760.

Bendat JS and Piersol, AG (2000). *Random data: Analysis and measurement procedures* (3rd edition), Wiley, New York.

Bartlett MS (1948)."Smoothing periodograms from time series with continuous spectral," *Nature*, **161**(5), 686−687.

Beck JL (1978). "Determining models of structures from earthquake records," *Report EERL78-01*, California Institute of Technology.

Beck JL and Katafygiotis LS (1998). "Updating Models and Their Uncertainties. Part I: Bayesian Statistical Framework," *Journal of Engineering Mechanics*, **124**(4), 455−461.

Bernal D (2000). "Extracting Flexibility Matrices from State-Space Realizations," *Proceedings of European COST F3 Conference on System Identification and Structural Health Monitoring*, 127−135.

Bernal D (2006). "Flexibility-based damage localization from stochastic realization results," *Journal of Engineering Mechanics*, **132**(6), 651−658.

Bernal D (2010). "Load vectors for damage location in systems identified from operational loads," *Journal of Engineering Mechanics*, **136**(1), 31−39.

Brechlin E, Bendel K and Keiper W (1998). "A New Scaled Modal Assurance Criterion for Eigenmodes Containing Rotational Degrees of Freedom," *Proceedings of International Seminar on Modal Analysis*, 197−206.

Brincker R, Anderson P, Kirkegaard PH and Ulfkjaer JP (1995). "Damage Detection in Laboratory Concrete Beams," *Proceeding of the 13th International Modal Analysis Conference*, 1, 668−674.

Caicedo JM, Dyke SJ and Johnson EA (2004). "Natural Excitation Technique and Eigensystem Realization Algorithm for Phase I of the IASC-ASCE Benchmark Problem: Simulated Data," *Journal of Engineering Mechanics*, **130**(1), 49−60.

Cawley P and Adams RD (1979). "The location of defects in structures from measurements of natural frequencies," *Journal of Strain Analysis*, **14**(2), 49−57.

Chang PC and Liu SC (2003). "Recent Research in Nondestructive Evaluation of Civil infrastructure," *Journal of Material of Civil Engineering* **15**(3), 298−304.

Christenson RE, Spencer BF, Hori N and Seto K (2003). "Coupled Building Control Using Acceleration Feedback," *Computer-Aided civil and infrastructure Engineering*, **18**(1), 4−18.

De Callafon RA, Moaveni B, Ponte JP, He X and Udd E. (2008) "General realization algorithm for modal identification of linear dynamic systems," *Journal of Engineering Mechanics*, **134**(9), 712−722.

Doebling SW, Farrar CR, Prime MB and Shevitz DW (1996). "Damage Identification and Health Monitoring of Structural and Mechanical Systems from Changes in Their Vibration Characteristics: A Literature Review", *Los Alamos National Laboratory Report*, LA-13070-MS, 1996.

Dyke SJ, Spencer BF, Sain MK and Carlson JD (1996). "Modeling and control of magnetorheological damper for seismic response reduction," *Smart Materials and Structures*, **5**(5), 565−575.

Elmasry MIS and Johnson EA (2002). "Parametric Frequency Domain Identification in Multiconfiguration Structures," *15th ASCE Engineering Mechanics Conference* (EM2002), 444−452.

Elmasry MIS (2005). "Health Monitoring of Structures under Ambient Vibrations Using Semiactive Devices," *Ph.D. dissertation, University of Southern California*, Los Angeles, CA.

Farrar CR, Doebling SW and Nix DA (2001). "Vibration-based structural damage identification," *Philosophical Transactions: Mathematical, Physical and Engineering Sciences*, **359**(1778), 131−149.

Farrar CR, Baker WE, Bell TM, Cone KM, Darling TW, Duffey TA, Eklund A and Migliori A (1994). "Dynamic Characterization and Damage Detection in the I-40 Bridge Over the Rio Grande," *Los Alamos National Laboratory report*, LA-12767-MS, 1994.

Farrar CR and Worden K (2007). "An introduction to structural health monitoring," *Philosophical Transaction of the Royal Society A*, **365**, 303−315.

Fanning P and Carden EP (2003). “A damage detection algorithm based on SISO measurements,” *Journal of Engineering Mechanics*, **129**(2), 202−209.

Fanning P and Carden EP (2004). “Experimentally validated added mass identification algorithm based on frequency response functions,” *Journal of Engineering Mechanics*, **130**(9), 1045−1051.

Frýba L and Pirner M (2001). “Load tests and modal analysis of bridges,” *Engineering Structures*, **23**, 102−109.

Fotsch D and Ewins DJ (2000). “Applications of MAC in the Frequency Domain,” *Proceedings of International Modal Analysis Conference*, 1225−1231

Fotsch D and Ewins DJ (2001). “Further Applications of the FMAC,” *Proceedings of International Modal Analysis Conference*, 635−639.

Ghanem R and Ferro G (2006). “Health monitoring for strongly non-linear systems using the Ensemble Kalman Filter,” *Structural Control and Health Monitoring*, 13(1), 245−259.

Hernandez-Garcia MR, Masri SF, Ghanem R, Figueiredo E and Farrar CR (2010). “An experimental investigation of change detection in uncertain chain-like systems,” *Journal of Sound and Vibration*, **239**(12), 395−409.

Heylen W and Lammens S (1996). “FRAC: A Consistent way of Comparing Frequency Response Functions,” *Proceeding of International Conference on Identification in Engineering*, Swansea, 48−57.

Heylen W (1990). “Extensions of the Modal Assurance Criterion,” *Journal of Vibrations and Acoustics*, **112**, 468−472.

Hoshiya M and Saito E (1984). “Structural identification by extended Kalman filter,” *Journal of Engineering Mechanics*, **110**(12), 1757−1771.

Hou J, Jankowski L and Ou J (2010). “Substructure Damage Identification Using Time Series of Local Measured Response,” *5th World Conference on Structural Control and Monitoring*, 178.

Housner GW, Soong TT and Masri SF (1994). “Second Generation of Active Structural Control in Civil Engineering,” *Microcomputer in Civil Engineering*, **11**(5), 289−296.

Housner GW, Bergman LA, Caughey TK, Chassiakos AG, Claus RO, Masri SF, Skelton RE, Soong TT, Spencer BF and Yao JTP (1997). “Structural Control: Past Present, and Future,” *Journal of Engineering Mechanics*, ASCE, **123**,897−971.

Huang CS and Yeh CH, (1999). “Some properties of randomdec signatures,” *Mechanical Systems and Signal Processing*, **13**(3), 491−507.

Hayes MH (1996). *Statistical Digital Signal Processing and Modeling*, Wiley, New York.

James GH, Carne TG and Lauffer JP (1993). "The natural excitation technique for modal parameter extraction from operating wind turbines," *Rep. No. SAND92-1666*, *UC-261*, Sandia National Laboratories, Sandia, N.M.

Jaynes ET (1968). "Prior probabilities," *IEEE transaction, System, Science & Cybernetics*, SSC-4, 227–241.

Jiang LJ, Tang J and Wang KW (2007). "An optimal sensitivity-enhancing feedback control approach via eigenstructure assignment for structural damage identification," *Journal of Vibration and Acoustics*, **129**(6), 771−783.

Johnson EA and Erkus B (2007). "Dissipativity and performance analysis of smart dampers via LMI synthesis," *Structural Control and Heath Monitoring*, **14**(3), 471−496.

Juang JN and Pappa RS (1985). "An Eigensystem Realization Algorithm For Modal Parameter Identification and Model Reduction," *Journal of Guidance Control and Dynamics*, **8**(5) 620−627.

Juang JN, Cooper JE and Wright JR (1988). "Eigensystem Realization Algorithm using data correlations (ERA/DC) for modal parameter identification," *Control, theory and advanced technology*, **4**(1), 5−14.

Kim JT and Stubbs N (1995). "Model-uncertainty impact and damage-detection accuracy in plate girder," *Journal of Structural Engineering*, **121**(10), 1409−1417.

Koh BH and Ray LR (2004). "Feedback controller design for sensitivity based damage localization," *Journal of Sound and Vibration*, **273**(1–2), 317−335.

Koh CG, See LM and Balendra T (1991). "Estimation of structural parameters in time domain: A substructure approach," *Earthquake Engineering & Structural Dynamics*, **20**(8), 787−801.

Koh CG and Shankar K (2003). "Substructural identification method without interface measurement," *Journal of Engineering Mechanics*, **129**(7), 769−776.

Law SS, Shi ZY and Zhang LM (1998). "Structural damage detection from incomplete and noisy modal test data," *Journal of Engineering Mechanics*, **124**(11), 1280−1288.

Lee U and Shin J (2002). "A frequency response function-based structural damage identification method," *Computers and Structures,* **80**(2), 117−132.

Lew JS and Juang JN (2002). "Structural damage detection using virtual passive controllers," *Journal of Guidance, Control and Dynamics*, **25**(3), 419−424.

Li GQ, Hao KC, Lu Y and Chen SW (1999). “A flexibility approach for damage identification of cantilever-type structures with bending and shear deformation,” *Computers and Structures*, **73**(6), 565−572.

Lieven NAJ and Ewins DJ (1988). “Spatial correlation of mode spaces: the coordinate modal assurance criterion (COMAC)”, *Proceedings of the 6th International Modal Analysis Conference*, 1063−1070.

Ljung L (1999). *System identification: Theory for the User* (2nd edition), Prentice Hall, Engelwood Cliffs, New Jersey.

Mahalanobis PC (1936). “On the generalized distance in statistics,” *Proceedings of the National Institute of Sciences of India* **2**(1): 49−55.

Masri SF, Berkey GA and Sassi H (1982). “Non-parametric Identification of a Class of Non-linear Multi-degree Dynamic Systems,” *Earthquake Engineering and Structural Dynamics*, **10**(1), 1−30.

Nayeri RD, Masri SF, Rhanem RG and Nigbor RL (2008). “A Novel Approach for the Structural Identification and Monitoring of A Full-scale 17-story Building Based on Ambient Vibration Measurements,” *Smart Materials and Structures*, **17**(2), 1−19.

Pintelon R and Schoukens J (2001). *System Identification: A Frequency Domain Approach*, Wiley-IEEE Press.

Quanser (2010). "Bench-Scale Shake Tables Move Earthquake Engineering Education to New Heights." Web page http://quanser.com/english/downloads/products/Earthquake/Quanser_EEC_PIS_v8_web.pdf accessed 30 October 2010.

Ramallo JC, Johnson EA and Spencer BF (2002). “Smart base isolation systems,” *Journal of Engineering Mechanics*, **128**(10), 1088−1099.

Rytter A (1993). “Vibration Based Inspection of Civil Engineering Structures,” Ph. D. Dissertation, Department of Building Technology and Structural Engineering, Aalborg University, Denmark.

Salawu OS and Williams C (1995). “Bridge assessment using forced-vibration testing”, *Journal of Structural Engineering*, **121**(2), 161−173.

Salawu OS (1997). “Detection of structural damage through changes in frequency: a review,” *Engineering Structures*, **19**(9), 718−723.

Shinozuka M, Yun CB and Imai HS (1982). “Identification of Linear Structural Dynamics Systems,” *Journal of the Engineering Mechanics Division*, **108**(12), 1371−1390.

Sohn H, Farrar CR, Hemez FM, Shunk DD, Stinemates DW and Nadler BR (2003). “Review of Structural Health Monitoring Literature: 1996-2001.” *Los Alamos National Laboratory Report*, *LA-13976-MS*, 2003.

Solbeck JA and Ray LR (2006). “Damage identification using sensitivity- enhancing control and identified models,” *Journal of Vibration and Acoustics*, **128**(2), 210−220.

Stubbs N, Broome TH and Osegueda R (1990a). “Nondestructive Construction Error Detection in Large Space Structures,” *AIAA Journal*, **28**(1), 146−152.

Stubbs N and Osegueda R (1990b). “Global Non-Destructive Damage Evaluation in Solids,” *Modal Analysis: The International Journal of Analytical and Experimental Modal Analysis*, **5**(2), 67−79.

Tee KF, Koh CG and Quek ST (2005). “Substructural first- and second-order model identification for structural damage assessment,” *Earthquake Engineering and Structural Dynamics*, **34**(15), 1755−1775.

Udwadia FE, Sharma DK and Shah PC (1978). “Uniqueness of Damping and Stiffness Distributions in the Identification of Soil and Structural Systems,” *Journal of Applied Mechanics*, **45**(3), 181−187.

Wahab MMA and De Roeck G (1999). “Damage detection in bridges using modal curvatures: applications to a real damage scenario,” *Journal of Sound and Vibration*, **226**(2), 217−235.

Wei JC, Wang W and Allemang RJ (1990). “Model Correlation and Orthogonality Criteria Based on Reciprocal Modal Vectors,” *Proceedings of SAE Noise and Vibration Conference*, 607−616.

West WM (1984). “Illustration of the Use of Modal Assurance Criterion to Detect Structural Changes in an Orbiter Test Specimen,” *Proceeding of Air Force Conference on Aircraft Structural Integrity*, 1–6.

Whittome TR and Dodds CJ (1983). “Monitoring Offshore Structures by Vibration Techniques,” *Proceeding of Design in Offshore Structures Conference*, 93−100.

Wylie CR and Barrett LC(1982). *Advanced Engineering Mathematics* (5th edition). McGraw-Hill Inc.

Wu M and Smyth AW (2007). “Application of the unscented Kalman filter for real-time nonlinear structural system identification,” *Structural Control and Health Monitoring*, **14**(7), 971−990.

Yang JSC and Caldwell D (1976). “Measurement of damping and the detection of damages in structures by the random decrement technique,” *Shock and Vibration Bulletin*, **46**(4), 129−136.

Yan YJ, Yam LH, Cheng L and Yu L (2006). “FEM modeling method of damage structures for structural damage detection,” *Composite Structures*, **72**(2), 193−199.

Yang JN, Pan S and Huang H (2007). “An adaptive extended Kalman filter for structural damage identifications II: unknown inputs,” *Structural Control and Health Monitoring*, **14**(3), 497−521.

Yuen KV and Katafygiotis LS (2006). “Substructure identification and health monitoring using noisy response measurements only,” *Computer-Aided Civil and Infrastructure Engineering*, **21**(4), 280−291.

Yun CB and Lee HJ (1997). “Substructural Identification for Damage Estimation of Structures,” *Structural Safety*, **19**(1), 121−140.

Zheng H and Mita A (2008). “ Damage indicator defined as the distance between ARMA models for structural health monitoring,” *Structural Control and Health Monitoring*, **15**(7), 992−1005.

Appendices

Appendix A: The Properties of Circular Complex Gaussian Random Variables

Lemma 1

Let $x(n)$ ($n=0,\ldots,N-1$) be a real zero-mean discrete-time Gaussian white random process, then

1) The discrete Fourier transform X_k of $x(n)$, evaluated at the discrete frequency $2\pi k/N$, is a circular complex Gaussian variable, which means that the real part and the imaginary part of X_k are jointly Gaussian, independent of each other, and with equal variance.

2) If $k\neq j$ are two arbitrary nonnegative integers no more than $(N-1)/2$, the discrete Fourier transform of $x(n)$ evaluated at two different discrete frequencies $2\pi k/N$ and $2\pi j/N$, X_k and X_j, are independent.

3) If X_k is a circular complex Gaussian random variable and A be a constant complex number, then AX_k is a circular complex Gaussian random variable.

4) If X_k and X_j are two independent circular complex Gaussian random variables, then X_k+X_j is a circular complex Gaussian random variable.

5) If a real random process $y(n)$ is the combined output of several independent real zero-mean white Gaussian processes passing through a linear system, then

   a) The discrete Fourier transform of $y(n)$ evaluated at certain discrete frequency, Y_k, is circular complex Gaussian variable;

b) The discrete Fourier transform of $y(n)$ evaluate at two different discrete frequencies, Y_k and Y_j ($j\neq k$), are independent.

Proof:

Before beginning to prove the lemma, the following Equation (A1) is proved first.

$$\sum_{n=0}^{N-1} e^{-2\pi\cdot i\cdot kn/N} = \begin{cases} N & k=0 \\ 0 & k\in\{-N+1,\cdots,-1,1,\cdots,N-1\} \end{cases} \tag{A1}$$

<u>Proof for (A1)</u>

If k=0,

$$\sum_{n=0}^{N-1} e^{-2\pi\cdot i\cdot kn/N} = \sum_{n=0}^{N-1} e^{0} = \sum_{n=0}^{N-1} 1 = N$$

If $k\neq 0$

$$\sum_{n=0}^{N-1} e^{-2\pi\cdot i\cdot kn/N} = \sum_{n=0}^{N-1}\left(e^{-2\pi\cdot i\cdot k/N}\right)^{n} = \left(1-e^{-2\pi\cdot i\cdot k}\right)/\left(1-e^{-2\pi\cdot i\cdot k/N}\right)$$
$$=(1-1)/\left(1-e^{-2\pi\cdot i\cdot k/N}\right)=0$$

QED

<u>Proof for (1)</u>

Since $x(n)$ si a zero mean white Gaussian random process, therefore

$$\mathrm{E}[x(n)]=0,\quad \mathrm{E}[x(m)x(n)]=\delta_{mn}=\begin{cases}0, & m\neq n \\ 1, & m=n\end{cases}$$

The Fourier transform of process $x(n)$ can be calculated as

$$X_k = \sum_{n=0}^{N-1} x(n) e^{-2\pi\cdot i\cdot kn/N} \quad (k=0,\ldots,N-1)\,,$$

$$\mathrm{Re}[X_k] = \sum_{n=0}^{N-1} x(n)\cos\left(-\frac{2\pi}{N}kn\right), \quad \mathrm{Im}[X_k] = \sum_{n=0}^{N-1} x(n)\sin\left(-\frac{2\pi}{N}kn\right)$$

Since the process $x(n)$ is a Gaussian process, $\mathrm{Re}[X_k]$ and $\mathrm{Im}[X_k]$ are Gaussian random variables and the mean, covariance and covariance of these two random variables can be evaluated as follows,

$$\mathrm{E}\{\mathrm{Re}[X_k]\} = \sum_{n=0}^{N-1} \mathrm{E}\{x(n)\}\cos\left(-\frac{2\pi}{N}kn\right) = 0$$

$$\mathrm{E}\{\mathrm{Im}[X_k]\} = \sum_{n=0}^{N-1} \mathrm{E}\{x(n)\}\sin\left(-\frac{2\pi}{N}kn\right) = 0$$

$$\mathrm{E}\{\mathrm{Re}[X_k]\cdot \mathrm{Im}[X_k]\} = \sum_{n=0}^{N-1}\sum_{m=0}^{N-1} \mathrm{E}[x(n)x(m)]\cos\left(-\frac{2\pi}{N}km\right)\sin\left(-\frac{2\pi}{N}kn\right)$$

$$= \sum_{n=0}^{N-1} \cos\left(-\frac{2\pi}{N}kn\right)\sin\left(-\frac{2\pi}{N}kn\right)$$

$$= \frac{1}{-4i}\sum_{n=0}^{N-1}\left(e^{2\pi\cdot i\cdot kn/N} + e^{-2\pi\cdot i\cdot kn/N}\right)\left(e^{2\pi\cdot i\cdot kn/N} - e^{-2\pi\cdot i\cdot kn/N}\right)$$

$$= \frac{1}{-4i}\sum_{n=0}^{N-1}\left(e^{4\pi\cdot i\cdot kn/N} - e^{-4\pi\cdot i\cdot kn/N}\right) = 0 \qquad \text{(because of Equation (A1))} \tag{A2}$$

$$\mathrm{VAR}\{\mathrm{Re}[X_k]\} = \mathrm{E}\{\mathrm{Re}[X_k]^2\} = \sum_{n=0}^{N-1}\sum_{m=0}^{N-1} \mathrm{E}[x(n)x(m)]\cos\left(-\frac{2\pi}{N}kn\right)\cos\left(-\frac{2\pi}{N}km\right)$$

$$= \sum_{n=0}^{N-1} \cos^2\left(-\frac{2\pi}{N}kn\right) = \frac{1}{4}\sum_{n=0}^{N-1}\left(e^{2\pi\cdot i\cdot kn/N} + e^{-2\pi\cdot i\cdot kn/Nn}\right)^2$$

$$= \frac{1}{4}\sum_{n=0}^{N-1}\left(e^{4\pi\cdot i\cdot kn/N} + e^{-4\pi\cdot i\cdot kn/N} + 2\right) = \frac{1}{2}N \tag{A3}$$

$$\mathrm{VAR}\{\mathrm{Im}[X_k]\} = \mathrm{E}\{\mathrm{Im}[X_k]^2\} = \sum_{n=0}^{N-1}\sum_{m=0}^{N-1} \mathrm{E}[x(n)x(m)]\sin\left(-\frac{2\pi}{N}kn\right)\sin\left(-\frac{2\pi}{N}km\right)$$

$$= \sum_{n=0}^{N-1} \sin^2\left(-\frac{2\pi}{N}kn\right) = \frac{1}{-4}\sum_{n=0}^{N-1}\left(e^{2\pi\cdot i\cdot kn/N} - e^{-2\pi\cdot i\cdot kn/N}\right)^2$$

$$= \frac{1}{-4}\sum_{n=0}^{N-1}\left(e^{4\pi\cdot i\cdot kn/N} + e^{-4\pi\cdot i\cdot kn/N} - 2\right) = \frac{1}{2}N \tag{A4}$$

According to the results for Equation (A2), (A3) and (A4), $\mathrm{Re}[X_k]$ and $\mathrm{Im}[X_k]$ are zero-mean and mutually independent Gaussian random variables and their variances are

$$\mathrm{VAR}\{\mathrm{Re}[X_k]\} = \mathrm{VAR}\{\mathrm{Im}[X_k]\} = \mathrm{E}\left[|X_k|^2/2\right].$$

QED

Proof for (2):

$$X_k = \sum_{n=0}^{N-1} x(n)e^{-2\pi\cdot i\cdot kn/N}, \ \mathrm{Re}[X_k] = \sum_{n=0}^{N-1} x(n)\cos\left(-\frac{2\pi}{N}kn\right), \ \mathrm{Im}[X_k] = \sum_{n=0}^{N-1} x(n)\sin\left(-\frac{2\pi}{N}kn\right)$$

$$X_j = \sum_{n=0}^{N-1} x(n)e^{-2\pi\cdot i\cdot jn/N}, \ \mathrm{Re}[X_j] = \sum_{n=0}^{N-1} x(n)\cos\left(-\frac{2\pi}{N}jn\right), \ \mathrm{Im}[X_j] = \sum_{n=0}^{N-1} x(n)\sin\left(-\frac{2\pi}{N}jn\right)$$

Since X_k and X_j are zero-mean complex, the covariance of these two random variables is

$$\begin{aligned}\mathrm{COV}\{X_k X_j\} &= \mathrm{E}\{(\mathrm{Re}[X_k] + i\cdot\mathrm{Im}[X_k])(\mathrm{Re}[X_j] + i\cdot\mathrm{Im}[X_j])\} \\ &= \mathrm{E}\{\mathrm{Re}[X_k]\cdot\mathrm{Re}[X_j]\} + i\cdot\mathrm{E}\{\mathrm{Re}[X_k]\cdot\mathrm{Im}[X_j]\} + \\ &\quad i\cdot\mathrm{E}\{\mathrm{Im}[X_k]\cdot\mathrm{Re}[X_j]\} - \mathrm{E}\{\mathrm{Im}[X_k]\cdot\mathrm{Im}[X_j]\}\end{aligned} \tag{A5}$$

The four expected values of the production of the real and imaginary parts of X_k and X_j in the above equation can be calculated as follows

$$\mathrm{E}\{\mathrm{Re}[X_k]\cdot\mathrm{Im}[X_j]\} = \sum_{n=0}^{N-1}\sum_{m=0}^{N-1}\mathrm{E}[x(n)x(m)]\cos\left(-\frac{2\pi}{N}km\right)\sin\left(-\frac{2\pi}{N}jn\right)$$

$$= \sum_{n=0}^{N-1} \cos\left(-\frac{2\pi}{N}kn\right)\sin\left(-\frac{2\pi}{N}jn\right) = \frac{1}{-4i}\sum_{n=0}^{N-1}\left(e^{2\pi\cdot i\cdot kn/N} + e^{-2\pi\cdot i\cdot kn/N}\right)\left(e^{2\pi\cdot i\cdot jn/N} - e^{-2\pi\cdot i\cdot jn/N}\right)$$

$$= \frac{1}{4i}\sum_{n=0}^{N-1}\left(e^{2\pi\cdot i\cdot(k+j)n/N} - e^{2\pi\cdot i\cdot(k-j)n/N} + e^{2\pi\cdot i\cdot(j-k)n/N} - e^{-2\pi\cdot i\cdot(k+j)n/N}\right) = 0 \qquad \text{(A6)}$$

Since $(k+j),(k-j),(j-k),(-k-j) \in \{-N+1,\cdots,-1,1,\cdots,N-1\}$, using the result of (A1) it is easy to get the final result of (A6).

$$\mathrm{E}\{\mathrm{Re}[X_k]\cdot\mathrm{Re}[X_j]\} = \sum_{n=0}^{N-1}\sum_{m=0}^{N-1}\mathrm{E}[x(n)x(m)]\cos\left(-\frac{2\pi}{N}km\right)\cos\left(-\frac{2\pi}{N}jn\right)$$

$$= \sum_{n=0}^{N-1} \cos\left(-\frac{2\pi}{N}kn\right)\cos\left(-\frac{2\pi}{N}jn\right) = \frac{1}{4}\sum_{n=0}^{N-1}\left(e^{2\pi\cdot i\cdot kn/N} + e^{-2\pi\cdot i\cdot kn/N}\right)\left(e^{2\pi\cdot i\cdot jn/N} + e^{-2\pi\cdot i\cdot jn/N}\right)$$

$$= \frac{1}{4}\sum_{n=0}^{N-1}\left(e^{2\pi\cdot i\cdot(k+j)n/N} + e^{2\pi\cdot i\cdot(k-j)n/N} + e^{2\pi\cdot i\cdot(j-k)n/N} + e^{-2\pi\cdot i\cdot(k+j)n/N}\right) = 0 \qquad \text{(A7)}$$

$$\mathrm{E}\{\mathrm{Im}[X_k]\cdot\mathrm{Im}[X_j]\} = \sum_{n=0}^{N-1}\sum_{m=0}^{N-1}\mathrm{E}[x(n)x(m)]\sin\left(-\frac{2\pi}{N}km\right)\sin\left(-\frac{2\pi}{N}jn\right)$$

$$= \sum_{n=0}^{N-1} \sin\left(-\frac{2\pi}{N}kn\right)\sin\left(-\frac{2\pi}{N}jn\right) = \frac{1}{-4}\sum_{n=0}^{N-1}\left(e^{2\pi\cdot i\cdot kn/N} - e^{-2\pi\cdot i\cdot kn/N}\right)\left(e^{2\pi\cdot i\cdot jn/N} - e^{-2\pi\cdot i\cdot jn/N}\right)$$

$$= \frac{1}{-4}\sum_{n=0}^{N-1}\left(e^{2\pi\cdot i\cdot(k+j)n/N} - e^{2\pi\cdot i\cdot(k-j)n/N} - e^{2\pi\cdot i\cdot(j-k)n/N} + e^{-2\pi\cdot i\cdot(k+j)n/N}\right) = 0 \qquad \text{(A8)}$$

Putting the results form Equations (A6)~(A8) back into (A5)

$$\mathrm{COV}\{X_k X_j\} = 0 \quad (j \neq k)$$

Therefore, X_k and X_j are independent if $j \neq k$.

QED

Proof for (3):

Let $A=a+b\cdot i$,

$$\mathrm{Re}[AX_k]=a\,\mathrm{Re}[X_k]-b\,\mathrm{Im}[X_k],\ \mathrm{Im}[AX_k]=a\,\mathrm{Im}[X_k]+b\,\mathrm{Re}[X_k]$$

Since X_k is a circular complex Gaussian random variable, $\mathrm{Re}[X_k]$ and $\mathrm{Im}[X_k]$ are independent, zero mean, and $\mathrm{VAR}\{\mathrm{Re}[X_k]\}=\mathrm{VAR}\{\mathrm{Im}[X_k]\}=\sigma^2/2$.

$$\mathrm{E}\{\mathrm{Re}[AX_k]\}=a\mathrm{E}\{\mathrm{Re}[X_k]\}-b\mathrm{E}\{\mathrm{Im}[X_k]\}=0$$

$$\mathrm{E}\{\mathrm{Im}[AX_k]\}=a\mathrm{E}\{\mathrm{Im}[X_k]\}+b\mathrm{E}\{\mathrm{Re}[X_k]\}=0$$

$$\mathrm{VAR}\{\mathrm{Re}[AX_k]\}=a^2\mathrm{VAR}\{\mathrm{Re}[X_k]\}+b^2\mathrm{VAR}\{\mathrm{Im}[X_k]\}=(a^2+b^2)\sigma^2/2$$

$$\mathrm{VAR}\{\mathrm{Im}[AX_k]\}=a^2\mathrm{VAR}\{\mathrm{Im}[X_k]\}+b^2\mathrm{VAR}\{\mathrm{Re}[X_k]\}=(a^2+b^2)\sigma^2/2$$

Therefore, AX_k is a circular complex Gaussian random variable.

QED

Proof for (4):

Since X_k and X_j are independent, Re[X_k], Re[X_j], Im[X_k] and Im[X_j] are independent of one another.

$\mathrm{Re}[X_k+X_j]=\mathrm{Re}[X_k]+\mathrm{Re}[X_j]$ are independent of $\mathrm{Im}[X_k+X_j]=\mathrm{Im}[X_k]+\mathrm{Im}[X_j]$.

It is also easy to verify that $\mathrm{VAR}\{\mathrm{Re}[X_k+X_j]\}=\mathrm{VAR}\{\mathrm{Im}[X_k+X_j]\}=\mathrm{E}\{|X_k+X_j|^2\}/2$.

Therefore, X_k+X_j is a circular complex Gaussian random variable.

QED

Proof for (5a):

$$Y_k = \sum_{m=1}^{p} H_m\left(e^{2\pi\cdot i\cdot k/N}\right)\cdot X_k^{(m)}$$

where $H_m(e^{2\pi ik/N})$ is the transfer function from the m^{th} input to the output evaluated at frequency $2\pi k/N$, $X_k^{(m)}$ is the discrete Fourier transform of the m^{th} input evaluated at frequency $2\pi k/N$.

Using the results from lemmas (1), (3) and (4), it can be easily shown that Y_k is a circular complex Gaussian random variable with the described properties.

QED

Proof for (5b):

$$Y_k = \sum_{m=1}^{p} H_m\left(e^{2\pi\cdot i\cdot k/N}\right)\cdot X_k^{(m)}\ ;\ Y_j = \sum_{m=1}^{p} H_m\left(e^{2\pi\cdot i\cdot k/N}\right)\cdot X_j^{(m)}$$

According to the result from Lemma 1(2) that $X_k^{(m)}$ and $X_j^{(m)}$ are independent for any m if $k \neq j$, Y_k and X_j are independent.

QED

Appendix B: Proof of Equations (5.21a)~(5.21i)

Before the formal proof of Equations (5.21a)~(5.21e), the following lemma is proved first.

Lemma 1

Given the four assumptions in section 5.5, the following properties hold:

$$\mathrm{E}\left[N_{\ddot{x}_j y,l} \big/ S_{(\ddot{x}_n-\ddot{x}_{n-1})y,l}\right]=0 \quad j\in\{n-1,n\} \text{ and } l\in Z[1,N] \tag{a}$$

$$\mathrm{E}\left[\frac{N_{\ddot{x}_j y,l}}{S_{(\ddot{x}_n-\ddot{x}_{n-1})y,l}}\frac{N_{\ddot{x}_k y,m}}{S_{(\ddot{x}_n-\ddot{x}_{n-1})y,m}}\right]=0 \quad \forall j,k\in\{n-1,n\} \text{ and } l,m\in Z[1,N] \tag{b}$$

$$\mathrm{E}\left\{\frac{N_{\ddot{x}_j y,l}}{S_{(\ddot{x}_n-\ddot{x}_{n-1})y,l}}\left[\frac{N_{\ddot{x}_k y,m}}{S_{(\ddot{x}_n-\ddot{x}_{n-1})y,m}}\right]^*\right\}=\delta_{lm}\delta_{jk}\mathrm{E}\left[\frac{\left|N_{\ddot{x}_j y,l}\right|^2}{\left|S_{(\ddot{x}_n-\ddot{x}_{n-1})y,l}\right|^2}\right] \quad j,k\in\{n-1,n\} \text{ and } l,m\in Z[1,N] \tag{c}$$

where Z[1,*N*] denotes a set containing natural numbers from 1 to *N*.

<u>Proof for Lemma 1(a)</u>

$$\begin{aligned}
\mathrm{E}\left[N_{\ddot{x}_j y,l} \big/ S_{(\ddot{x}_n-\ddot{x}_{n-1})y,l}\right] &= \mathrm{E}\left[\frac{\sum_{q=1}^{Q}\left(Y_l^{(q)}+N_{y,l}^{(q)}\right)^*\left(\ddot{X}_{j,l}^{(q)}+N_{\ddot{x}_j,l}^{(q)}\right)-\sum_{q=1}^{Q}Y_l^{(q)*}\ddot{X}_j^{(q)}}{\sum_{q=1}^{Q}Y_l^{(q)*}\left(\ddot{X}_{n,l}^{(q)}-\ddot{X}_{n-1,l}^{(q)}\right)}\right] \\
&= \mathrm{E}\left[\frac{\sum_{q=1}^{Q}\left(Y_l^{(q)*}N_{\ddot{x}_j,l}^{(q)}+N_{y,l}^{(q)*}\ddot{X}_{j,l}^{(q)}+N_{y,l}^{(q)*}N_{\ddot{x}_j,l}^{(q)}\right)}{\sum_{q=1}^{Q}Y_l^{(q)*}\left(\ddot{X}_{n,l}^{(q)}-\ddot{X}_{n-1,l}^{(q)}\right)}\right] \\
&= \mathrm{E}\left[\frac{\sum_{q=1}^{Q}Y_l^{(q)*}N_{\ddot{x}_j,l}^{(q)}}{\sum_{q=1}^{Q}Y_l^{(q)*}\left(\ddot{X}_{n,l}^{(q)}-\ddot{X}_{n-1,l}^{(q)}\right)}\right]+\mathrm{E}\left[\frac{\sum_{q=1}^{Q}N_{y,l}^{(q)*}\ddot{X}_{j,l}^{(q)}}{\sum_{q=1}^{Q}Y_l^{(q)*}\left(\ddot{X}_{n,l}^{(q)}-\ddot{X}_{n-1,l}^{(q)}\right)}\right]+\mathrm{E}\left[\frac{\sum_{q=1}^{Q}N_{y,l}^{(q)*}N_{\ddot{x}_j,l}^{(q)}}{\sum_{q=1}^{Q}Y_l^{(q)*}\left(\ddot{X}_{n,l}^{(q)}-\ddot{X}_{n-1,l}^{(q)}\right)}\right]
\end{aligned} \tag{B1}$$

The first term in the above equation equals zero, which can be proved as follows

$$\mathrm{E}\left[\frac{\sum_{q=1}^{Q} Y_l^{(q)*} N_{\ddot{x}_j,l}^{(q)}}{\sum_{q=1}^{Q} Y_l^{(q)*}\left(\ddot{X}_{n,l}^{(q)} - \ddot{X}_{n-1,l}^{(q)}\right)}\right] = \sum_{p=1}^{Q}\left\{\mathrm{E}\left[\frac{Y_l^{(p)*}}{\sum_{q=1}^{Q} Y_l^{(q)*}\left(\ddot{X}_{n,l}^{(q)} - \ddot{X}_{n-1,l}^{(q)}\right)}\right]\cdot \mathrm{E}\left[N_{\ddot{x}_j,l}^{(p)}\right]\right\}$$

$$= \sum_{p=1}^{Q}\left\{\mathrm{E}\left[\frac{Y_l^{(p)*}}{\sum_{q=1}^{Q} Y_l^{(q)*}\left(\ddot{X}_{n,l}^{(q)} - \ddot{X}_{n-1,l}^{(q)}\right)}\right]\cdot 0\right\} = 0 \tag{B2}$$

The first equality in the above equation uses the assumption that the measurement noise is independent of the true structural responses. Similarly, the second and third terms in Equation (B1) also equal zero, assuming y is not $\ddot{x}_j$ (*i.e.*, following the selection rules of section 5.4).

Therefore, $\mathrm{E}\left[N_{\ddot{x}_j y,l} / S_{(\ddot{x}_n - \ddot{x}_{n-1})y,l}\right] = 0 \quad j \in \{n-1, n\}$ and $l \in Z[1, N]$

QED

Proof for Lemma 1(b)

$$\mathrm{E}\left[\frac{N_{\ddot{x}_j y,l}}{S_{(\ddot{x}_n - \ddot{x}_{n-1})y,l}} \frac{N_{\ddot{x}_k y,m}}{S_{(\ddot{x}_n - \ddot{x}_{n-1})y,m}}\right]$$

$$= \mathrm{E}\left[\frac{\left[\sum_{q=1}^{Q}\left(Y_l^{(q)*} N_{\ddot{x}_j,l}^{(q)} + N_{y,l}^{(q)*}\ddot{X}_{j,l}^{(q)} + N_{y,l}^{(q)*} N_{\ddot{x}_j,l}^{(q)}\right)\right]}{\sum_{q=1}^{Q} Y_l^{(q)*}\left(\ddot{X}_{n,l}^{(q)} - \ddot{X}_{n-1,l}^{(q)}\right)} \frac{\left[\sum_{p=1}^{Q}\left(Y_m^{(p)*} N_{\ddot{x}_k,m}^{(p)} + N_{y,m}^{(p)*}\ddot{X}_{k,m}^{(p)} + N_{y,m}^{(p)*} N_{\ddot{x}_k,m}^{(p)}\right)\right]}{\sum_{p=1}^{Q} Y_m^{(p)*}\left(\ddot{X}_{n,m}^{(p)} - \ddot{X}_{n-1,m}^{(p)}\right)}\right]$$

$$= \mathrm{E}\left[\frac{\sum_{q=1}^{Q}\sum_{p=1}^{Q} Y_l^{(q)*} N_{\ddot{x}_j,l}^{(q)} Y_m^{(p)*} N_{\ddot{x}_k,m}^{(p)}}{\left[\sum_{q=1}^{Q} Y_l^{(q)*}\left(\ddot{X}_{n,l}^{(q)} - \ddot{X}_{n-1,l}^{(q)}\right)\right]\left[\sum_{p=1}^{Q} Y_m^{(p)*}\left(\ddot{X}_{n,m}^{(p)} - \ddot{X}_{n-1,m}^{(p)}\right)\right]}\right] + \text{other 8 terms} \tag{B3}$$

The first term in the above equation can be simplified as

$$\begin{aligned}
&\mathrm{E}\left[\frac{\sum_{q=1}^{Q}\sum_{p=1}^{Q}Y_l^{(q)^*}N_{\ddot{x}_j,l}^{(q)}Y_m^{(p)^*}N_{\ddot{x}_k,m}^{(p)}}{\left[\sum_{q=1}^{Q}Y_l^{(q)^*}\left(\ddot{X}_{n,l}^{(q)}-\ddot{X}_{n-1,l}^{(q)}\right)\right]\left[\sum_{p=1}^{Q}Y_m^{(p)^*}\left(\ddot{X}_{n,m}^{(p)}-\ddot{X}_{n-1,m}^{(p)}\right)\right]}\right] \\
&=\sum_{q=1}^{Q}\sum_{p=1}^{Q}\left\{\mathrm{E}\left[\frac{Y_l^{(q)^*}Y_m^{(p)^*}}{\left[\sum_{q=1}^{Q}Y_l^{(q)^*}\left(\ddot{X}_{n,l}^{(q)}-\ddot{X}_{n-1,l}^{(q)}\right)\right]\left[\sum_{p=1}^{Q}Y_m^{(p)^*}\left(\ddot{X}_{n,m}^{(p)}-\ddot{X}_{n-1,m}^{(p)}\right)\right]}\right]\cdot\mathrm{E}\left[N_{\ddot{x}_j,l}^{(q)}N_{\ddot{x}_k,m}^{(p)}\right]\right\}
\end{aligned} \tag{B4}$$

Applying the assumption that the measurement noise is a white Gaussian process, it can easily be shown that

$$\mathrm{E}\left[N_{\ddot{x}_j,l}^{(q)}N_{\ddot{x}_k,m}^{(p)}\right]=0 \quad \forall j,k\in\{n-1,n\}\ \&\ \forall l,m\in Z[1,N]\ \&\ \forall p,q\in Z[1,Q] \tag{B5}$$

Applying the result of Equation B5, Equation B4 can finally be simplified as

$$\mathrm{E}\left[\frac{\sum_{q=1}^{Q}\sum_{p=1}^{Q}Y_l^{(q)^*}N_{\ddot{x}_j,l}^{(q)}Y_m^{(p)^*}N_{\ddot{x}_k,m}^{(p)}}{\left[\sum_{q=1}^{Q}Y_l^{(q)^*}\left(\ddot{X}_{n,l}^{(q)}-\ddot{X}_{n-1,l}^{(q)}\right)\right]\left[\sum_{p=1}^{Q}Y_m^{(p)^*}\left(\ddot{X}_{n,m}^{(p)}-\ddot{X}_{n-1,m}^{(p)}\right)\right]}\right]=0 \tag{B6}$$

Following similar steps, it can be shown that other eight terms in Equation B3 are all equal to zero.

Therefore,

$$\mathrm{E}\left[\frac{N_{y\ddot{x}_j,l}}{S_{y(\ddot{x}_n-\ddot{x}_{n-1}),l}}\frac{N_{y\ddot{x}_k,m}}{S_{y(\ddot{x}_n-\ddot{x}_{n-1}),m}}\right]=0 \quad \begin{array}{l} j,k\in\{n-1,n\}\text{ and } l,m\in Z[1,N] \\ \text{and } j\neq k \text{ and } l\neq m \\ \text{and } y \text{ is neither } \ddot{x}_j \text{ nor } \ddot{x}_k \end{array}$$

QED

Proof for Lemma 1(c)

$$\mathrm{E}\left[\frac{N_{\ddot{x}_j y,l}}{S_{(\ddot{x}_n-\ddot{x}_{n-1})y,l}}\frac{N_{\ddot{x}_k y,m}{}^*}{S_{(\ddot{x}_n-\ddot{x}_{n-1})y,m}{}^*}\right]$$

$$=\mathrm{E}\left[\frac{\left[\sum_{q=1}^{Q}Y_l^{(q)*}N_{\ddot{x}_j,l}^{(q)}+N_{y,l}^{(q)*}\ddot{X}_{j,l}^{(q)}+N_{y,l}^{(q)*}N_{\ddot{x}_j,l}^{(q)}\right]}{\sum_{q=1}^{Q}Y_l^{(q)*}\left(\ddot{X}_{n,l}^{(q)}-\ddot{X}_{n-1,l}^{(q)}\right)}\frac{\left[\sum_{p=1}^{Q}Y_m^{(p)*}N_{\ddot{x}_k,m}^{(p)}+N_{y,m}^{(p)*}\ddot{X}_{k,m}^{(p)}+N_{y,m}^{(p)*}N_{\ddot{x}_k,m}^{(p)}\right]^*}{\left[\sum_{p=1}^{Q}Y_m^{(p)*}\left(\ddot{X}_{n,m}^{(p)}-\ddot{X}_{n-1,m}^{(p)}\right)\right]^*}\right]$$

$$=\mathrm{E}\left[\frac{\sum_{q=1}^{Q}\sum_{p=1}^{Q}\left\{\begin{aligned}&Y_l^{(q)*}N_{\ddot{x}_j,l}^{(q)}Y_m^{(p)}N_{\ddot{x}_k,m}^{(p)}{}^*+Y_l^{(q)*}N_{\ddot{x}_j,l}^{(q)}N_{y,m}^{(p)}\ddot{X}_{k,m}^{(p)*}+Y_l^{(q)*}N_{\ddot{x}_j,l}^{(q)}N_{y,m}^{(p)}N_{\ddot{x}_k,m}^{(p)}{}^*\\&+N_{y,l}^{(q)*}\ddot{X}_{j,l}^{(q)}Y_m^{(p)}N_{\ddot{x}_k,m}^{(p)}{}^*+N_{y,l}^{(q)*}\ddot{X}_{j,l}^{(q)}N_{y,m}^{(p)}\ddot{X}_{k,m}^{(p)*}+N_{y,l}^{(q)*}\ddot{X}_{j,l}^{(q)}N_{y,m}^{(p)}N_{\ddot{x}_k,m}^{(p)}{}^*\\&+N_{y,l}^{(q)*}N_{\ddot{x}_j,l}^{(q)}Y_m^{(p)}N_{\ddot{x}_k,m}^{(p)}{}^*+N_{y,l}^{(q)*}N_{\ddot{x}_j,l}^{(q)}N_{y,m}^{(p)}\ddot{X}_{k,m}^{(p)*}+N_{y,l}^{(q)*}N_{\ddot{x}_j,l}^{(q)}N_{y,m}^{(p)}N_{\ddot{x}_k,m}^{(p)}{}^*\end{aligned}\right\}}{\left[\sum_{q=1}^{Q}Y_l^{(q)*}\left(\ddot{X}_{n,l}^{(q)}-\ddot{X}_{n-1,l}^{(q)}\right)\right]\left[\sum_{p=1}^{Q}Y_m^{(p)*}\left(\ddot{X}_{n,m}^{(p)}-\ddot{X}_{n-1,m}^{(p)}\right)\right]^*}\right] \quad \text{(B7)}$$

Given the assumption that measurement noises are white Gaussian processes and the noise from different measurements are statistically independent, it can be easily shown that

$$\mathrm{E}\left[N_{\ddot{x}_j,l}^{(q)}N_{\ddot{x}_k,m}^{(p)}{}^*\right]=\delta_{jk}\delta_{lm}\delta_{pq}\mathrm{E}\left[\left|N_{\ddot{x}_j,l}\right|^2\right] \quad \begin{aligned}&\forall j,k\in\{n-1,n\}\text{ and }\forall l,m\in Z[1,N]\\&\text{and }\forall p,q\in Z[1,Q]\end{aligned} \quad \text{(B8)}$$

Utilizing the result of Equation (B8), Equation (B7) are simplified as

$$\mathrm{E}\left\{\frac{N_{\ddot{x}_j y,l}}{S_{(\ddot{x}_n-\ddot{x}_{n-1})y,l}}\left[\frac{N_{\ddot{x}_k y,m}}{S_{(\ddot{x}_n-\ddot{x}_{n-1})y,m}}\right]^*\right\}=\delta_{lm}\delta_{jk}\mathrm{E}\left[\frac{\left|N_{\ddot{x}_j y,l}\right|^2}{\left|S_{(\ddot{x}_n-\ddot{x}_{n-1})y,l}\right|^2}\right] \quad j,k\in\{n-1,n\}\text{ and }l,m\in Z[1,N]$$

QED

With the results from Lemma 1, Equation (5.21a)~(5.21i) are proved as follows

Proof for Equation 5.21a

$$\begin{aligned}\mathrm{E}\left[\varepsilon_{kn,l}\right] &= W_{11,l}\,\mathrm{E}\left[N_{\ddot{x}_{n-1}y,l}\big/S_{(\ddot{x}_n-\ddot{x}_{n-1})y,l}\right] + W_{12,l}\,\mathrm{E}\left[N_{\ddot{x}_n y,l}\big/S_{(\ddot{x}_n-\ddot{x}_{n-1})y,l}\right] \\ &= W_{11,l}\times 0 + W_{12,l}\times 0 = 0\end{aligned}$$

QED

Proof for Equation 5.21b

$$\begin{aligned}\mathrm{E}\left[\varepsilon_{cn,l}\right] &= W_{21,l}\,\mathrm{E}\left[N_{\ddot{x}_{n-1}y,l}\big/S_{(\ddot{x}_n-\ddot{x}_{n-1})y,l}\right] + W_{22,l}\,\mathrm{E}\left[N_{\ddot{x}_n y,l}\big/S_{(\ddot{x}_n-\ddot{x}_{n-1})y,l}\right] \\ &= W_{21,l}\times 0 + W_{22,l}\times 0 = 0\end{aligned}$$

QED

Proof for Equation 5.21c

$$\mathrm{E}\left[\varepsilon_{kn,l}\varepsilon_{kn,m}\right] = \mathrm{E}\left\{\begin{array}{l}\left[W_{11,l}\ N_{\ddot{x}_{n-1}y,l}\big/S_{(\ddot{x}_n-\ddot{x}_{n-1})y,l} + W_{12,l}\ N_{\ddot{x}_n y,l}\big/S_{(\ddot{x}_n-\ddot{x}_{n-1})y,l}\right] \\ \times\left[W_{11,m}\ N_{\ddot{x}_{n-1}y,m}\big/S_{(\ddot{x}_n-\ddot{x}_{n-1})y,m} + W_{12,m}\ N_{\ddot{x}_n y,m}\big/S_{(\ddot{x}_n-\ddot{x}_{n-1})y,m}\right]\end{array}\right\}$$

$$= W_{11,l}W_{11,m}\mathrm{E}\left[\frac{N_{\ddot{x}_{n-1}y,l}}{S_{(\ddot{x}_n-\ddot{x}_{n-1})y,l}}\cdot\frac{N_{\ddot{x}_{n-1}y,m}}{S_{(\ddot{x}_n-\ddot{x}_{n-1})y,m}}\right] + W_{11,l}W_{12,m}\mathrm{E}\left[\frac{N_{\ddot{x}_{n-1}y,l}}{S_{(\ddot{x}_n-\ddot{x}_{n-1})y,l}}\cdot\frac{N_{\ddot{x}_n y,m}}{S_{(\ddot{x}_n-\ddot{x}_{n-1})y,m}}\right]$$

$$+ W_{12,l}W_{11,m}\mathrm{E}\left[\frac{N_{\ddot{x}_n y,l}}{S_{(\ddot{x}_n-\ddot{x}_{n-1})y,l}}\cdot\frac{N_{\ddot{x}_{n-1}y,m}}{S_{(\ddot{x}_n-\ddot{x}_{n-1})y,m}}\right] + W_{12,l}W_{12,m}\mathrm{E}\left[\frac{N_{\ddot{x}_n y,l}}{S_{(\ddot{x}_n-\ddot{x}_{n-1})y,l}}\cdot\frac{N_{\ddot{x}_n y,m}}{S_{(\ddot{x}_n-\ddot{x}_{n-1})y,m}}\right]$$

$$= 0$$

Lemma 1(b) is used to simplify the results of the above equation. QED

Proof for Equation 5.21d

$$\mathrm{E}\left[\varepsilon_{kn,l}\varepsilon^{*}_{kn,m}\right] = \mathrm{E}\left\{\begin{array}{l}\left[W_{11,l}\ N_{\ddot{x}_{n-1}y,l}\big/S_{(\ddot{x}_n-\ddot{x}_{n-1})y,l} + W_{12,l}\ N_{\ddot{x}_n y,l}\big/S_{(\ddot{x}_n-\ddot{x}_{n-1})y,l}\right] \\ \times\left[W_{11,m}\ N_{\ddot{x}_{n-1}y,m}\big/S_{(\ddot{x}_n-\ddot{x}_{n-1})y,m} + W_{12,m}\ N_{\ddot{x}_n y,m}\big/S_{(\ddot{x}_n-\ddot{x}_{n-1})y,m}\right]^{*}\end{array}\right\}$$

$$= W_{11,l}W_{11,m}{}^{*}\mathrm{E}\left[\frac{N_{\ddot{x}_{n-1}y,l}}{S_{(\ddot{x}_n-\ddot{x}_{n-1})y,l}}\cdot\frac{N_{\ddot{x}_{n-1}y,m}{}^{*}}{S_{(\ddot{x}_n-\ddot{x}_{n-1})y,m}{}^{*}}\right] + W_{11,l}W_{12,m}{}^{*}\mathrm{E}\left[\frac{N_{\ddot{x}_{n-1}y,l}}{S_{(\ddot{x}_n-\ddot{x}_{n-1})y,l}}\cdot\frac{N_{\ddot{x}_n y,m}{}^{*}}{S_{(\ddot{x}_n-\ddot{x}_{n-1})y,m}{}^{*}}\right]$$

$$+ W_{12,l}W_{11,m}{}^{*}\mathrm{E}\left[\frac{N_{y\ddot{x}_n,l}}{S_{(\ddot{x}_n-\ddot{x}_{n-1})y,l}}\cdot\frac{N_{y\ddot{x}_{n-1},m}{}^{*}}{S_{(\ddot{x}_n-\ddot{x}_{n-1})y,m}{}^{*}}\right] + W_{12,l}W_{12,m}{}^{*}\mathrm{E}\left[\frac{N_{\ddot{x}_n y,l}}{S_{(\ddot{x}_n-\ddot{x}_{n-1})y,l}}\cdot\frac{N_{\ddot{x}_n y,m}{}^{*}}{S_{(\ddot{x}_n-\ddot{x}_{n-1})y,m}{}^{*}}\right]$$

$$= \left|W_{11,l}\right|^2\mathrm{E}\left[\left|N_{\ddot{x}_{n-1}y,l}\right|^2\Big/\left|S_{(\ddot{x}_n-\ddot{x}_{n-1})y,l}\right|^2\right] + \left|W_{12,l}\right|^2\mathrm{E}\left[\left|N_{\ddot{x}_n y,l}\right|^2\Big/\left|S_{(\ddot{x}_n-\ddot{x}_{n-1})y,l}\right|^2\right]$$

Lemma 1(c) is used to obtain the simplified result of the above equation. QED

The proof of Equation 5.21e is similar to the proof for Equation 5.21c.

The proof of Equation 5.21f is similar to the proof for Equation 5.21d.

The proof of Equation 5.21g is similar to the proof for Equation 5.21c.

The proof of Equation 5.21h is similar to the proof for Equation 5.21d.

The proof of Equation 5.21i is similar to the proof for Equation 5.21d.

Appendix C: Proof of Equation (5.22)~(5.26)

Proof for Equation 5.22

$$\mathrm{E}[\theta_{kn}] = \frac{1}{2}\sum_{l=1}^{N}\left\{\mathrm{E}[\varepsilon_{kn,l}] + \mathrm{E}[\varepsilon_{kn,l}^{*}]\right\} = \frac{1}{2}\sum_{l=1}^{N}\{0+0\} = 0$$

The result of Equation (5.21a) is used for this proof. QED

Proof for Equation 5.23

$$\mathrm{E}[\theta_{cn}] = \frac{1}{2}\sum_{l=1}^{N}\left\{\mathrm{E}[\varepsilon_{cn,l}] + \mathrm{E}[\varepsilon_{cn,l}^{*}]\right\} = \frac{1}{2}\sum_{l=1}^{N}\{0+0\} = 0$$

The result of Equation (5.21b) is used in this proof. QED

Proof for Equation 5.24

$$\begin{aligned}
\mathrm{VAR}[\theta_{kn}] &= \frac{1}{4}\mathrm{E}\left\{\sum_{l=1}^{N}\left[\varepsilon_{kn,l} + \varepsilon_{kn,l}^{*}\right]\right\}^{2} \\
&= \frac{1}{4}\sum_{l=1}^{N}\sum_{m=1}^{N}\mathrm{E}[\varepsilon_{kn,l}\varepsilon_{kn,m}] + \frac{1}{4}\sum_{l=1}^{N}\sum_{m=1}^{N}\mathrm{E}[\varepsilon_{kn,l}^{*}\varepsilon_{kn,m}^{*}] + \frac{1}{2}\sum_{l=1}^{N}\sum_{m=1}^{N}\mathrm{E}[\varepsilon_{kn,l}\varepsilon_{kn,m}^{*}] \\
&= \frac{1}{2}\sum_{l=1}^{N}\left\{|W_{11,l}|^{2}\mathrm{E}\left[|N_{\ddot{x}_{n-1}y,l}|^{2} \Big/ |S_{(\ddot{x}_{n}-\ddot{x}_{n-1})y,l}|^{2}\right] + |W_{12,l}|^{2}\mathrm{E}\left[|N_{\ddot{x}_{n}y,l}|^{2} \Big/ |S_{(\ddot{x}_{n}-\ddot{x}_{n-1})y,l}|^{2}\right]\right\}
\end{aligned}$$

The results of Equation (5.21c) & (5.21d) are used for this proof. QED

Proof for Equation 5.25

$$\begin{aligned}
\mathrm{VAR}[\theta_{cn}] &= \frac{1}{4}\mathrm{E}\left\{\sum_{l=1}^{N}\left[\varepsilon_{cn,l} + \varepsilon_{cn,l}^{*}\right]\right\}^{2} \\
&= \frac{1}{4}\sum_{l=1}^{N}\sum_{m=1}^{N}\mathrm{E}[\varepsilon_{cn,l}\varepsilon_{cn,m}] + \frac{1}{4}\sum_{l=1}^{N}\sum_{m=1}^{N}\mathrm{E}[\varepsilon_{cn,l}^{*}\varepsilon_{cn,m}^{*}] + \frac{1}{2}\sum_{l=1}^{N}\sum_{m=1}^{N}\mathrm{E}[\varepsilon_{cn,l}\varepsilon_{cn,m}^{*}] \\
&= \frac{1}{2}\sum_{l=1}^{N}\left\{|W_{21,l}|^{2}\mathrm{E}\left[|N_{\ddot{x}_{n-1}y,l}|^{2} \Big/ |S_{(\ddot{x}_{n}-\ddot{x}_{n-1})y,l}|^{2}\right] + |W_{22,l}|^{2}\mathrm{E}\left[|N_{\ddot{x}_{n}y,l}|^{2} \Big/ |S_{(\ddot{x}_{n}-\ddot{x}_{n-1})y,l}|^{2}\right]\right\}
\end{aligned}$$

The results of Equation (5.21e) & (5.21f) are used for this proof. QED

Proof for Equation 5.26

$$\mathrm{COV}[\theta_{kn}\theta_{cn}] = \frac{1}{4}\mathrm{E}\left\{\sum_{l=1}^{N}\left[\varepsilon_{kn,l} + \varepsilon_{kn,l}^{*}\right]\sum_{m=1}^{N}\left[\varepsilon_{cn,m} + \varepsilon_{cn,m}^{*}\right]\right\}$$

$$= \frac{1}{4}\sum_{l=1}^{N}\sum_{m=1}^{N}\mathrm{E}\left[\varepsilon_{kn,l}\varepsilon_{cn,m}\right] + \frac{1}{4}\sum_{l=1}^{N}\sum_{m=1}^{N}\mathrm{E}\left[\varepsilon_{kn,l}^{*}\varepsilon_{cn,m}^{*}\right] + \frac{1}{4}\sum_{l=1}^{N}\sum_{m=1}^{N}\mathrm{E}\left[\varepsilon_{kn,l}\varepsilon_{cn,m}^{*}\right] + \frac{1}{4}\sum_{l=1}^{N}\sum_{m=1}^{N}\mathrm{E}\left[\varepsilon_{kn,l}^{*}\varepsilon_{cn,m}\right]$$

$$= \frac{1}{4}\sum_{l=1}^{N}\left\{W_{11,l}W_{21,l}^{*}\mathrm{E}\left[\left|N_{\ddot{x}_{n-1}y,l}\right|^{2} \Big/ \left|S_{(\ddot{x}_n-\ddot{x}_{n-1})y,l}\right|^{2}\right] + W_{21,l}W_{22,l}^{*}\mathrm{E}\left[\left|N_{\ddot{x}_{n}y,l}\right|^{2} \Big/ \left|S_{(\ddot{x}_n-\ddot{x}_{n-1})y,l}\right|^{2}\right]\right\}$$

$$+ \frac{1}{4}\sum_{l=1}^{N}\left\{W_{11,l}^{*}W_{21,l}\mathrm{E}\left[\left|N_{\ddot{x}_{n-1}y,l}\right|^{2} \Big/ \left|S_{(\ddot{x}_n-\ddot{x}_{n-1})y,l}\right|^{2}\right] + W_{21,l}^{*}W_{22,l}\mathrm{E}\left[\left|N_{\ddot{x}_{n}y,l}\right|^{2} \Big/ \left|S_{(\ddot{x}_n-\ddot{x}_{n-1})y,l}\right|^{2}\right]\right\}$$

$$= \frac{1}{2}\sum_{l=1}^{N}\left\{\mathrm{Re}\left[W_{11,l}W_{21,l}^{*}\right]\mathrm{E}\left[\left|N_{\ddot{x}_{n-1}y,l}\right|^{2} \Big/ \left|S_{(\ddot{x}_n-\ddot{x}_{n-1})y,l}\right|^{2}\right] + \mathrm{Re}\left[W_{21,l}W_{22,l}^{*}\right]\mathrm{E}\left[\left|N_{\ddot{x}_{n}y,l}\right|^{2} \Big/ \left|S_{(\ddot{x}_n-\ddot{x}_{n-1})y,l}\right|^{2}\right]\right\}$$

The results of Equation (5.21g), (5.21h) and (5.21i) are used in the second-to-last step of the proof. Recalling the expression of factors $W_{11,l}$, $W_{12,l}$, $W_{21,l}$ and $W_{22,l}$ in Equation (3.26), it can easily be shown that

$$\mathrm{Re}\left[W_{11,l}W_{21,l}^{*}\right] = \mathrm{Re}\left[W_{21,l}W_{22,l}^{*}\right] = 0$$

Therefore, $\mathrm{COV}[\theta_{kn}\theta_{cn}] = 0$. QED

Appendix D: Identification Error Analysis of CSD_SUBID Method with Non-stationary Response

a) Top Story Case:

Using the integrity indexes to rewrite the optimization problem (5.56) gives

$$\underset{\beta_{kn},\beta_{cn}}{\arg\min} \quad J(\beta_{kn},\beta_{cn}) = \sum_{l=1}^{N} |\varepsilon_l|^2 = \sum_{l=1}^{N} \left| f_l(\beta_{kn},\beta_{cn}) - \hat{f}_l\left(\hat{S}_{\ddot{x}_n y}, \hat{S}_{\ddot{x}_{n-1} y}, \hat{S}_{\ddot{\Delta}_n y}\right) \right|^2 \tag{D1}$$

where $f_l(\beta_{kn},\beta_{cn}) = \dfrac{1}{1 - j\beta_{cn}\, c_n/(m_n\omega_l) - \beta_{kn} k_n/(m_n\omega_l^2)}$,

$$\hat{f}_l\left(\hat{S}_{\ddot{x}_n y}, \hat{S}_{\ddot{x}_{n-1} y}, \hat{S}_{\ddot{\Delta}_n y}\right) = \frac{\hat{P}_{\ddot{x}_{n-1} y,l} - \hat{P}_{\ddot{x}_n y,l}}{\hat{P}_{y\ddot{x}_{n-1},l} - \hat{P}_{f_n y,l}}.$$

Following the procedure proposed in the LSE identification error analysis section,

$$\mathbf{h}_l = \begin{bmatrix} \partial f_l/\partial\beta_{nk} \\ \partial f_l/\partial\beta_{nc} \end{bmatrix}^{\mathrm{T}}_{\beta_\bullet=1} = \begin{bmatrix} \dfrac{k_n/(m_n\omega_l^2)}{\left[1 - j\, c_n/(m_n\omega_l) - k_n/(m_n\omega_l^2)\right]^2} & \dfrac{jc_n/(m_n\omega_l)}{\left[1 - j\, c_n/(m_n\omega_l) - k_n/(m_n\omega_l^2)\right]^2} \end{bmatrix} \tag{D2}$$

$$\hat{\mathbf{h}}_l = \begin{bmatrix} \partial\hat{f}_l/\partial\hat{P}_{\ddot{x}_{n-1} y,l} \\ \partial\hat{f}_l/\partial\hat{P}_{\ddot{x}_n y,l} \\ \partial\hat{f}_l/\partial\hat{P}_{f_n y,l} \end{bmatrix}^{\mathrm{T}}_{\hat{P}_\bullet=P} = \begin{bmatrix} \dfrac{P_{\ddot{x}_n y,l} - P_{f_n y,l}}{\left(P_{\ddot{x}_{n-1} y,l} - P_{f_n y,l}\right)^2} \\ \dfrac{-1}{P_{\ddot{x}_{n-1} y,l} - P_{f_n y,l}} \\ \dfrac{\left(P_{\ddot{x}_{n-1} y,l} - P_{\ddot{x}_n y,l}\right)}{\left(P_{\ddot{x}_{n-1} y,l} - P_{f_n y,l}\right)^2} \end{bmatrix}^{\mathrm{T}} \tag{D3}$$

where $\beta_\bullet = 1$ is the abbreviation for $\beta_{kn} = 1$ and $\beta_{cn} = 1$; $\hat{P}_\bullet = P_\bullet$ is the abbreviation of $\hat{P}_{\ddot{x}_{n-1} y,l} = P_{\ddot{x}_{n-1} y,l}$, $\hat{P}_{\ddot{x}_n y,l} = P_{\ddot{x}_n y,l}$ and $\hat{P}_{f_n y,l} = P_{f_n y,l}$ for the sake of notational simplicity. Rearranging Equation (5.55) gives

$$P_{\ddot{x}_{n-1} y} - P_{f_n y} = \left(P_{\ddot{x}_{n-1} y} - P_{\ddot{x}_n y}\right)\left[1 - j\, c_n/(m_n\omega) - k_n/(m_n\omega^2)\right] \tag{D4}$$

Using the right side of (D4) to replace the term in (D3) that equals the left side of (D4), and simplifying gives

$$\hat{\mathbf{h}}_l = \frac{1}{\left(P_{\ddot{x}_{n-1}y,l} - P_{\ddot{x}_n y,l}\right)} \begin{bmatrix} -\left[j c_n/(m_n\omega_l) + k_n/(m_n\omega_l^2)\right] \Big/ \left[1 - j c_n/(m_n\omega_l) - k_n/(m_n\omega_l^2)\right]^2 \\ -1\Big/\left[1 - j c_n/(m_n\omega_l) - k_n/(m_n\omega_l^2)\right] \\ 1\Big/\left[1 - j c_n/(m_n\omega_l) - k_n/(m_n\omega_l^2)\right]^2 \end{bmatrix}^{\mathrm{T}} \quad \text{(D5)}$$

Using the result of (D2),

$$\left[\sum_{l=1}^{N} \mathrm{Re}\left(\mathbf{h}_l^{\mathrm{T}} \mathbf{h}_l^*\right)\right]^{-1} = \begin{bmatrix} 1/A_1 & 0 \\ 0 & 1/A_2 \end{bmatrix} \quad \text{(D6)}$$

where $A_1 = \sum_{l=1}^{N} \frac{k_n^2/(m_n^2\omega_l^4)}{\left|1 - j c_n/(m_n\omega_l) - k_n/(m_n\omega_l^2)\right|^4}$; $A_2 = \sum_{l=1}^{N} \frac{c_n^2/(m_n^2\omega_l^2)}{\left|1 - j c_n/(m_n\omega_l) - k_n/(m_n\omega_l^2)\right|^4}$.

Then, applying the error analysis method in Equation (3.19) with the result of (D2), (D5) and (D6), the relative identification error of the top story parameters can be written as

$$\begin{bmatrix} \theta_{kn} \\ \theta_{cn} \end{bmatrix} \approx \sum_{l=1}^{N} \mathrm{Re}\left\{ \begin{bmatrix} W_{11,l} & W_{12,l} \\ W_{21,l} & W_{22,l} \end{bmatrix} \cdot \begin{bmatrix} N_{\ddot{x}_{n-1}y,l} / P_{(\ddot{x}_n - \ddot{x}_{n-1})y,l} \\ N_{\ddot{x}_n y,l} / P_{(\ddot{x}_n - \ddot{x}_{n-1})y,l} \end{bmatrix} + \begin{bmatrix} W_{13,l} \\ W_{23,l} \end{bmatrix} \frac{N_{f_n y,l}}{S_{(\ddot{x}_n - \ddot{x}_{n-1})y,l}} \right\} \quad \text{(D7)}$$

where

$$W_{11,l} = \frac{1}{A_1} \frac{k_n/(m_n\omega_l^2) \cdot \left[j c_n/(m_n\omega_l) + k_n/(m_n\omega_l^2)\right]}{\left|1 - j c_n/(m_n\omega_l) - k_n/(m_n\omega_l^2)\right|^4},$$

$$W_{21,l} = \frac{1}{A_2} \frac{j c_n/(m_n\omega_l) \cdot \left[j c_n/(m_n\omega_l) + k_n/(m_n\omega_l^2)\right]}{\left|1 - j c_n/(m_n\omega_l) - k_n/(m_n\omega_l^2)\right|^4},$$

$$W_{12,l} = \frac{1}{A_1} \frac{k_n/(m_n\omega_l^2)}{\left|1 - j c_n/(m_n\omega_l) - k_n/(m_n\omega_l^2)\right|^2 \left[1 - j c_n/(m_n\omega_l) - k_n/(m_n\omega_l^2)\right]^*},$$

$$W_{22,l} = \frac{1}{A_2} \frac{-jc_n/(m_n\omega_l)}{\left|1-jc_n/(m_n\omega_l)-k_n/(m_n\omega_l^2)\right|^2\left[1-jc_n/(m_n\omega_l)-k_n/(m_n\omega_l^2)\right]^*},$$

$$W_{13,l} = \frac{1}{A_1} \frac{-k_n/(m_n\omega_l^2)}{\left|1-jc_n/(m_n\omega_l)-k_n/(m_n\omega_l^2)\right|^4},\ W_{23,l} = \frac{1}{A_2} \frac{jc_n/(m_n\omega_l)}{\left|1-jc_n/(m_n\omega_l)-k_n/(m_n\omega_l^2)\right|^4}.$$

b) Non-top Story Case:

Using the integrity index, the identification problem (5.63) can be rewritten as

$$\arg\min_{\beta_{ki},\beta_{ci}} \quad J(\beta_{ki},\beta_{ci}) = \sum_{l=1}^{N}\left|g_l(\beta_{ki},\beta_{ci}) - \hat{g}_l(\hat{P}_{\ddot{x}_{i-1}y},\hat{P}_{\ddot{x}_i y},\hat{P}_{\ddot{x}_{i+1}y},\beta_{k(i+1)},\beta_{c(i+1)},\hat{P}_{f_i y})\right|^2 \tag{D8}$$

where $g_l(\beta_{ki},\beta_{ci}) = \dfrac{1}{1-j\beta_{ki}\,c_i/(m_i\omega_l)-\beta_{ci}\,k_i/(m_i\omega_l^2)}$;

$$\hat{g}_l\left(\hat{P}_{\ddot{x}_{i-1}y},\hat{P}_{\ddot{x}_i y},\hat{P}_{\ddot{x}_{i+1}y},\beta_{k(i+1)},\beta_{c(i+1)},\hat{P}_{f_i y}\right) = \frac{\hat{P}_{\ddot{x}_{i-1}y,l}-\hat{P}_{\ddot{x}_i y,l}}{\hat{P}_{\ddot{x}_{i-1}y,l}+(\hat{P}_{\ddot{x}_{i+1}y,l}-\hat{P}_{\ddot{x}_i y,l})[j\beta_{c(i+1)}c_{i+1}/(m_i\omega_l)+\beta_{k(i+1)}k_{i+1}/(m_i\omega_l^2)]-\hat{P}_{f_i y,l}}.$$

Following a procedure similar to the top story gives

$$\mathbf{h}_l = \left[\frac{\partial g_l}{\partial\beta_{ki}} \quad \frac{\partial g_l}{\partial\beta_{ci}}\right]_{\beta_\bullet=1} = \left[\frac{k_i/(m_i\omega_l^2)}{\left[1-jc_i/(m_i\omega_l)-k_i/(m_i\omega_l^2)\right]^2} \quad \frac{jc_i/(m_i\omega_l)}{\left[1-jc_i/(m_i\omega_l)-k_i/(m_i\omega_l^2)\right]^2}\right] \tag{D9}$$

$$
\hat{\mathbf{h}}_l = \left[\frac{\partial \hat{f}_l}{\partial \hat{P}_{\ddot{x}_{i-1}y,l}} \quad \frac{\partial \hat{f}_l}{\partial \hat{P}_{\ddot{x}_{i}y,l}} \quad \frac{\partial \hat{f}_l}{\partial \hat{P}_{\ddot{x}_{i+1}y,l}} \quad \frac{\partial \hat{f}_l}{\partial \beta_{k(i+1)}} \quad \frac{\partial \hat{f}_l}{\partial \beta_{c(i+1)}} \quad \frac{\partial \hat{f}_l}{\partial \hat{P}_{f_i y,l}} \right]_{\substack{\hat{P}_{\bullet} = P_{\bullet} \\ \beta_{\bullet} = 1}}
$$

$$
= \left[\begin{array}{c}
\dfrac{\left\{ -P_{f_i y,l} + P_{\ddot{x}_{i-1}y,l} + \left(P_{\ddot{x}_{i+1}y,l} - P_{\ddot{x}_{i}y,l}\right)\left[jc_{i+1}/(m_i\omega_l) + k_{i+1}/(m_i\omega_l^2)\right]\right\} - \left(P_{\ddot{x}_{i-1}y,l} - P_{\ddot{x}_{i}y,l}\right)}{\left\{ -P_{f_i y,l} + P_{\ddot{x}_{i-1}y,l} + \left(P_{\ddot{x}_{i+1}y,l} - P_{\ddot{x}_{i}y,l}\right)\left[jc_{i+1}/(m_i\omega_l) + k_{i+1}/(m_i\omega_l^2)\right]\right\}^2} \\
\dfrac{\left\{ -P_{\ddot{x}_{i-1}y,l} - \left[\left(P_{\ddot{x}_{i+1}y,l} - P_{\ddot{x}_{i}y,l}\right) + \left(P_{\ddot{x}_{i-1}y,l} - P_{\ddot{x}_{i-1}y,l}\right)\right]\left[jc_{i+1}/(m_i\omega_l) + k_{i+1}/(m_i\omega_l^2)\right] + P_{f_i y,l}\right\}}{\left\{ -P_{f_i y,l} + P_{\ddot{x}_{i-1}y,l} + \left(P_{\ddot{x}_{i+1}y,l} - P_{\ddot{x}_{i}y,l}\right)\left[jc_{i+1}/(m_i\omega_l) + k_{i+1}/(m_i\omega_l^2)\right]\right\}^2} \\
\dfrac{\left(P_{\ddot{x}_{i}y,l} - P_{\ddot{x}_{i-1}y,l}\right)\left[jc_{i+1}/(m_i\omega_l) + k_{i+1}/(m_i\omega_l^2)\right]}{\left\{ -P_{f_i y,l} + P_{\ddot{x}_{i-1}y,l} + \left(P_{\ddot{x}_{i+1}y,l} - P_{\ddot{x}_{i}y,l}\right)\left[jc_{i+1}/(m_i\omega_l) + k_{i+1}/(m_i\omega_l^2)\right]\right\}^2} \\
\dfrac{\left(P_{\ddot{x}_{i}y,l} - P_{\ddot{x}_{i-1}y,l}\right)\left(P_{\ddot{x}_{i+1}y,l} - P_{\ddot{x}_{i}y,l}\right)\left[k_{i+1}/(m_i\omega_l^2)\right]}{\left\{ -P_{f_i y,l} + P_{\ddot{x}_{i-1}y,l} + \left(P_{\ddot{x}_{i+1}y,l} - P_{\ddot{x}_{i}y,l}\right)\left[jc_{i+1}/(m_i\omega_l) + k_{i+1}/(m_i\omega_l^2)\right]\right\}^2} \\
\dfrac{\left(P_{\ddot{x}_{i}y,l} - P_{\ddot{x}_{i-1}y,l}\right)\left(P_{\ddot{x}_{i+1}y,l} - P_{\ddot{x}_{i}y,l}\right)\left[jc_{i+1}/(m_i\omega_l)\right]}{\left\{ -P_{f_i y,l} + P_{\ddot{x}_{i-1}y,l} + \left(P_{\ddot{x}_{i+1}y,l} - P_{\ddot{x}_{i}y,l}\right)\left[jc_{i+1}/(m_i\omega_l) + k_{i+1}/(m_i\omega_l^2)\right]\right\}^2} \\
\dfrac{\left(P_{\ddot{x}_{i-1}y,l} - P_{\ddot{x}_{i}y,l}\right)}{\left\{ -P_{f_i y,l} + P_{\ddot{x}_{i-1}y,l} + \left(P_{\ddot{x}_{i+1}y,l} - P_{\ddot{x}_{i}y,l}\right)\left[jc_{i+1}/(m_i\omega_l) + k_{i+1}/(m_i\omega_l^2)\right]\right\}^2}
\end{array} \right]^{\mathrm{T}} \qquad \text{(D10)}
$$

Rearranging Equation (5.61) gives

$$
\begin{aligned}
&-P_{f_i y} + P_{\ddot{x}_{i-1}y} + (P_{\ddot{x}_{i+1}y} - P_{\ddot{x}_{i}y})[jc_{i+1}/(m_i\omega) + k_{i+1}/(m_i\omega^2)] \\
&= \left(P_{\ddot{x}_{i-1}y} - P_{\ddot{x}_{i}y}\right)\left[1 - jc_i/(m_i\omega) - k_i/(m_i\omega^2)\right]
\end{aligned} \qquad \text{(D11)}
$$

Using the right side of (D11) to replace the terms in (D10) that equals to the left side of (D11) and simplifying will give

$$\hat{\mathbf{h}}_l = \begin{bmatrix} \dfrac{1}{\left(P_{\ddot{x}_i y,l} - P_{\ddot{x}_{i-1} y,l}\right)} \dfrac{j c_i/(m_i\omega_l) + k_i/(m_i\omega_l^2)}{\left[1 - j c_i/(m_i\omega_l) - k_i/(m_i\omega_l^2)\right]^2} \\ \dfrac{1}{\left(P_{\ddot{x}_i y,l} - P_{\ddot{x}_{i-1} y,l}\right)} \dfrac{\left[1 - j\left(c_{i+1} + c_i\right)/(m_i\omega_l) - \left(k_{i+1} + k_i\right)/(m_i\omega_l^2)\right]}{\left[1 - j c_i/(m_i\omega_l) - k_i/(m_i\omega_l^2)\right]^2} \\ \dfrac{1}{\left(P_{\ddot{x}_i y,l} - P_{\ddot{x}_{i-1} y,l}\right)} \dfrac{j c_{i+1}/(m_i\omega_l) + k_{i+1}/(m_i\omega_l^2)}{\left[1 - j c_i/(m_i\omega_l) - k_i/(m_i\omega_l^2)\right]^2} \\ \dfrac{\left(P_{\ddot{x}_{i+1} y,l} - P_{\ddot{x}_i y,l}\right)}{\left(P_{\ddot{x}_i y,l} - P_{\ddot{x}_{i-1} y,l}\right)} \dfrac{k_{i+1}/(m_i\omega_l^2)}{\left[1 - j c_i/(m_i\omega_l) - k_i/(m_i\omega_l^2)\right]^2} \\ \dfrac{\left(P_{\ddot{x}_{i+1} y,l} - P_{\ddot{x}_i y,l}\right)}{\left(P_{\ddot{x}_i y,l} - P_{\ddot{x}_{i-1} y,l}\right)} \dfrac{j c_{i+1}/(m_i\omega_l)}{\left[1 - j c_i/(m_i\omega_l) - k_i/(m_i\omega_l^2)\right]^2} \\ \dfrac{1}{\left(P_{\ddot{x}_i y,l} - P_{\ddot{x}_{i-1} y,l}\right)} \dfrac{-1}{\left[1 - j c_i/(m_i\omega_l) - k_i/(m_i\omega_l^2)\right]^2} \end{bmatrix} \tag{D12}$$

Then, applying the error analysis method in Equation (3.19) with the results of Equations (D9) and (D12), the relative identification error of the i^{th} story parameters can be obtained as

$$\begin{aligned} \begin{bmatrix} \theta_{ki} \\ \theta_{ci} \end{bmatrix} \approx \sum_{l=1}^{N} \mathrm{Re}\left\{ \begin{bmatrix} U_{11,l} & U_{12,l} & U_{13,l} \\ U_{21,l} & U_{22,l} & U_{23,l} \end{bmatrix} \cdot \begin{bmatrix} N_{\ddot{x}_{i-1} y,l} / P_{(\ddot{x}_i - \ddot{x}_{i-1}) y,l} \\ N_{\ddot{x}_i y,l} / P_{(\ddot{x}_i - \ddot{x}_{i-1}) y,l} \\ N_{\ddot{x}_{i+1} y,l} / P_{(\ddot{x}_i - \ddot{x}_{i-1}) y,l} \end{bmatrix} + \begin{bmatrix} U_{16,l} \\ U_{26,l} \end{bmatrix} \frac{N_{y f_i,l}}{P_{(\ddot{x}_i - \ddot{x}_{i-1}) y,l}} \right\} \\ + \sum_{l=1}^{N} \mathrm{Re}\left\{ \begin{bmatrix} U_{14,l} & U_{15,l} \\ U_{24,l} & U_{25,l} \end{bmatrix} \cdot \begin{bmatrix} \dfrac{P_{(\ddot{x}_{i+1} - \ddot{x}_i) y,l}}{P_{(\ddot{x}_i - \ddot{x}_{i-1}) y,l}} \theta_{k(i+1)} \\ \dfrac{P_{(\ddot{x}_{i+1} - \ddot{x}_i) y,l}}{P_{(\ddot{x}_i - \ddot{x}_{i-1}) y,l}} \theta_{c(i+1)} \end{bmatrix} \right\} \end{aligned} \tag{D13}$$

where $U_{ij,l}$ are weighting factors as follows,

$$B_1 = \sum_{l=1}^{N} \frac{k_i^2/(m_i^2\omega_l^4)}{\left|1 - j c_i/(m_i\omega_l) - k_i/(m_i\omega_l^2)\right|^4}, \; B_2 = \sum_{l=1}^{N} \frac{c_i^2/(m_i^2\omega_l^2)}{\left|1 - j c_i/(m_i\omega_l) - k_i/(m_i\omega_l^2)\right|^4}$$

$$U_{11,l} = \frac{1}{B_1} \frac{k_i/(m_i\omega_l^2) \cdot \left[j c_i/(m_i\omega_l) + k_i/(m_i\omega_l^2)\right]}{\left|1 - j c_i/(m_i\omega_l) - k_i/(m_i\omega_l^2)\right|^4},$$

$$U_{21,l} = \frac{1}{B_2}\frac{-jc_i/(m_i\omega_l)\cdot\left[jc_i/(m_i\omega_l)+k_i/(m_i\omega_l^2)\right]}{\left|1-j\,c_i/(m_i\omega_l)-k_i/(m_i\omega_l^2)\right|^4},$$

$$U_{12,l} = \frac{1}{B_1}\frac{k_i/(m_i\omega_l^2)\cdot\left[1-j\left(c_{i+1}+c_i\right)/(m_i\omega_l)-\left(k_{i+1}+k_i\right)/(m_i\omega_l^2)\right]}{\left|1-j\,c_i/(m_i\omega_l)-k_i/(m_i\omega_l^2)\right|^4},$$

$$U_{22,l} = \frac{1}{B_2}\frac{-jc_i/(m_i\omega_l)\cdot\left[1-j\left(c_{i+1}+c_i\right)/(m_i\omega_l)-\left(k_{i+1}+k_i\right)/(m_i\omega_l^2)\right]}{\left|1-j\,c_i/(m_i\omega_l)-k_i/(m_i\omega_l^2)\right|^4},$$

$$U_{13,l} = \frac{1}{B_1}\frac{k_i/(m_i\omega_l^2)\cdot\left[jc_{i+1}/\left(m_i\omega_l\right)+k_{i+1}/(m_i\omega_l^2)\right]}{\left|1-j\,c_i/\left(m_i\omega_l\right)-k_i/(m_i\omega_l^2)\right|^4},$$

$$U_{23,l} = \frac{1}{B_2}\frac{-jc_i/(m_i\omega_l)\cdot\left[jc_{i+1}/(m_i\omega_l)+k_{i+1}/(m_i\omega_l^2)\right]}{\left|1-j\,c_i/(m_i\omega_l)-k_i/(m_i\omega_l^2)\right|^4},$$

$$U_{14,l} = \frac{1}{B_1}\frac{k_ik_{i+1}/(m_i^2\omega_l^4)}{\left|1-j\,c_i/(m_i\omega_l)-k_i/(m_i\omega_l^2)\right|^4},\; U_{24,l} = \frac{1}{B_2}\frac{-jk_{i+1}c_i/(m_i^2\omega_l^3)}{\left|1-j\,c_i/(m_i\omega_l)-k_i/(m_i\omega_l^2)\right|^4},$$

$$U_{15,l} = \frac{1}{B_1}\frac{jk_ic_{i+1}/(m_i^2\omega_l^3)}{\left|1-j\,c_i/(m_i\omega_l)-k_i/(m_i\omega_l^2)\right|^4},\; U_{25,l} = \frac{1}{B_2}\frac{c_ic_{i+1}/(m_i^2\omega_l^2)}{\left|1-j\,c_i/(m_i\omega_l)-k_i/(m_i\omega_l^2)\right|^4},$$

$$U_{16,l} = \frac{1}{B_1}\frac{-k_i/(m_i\omega_l^2)}{\left|1-j\,c_i/(m_i\omega_l)-k_i/(m_i\omega_l^2)\right|^4},\; U_{26,l} = \frac{1}{B_2}\frac{jc_i/(m_i\omega_l)}{\left|1-j\,c_i/(m_i\omega_l)-k_i/(m_i\omega_l^2)\right|^4}.$$

Appendix E: Identification Error Analysis of Power Spectral Density Based Substructure Identification Method for Frame Structures

a) Top Story Case:

Using the integrity indexes to rewrite the optimization problem (8.25) gives

$$\underset{\beta_{kn},\beta_{cn}}{\arg\min} \quad J(\beta_{kn},\beta_{cn}) = \sum_{l=1}^{N} \left|\varepsilon_l\right|^2 = \sum_{l=1}^{N} \left| f_l(\beta_{kn},\beta_{cn}) - \hat{f}_l(\hat{S}_{\ddot{x}_n y}, \hat{S}_{\ddot{x}_{n-1} y}, , \hat{S}_{\ddot{\Delta}_n y}) \right|^2 \tag{E1}$$

where $f_l(\beta_{kn},\beta_{cn}) = \dfrac{1}{1 - j\beta_{cn}\, c_n/(m_n\omega_l) - \beta_{kn} k_n/(m_n\omega_l^2)}$,

$$\hat{f}_l(\hat{S}_{\ddot{x}_n y}, \hat{S}_{\ddot{x}_{n-1} y}, , \hat{S}_{\ddot{\Delta}_n y}) = \frac{\hat{S}_{\ddot{x}_{n-1} y,l} - \hat{S}_{\ddot{x}_n y,l} - \hat{S}_{\ddot{\Delta}_n y,l}}{\hat{S}_{\ddot{x}_{n-1} y,l} - \hat{S}_{\ddot{\Delta}_n y,l}}.$$

Following the procedure proposed in the LSE identification error analysis section,

$$\mathbf{h}_l = \begin{bmatrix} \partial f_l/\partial\beta_{nk} \\ \partial f_l/\partial\beta_{nc} \end{bmatrix}^{\mathrm{T}}_{\beta_\bullet=1} = \begin{bmatrix} \dfrac{k_n/(m_n\omega_l^2)}{\left[1 - j\,c_n/(m_n\omega_l) - k_n/(m_n\omega_l^2)\right]^2} & \dfrac{jc_n/(m_n\omega_l)}{\left[1 - j\,c_n/(m_n\omega_l) - k_n/(m_n\omega_l^2)\right]^2} \end{bmatrix} \tag{E2}$$

$$\hat{\mathbf{h}}_l = \begin{bmatrix} \partial\hat{f}_l/\partial\hat{S}_{\ddot{x}_{n-1} y,l} \\ \partial\hat{f}_l/\partial\hat{S}_{\ddot{x}_n y,l} \\ \partial\hat{f}_l/\partial\hat{S}_{\ddot{\Delta}_n y,l} \end{bmatrix}^{\mathrm{T}}_{\hat{S}_\bullet = S_\bullet} = \begin{bmatrix} \dfrac{S_{\ddot{x}_n y,l}}{(\hat{S}_{\ddot{x}_{n-1} y,l} - \hat{S}_{\ddot{\Delta}_n y,l})^2} & \dfrac{-1}{(\hat{S}_{\ddot{x}_{n-1} y,l} - \hat{S}_{\ddot{\Delta}_n y,l})} & \dfrac{-S_{\ddot{x}_n y,l}}{(\hat{S}_{\ddot{x}_{n-1} y,l} - \hat{S}_{\ddot{\Delta}_n y,l})^2} \end{bmatrix}^{\mathrm{T}} \tag{E3}$$

where $\beta_\bullet = 1$ is the abbreviation for $\beta_{kn} = 1$ and $\beta_{cn} = 1$; $\hat{S}_\bullet = S_\bullet$ is the abbreviation of $\hat{S}_{\ddot{x}_{n-1} y,l} = S_{\ddot{x}_{n-1} y,l}$, $\hat{S}_{\ddot{x}_n y,l} = S_{\ddot{x}_n y,l}$ and $\hat{S}_{\ddot{\Delta}_n y,l} = S_{\ddot{\Delta}_n y,l}$, for the sake of notational simplicity. Rearranging Equation (8.23) gives

$$S_{\ddot{x}_{n-1} y} - S_{\ddot{\Delta}_n y} = (S_{\ddot{x}_{n-1} y} - S_{\ddot{x}_n y} - S_{\ddot{\Delta}_n y})\left[1 - j\,c_n/(m_n\omega) - k_n/(m_n\omega^2)\right] \tag{E4}$$

$$S_{\ddot{x}_n y}\big/(\hat{S}_{\ddot{x}_{n-1} y} - \hat{S}_{\ddot{\Delta}_n y}) = -\left[j\,c_n/(m_n\omega) + k_n/(m_n\omega^2)\right]\big/\left[1 - j\,c_n/(m_n\omega) - k_n/(m_n\omega^2)\right] \tag{E5}$$

Using the results of Equations (E4) and (E5) to simplify Equation (E3) gives

$$\hat{\mathbf{h}}_l = \frac{1}{(S_{\ddot{x}_{n-1}y,l} - S_{\ddot{x}_n y,l} - S_{\ddot{\Delta}_n y,l})} \begin{bmatrix} \dfrac{-jc_n/(m_n\omega_l) - k_n/(m_n\omega_l^2)}{\left[1 - jc_n/(m_n\omega_l) - k_n/(m_n\omega_l^2)\right]^2} \\ \dfrac{-1}{1 - jc_n/(m_n\omega_l) - k_n/(m_n\omega_l^2)} \\ \dfrac{jc_n/(m_n\omega_l) + k_n/(m_n\omega_l^2)}{\left[1 - jc_n/(m_n\omega_l) - k_n/(m_n\omega_l^2)\right]^2} \end{bmatrix}^{\mathrm{T}} \tag{E6}$$

Using the result of (E2),

$$\left[\sum_{l=1}^{N} \mathrm{Re}\left(\mathbf{h}_l^{\mathrm{T}}\mathbf{h}_l^*\right)\right]^{-1} = \begin{bmatrix} 1/A_1 & 0 \\ 0 & 1/A_2 \end{bmatrix} \tag{E7}$$

where $A_1 = \sum_{l=1}^{N} \dfrac{k_n^2/(m_n^2\omega_l^4)}{\left|1 - jc_n/(m_n\omega_l) - k_n/(m_n\omega_l^2)\right|^4}$; $A_2 = \sum_{l=1}^{N} \dfrac{c_n^2/(m_n^2\omega_l^2)}{\left|1 - jc_n/(m_n\omega_l) - k_n/(m_n\omega_l^2)\right|^4}$.

Then, applying the error analysis method in Equation (3.19) with (E2), (E6) and (E7), the relative identification error of the top story parameters can be written as

$$\begin{bmatrix} \theta_{nk} \\ \theta_{nc} \end{bmatrix} \approx \sum_{l=1}^{N} \mathrm{Re}\left\{ \begin{bmatrix} W_{11,l} & W_{12,l} & W_{13,l} \\ W_{21,l} & W_{22,l} & W_{23,l} \end{bmatrix} \cdot \begin{bmatrix} N_{\ddot{x}_{n-1}y,l} / S_{(\ddot{x}_n - \ddot{x}_{n-1} + \ddot{\Delta}_n)y,l} \\ N_{\ddot{x}_n y,l} / S_{(\ddot{x}_n - \ddot{x}_{n-1} + \ddot{\Delta}_n)y,l} \\ N_{\ddot{\Delta}_n y,l} / S_{(\ddot{x}_n - \ddot{x}_{n-1} + \ddot{\Delta}_n)y,l} \end{bmatrix} \right\} \tag{E8}$$

where $W_{11,l} = \dfrac{1}{A_1} \dfrac{-k_n/(m_n\omega_l^2) \cdot \left[jc_n/(m_n\omega_l) + k_n/(m_n\omega_l^2)\right]}{\left|1 - jc_n/(m_n\omega_l) - k_n/(m_n\omega_l^2)\right|^4}$,

$$W_{21,l} = \frac{1}{A_2} \frac{-jc_n/(m_n\omega_l) \cdot \left[jc_n/(m_n\omega_l) + k_n/(m_n\omega_l^2)\right]}{\left|1 - jc_n/(m_n\omega_l) - k_n/(m_n\omega_l^2)\right|^4},$$

$$W_{12,l} = \frac{1}{A_1} \frac{k_n/(m_n\omega_l^2)}{\left|1 - jc_n/(m_n\omega_l) - k_n/(m_n\omega_l^2)\right|^2 \left[1 - jc_n/(m_n\omega_l) - k_n/(m_n\omega_l^2)\right]^*},$$

$$W_{22,l} = \frac{1}{A_2} \frac{jc_n/(m_n\omega_l)}{\left|1 - jc_n/(m_n\omega_l) - k_n/(m_n\omega_l^2)\right|^2 \left[1 - jc_n/(m_n\omega_l) - k_n/(m_n\omega_l^2)\right]^*},$$

$$W_{13,l} = \frac{1}{A_1} \frac{k_n/(m_n\omega_l^2)\cdot\left[jc_n/(m_n\omega_l) + k_n/(m_n\omega_l^2)\right]}{\left|1 - jc_n/(m_n\omega_l) - k_n/(m_n\omega_l^2)\right|^4} = -W_{11,l},$$

$$W_{23,l} = \frac{1}{A_2} \frac{jc_n/(m_n\omega_l)\cdot\left[jc_n/(m_n\omega_l) + k_n/(m_n\omega_l^2)\right]}{\left|1 - jc_n/(m_n\omega_l) - k_n/(m_n\omega_l^2)\right|^4} = -W_{21,l}.$$

b) Non-top Story Case:

Using the integrity index, the identification problem (8.26) can be rewritten as

$$\arg\min_{\beta_{ki},\beta_{ci}} \quad J(\beta_{ki},\beta_{ci}) = \sum_{l=1}^{N} \left| g_l(\beta_{ki},\beta_{ci}) - \hat{g}_l(\hat{S}_{\ddot{x}_{i-1}y}, \hat{S}_{\ddot{x}_i y}, \hat{S}_{\ddot{x}_{i+1}y}, \hat{S}_{\ddot{\Delta}_i y}, \hat{S}_{\ddot{\Delta}_{i+1}y}, \beta_{k(i+1)}, \beta_{c(i+1)}) \right|^2 \quad \text{(E9)}$$

where $g_l(\beta_{ki},\beta_{ci}) = \dfrac{1}{1 - j\beta_{ki}\, c_i/(m_i\omega_l) - \beta_{ci}\, k_i/(m_i\omega_l^2)}$;

$$\hat{g}_l(\hat{S}_{\ddot{x}_{i-1}y}, \hat{S}_{\ddot{x}_i y}, \hat{S}_{\ddot{x}_{i+1}y}, \hat{S}_{\ddot{\Delta}_{i-1}y}, \hat{S}_{\ddot{\Delta}_i y}, \beta_{k(i+1)}, \beta_{c(i+1)}) = \frac{\hat{S}_{\ddot{x}_{i-1}y,l} - \hat{S}_{\ddot{x}_i y,l} - \hat{S}_{\ddot{\Delta}_i y,l}}{(\hat{S}_{\ddot{x}_{i-1}y,l} - \hat{S}_{\ddot{\Delta}_i y,l}) + (\hat{S}_{\ddot{x}_{i+1}y,l} - \hat{S}_{\ddot{x}_i y,l} + \hat{S}_{\ddot{\Delta}_{i+1}y,l})[j\beta_{c(i+1)}c_{i+1}/(m_i\omega_l) + \beta_{k(i+1)}\, k_{i+1}/(m_i\omega_l^2)]}.$$

Following a procedure similar to the top story gives

$$\mathbf{h}_l = \left[\frac{\partial g_l}{\partial \beta_{ki}} \quad \frac{\partial g_l}{\partial \beta_{ci}}\right]_{\beta_\bullet = 1} = \left[\frac{k_i/(m_i\omega_l^2)}{\left[1 - jc_i/(m_i\omega_l) - k_i/(m_i\omega_l^2)\right]^2} \quad \frac{jc_i/(m_i\omega_l)}{\left[1 - jc_i/(m_i\omega_l) - k_i/(m_i\omega_l^2)\right]^2}\right]$$

(E10)

$$\hat{\mathbf{h}}_l = \left[\frac{\partial \hat{g}_l}{\partial \hat{S}_{y\ddot{x}_{i-1},l}} \quad \frac{\partial \hat{g}_l}{\partial \hat{S}_{y\ddot{x}_{i},l}} \quad \frac{\partial \hat{g}_l}{\partial \hat{S}_{y\ddot{x}_{i+1},l}} \quad \frac{\partial \hat{g}_l}{\partial \hat{S}_{y\ddot{\Delta}_{i},l}} \quad \frac{\partial \hat{g}_l}{\partial \hat{S}_{y\ddot{\Delta}_{i+1},l}} \quad \frac{\partial \hat{g}_l}{\partial \beta_{k(i+1)}} \quad \frac{\partial \hat{g}_l}{\partial \beta_{c(i+1)}} \right]_{\substack{\hat{S}_\bullet = S_\bullet \\ \beta_\bullet = 1}}$$

$$= \begin{bmatrix} \dfrac{\left\{ S_{\ddot{x}_i y,l} + (S_{\ddot{x}_{i+1}y,l} - S_{\ddot{x}_i y,l})\left[jc_{i+1}/(m_i\omega_l) + k_{i+1}/(m_i\omega_l^2)\right]\right\}}{\left\{(S_{\ddot{x}_{i-1}y,l} - S_{\ddot{\Delta}_i y,l}) + (S_{\ddot{x}_{i+1}y,l} - S_{\ddot{x}_i y,l} + S_{\ddot{\Delta}_{i+1}y,l})\left[jc_{i+1}/(m_i\omega_l) + k_{i+1}/(m_i\omega_l^2)\right]\right\}^2} \\ \dfrac{\left\{ -(S_{\ddot{x}_{i-1}y,l} - S_{\ddot{\Delta}_i y,l}) - (S_{\ddot{x}_{i+1}y,l} - S_{\ddot{x}_{i-1}y,l} + S_{\ddot{\Delta}_{i+1}y,l} + S_{\ddot{\Delta}_i y,l})\left[jc_{i+1}/(m_i\omega_l) + k_{i+1}/(m_i\omega_l^2)\right]\right\}}{\left\{(S_{\ddot{x}_{i-1}y,l} - S_{\ddot{\Delta}_i y,l}) + (S_{\ddot{x}_{i+1}y,l} - S_{\ddot{x}_i y,l} + S_{\ddot{\Delta}_{i+1}y,l})\left[jc_{i+1}/(m_i\omega_l) + k_{i+1}/(m_i\omega_l^2)\right]\right\}^2} \\ \dfrac{-(S_{\ddot{x}_{i-1}y,l} - S_{\ddot{x}_i y,l} - S_{\ddot{\Delta}_i y,l})\left[jc_{i+1}/(m_i\omega_l) + k_{i+1}/(m_i\omega_l^2)\right]}{\left\{(S_{\ddot{x}_{i-1}y,l} - S_{\ddot{\Delta}_i y,l}) + (S_{\ddot{x}_{i+1}y,l} - S_{\ddot{x}_i y,l} + S_{\ddot{\Delta}_{i+1}y,l})\left[jc_{i+1}/(m_i\omega_l) + k_{i+1}/(m_i\omega_l^2)\right]\right\}^2} \\ \dfrac{-\left\{ S_{\ddot{x}_i y,l} + (S_{\ddot{x}_{i+1}y,l} - S_{\ddot{x}_i y,l})\left[jc_{i+1}/(m_i\omega_l) + k_{i+1}/(m_i\omega_l^2)\right]\right\}}{\left\{(S_{\ddot{x}_{i-1}y,l} - S_{\ddot{\Delta}_i y,l}) + (S_{\ddot{x}_{i+1}y,l} - S_{\ddot{x}_i y,l} + S_{\ddot{\Delta}_{i+1}y,l})\left[jc_{i+1}/(m_i\omega_l) + k_{i+1}/(m_i\omega_l^2)\right]\right\}^2} \\ \dfrac{-(S_{\ddot{x}_{i-1}y,l} - S_{\ddot{x}_i y,l} - S_{\ddot{\Delta}_i y,l})\left[jc_{i+1}/(m_i\omega_l) + k_{i+1}/(m_i\omega_l^2)\right]}{\left\{(S_{\ddot{x}_{i-1}y,l} - S_{\ddot{\Delta}_i y,l}) + (S_{\ddot{x}_{i+1}y,l} - S_{\ddot{x}_i y,l} + S_{\ddot{\Delta}_{i+1}y,l})\left[jc_{i+1}/(m_i\omega_l) + k_{i+1}/(m_i\omega_l^2)\right]\right\}^2} \\ \dfrac{(S_{\ddot{x}_{i-1}y,l} - S_{\ddot{x}_i y,l} - S_{\ddot{\Delta}_i y,l})(S_{\ddot{x}_{i+1}y,l} - S_{\ddot{x}_i y,l} + S_{\ddot{\Delta}_{i+1}y,l})\, k_{i+1}/(m_i\omega_l^2)}{\left\{(S_{\ddot{x}_{i-1}y,l} - S_{\ddot{\Delta}_i y,l}) + (S_{\ddot{x}_{i+1}y,l} - S_{\ddot{x}_i y,l} + S_{\ddot{\Delta}_{i+1}y,l})\left[jc_{i+1}/(m_i\omega_l) + k_{i+1}/(m_i\omega_l^2)\right]\right\}^2} \\ \dfrac{(S_{\ddot{x}_{i-1}y,l} - S_{\ddot{x}_i y,l} - S_{\ddot{\Delta}_i y,l})(S_{\ddot{x}_{i+1}y,l} - S_{\ddot{x}_i y,l} + S_{\ddot{\Delta}_{i+1}y,l})\, jc_{i+1}/(m_i\omega_l)}{\left\{(S_{\ddot{x}_{i-1}y,l} - S_{\ddot{\Delta}_i y,l}) + (S_{\ddot{x}_{i+1}y,l} - S_{\ddot{x}_i y,l} + S_{\ddot{\Delta}_{i+1}y,l})\left[jc_{i+1}/(m_i\omega_l) + k_{i+1}/(m_i\omega_l^2)\right]\right\}^2} \end{bmatrix}^{\mathrm{T}} \tag{E11}$$

Rearranging Equation (8.24) gives

$$\begin{aligned} &(S_{\ddot{x}_{i-1}y} - S_{\ddot{\Delta}_i y}) + (S_{\ddot{x}_{i+1}y} - S_{\ddot{x}_i y} + S_{\ddot{\Delta}_{i+1}y})\left[\frac{jc_{i+1}}{(m_i\omega)} + \frac{k_{i+1}}{(m_i\omega^2)} \right] = \\ &(S_{\ddot{x}_{i-1}y} - S_{\ddot{x}_i y} - S_{\ddot{\Delta}_i y})\left[1 - \frac{jc_i}{(m_i\omega)} - \frac{k_i}{(m_i\omega^2)} \right] \end{aligned} \tag{E12}$$

Using Equation (E12) to simplify Equation (E11) gives

$$\hat{\mathbf{h}}_l = \begin{bmatrix} \dfrac{j c_i/(m_i\omega_l) + k_i/(m_i\omega_l^2)}{(S_{\ddot{x}_i y,l} - S_{\ddot{x}_{i-1} y,l} + S_{\ddot{\Delta}_i y,l})\left[1 - j c_i/(m_i\omega_l) - k_i/(m_i\omega_l^2)\right]^2} \\ \dfrac{\left[1 - j(c_{i+1}+c_i)/(m_i\omega_l) - (k_{i+1}+k_i)/(m_i\omega_l^2)\right]}{(S_{\ddot{x}_i y,l} - S_{\ddot{x}_{i-1} y,l} + S_{\ddot{\Delta}_i y,l})\left[1 - j c_i/(m_i\omega_l) - k_i/(m_i\omega_l^2)\right]^2} \\ \dfrac{j c_{i+1}/(m_i\omega_l) + k_{i+1}/(m_i\omega_l^2)}{(S_{\ddot{x}_i y,l} - S_{\ddot{x}_{i-1} y,l} + S_{\ddot{\Delta}_i y,l})\left[1 - j c_i/(m_i\omega_l) - k_i/(m_i\omega_l^2)\right]^2} \\ \dfrac{- j c_i/(m_i\omega_l) - k_i/(m_i\omega_l^2)}{(S_{\ddot{x}_i y,l} - S_{\ddot{x}_{i-1} y,l} + S_{\ddot{\Delta}_i y,l})\left[1 - j c_i/(m_i\omega_l) - k_i/(m_i\omega_l^2)\right]^2} \\ \dfrac{- j c_{i+1}/(m_i\omega_l) - k_{i+1}/(m_i\omega_l^2)}{(S_{\ddot{x}_i y,l} - S_{\ddot{x}_{i-1} y,l} + S_{\ddot{\Delta}_i y,l})\left[1 - j c_i/(m_i\omega_l) - k_i/(m_i\omega_l^2)\right]^2} \\ \dfrac{-(S_{\ddot{x}_{i+1} y,l} - S_{\ddot{x}_i y,l} + S_{\ddot{\Delta}_{i+1} y,l})\left[k_{i+1}/(m_i\omega_l^2)\right]}{(S_{\ddot{x}_i y,l} - S_{\ddot{x}_{i-1} y,l} + S_{\ddot{\Delta}_i y,l})\left[1 - j c_i/(m_i\omega_l) - k_i/(m_i\omega_l^2)\right]^2} \\ \dfrac{-(S_{\ddot{x}_{i+1} y,l} - S_{\ddot{x}_i y,l} + S_{\ddot{\Delta}_{i+1} y,l})\left[j c_{i+1}/(m_i\omega_l)\right]}{(S_{\ddot{x}_i y,l} - S_{\ddot{x}_{i-1} y,l} + S_{\ddot{\Delta}_i y,l})\left[1 - j c_i/(m_i\omega_l) - k_i/(m_i\omega_l^2)\right]^2} \end{bmatrix}^{\mathrm{T}} \tag{E13}$$

Then, applying the error analysis method in Equation (3.19) with Equations (E10) and (E13), the relative identification error of the i^{th} story parameters can be obtained as

$$\begin{bmatrix} \theta_{ki} \\ \theta_{ci} \end{bmatrix} \approx \sum_{l=1}^{N} \mathrm{Re}\left\{ \begin{bmatrix} U_{11,l} & U_{12,l} & U_{13,l} & U_{14,l} & U_{15,l} \\ U_{22,l} & U_{22,l} & U_{23,l} & U_{24,l} & U_{25,l} \end{bmatrix} \cdot \begin{bmatrix} N_{\ddot{x}_{i-1} y,l} / S_{(\ddot{x}_i - \ddot{x}_{i-1} + \ddot{\Delta}_i) y,l} \\ N_{\ddot{x}_i y,l} / S_{(\ddot{x}_i - \ddot{x}_{i-1} + \ddot{\Delta}_i) y,l} \\ N_{\ddot{x}_{i+1} y,l} / S_{(\ddot{x}_i - \ddot{x}_{i-1} + \ddot{\Delta}_i) y,l} \\ N_{\ddot{\Delta}_i y,l} / S_{(\ddot{x}_i - \ddot{x}_{i-1} + \ddot{\Delta}_i) y,l} \\ N_{\ddot{\Delta}_{i+1} y,l} / S_{(\ddot{x}_i - \ddot{x}_{i-1} + \ddot{\Delta}_i) y,l} \end{bmatrix} \right\} + \sum_{l=1}^{N} \mathrm{Re}\left\{ \begin{bmatrix} U_{16,l} & U_{17,l} \\ U_{26,l} & U_{27,l} \end{bmatrix} \cdot \begin{bmatrix} \dfrac{S_{(\ddot{x}_{i+1} - \ddot{x}_i + \ddot{\Delta}_{i+1}) y,l}}{S_{(\ddot{x}_i - \ddot{x}_{i-1} + \ddot{\Delta}_i) y,l}} \theta_{k(i+1)} \\ \dfrac{S_{(\ddot{x}_{i+1} - \ddot{x}_i + \ddot{\Delta}_{i+1}) y,l}}{S_{(\ddot{x}_i - \ddot{x}_{i-1} + \ddot{\Delta}_i) y,l}} \theta_{c(i+1)} \end{bmatrix} \right\} \tag{E14}$$

where $U_{ij,l}$ are weighting factors as follows,

$$B_1 = \sum_{l=1}^{N} \frac{k_i^2 / (m_i^2 \omega_l^4)}{\left| 1 - j\, c_i / (m_i \omega_l) - k_i / (m_i \omega_l^2) \right|^4}\,,\;\; B_2 = \sum_{l=1}^{N} \frac{c_i^2 / (m_i^2 \omega_l^2)}{\left| 1 - j\, c_i / (m_i \omega_l) - k_i / (m_i \omega_l^2) \right|^4}\,,$$

$$U_{11,l} = \frac{1}{B_1} \frac{k_i / (m_i \omega_l^2) \cdot \left[j c_i / (m_i \omega_l) + k_i / (m_i \omega_l^2) \right]}{\left| 1 - j\, c_i / (m_i \omega_l) - k_i / (m_i \omega_l^2) \right|^4}\,,$$

$$U_{21,l} = \frac{1}{B_2} \frac{- j c_i / (m_i \omega_l) \cdot \left[j c_i / (m_i \omega_l) + k_i / (m_i \omega_l^2) \right]}{\left| 1 - j\, c_i / (m_i \omega_l) - k_i / (m_i \omega_l^2) \right|^4}\,,$$

$$U_{12,l} = \frac{1}{B_1} \frac{k_i / (m_i \omega_l^2) \cdot \left[1 - j\left(c_{i+1} + c_i\right) / (m_i \omega_l) - \left(k_{i+1} + k_i\right) / (m_i \omega_l^2) \right]}{\left| 1 - j\, c_i / (m_i \omega_l) - k_i / (m_i \omega_l^2) \right|^4}\,,$$

$$U_{22,l} = \frac{1}{B_2} \frac{- j c_i / (m_i \omega_l) \cdot \left[1 - j\left(c_{i+1} + c_i\right) / (m_i \omega_l) - \left(k_{i+1} + k_i\right) / (m_i \omega_l^2) \right]}{\left| 1 - j\, c_i / (m_i \omega_l) - k_i / (m_i \omega_l^2) \right|^4}\,,$$

$$U_{13,l} = \frac{1}{B_1} \frac{k_i / (m_i \omega_l^2) \cdot \left[j c_{i+1} / (m_i \omega_l) + k_{i+1} / (m_i \omega_l^2) \right]}{\left| 1 - j\, c_i / (m_i \omega_l) - k_i / (m_i \omega_l^2) \right|^4}\,,$$

$$U_{23,l} = \frac{1}{B_2} \frac{- j c_i / (m_i \omega_l) \cdot \left[j c_{i+1} / (m_i \omega_l) + k_{i+1} / (m_i \omega_l^2) \right]}{\left| 1 - j\, c_i / (m_i \omega_l) - k_i / (m_i \omega_l^2) \right|^4}\,,$$

$$U_{14,l} = \frac{1}{B_1} \frac{- k_i / (m_i \omega_l^2) \cdot \left[j c_i / (m_i \omega_l) + k_i / (m_i \omega_l^2) \right]}{\left| 1 - j\, c_i / (m_i \omega_l) - k_i / (m_i \omega_l^2) \right|^4} = -U_{11,l}\,,$$

$$U_{24,l} = \frac{1}{B_2} \frac{j c_i / \left(m_i \omega_l\right) \cdot \left[j c_i / (m_i \omega_l) + k_i / (m_i \omega_l^2) \right]}{\left| 1 - j\, c_i / (m_i \omega_l) - k_i / (m_i \omega_l^2) \right|^4} = -U_{21,l}\,,$$

$$U_{15,l} = \frac{1}{B_1} \frac{- k_i / (m_i \omega_l^2) \cdot \left[j c_{i+1} / (m_i \omega_l) + k_{i+1} / (m_i \omega_l^2) \right]}{\left| 1 - j\, c_i / (m_i \omega_l) - k_i / (m_i \omega_l^2) \right|^4} = U_{13,l}\,,$$

$$U_{25,l} = \frac{1}{B_2} \frac{j c_i / (m_i \omega_l) \cdot \left[j c_{i+1} / (m_i \omega_l) + k_{i+1} / (m_i \omega_l^2) \right]}{\left| 1 - j\, c_i / (m_i \omega_l) - k_i / (m_i \omega_l^2) \right|^4} = U_{23,l}\,,$$

$$U_{16,l} = \frac{1}{B_1} \frac{-k_i k_{i+1} / (m_i^2 \omega_l^4)}{\left|1 - j\, c_i / (m_i \omega_l) - k_i / (m_i \omega_l^2)\right|^4}\,,\; U_{26,l} = \frac{1}{B_2} \frac{j k_{i+1} c_i / (m_i^2 \omega_l^3)}{\left|1 - j\, c_i / (m_i \omega_l) - k_i / (m_i \omega_l^2)\right|^4}\,,$$

$$U_{17,l} = \frac{1}{B_1} \frac{-j k_i c_{i+1} / (m_i^2 \omega_l^3)}{\left|1 - j\, c_i / (m_i \omega_l) - k_i / (m_i \omega_l^2)\right|^4}\,,\; U_{27,l} = \frac{1}{B_2} \frac{-c_i c_{i+1} / (m_i^2 \omega_l^2)}{\left|1 - j\, c_i / (m_i \omega_l) - k_i / (m_i \omega_l^2)\right|^4}\,.$$